

Chirality Pure Carbon Nanotubes: Growth, Sorting, and Characterization

Feng Yang, Meng Wang, Daqi Zhang, Juan Yang, Ming Zheng*, and Yan Li*



Cite This: <https://dx.doi.org/10.1021/acs.chemrev.9b00835>



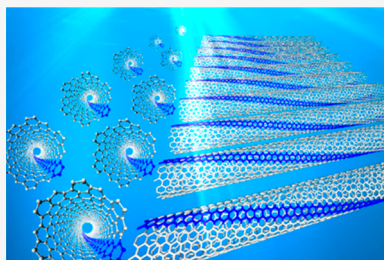
Read Online

ACCESS |

Metrics & More

Article Recommendations

ABSTRACT: Single-walled carbon nanotubes (SWCNTs) have been attracting tremendous attention owing to their structure (chirality) dependent outstanding properties, which endow them with great potential in a wide range of applications. The preparation of chirality-pure SWCNTs is not only a great scientific challenge but also a crucial requirement for many high-end applications. As such, research activities in this area over the last two decades have been very extensive. In this review, we summarize recent achievements and accumulated knowledge thus far and discuss future developments and remaining challenges from three aspects: controlled growth, postsynthesis sorting, and characterization techniques. In the growth part, we focus on the mechanism of chirality-controlled growth and catalyst design. In the sorting part, we organize and analyze existing literature based on sorting targets rather than methods. Since chirality assignment and quantification is essential in the study of selective preparation, we also include in the last part a comprehensive description and discussion of characterization techniques for SWCNTs. It is our view that even though progress made in this area is impressive, more efforts are still needed to develop both methodologies for preparing ultrapure (e.g., >99.99%) SWCNTs in large quantity and nondestructive fast characterization techniques with high spatial resolution for various nanotube samples.



CONTENTS

1. Introduction
 - 1.1. Structure and Properties of SWCNTs
 - 1.2. Brief Account of Structure-Dependent Application of SWCNTs
 - 1.3. Overview of Structure-Controlled Preparation of SWCNTs
2. Structure-Controlled Growth of SWCNTs
 - 2.1. Growth Mechanism and Role of Catalysts
 - 2.1.1. Catalytic Nucleation and Growth of SWCNTs
 - 2.1.2. Theoretical Models of Chirality Controlled Growth of SWCNTs
 - 2.2. Diameter- and Conductivity-Controlled Growth of SWCNTs
 - 2.2.1. Diameter-Controlled Growth of SWCNTs
 - 2.2.2. Selective Growth of Semiconducting SWCNTs
 - 2.3. Chirality Controlled Growth of SWCNTs from Catalysts
 - 2.3.1. Catalyst Design
 - 2.3.2. Kinetic Control
 - 2.3.3. Strategy for Chirality-Specific Growth of SWCNTs
 - 2.4. SWCNTs Initiated by Predesigned Nano-carbon Segments

B	2.4.1. Synthesis of SWCNTs from Nanocarbon Segments	U
B	2.4.2. Chirality-Specified SWCNTs by Elongation of Nanocarbon Segments	W
B	2.5. Open Questions and Challenges in Chirality-Controlled Growth of SWCNTs	W
C	2.5.1. Understanding the Growth Mechanism	W
D	2.5.2. How Far Can Selective Growth Practically Go?	W
D	3. Sorting SWCNTs	X
D	3.1. A Brief Account of Sorting SWCNTs in Solution	X
G	3.1.1. Challenges in SWCNT Sorting	X
G	3.1.2. Strategies for Dispersion of SWCNTs	Y
I	3.1.3. Methodologies and Mechanisms of Sorting SWCNTs	Z
L	3.2. Length, Diameter, and Conductivity Based Sorting of SWCNTs	AB
N	3.2.1. Length-Based Sorting of SWCNTs	AB
N	3.2.2. Diameter-Based Sorting of SWCNTs	AC
R	3.2.3. Conductivity-Based Sorting of SWCNTs	AC
T	3.3. Sorting SWCNTs by Chirality	AE

Received: December 24, 2019

3.3.1. Sorting SWCNTs Dispersed by Surfactants	AE
3.3.2. Sorting SWCNTs Dispersed by DNA	AF
3.3.3. Sorting SWCNTs Dispersed by Polymers	AG
3.4. Enantiomer-Based Sorting of SWCNTs	AG
3.4.1. Chirality-Enriched Enantiomer of SWCNTs	AH
3.4.2. Single-Chirality Enantiomers of SWCNTs	AH
3.5. Other Purification Techniques	AI
3.5.1. Electrical Break Down	AI
3.5.2. Selective Chemical Reaction	AJ
3.6. Future Perspectives on SWCNT Sorting	AJ
4. Chirality Assignment and Quantification of SWCNTs	AJ
4.1. Chirality Assignment	AJ
4.1.1. Basic Principles	AJ
4.1.2. Resonant Raman Spectroscopy	AK
4.1.3. Photoluminescence Spectroscopy	AN
4.1.4. Absorption Spectroscopy	AO
4.1.5. Rayleigh Scattering Spectroscopy	AP
4.1.6. Circular Dichroism Spectroscopy	AQ
4.1.7. Scanning Tunneling Microscopy	AQ
4.1.8. Transmission Electron Microscopy	AQ
4.1.9. Other Methods	AR
4.1.10. Combination of Multiple Techniques	AR
4.2. Chirality Quantification	AS
4.2.1. Quantification of Ensemble SWCNTs	AS
4.2.2. Quantification of On-Substrate Individual SWCNTs	AU
4.2.3. Limitations of Present Quantitative Methods	AU
4.2.4. Combination of Multiple Techniques	AV
5. Concluding Remarks and Perspectives	AV
5.1. Summary of the Present Research	AW
5.2. Remaining Challenges	AW
5.2.1. Growth Mechanism of Chirality-Controlled SWCNTs	AW
5.2.2. Scalable Growth of Ultrapure Single-Chirality SWCNTs and Their Quantification	AW
5.2.3. Low-Cost Sorting of Single-Chirality SWCNTs for Large Scale Production	AW
5.3. Future Outlook	AW
Author Information	AX
Corresponding Authors	AX
Authors	AX
Notes	AX
Biographies	AX
Acknowledgments	AX
References	AX

1. INTRODUCTION

As one of the amazing allotropes of carbon, carbon nanotubes (CNTs) have attracted much attention since early 1990s,^{1,2} partially evidenced by the increasing number of annual publications (Figure 1). Indeed, CNTs are among the most studied materials in chemistry and related fields in the past three decades. Research and development of CNT applications keep on expanding as well, covering energy harvesting, energy storage, water treatment, ultrahigh-conduction films and fibers, electronics, photonics, display, biomedicine, and composites, etc.^{3–10} Many of these applications are enabled by the

outstanding properties of single-walled CNTs (SWCNTs),² which are endowed by their unique structure, honeycombs of sp^2 carbon with specific arrangements of the hexagons designated by a pair of chiral indices. Therefore, the availability of chirality-pure SWCNTs has always been at the root of CNT research because of its importance in both science and technology.^{11–18}

Though the preparation of chirality-pure SWCNTs is no doubt one of the most important challenges in the field, chirality-pure SWCNTs are becoming increasingly accessible. Recently, there has been significant progress in both chirality-specific growth and sorting. Therefore, we intend to review the developments and new findings in the field and identify directions for future studies. Our review will cover three aspects: controlled growth, postsynthesis sorting, and characterization.

1.1. Structure and Properties of SWCNTs

A SWCNT can be viewed as a cylinder rolled up from a monolayer graphene via a chiral vector $C_h = na_1 + ma_2 \equiv (n,m)$, where a_1 and a_2 are lattice unit vectors of the graphene sheet (Figure 2); (n,m) defines the “chirality” or “helicity” of a SWCNT. The diameter (d_t) and chiral angle (θ) of a SWCNT are calculated by $d_t = C_h/\pi = a_{CC}\sqrt{3(m^2 + n^2 + nm)}/\pi$ and $\theta = \tan^{-1} \frac{\sqrt{3}m}{2n+m}$. The tube ends are “armchair”-shaped when $n = m$ ($\theta = 30^\circ$) and “zigzag”-shaped when $m = 0$ ($\theta = 0^\circ$). A SWCNT is right-handed if $n - m > 0$ and left-handed otherwise.¹⁹

Let us see how (n,m) determines the band structure of a SWCNT and makes it either a semiconducting SWCNT (s-SWCNT) or a metallic SWCNT (m-SWCNT). The electronic structure of a SWCNT can originate from that of single layer graphene according to the hexagonal Brillouin zone. The Brillouin zone of a SWCNT can be seen as a set of parallel lines with equal spacings cutting in the graphene Brillouin zone (Figure 2b).²⁰ SWCNTs are classified into three groups, according to $(m - n) \text{ MOD } 3 = 0, 1, \text{ and } 2$. For a MOD-0 SWCNT, a cutting line crosses the K point (valence and conduction bands touch), and thus it is metallic with continuous density of states (DOS) at the Fermi energy (Figure 2c). Since no allowed cutting lines cross the K point, MOD-1 and MOD-2 SWCNTs are semiconducting, exhibiting chirality-dependent transitional energies (E_{ii}) (Figure 2d).

1.2. Brief Account of Structure-Dependent Application of SWCNTs

CNTs present outstanding thermal, electrical, and mechanical properties and have found applications in various fields.^{3,21} For instance, CNTs were used as conductive fillers in plastics²² and in lithium ion batteries because of their electrical conductivity and mechanical integrity.^{23,24} Furthermore, CNTs present high elastic modulus and tensile strength²⁵ and hence can act as superior materials for fabricating high-performance ultralight multifunctional fibers with specific strength, stiffness, and thermal and electrical conductivity.^{26,27}

SWCNTs hold great potential in electronic, quantum-photonic, and biomedical applications.^{4,6,28,29} SWCNTs are compatible with important biomolecules (e.g., DNA and proteins) in both spatial dimensions and chemical properties and thus are promising in biomedical applications.⁴ High water permeability and ion selectivity through the inner channel of a CNT opens possibilities to use CNTs in membrane separation.²⁸ High-quality SWCNTs are considered to be promising alternative materials in next generation electronics

because of their proper band gap and low carrier scattering.^{9,30–36} Here are some milestones in SWCNT-based electronics: the first SWCNT transistor in 1998,³⁷ the first SWCNT radio in 2007,³⁸ the first SWCNT computer in 2013,³¹ complementary SWCNT transistors with gate length of 5 nm in 2017,³⁴ and SWCNT-based modern microprocessor in 2019.³⁹ Furthermore, SWCNTs are particularly attractive in fabricating transparent conductive films (TCFs) for flexible devices owing to their outstanding conductivity, stability, and flexibility. These outstanding properties of SWCNT TCFs enable their applications in photovoltaics and many electronic or optoelectronic devices.^{5,40–43} Commercialization of SWCNT-based TCFs in the near future is expected.

Despite the promising performance of SWCNTs in various applications, many high-end applications require SWCNTs with specific structures. For example, high-performance field effect transistor (FETs) using high-density horizontally aligned s-SWCNTs achieved mobilities of $1600 \text{ cm}^2 \cdot \text{V}^{-1} \cdot \text{s}^{-1}$, on-state current density of $150 \mu\text{A} \cdot \mu\text{m}^{-1}$, and on/off ratio of more than 10^4 simultaneously.⁴⁴ In addition, chirality-specific s-SWCNTs are ideal bioimaging probes with intrinsic emission located in the

second near-infrared window covering wavelengths between 1.0 and $1.4 \mu\text{m}$, which was first demonstrated by Dai et al.⁴⁵ Chirality-pure SWCNTs provide high imaging sensitivity and resolution and reduced dosage during imaging. Strano et al. demonstrated that highly purified (6,5) SWCNTs possessed higher efficiency than mixtures of SWCNTs when acting as the active photoabsorption layer in an all carbon solar cell.⁴⁶ Adding 20% of (6,4) tubes to the (6,5) tubes led to a 30-fold decay in power conversion efficiency. The reason is that the heterojunction of pure (6,5) SWCNTs and fullerene presents a lower energy barrier for holes. Flavel et al. demonstrated that the efficiency of polymer-free SWCNT–fullerene solar cells depends on SWCNT diameter.⁴⁷

1.3. Overview of Structure-Controlled Preparation of SWCNTs

To harness the extraordinary properties and achieve optimal performance of SWCNTs in various applications, the production of SWCNTs with single chirality is highly desirable. Huge efforts have been directed to the preparation of chirality-pure SWCNTs. There are mainly two pathways to this goal, one

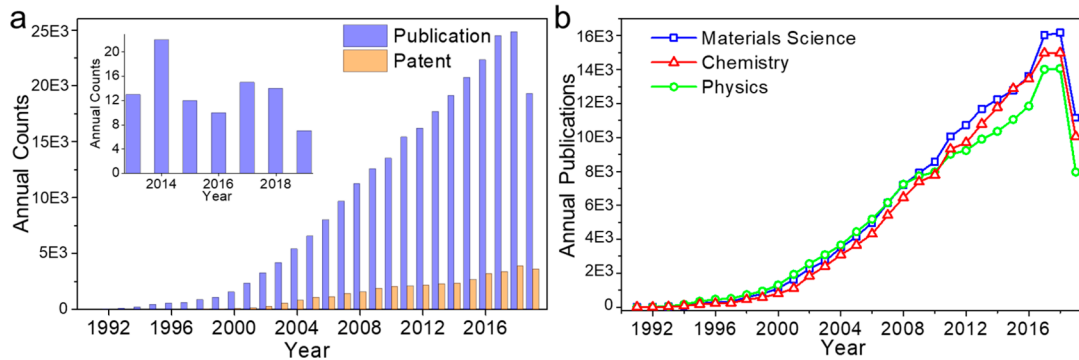


Figure 1. (a) Trends in research on CNTs represented as number of journal publications and patents from 1991 to 2019 (Data from ISI Web of Science on December 7, 2019). Inset shows research on CNTs published in *Science* and *Nature* in the last 7 years. (b) Trends in research on CNTs represented as number of journal publications in the fields of Chemistry, Materials Science, and Physics from 1991 to 2019 (Data from ISI Web of Science).

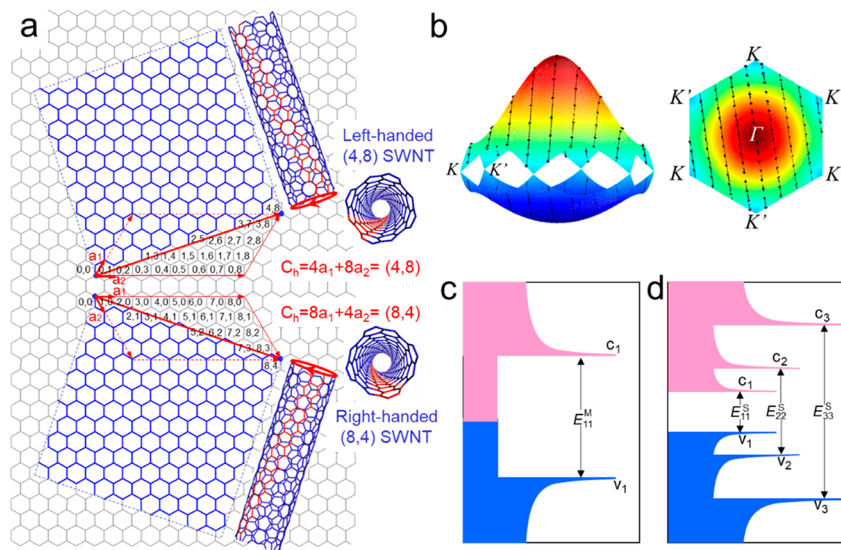


Figure 2. (a) Schematic illustration of a right-handed (8,4) and a left-handed (4,8) SWCNT rolled up from graphene sheets. (b) Calculated energy dispersion (E vs k) contours for the conduction and valence bands of a graphene layer in the first Brillouin zone using the π -band nearest neighbor tight binding model. Right, side view; left, vertical view. (c, d) DOS plots and corresponding electronic transitions of a m-SWCNT (c) and a s-SWCNT (d).

is direct synthesis and the other is postsynthesis purification and separation.

Chemical vapor deposition (CVD) is presently a dominant methodology to synthesize SWCNTs. Figure 3 summarizes the

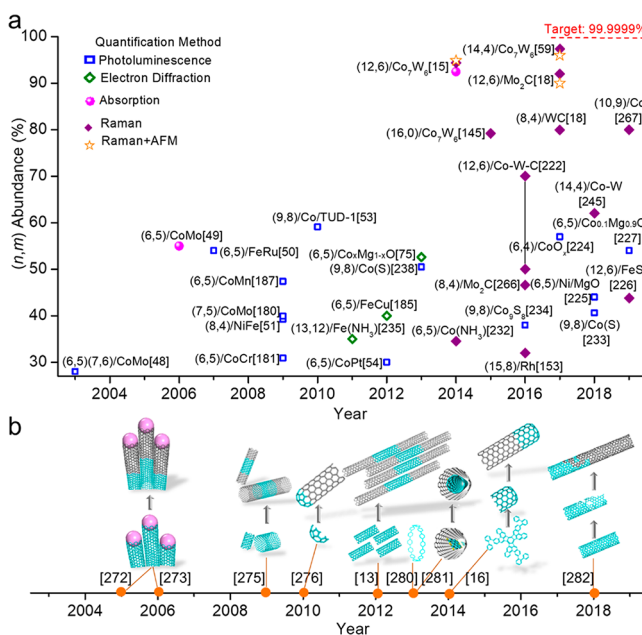


Figure 3. Reports on chirality-controlled growth of SWCNTs with catalysts (a) and amplification of SWCNT segments (b). Corresponding references are shown. Adapted from ref 64. Copyright 2016 American Chemical Society.

main progress in selective growth of chirality-enriched SWCNTs. Relying on the rational design and optimization of both catalysts and growth conditions,^{15,18,48–58} the highest chiral purity ever reported is 97% for (14,4) tubes.⁵⁹ Segments of nanocarbon have also been used as the seeds to grow SWCNTs with specified chiralities.^{13,16} Yet chiral purity of the products obtained by this method has not been quantified and reported.

Postgrowth separation based on solution-sorting techniques has been shown to be a reliable route to obtain high-purity species of SWCNTs with various (*n,m*) as summarized in Figure 4. Many effective dispersion systems (e.g., DNA,¹¹ polymer,⁶⁰ and surfactant) and separation techniques (e.g., dielectrophoresis,⁶¹ density gradient ultracentrifugation (DGU),¹⁴ ion-exchange chromatography (IEX),⁶² gel column chromatography (GCC),¹² aqueous two-phase (ATP) extraction⁶³) have been developed to achieve diameter-, conductivity-, chirality-, and enantiomer-based separation and sorting of SWCNTs.

The preparation of chirality-pure SWCNTs is important both scientifically and for application potential. Huge progress has been made, yet great challenges still lie ahead. Herein, we systematically review pathways of controlled growth and postsynthesis sorting to achieve chirality-pure SWCNTs. More importantly, we will discuss and compare advantages and disadvantages of various strategies, aiming to reveal the future development of precise and controllable preparation. Since reliable characterization is the prerequisite for controlled preparation, we will provide an up-to date overview of methodologies to determine chiral index and quantify the purity, with an emphasis on the applicability of each method. Specifically, we will suggest reliable methodology that combines

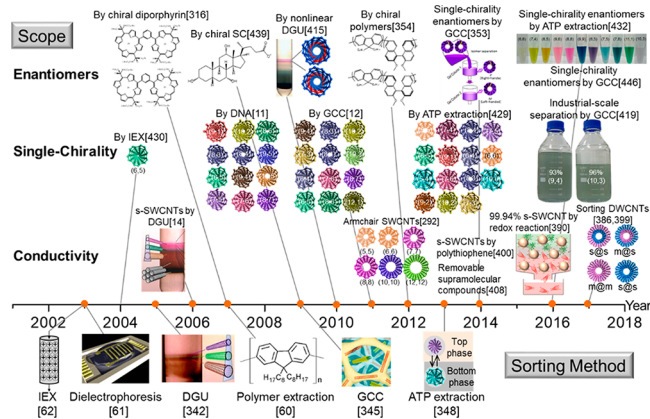


Figure 4. Time line of sorting SWCNTs. Reproduced with permission from the following: ref 14, Copyright 2006 Nature Publishing Group; ref 61, 2003 Copyright American Association for the Advancement of Science; ref 342, Copyright 2005 American Chemical Society; ref 345, Copyright 2009 American Chemical Society; ref 353, Copyright 2014 American Chemical Society; ref 390, Copyright 2016 American Chemical Society; ref 415, Copyright 2010 Nature Publishing Group; ref 419, 2016 Nature Publishing Group; ref 432, Copyright 2016 American Chemical Society.

different techniques. At the end, we will discuss the challenges and opportunities and expound our outlook in this field.

2. STRUCTURE-CONTROLLED GROWTH OF SWCNTs

Chirality-specific growth of SWCNTs presents the advantage of providing high-quality products with well-graphitized structure in large quantity. CVD offers multiple parameters for catalysts, substrates, and growth conditions to achieve better control of the synthesis. In this section, we will first introduce the growth mechanism of CNTs, because a deep understanding and knowledge of the growth mechanism of CNTs is the first step to realizing controllable synthesis. Then we will introduce the major experimental achievements in controlled growth of SWCNTs in diameter, conductivity, and eventually chirality. In the end, we will discuss open questions and remaining challenges in the field.

2.1. Growth Mechanism and Role of Catalysts

2.1.1. Catalytic Nucleation and Growth of SWCNTs. *Nucleation of SWCNTs.* Catalysts play core roles in growing SWCNTs in the CVD synthesis. Metal nanoparticles are normally used as catalysts for SWCNT growth.^{65–68} Fe, Cu, Co, and Ni are the most frequently used catalysts. Many other transition metals such as Cr, Mn, Mo, Ag, Au, Pd, and Pt are also adopted. There are reports on oxides and other nonmetal catalysts. However, none of them is as efficient as metals in catalyzing SWCNT growth.⁶⁹ Depending on the properties of the metal catalysts and CVD conditions, the growth process undergoes either a vapor–liquid–solid (VLS) or a vapor–solid–solid (VSS) mechanism by base- or tip-growth mode with tubes perpendicular or tangential to the catalyst nanoparticles (Figure 5).

High temperature (normally >800 °C) is generally required for growing CNTs of well-graphitized structure; thus the nanosized catalyst particles are normally in liquid state during the CVD process.^{70,71} In this case, CNTs grow via a VLS process, progressing from catalyzed decomposition of carbon precursors, to dissolution of carbon species in the liquid catalyst,

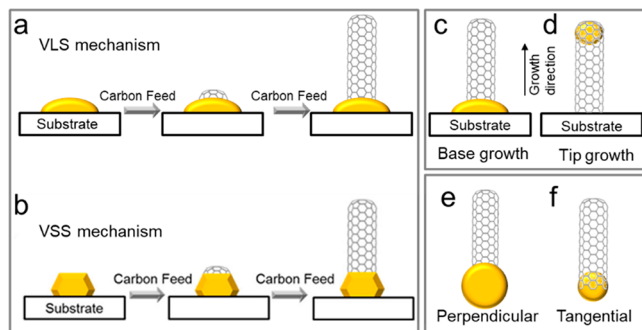


Figure 5. Scheme of the SWCNT growth mechanisms. (a, b) VLS (a) and VSS (b) mechanisms; (c, d) Base (c) and tip (d) growth mode; (e, f) Perpendicular (e) and tangential (f) growth mode. Panels a, e, and f reproduced with permission from ref 56. Copyright 2017 Springer. Panel b reproduced from ref 64. Copyright 2016 American Chemical Society.

nucleation of a tube cap on the catalyst, lift-off of the cap, and elongation of the tube (Figure 5a).^{56,68,72}

When growth is performed at relatively lower temperature, CNTs can also grow via a VSS process (Figure 5b).⁶⁴ *In situ* studies using environmental transmission electron microscope (ETEM) more often showed that the nanoparticles maintain a crystallized state during CNT growth^{15,69,73–76} because the observations were normally performed at lower temperature (400–650 °C) than the normal CVD process. In the VSS process, carbon atoms may migrate on the surface of solid catalysts to form nanotubes without dissolving into the catalyst.^{75,77,78}

The catalysts for growing SWCNTs are generally loaded on substrates or supports. A strong metal–substrate interaction could anchor the catalyst on the support, pushing lift-off of the SWCNT from the substrate. Such a growth mode is called base growth (Figure 5c).^{79,80} In contrast, a weak catalyst–substrate interaction leads to growth of the SWCNTs by the tip-growth mode (Figure 5d).⁸¹

It has been widely accepted that a size correlation exists between the tube and its seeding catalyst particle. Loiseau et al. found by TEM observation that there are two configurations of a tube wall on a catalyst nanoparticle, so-called tangential and perpendicular modes.⁸² The tangential mode yields a SWCNT with diameter equal to the particle size, while the perpendicular one yields a SWCNT with a diameter smaller than the catalyst (Figure 5e,f).

It is obvious that the properties of the catalysts, including composition, carbon solubility, melting point, crystal structure, surface energy, interaction with the support, etc., affect the structure of the resultant SWCNTs. Understanding the mechanisms of SWCNT nucleation and growth on catalyst nanoparticles at atomic scale is vital to the controllable synthesis of SWCNTs.

Atomistic Modeling. Theoretical simulation using molecular dynamics (MD), tight binding (TB), reactive force field, and density functional theory (DFT) provides information on SWCNT growth, such as growth mode,^{83,84} defect evolution,^{85–87} chirality transfer,^{88,89} and growth rate.⁹⁰ Nucleation of a carbon cap on catalysts via the VLS mode has been intensively investigated. Pioneering MD simulations on SWCNT nucleation were developed by Shibuta and Maruyama based on an empirical force field.⁸³ They found that the sp^2 carbon network arises from a carbon-saturated Ni cluster (Figure 6a). In VLS

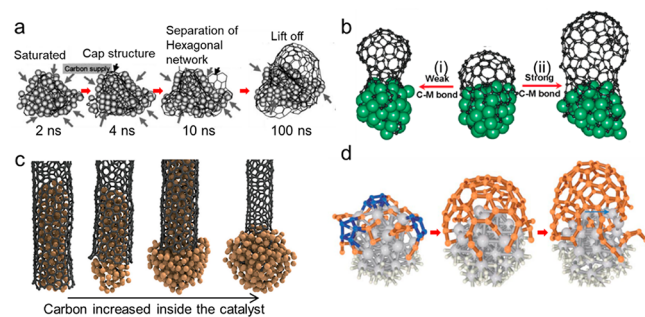


Figure 6. (a) Snapshots of the Ni_{108} cluster-catalyzed growth process of the cap structure. Reproduced with permission from ref 83. Copyright 2003 Elsevier. (b) MD simulations of SWCNT growth with different carbon–metal interaction strengths. The open end of a carbon cap on an Fe_{50} catalyst particle closes after addition of carbon atoms when the carbon–metal interaction is changed to be weak (i) and remains open to support SWCNT elongation when the carbon–metal interaction is strong (ii). Reproduced from ref 96. Copyright 2008 American Chemical Society. (c) SWCNT–catalyst configurations showing tangential (left) and perpendicular modes (right). Reproduced with permission from ref 98. Copyright 2017 Springer. (d) Snapshot of a sp^2 carbon network nucleating on the surface of Fe cluster by MD simulation. Reproduced with permission from ref 78. Copyright 2005 American Physical Society.

growth mode, the solubility of carbon in a metal catalyst and metal–carbon interactions are two critical factors for nanotube formation.^{83,91–95} Ding et al. considered a metal carbide phase in the SWCNT nucleation process.^{94,95} They showed that an optimal interaction between carbon and catalyst is very important for SWCNT nucleation.⁹⁶ An interaction that is too strong will result in the encapsulation of the catalyst, and one that is too weak will cause the lifting of the SWCNT from the catalyst (Figure 6b).

The phase diagrams of the metal–carbon mixtures can help to understand the interaction between metal catalyst and carbon. Bichara et al. calculated carbon adsorption isotherms on a Ni cluster with TB simulation and showed that carbon-enriched Ni clusters tend to dewet the graphitic wall.⁹¹ Their later work combining simulation and TEM observations demonstrated that the carbon solubility inside the catalyst determines the growth mode (perpendicular or tangential) (Figure 6c).^{97,98} When carbon is highly enriched in the nanoparticles, a perpendicular growth mode will happen. Conversely, when carbon feeding is lower, a tangential growth mode will take place. However, the mechanism of the VSS growth mode was rarely reported. Raty et al. found with MD simulations that carbon atoms do not diffuse into the iron cluster because of the weak adhesion between the graphitic wall and Fe cluster, indicating that the growth follows the VSS growth mode (Figure 6d).⁷⁸

Although simulations provide a basic sketch of nanotube formation, the correlation to experimental growth conditions is still a big challenge. For example, most of the simulations are performed on a free-standing catalyst particle, ignoring the catalyst–support interactions, and at a significantly higher temperature compared to the typical catalytic CVD experimental conditions. Therefore, direct atomic scale observations are needed to elucidate the nucleation and growth process of SWCNTs under growth conditions.

In situ Study on Catalysts during SWCNT Nucleation. *In situ* techniques such as environmental TEM (ETEM),⁷³ atmospheric X-ray photoelectron spectroscopy,⁷⁷ synchrotron based X-ray absorption spectroscopy (XAS),^{99,100} and X-ray diffrac-

tion (XRD)¹⁰¹ have been applied to follow the CVD conditions and reveal the structure of the catalyst during CNT growth. Among them, ETEM is an effective tool to directly image nanotube growth in real time.

In the early stages, several groups found that the nucleation of a CNT always accompanies the reconstruction of the catalyst during CNT growth.^{73,74} Another ETEM study showed that solid Fe₃C

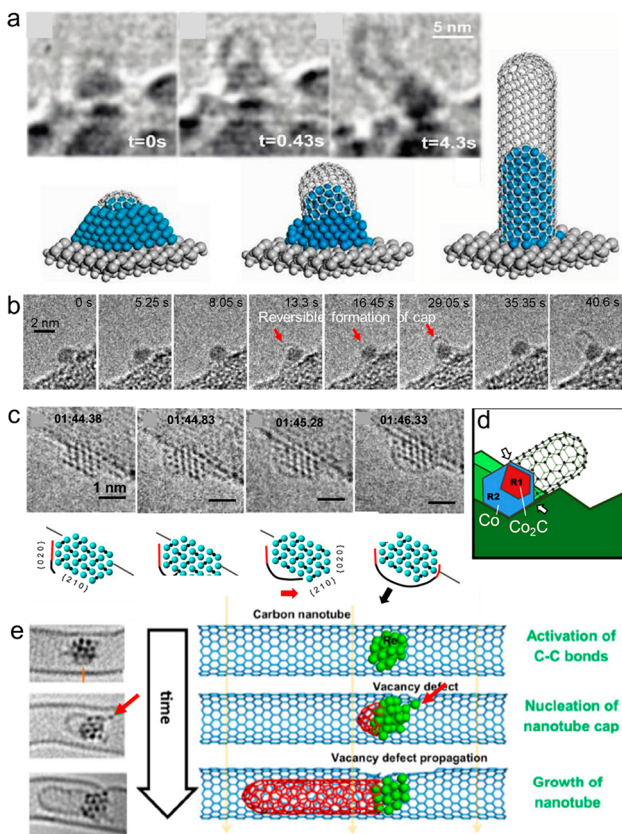


Figure 7. *In situ* observation of SWCNT nucleation. (a) Time-sequenced ETEM images of Ni-catalyzed CNT growth via a base mode. Reproduced from ref 74. Copyright 2006 American Chemical Society. (b) Time-sequenced ETEM images of Fe₃C catalyzed CNT growth. Reproduced from ref 102. Copyright 2008 American Chemical Society. (c) Time-resolved ETEM images of cap formation on the step of a Co nanocrystal and the corresponding atomic models. Reproduced from ref 103. Copyright 2014 American Chemical Society. (d) Schematic showing the configuration of SWCNT and Co-Co₂C. Reproduced with permission from ref 110. Copyright 2017 Elsevier. (e) Time sequenced AC-HRTEM images following the nucleation of a SWCNT on a Re cluster embedded in a SWCNT and corresponding schematics. Reproduced from ref 109. Copyright 2018 American Chemical Society.

catalysts structurally fluctuate and carbon caps reversibly form on catalysts (Figure 7b).¹⁰² Limited by the resolution of *in situ* TEM, the atomic-scale structure of the catalyst and cap was still unreachable at that time. With the recent development of advanced aberration-corrected ETEM, some new deep insights into the growth mechanism have been proposed. Sharma et al. found an approach of cap formation in which the single layer graphene converts to a curved cap on the atomic step of a Co₃C nanocrystal. The step of the catalyst acts as anchoring site to stabilize the cap, and then the cap lifts off from the catalyst to grow longer (Figure 7c).¹⁰³ The interfacial step induced nucleation of CNTs was also observed in Ni catalysts.^{104,105}

Besides introducing gaseous carbon stocks into the ETEM chamber, researchers also used host multiwall CNTs (MWCNTs) containing metal nanoparticles as a nanoreactor. Carbon from the graphitic walls of the host tube served as carbon source to grow a smaller tube inside.^{106–109} Kaiser's group used the e-beam of an aberration-corrected high-resolution TEM (AC-HRTEM) to supply the energy to drive nanotube growth on a sub-nanometer Re cluster embedded in a host SWCNT. They revealed that the dynamic single Re atoms contribute to the nucleation of a cap and the ordered crystalline Re phase accelerates the growth efficiency of the nanotube (Figure 7e).¹⁰⁹

Uncovering the composition and structure of the active catalysts in working conditions is important for comprehending the growth mechanism of SWCNTs. It has been reported that metals,^{74,75,77,111} alloys,¹¹² carbides,^{102,113} and inhomogeneous metal-carbides^{110,114,115} can all act as active species during the nanotube growth. Bichara et al. proved by MD simulation that the carbon solubility in Ni catalyst depends on both the size and state of the catalysts.^{91,116} These theoretical predictions were also evidenced by the ETEM observations.

On the other hand, much direct evidence probed by *in situ* TEM and XAS shows that active metal catalysts, such as transitional metals Fe,¹¹⁷ Co,^{75,111} Ni,^{74,77} Pt,^{99,118} Au,¹⁰⁷ and FePt alloy,¹¹² maintain a metallic state and there is no carbon diffusion into the nanoparticles when fed with carbon. When comparing these ETEM results systematically, we found that the active species, even for the same metal element, can be different (Table 1). For the case of cobalt-catalyzed CVD growth of

Table 1. Summary of Active Species in Cobalt-Catalyzed Growth of CNTs by ETEM

catalyst	active species	product	ETEM condition	ref
Co/MgO	Co	SWCNTs	600 °C, CO 630 Pa	75
Co/MgO	Co ₃ C	SWCNTs	700 °C, CO 530–760 Pa	119
Co/SiO ₂	Co + Co ₃ C	MWCNTs	550 °C, C ₂ H ₂ 3 Pa	115
CoMo/MgO	Co ₂ C	SWCNTs	625 °C, C ₂ H ₂ 0.005 Pa	103
CoMo/MgO	Co + Co ₂ C	SWCNTs	650 °C, C ₂ H ₂ 0.01 Pa	110

CNTs, He et al. realized the preferential growth of (6,5) SWCNTs with MgO-stabilized Co catalysts.⁷⁵ These stabilized Co nanoparticles maintain a metallic state and act as active species for nanotube nucleation, demonstrated by ETEM at 600 °C in 630 Pa of CO. In contrast, other ETEM results demonstrated that the metallic Co particles transform to cobalt carbides (Co₂C or Co₃C) in CO¹¹⁹ or to structurally inhomogeneous Co–Co₂C^{110,114} or Co–Co₃C¹¹⁵ in a C₂H₂ environment (Table 1). For example, Sharma et al.¹¹⁰ showed that a carbon gradient exists in MgO supported Co nanoparticles. The carbon-rich phase (Co₂C) is generally in contact with the support (MgO), and the carbon-poor phase (metallic Co) is in contact with the SWCNT rim (Figure 7d). Such a carbon gradient acts as a driving force for carbon atom diffusion toward the surface over the particle.¹¹⁰

After carefully analyzing these ETEM studies with different conclusions on active species for CNT growth, we believe that the carbon feeding conditions played important roles. The active catalyst species can be different depending on CVD conditions, which was also evidenced when using Ni^{73,77,104} and Fe^{102,113,120,121} to do the study. Besides the CVD conditions, the phase of metals also affects the type of active catalyst

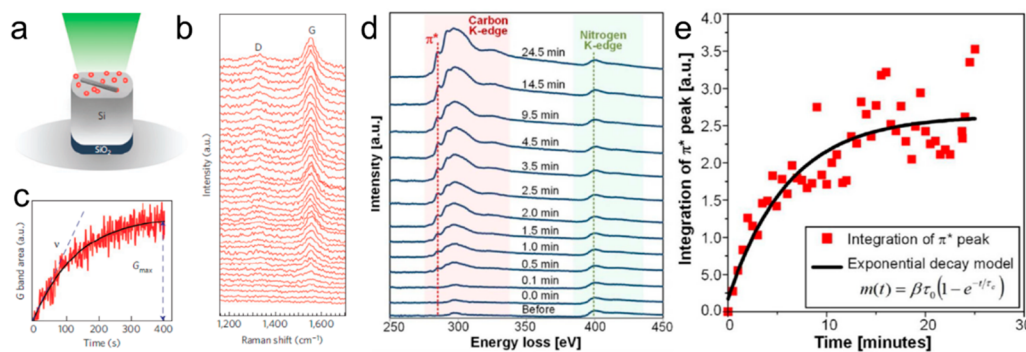


Figure 8. *In situ* measurements of growth rate of SWCNTs. (a–c) Raman. Reproduced with permission from ref 123. Copyright 2012 Nature Publishing Group. (d, e) EELS. Reproduced from ref 124. Copyright 2016 American Chemical Society.

species.^{117,122} For example, for γ -rich Fe nanoparticles, Hofmann et al. identified that metallic Fe acts as the active species for the nucleation of CNTs by *in situ* XRD, whereas for α -rich Fe nanoparticles, carbonized Fe_3C is responsible for growing CNTs.¹¹⁷

Compared to ETEM, *in situ* XRD has the advantage of reflecting the overall information but also some disadvantages. Since diffractions from well-crystallized particles (normally with larger diameters) often dominate the XRD patterns, information on the nanoparticles that catalyze nanotube growth might be absent since these catalyst particles are normally smaller in size and less ordered in structure.

The above *in situ* studies indicate that the composition and state of catalysts play important roles in catalyzing the tube growth. Therefore, precisely modulating the structure of the active catalyst is important for controlled growth of SWCNTs.

In Situ Study of the Growth Rate of SWCNTs. Revealing the growth rate of SWCNTs of different structures can provide information on growth kinetics. Both ETEM¹¹⁹ and Raman spectrometry incorporated with a reaction cell for tube growth¹²³ have been used to measure the growth rate of SWCNTs. The tube length, which is positively proportional to numbers of carbon atoms, can be derived from the peak intensity of G-band in the time-resolved Raman spectra (Figure 8a–c). When ETEM is used, the tube length is directly measured from the time-sequenced TEM images; then growth rate can be plotted as a function of tube length and time.¹¹⁹ This is a straightforward method. *In situ* electron energy loss spectroscopy (EELS) in ETEM can also offer the information on tube length from the intensity of the electron energy loss peak of carbon (Figure 8d,e).¹²⁴ These *in situ* studies show that the growth rate varies tube by tube and is often heterogeneous during the nucleation and expanding stages (Figure 8c,e).

It is obvious that ETEM presents much higher spatial and temporal resolution than *in situ* Raman and subsequently superior accuracy in the growth rate. There are additional factors that bring down the accuracy of the Raman method. One is that other carbon species may also contribute to the intensity of Raman bands; another is that band intensity also depends on the orientation of SWCNTs. Therefore, ETEM is preferred for the study of growth rate of SWCNTs.

2.1.2. Theoretical Models of Chirality Controlled Growth of SWCNTs. **Epitaxial Growth Model.** Predesigned chiral catalysts were broadly used to synthesize organic molecules with designed chiralities.¹²⁵ This strategy may also be used to control the chirality of SWCNTs. In 2006, Robertson et al. first proposed the epitaxial model, predicting the selective

growth of SWCNTs on solid catalysts.^{126,127} They found that the energy of different chiral caps relaxed on Ni(111) surfaces varies with the chirality (Figure 9). There are two hypotheses in

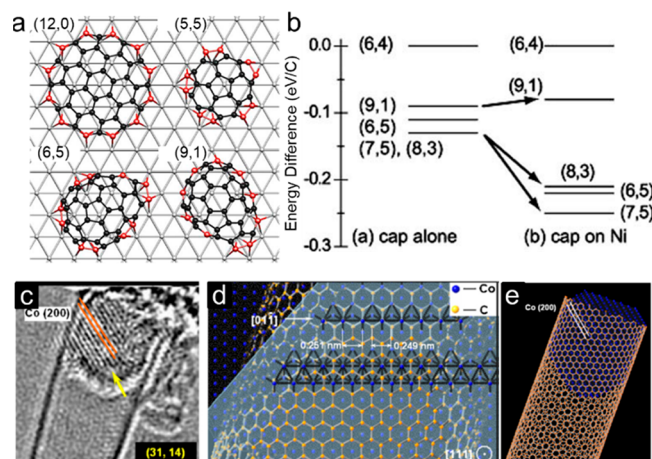


Figure 9. Epitaxial growth model. (a) Relaxed chiral caps on Ni(111). (b) Excess energies for chiral caps alone and caps on Ni(111) with the reference of the (6,4) cap. Reproduced with permission from ref 126. Copyright 2006 Elsevier. (c–e) TEM image (c) and schematic illustrations (d, e) showing the epitaxial relation between catalyst and SWCNTs. Reproduced with permission from ref 130. Copyright 2008 Elsevier.

the epitaxial growth model. First, the catalysts should keep their structure at high temperature in the CVD process. The strong interaction between catalyst and substrate can help to improve the crystallinity of the catalyst and thus limit carbon dissolution into the catalyst.¹²⁸ Second, the chirality of the cap should be retained when it converts to a tube. This model was used to explain the selective growth of SWCNTs including the selective growth of (8,4) SWCNTs with bimetallic $\text{Fe}_x\text{Ni}_{1-x}$ catalyst.^{51,129} Another epitaxial growth model proposed by Zhu et al. shows that a curved tube wall matches the lattice structure of a three-dimensional (3D) nanoparticle (Figure 9c–e).¹³⁰

Thermodynamics and Kinetics of SWCNT Chirality Control. Simulations have also indicated that the growth of SWCNTs is determined by both thermodynamic and kinetic processes.^{131–136} The interfacial energy between a tube and the catalyst is the dominant thermodynamic factor during the nucleation,^{127,137} whereas the carbon feeding, growth rate, carbon insertion into the tube, and chirality maintenance are part of the kinetic factors.^{87,136,138} For instance, it is believed that

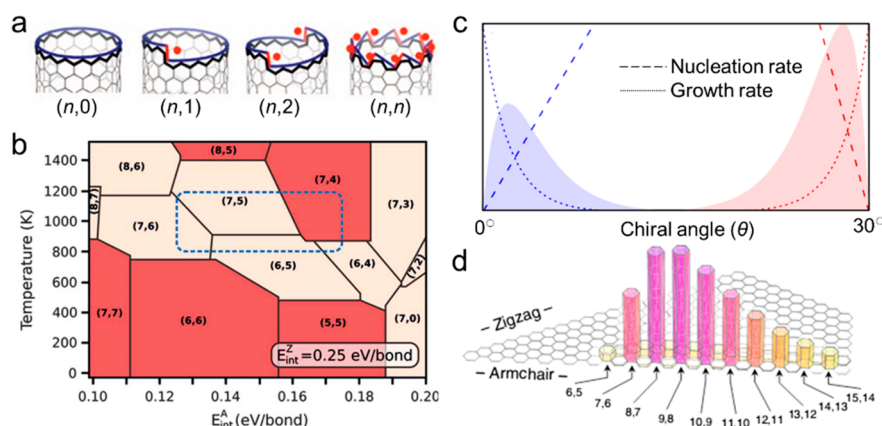


Figure 10. (a) Edge of a SWCNT viewed as a set of “cozy corners” (●) for C attachment. Reproduced with permission from ref 138. Copyright 2009 National Academy of Sciences of the USA. (b) Chirality phase diagram. Reproduced with permission from ref 143. Copyright 2018 American Association for the Advancement of Science. (c) Abundance distributions reflected as the product of nucleation and growth rate terms. (d) (n,m) distribution. Reproduced with permission from ref 135. Copyright 2014 Nature Publishing Group.

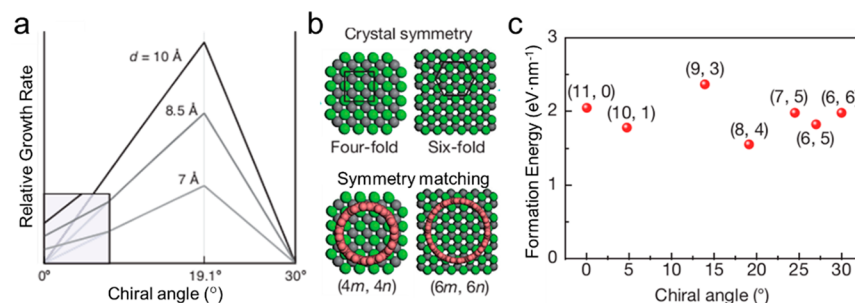


Figure 11. (a) Chiral angle as a function of growth rate of SWCNTs. Reproduced with permission from ref 135. Copyright 2014 Nature Publishing Group. (b) Atomic model of WC (100) with quasi-4-fold symmetry and Mo₂C (001) with 6-fold symmetry. (c) DFT calculations of the formation energy of tubes on the (100) plane of the WC. Reproduced with permission from ref 18. Copyright 2017 Nature Publishing Group.

C_2 dimer insertion during SWCNT growth presents a lower energy barrier.¹³⁹ The thermodynamic and kinetic factors work together to influence the (n,m) distributions of as-grown SWCNTs. From many approaches to chirality-enriched growth, SWCNTs with large chiral angles, such as (6,5), (7,5), and (7,6), are more often observed in various samples.¹³⁸ According to the DFT calculations based on the classical crystal screw theory, the growth rate of SWCNTs via a VLS mechanism is positively proportional to the chiral angle, and thus growing SWCNTs with larger chiral angle is favorable (Figure 10a).^{123,140,141} This is due to the bigger number of kinks in chiral nanotubes attached on molten catalysts acting as the active carbon insertion sites. Since the achiral zigzag and even armchair SWCNTs have no kinks in their end structures, their growth rates should be very low. Ding et al. further demonstrated that in the VLS mode, the chirality was determined kinetically by the sixth pentagon, which means that chirality cannot be controlled in the VLS mode.⁸⁷

Hedman et al. calculated the energetic stability of all (n,m) tube segments by DFT and compared it with the reported chiral abundances. The chiral selectivity was ascribed to thermodynamic control at the early stages of SWCNT nucleation.¹⁴² However, the energetic contribution of the interface with catalyst was not included in this study. Bichara et al. plotted the phase diagram of tube chirality with temperature and energy (Figure 10b).¹⁴³ They introduced the configuration entropy and interfacial energy of catalyst–SWCNT to explain the temperature evolution of the chirality selectivity. This chirality phase

diagram may guide the rational selection of catalysts and growth parameters.

Yakobson et al. proposed a model involving both thermodynamics and kinetics to explain the chirality-enriched growth of SWCNTs.¹³⁵ The (n,m) abundance ($A_{n,m}$) was computed by $A_{n,m} = N_{n,m}R_{n,m}$, where $N_{n,m}$ is the thermodynamic nucleation probability and $R_{n,m}$ is the kinetic growth rate of (n,m) SWCNTs. For solid catalysts, the resultant (n,m) abundance exhibited a peaked distribution near armchair or zigzag types, taking $N_{n,m} \approx e^{-\theta}$ and $R_{n,m} \approx \theta$. For liquid catalysts, the $N_{n,m}$ is weakly dependent on θ , resulting a broader abundance distribution. The favorable growth kinetics of SWCNTs with large chiral angle, such as (6,5), (7,5), and (7,6) are well interpreted by this model (Figure 10c, d).

For liquid catalysts, the abundance of ($2m,m$) tubes ($\theta = 19.1^\circ$) could be increased by improving the growth kinetics (Figure 11a). However, it is still difficult to achieve a high purity of ($2m,m$) with normal catalysts. Zhang et al. proposed the theory of crystal symmetry matching between the SWCNTs and the surface of solid carbide catalysts.¹⁸ They calculated formation energies of SWCNTs with different chiralities but similar diameters on WC (100) surface. Evidently, the (8,4) SWCNT and WC (100) plane have a 4-fold or quasi 4-fold symmetry, respectively. The symmetry match contributes to a structural match between the (8,4) tube and the WC nanoparticles and lowers the formation energy of (8,4) tubes with respect to tubes of other chosen chiralities (Figure 11b,c). They concluded that symmetry match is the intrinsic

thermodynamic factor for chirality-selective growth of SWCNTs. Wang and Ding further proposed a mechanism to understand the origin of chiral SWCNTs grown on solid catalysts. The mechanism has to satisfy three criteria: (i) thermodynamic selection of SWCNTs that possesses the same structural symmetry as that of the catalyst surface; (ii) kinetic elimination of achiral SWCNTs with extremely low growth rates; (iii) rough control over the catalyst particle size leading to SWCNTs with only one or a few dominant chiralities.¹⁴⁴

Catalysts with Unique Structure. Li et al.⁶⁴ proposed that a catalyst with stable and unique structure is critical for chirality-specific growth of SWCNTs by offering selective structural match between catalysts and nanotubes. Tungsten-based intermetallic compounds have lower structural symmetry and inhomogeneity of each crystal plane, which can be used to recognize a specific (n,m) SWCNT. There is a perfect structural match between a (12,6) tube and the (0012) plane of Co_7W_6 (space group $R\bar{3}m$) revealed by DFT simulation. Face-centered-cubic (fcc) Co catalysts with higher crystal symmetry (space group $Fm\bar{3}m$), however, show very low differentiation among SWCNTs with various chiralities. Better structural matching between a SWCNT and a crystal plane of the catalyst presents a lower formation energy for the SWCNT. So the chirality selectivity possesses an energetic ascendancy (Figure 12).^{15,64} This model was further proven to be valid for (16,0) and (14,4) SWCNTs grown around the Co_7W_6 (116) and (1010) planes, respectively.^{59,145}

2.2. Diameter- and Conductivity-Controlled Growth of SWCNTs

2.2.1. Diameter-Controlled Growth of SWCNTs.

Diameter control is the beginning step toward chirality controlled growth of SWCNTs. It was found that both catalyst^{56,68} and growth conditions^{146–148} affect the size of the tubes formed. Modulating the size of the catalyst is most often used to regulate the diameter of SWCNTs.^{68,149–152} There are mainly two important issues in controlling the size of catalysts. One is to synthesize catalyst nanoparticles with uniform size. The other is to prevent catalyst aggregation and ripening. Here we discuss the common approaches toward these two aspects.

Synthesis of Uniform Catalyst Nanoparticles. Solution-based pathways are most often used in synthesis of uniform nanoparticles. A key to achieve this target is the rational choice of capping agents. Capping agents absorbing on a nanoparticle surface can prevent overgrowth and aggregation of nanoparticles. Li et al. reported a feasible strategy to prepare monodispersed Fe–Mo nanoparticles by thermally decomposing the iron and molybdenum carbonyl complexes under the protection of long-chain amine and carboxylic acid (Figure 13a).¹⁴⁹ This method also showed its success in obtaining nearly monodispersed Fe¹⁵⁰ and Rh¹⁵³ nanoparticles. These uniform nanoparticles are effective catalysts for diameter-controlled growth of SWCNTs.

It has been demonstrated that protein cage apoferritin with Fe,⁸⁰ Co,¹⁵⁸ or Au loaded¹⁵⁹ is a promising precursor to prepare discrete catalyst nanoparticles for the growth of SWCNTs. This was first proposed by Dai et al.⁸⁰ The empty core of an apoferritin is used as a confined space to house iron species of restricted numbers. By depositing these iron-loaded ferritins on substrates, discrete catalytic nanoparticles with uniform sizes were prepared (Figure 13b).^{80,160} Polymers including dendrimers¹⁵⁴ and block copolymers^{155,161} with functional groups in the repeat units can also be employed as nanoreactors to trap a

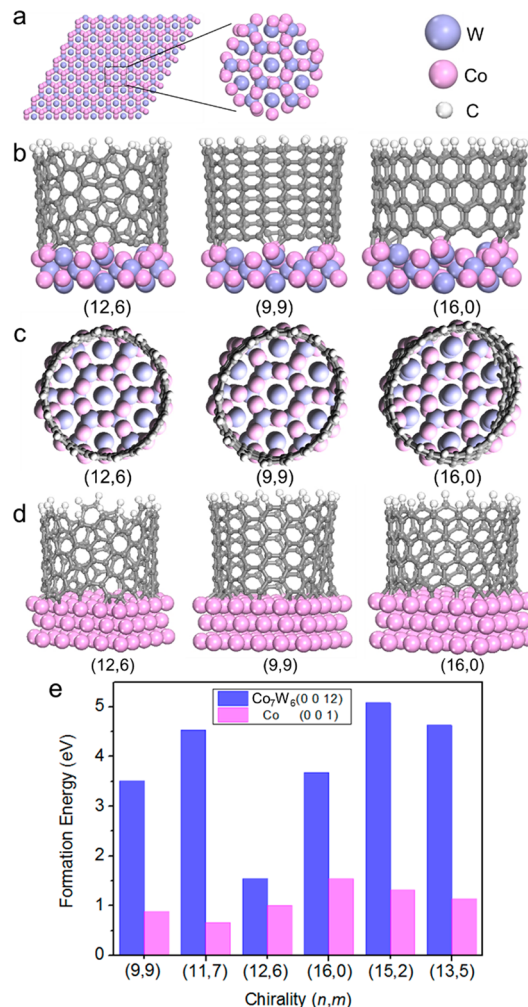


Figure 12. (a) Atomic model of Co_7W_6 (0012) plane. (b, c) Side views (b) and top views (c) of interfaces between SWCNTs and Co_7W_6 (0012) plane. (d) Side views of interfaces between SWCNTs and fcc Co(001) plane. Reproduced with permission from ref 15. Copyright 2014 Nature Publishing Group. (e) Formation energy of SWCNTs around Co_7W_6 (0012) and fcc-Co(001). Reproduced from ref 64. Copyright 2016 American Chemical Society.

fixed number of metal ions. For example, Dai et al. used dendrimer macromolecules with coordinative functional groups as hosts to trap metal ions. The resultant SWCNTs display similar diameter distribution of 1–2 nm to those discrete catalyst nanoparticles (Figure 13b).¹⁵⁴ These results show that engineering the catalyst size is effective for controlling the tube diameter.

Polyoxometalates are a family of molecular clusters composed of oxygen and a fixed number of metal atoms and are often denoted with only the metal atoms (e.g., $\{\text{M}_x\}$) for convenience.¹⁶² The nanoscaled clusters such as $\{\text{Mo}_{84}\text{Fe}_{30}\}$,^{151,163–165} $\{\text{W}_{39}\text{Fe}_6\}$,¹⁶⁶ and $\{\text{Mo}_{132}\}$ ¹⁶⁷ are superior precursors to prepare nanoparticles with uniform size for controlling SWCNT diameter. The $\{\text{Mo}_{84}\text{Fe}_{30}\}$ nanocluster was first demonstrated by Liu et al. as precursor to prepare nanoparticles with controlled size.¹⁵¹ The resulting SWCNTs present a narrow diameter distribution of 1.0 ± 0.18 nm (Figure 13c). Li et al. prepared well-aligned sub-nanometer SWCNTs (0.76 ± 0.16 nm) on ST-cut quartz, attributed to the uniform catalyst nanoparticles formed from the $\{\text{Mo}_{84}\text{Fe}_{30}\}$ cluster and

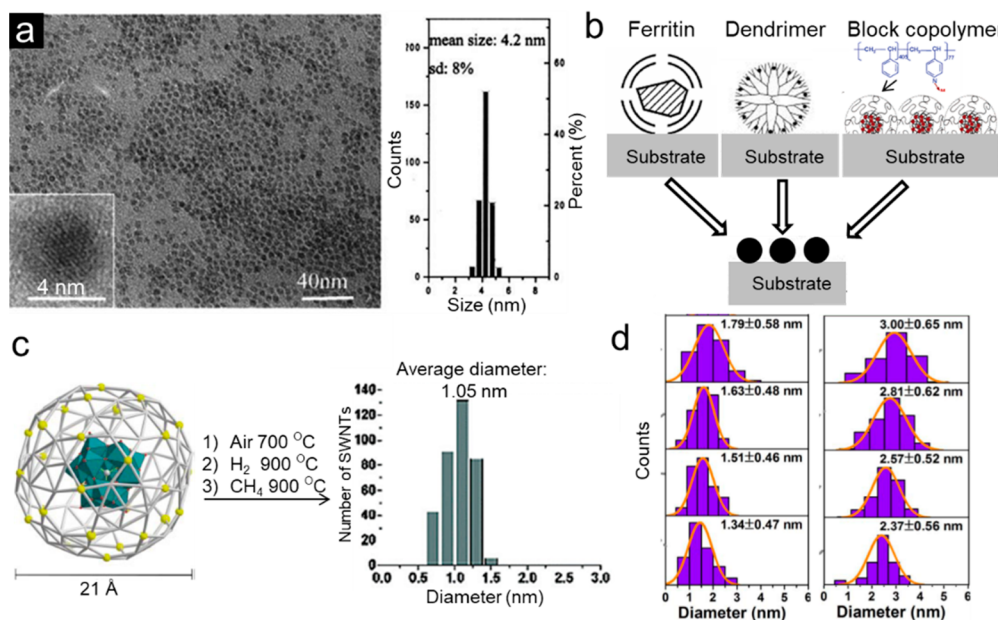


Figure 13. (a) TEM image of FeMo nanoparticles synthesized with protective agent and corresponding histogram of the nanoparticle sizes. Reproduced from ref 149. Copyright 2001 American Chemical Society. (b) Schematic process for SWCNT synthesis by CVD on catalytic nanoparticles derived from ferritin, polyamidoamine dendrimer template, and block copolymer micelle. Reproduced from ref 80, ref 154, and ref 155. Copyright 2001, 2002, and 2006 American Chemical Society. (c) The structure of $\{Mo_{132}\}$ cluster and diameter distribution of the SWCNTs grown on FeMo catalyst. Reproduced with permission from ref 156. Copyright 2000 Wiley, and ref 151, Copyright 2002 American Chemical Society. (d) Diameter distribution histograms of SWCNT forest grown with catalyst nanoparticles by arc-plasma deposition. Reproduced with permission from ref 157. Copyright 2014 Nature Publishing Group.

the confinement effect of the quartz substrates.¹⁶³ However, it is difficult to obtain uniform Mo containing nanoparticles, because MoO₃ is easily sublimated during annealing in air at temperatures higher than 700 °C.^{163,165} Based on this consideration, Zhang et al. treated the $\{Mo_{132}\}$ cluster at a lower temperature (300 °C) to inhibit the formation of volatile MoO₃ and then obtained uniform Mo₂C nanoparticles after introducing the carbon feedstocks; 85% of the resultant nanotubes present a diameter of 1.0–1.3 nm.¹⁶⁷ Compared with the Mo-containing clusters, W based nanocatalysts may be a better choice since WO₃ is more stable.¹⁵⁶

However, normally a polyoxometalate cluster does not contain sufficient metal atoms to form a 1–3 nm catalyst nanoparticle. Thus, a small degree of molecular aggregation is essential to achieve the critical size necessary for catalyzing tube growth.¹⁶⁵ However, the controlled aggregation of clusters is still challenging.

Deposition of Catalyst Nanoparticles on Substrates. Uniform nanoparticles are normally deposited on certain catalyst supports to further grow SWCNTs. The deposition may rely on electrostatic,¹⁵¹ hydrophobic,¹⁶⁸ and coordination interactions between the nanoparticles and the catalyst supports.¹⁶⁹ There are still other approaches to directly deposit catalyst nanoparticles with narrow size distribution on flat substrates, such as sputtering,¹⁷⁰ arc plasma deposition,¹⁵⁷ dip coating,¹⁷¹ and electron beam deposition.¹⁷² For example, Futaba et al. precisely modulated the catalyst size and density by using arc plasma deposition and realized the controlled growth of a SWCNT forest with a diameter resolution of 1 Å (Figure 13d).¹⁵⁷

Preventing Aggregation and Ripening of Catalysts. When a dispersion of catalyst nanoparticles is put on supports, the particles tend to aggregate and form random agglomerates. Therefore, preventing the aggregation of catalysts is also

important in controlling the size of catalysts and consequently the tube diameter. Surface modification of the substrates or the catalysts or both^{151,168,173} can enhance the interaction between the catalyst and substrate or support,^{174,175} stabilizing the catalysts. Liu et al. modified a silicon dioxide surface using 3-aminopropyltriethoxysilane. The modified surface terminated by amine groups becomes positively charged, so the negatively charged catalyst nanoparticles were anchored and uniformly distributed on these substrates.¹⁵¹

Increasing the interparticle distance can reduce the chance of aggregation.¹⁷⁶ Maekawa et al. grew an ultradense triple-walled CNT (TWCNT) forest using monodisperse hollow Fe₃O₄ nanoparticles as catalyst precursors (Figure 14a–c). The monodisperse nanoparticles shrank on account of the hollowness, while the phase transitioned from iron oxide to pure iron, and consequently the interparticle distance increased avoiding nanoparticle aggregation at high temperature. The resultant discrete Fe nanoparticles catalyzed the growth of TWCNTs with uniform diameter.¹⁷⁶ Cheng's group developed a kind of Co nanoparticle partially capped by carbon as a catalyst to grow SWCNTs with controlled diameter. This was realized by reducing (Co(CN)₆)₃ confined in a self-assembled copolymer. The as-formed carbon partially capped the catalyst, acting as a protective shell to inhibit the aggregation of the Co nanoparticles (Figure 14d–f).¹⁷³

During the reduction process, Ostwald ripening often happens, decreasing the uniformity of the catalyst nanoparticles. The rational selection of catalyst supports is one of the key points in suppressing Ostwald ripening as well as aggregation. Various catalyst supports, including mesoporous materials (e.g., MCM-41,^{177–183} TUD-1,⁵³ zeolite¹⁸⁴), metal,^{175,185,186} and high surface area oxides (e.g., MgO, SiO₂, Al₂O₃),^{49,75,187} were widely used because of their strong interaction with the catalysts. Pfefferle et al. systematically studied metal nanoparticles of

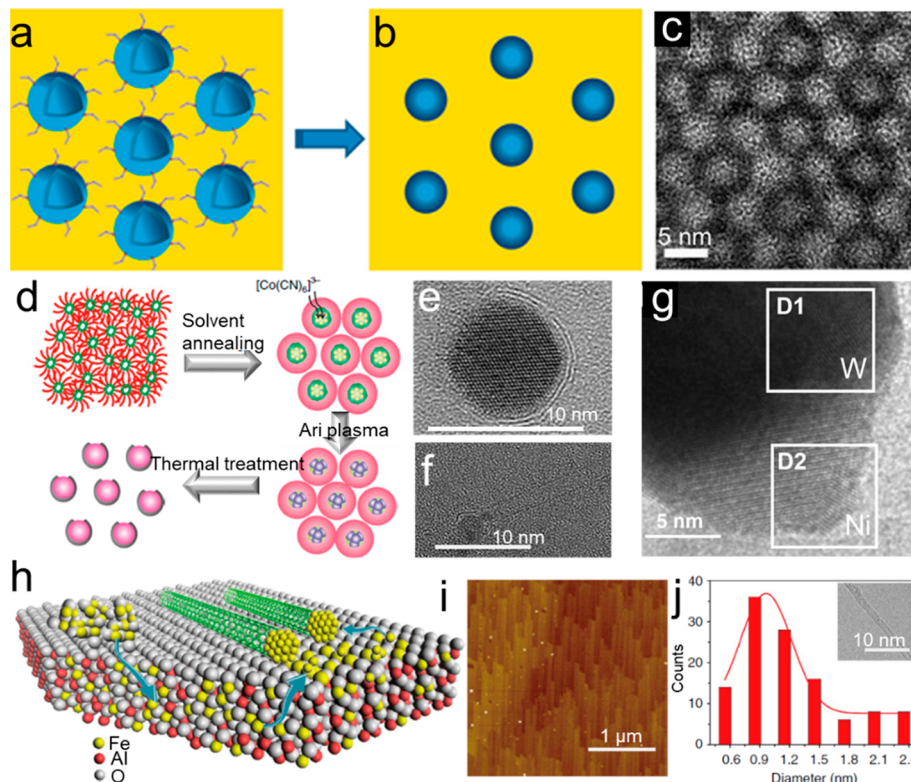


Figure 14. (a–c) Schematic diagram of densely packed hollow nanoparticles with ligand attached to the particles (a) and suppression of agglomeration of nanoparticles owing to the shrinkage of the hollow nanoparticles (b); TEM image of uniform hollow Fe_3O_4 nanoparticles (c). Reproduced from ref 176. Copyright 2014 American Chemical Society. (d–f) Formation of carbon-coated Co nanoparticles (d), HRTEM image of Co nanoparticle with acorn-like structure (e), and SWCNT grown from catalyst seed (f). Reproduced with permission from ref 173. Copyright 2016 Nature Publishing Group. (g) HRTEM image of the freshly reduced W supported Ni catalyst. Reproduced with permission from ref 175. Copyright 2017 Elsevier. (h–j) Schematic of the growth of high-density horizontal SWCNT arrays by reducing Fe buried into the substrate to suppress aggregation (h), atomic force microscopy (AFM) image of substrate after reduction in hydrogen (i), diameter distribution of SWCNTs (inset, HRTEM image of a SWCNT) (j). Reproduced with permission from ref 174. Copyright 2015 Nature Publishing Group.

Co ,¹⁷⁷ $\text{Co}-\text{Mn}$,¹⁸⁰ $\text{Co}-\text{Cr}$,¹⁸¹ $\text{Co}-\text{Mo}$,¹⁸² incorporated on MCM-41 and realized the growth of SWCNTs with narrow diameter distribution. The metal nanoparticles confined in nanosized channels of MCM-41 present a uniform and small size. However, the nanosized channels of mesoporous materials might be destroyed at temperatures higher than $700\text{ }^\circ\text{C}$. Li et al.¹⁷⁵ reported Ni nanoparticles that are anchored by W/WO_x ; therefore, the Ni nanoparticles were stabilized with uniform sizes (Figure 14g). Using these stabilized Ni catalysts, they achieved the growth of SWCNTs with a controlled diameter of $1.3 \pm 0.1\text{ nm}$ under a broad window of temperature ($850\text{--}950\text{ }^\circ\text{C}$) and carbon feeding conditions.¹⁷⁵ Zhang et al. designed a special annealing process at a temperature of $1100\text{ }^\circ\text{C}$ that buries Fe_2O_3 in the sapphire substrate to reduce catalyst aggregation.¹⁷⁴ Since Fe_2O_3 has a similar crystal structure to sapphire, Al^{3+} can be partially replaced by Fe^{3+} in the sapphire due to the entropy effect. As shown in Figure 14h–j, Fe^{3+} ions were reduced by H_2 and released from the substrate, forming the active catalyst on the surface to grow SWCNTs. A strong interaction with the substrate can suppress the aggregation of Fe catalysts on sapphire.

Size Correlation between Catalysts and SWCNTs. It is often observed that the diameter distribution of SWCNTs depends on the size distribution of the catalyst nanoparticles. Several statistical TEM/AFM measurements addressed the nanoparticle–nanotube size relation. The ratio between the diameter of a tube and that of its seeding catalyst (d_t/d_{NP}) was found to be

approximately 1:1^{80,188} or larger (Figure 15).^{153,159,189–192} However, it is hard to obtain catalysts with identical size and

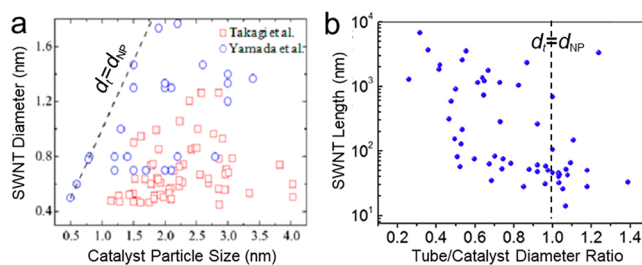


Figure 15. (a) Correlation between size of Au catalysts and that of SWCNTs growing on it; rectangles and circles represent data from ref 159 and ref 190, respectively. Reproduced with permission from ref 193. Copyright 2014 Yoshikazu Homma. (b) SWCNT length plots as a function of tube/particle diameter ratio, which are measured by TEM. Reproduced with permission from ref 189. Copyright 2017 Elsevier.

to maintain the size during the CVD process. The aggregation, evaporation, and Ostwald ripening of the catalysts during the CVD process definitely affect the size of the catalyst nanoparticles, unavoidably introducing more uncertainty to the correlation between the sizes of catalysts and SWCNTs.

Another important issue is the growth mode of nanotubes on nanoparticles, that is, the so-called tangential and perpendicular growth modes shown in Figure 5e,f,⁸² which have been

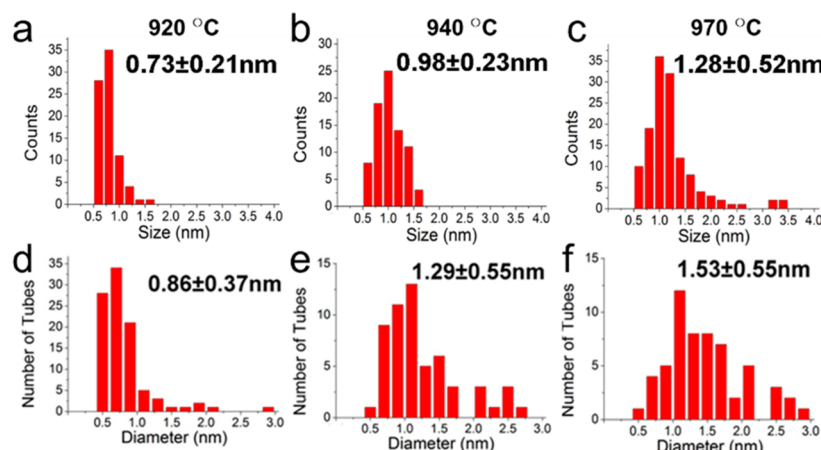


Figure 16. Size distributions of molecular Fe–Mo catalyst prepared at 920 °C, 940 °C, and 970 °C (a–c) and corresponding diameter distributions of as-grown SWCNTs (d–f). Reproduced with permission from ref 163. Copyright 2013 Springer.

discussed in section 2.1.1. Growing tubes in a perpendicular mode decouples the size correlation between tubes and nanoparticles. Tangential mode results in SWCNTs with similar diameter to the catalysts. However, as discussed above, it is almost impossible to obtain nanoparticles with identical size. Furthermore, it was also reported that the tube diameter may not be fully related to the catalyst size.¹⁵³ From all of the above issues, though the SWCNT diameter can be controlled to some extent, the precise control of tube diameter is hard to realize by catalyst size engineering.

Carbon feeding conditions also affect the diameter distribution of SWCNTs. By tuning the ethane concentration from 140 to 14400 ppm, Lu and Liu found that the average tube diameter shifts from 0.91 to 1.78 nm using the same catalysts with a broad size distribution.¹⁴⁷ They believed that catalyst nanoparticles of different sizes require their own optimized carbon feeding conditions to nucleate nanotubes. For a given CVD condition, carbon feed is insufficient for larger particles to nucleate tubes, while carbon is excessive in smaller particles and thus catalysts are encapsulated and poisoned. Only a fraction of particles with a suitable size can nucleate SWCNTs. This hypothesis of suitable nucleation conditions has been verified by additional experiments. Li et al. carefully compared the size of catalysts and SWCNTs and found that the size distribution of catalysts is narrower than that of SWCNTs (Figure 16).¹⁶³ This was caused by the selection of active nanoparticles with certain size by the carbon feeding conditions.

In summary, the correlation among the tube diameter, the catalyst size, and the carbon feeding conditions is important for diameter control. A rational choice and design of the catalysts, supports, and growth conditions are necessary to improve the uniformity of the diameters of the resultant SWCNTs.

2.2.2. Selective Growth of Semiconducting SWCNTs.

Direct growth of s-SWCNTs is another important step in the controlled synthesis of nanotubes. Since m-SWCNTs possess DOS near the Fermi level, they present lower ionization energy and higher reactivity than s-SWCNTs. Therefore, the most widely used strategy to obtain s-SWCNTs is selectively suppressing or etching m-SWCNTs during CVD growth. Great efforts have been devoted to creating a suitable reactive environment to achieve this goal. Radicals such as $\cdot\text{H}$, $\cdot\text{OH}$, and $\cdot\text{CH}_x$ induced by water,¹⁹⁴ methanol,^{195,196} isopropanol,¹⁹⁷ oxygen,^{198–200} plasma,²⁰¹ and UV light²⁰² have been proven effective in reacting with m-SWCNTs.

An early pioneering work was the direct growth of aligned s-SWCNTs with diameters of 1.55 to 1.78 nm on quartz wafers by addition of a suitable amount of methanol to ethanol feedstocks.¹⁹⁵ More than 95% of the SWCNTs were semiconducting as confirmed by Raman measurements and the transport property of FETs (Figure 17a,b). There are two possible factors working synergistically in this process: the strong interaction between the nanotube and the lattice of quartz restrains the distribution of tube diameter; $\cdot\text{OH}$ radicals decomposed from methanol react with m-SWCNTs. Later on, it was demonstrated that the $\cdot\text{OH}$ radicals not only etch m-SWCNTs but also destroy the small diameter tubes,¹⁹⁶ further verifying the importance of the uniformity of the diameters for higher selectivity toward s-SWCNTs. Moreover, there is a competition between growth rate and etching rate for s- and m-SWCNTs. Only both etching rate of m-SWCNTs being higher than that of s-SWCNTs and the etching rate of m-SWCNTs being higher than the growth rate of m-SWCNTs can ensure high-selectivity toward s-SWCNTs (Figure 17e).¹⁹⁴ Other techniques such as plasma²⁰¹ and UV irradiation assisted CVD²⁰² were also used to selectively produce s-SWCNTs. Zhang et al. proposed to prepare s-SWCNTs with UV assisted CVD. They attributed the enrichment of s-SWCNTs to the reaction between radicals and m-SWCNTs during the initial nucleation of m-SWCNTs (Figure 17f,g).²⁰² In addition to oxidative etchants, Liu and Cheng and co-workers also introduced H_2 as a reductive etchant to selectively remove m-SWCNTs to prepare s-SWCNTs (Figure 17h).^{173,203}

In most of the approaches, the selective growth window is very narrow. This makes the selectivity fluctuate trial by trial. One of the important reasons might be the sensitivity of etchant concentration due to their instability. Li et al.¹⁹⁹ developed a reliable and repeatable method to grow s-SWCNTs with high selectivity. They used CeO_2 as catalyst support. CeO_2 can offer active oxygen due to the transformation of Ce^{IV} to Ce^{III} .²⁰⁵ Therefore, CeO_2 is capable of providing a stable and proper oxidative environment for the *in situ* etching of m-SWCNTs during the tube nucleation stage; thus s-SWCNTs of high purity are obtained (Figure 17c,d).

Other than the difference in reactivity between s- and m-SWCNTs, modulating the barrier of nucleation was also demonstrated. Jiang et al. introduced extra electrons to the catalyst particles, which significantly amplified the difference in renucleation barrier between m- and s-SWCNTs, so that

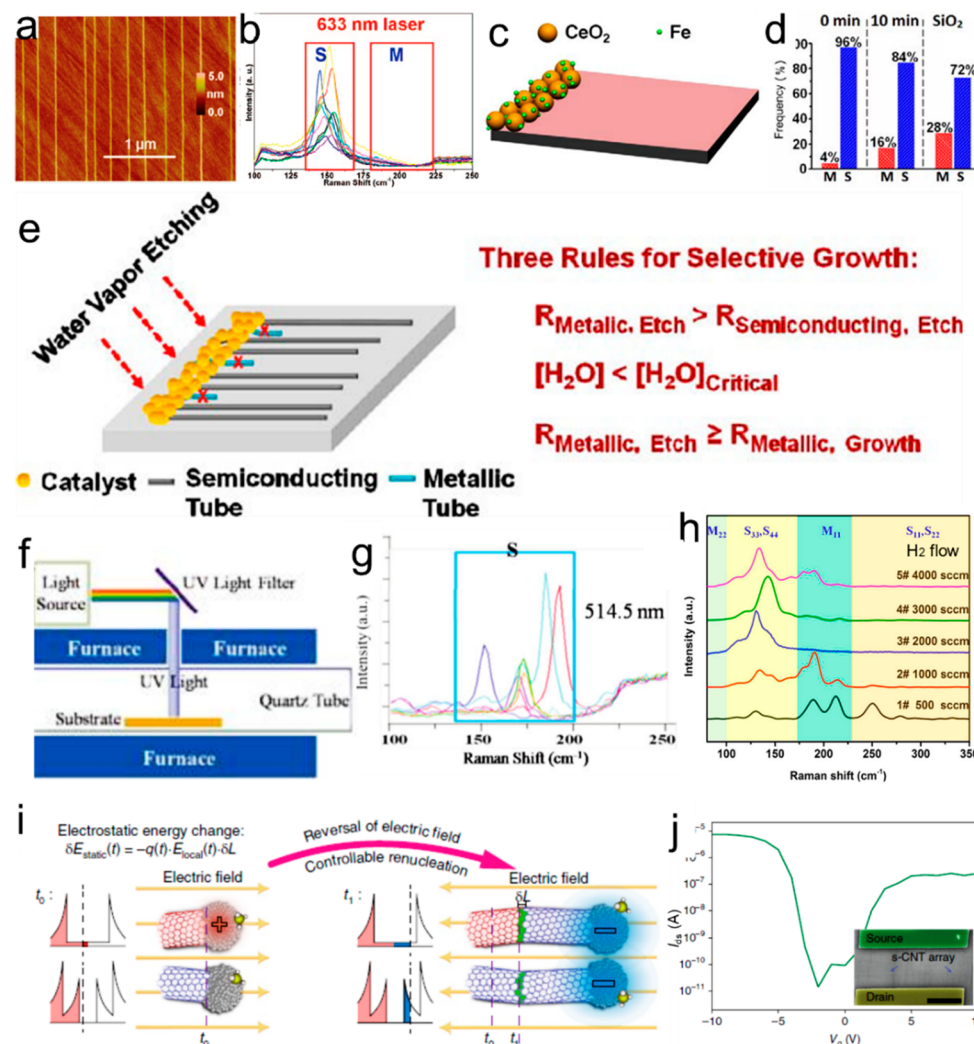


Figure 17. (a, b) AFM (a) and Raman (b) measurements of SWCNTs grown by using ethanol mixed with methanol as carbon sources. Reproduced from ref 195. Copyright 2009 American Chemical Society. (c, d) Scheme of selective growth of s-SWCNTs by using Fe supported on oxidative CeO_2 support (c). Statistics of m-/s-SWCNTs by using Fe/ CeO_2 reduced with H_2 for 0 and 10 min. The SWCNTs grown from Fe/ SiO_2 were used as reference (d). Reproduced from ref 199. Copyright 2014 American Chemical Society. (e) Scheme of selective growth of s-SWCNTs by using H_2O vapor as etchant. Reproduced from ref 194. Copyright 2012 American Chemical Society. (f) UV light-assisted CVD reactors used for the synthesis of s-SWCNTs (f) and Raman spectra (g). Reproduced from ref 202. Copyright 2009 American Chemical Society. (h) Raman spectra of SWCNTs grown under different flow of H_2 . Reproduced from ref 203. Copyright 2013 American Chemical Society. (i) Twisting the chirality of SWCNTs by reversing the electric field to grow s-SWCNTs. (j) $I-V$ curve of the s-SWCNT-array FET. Reproduced with permission from ref 204. Copyright 2018 Nature Publishing Group.

metallic tubes were twisted into semiconducting ones when incorporating new carbon (Figure 17i).²⁰⁴ Nearly defect-free s-SWCNT arrays with purity of 99.6% (estimated from FET measurements) to 99.9% (estimated from scanning electron microscopy (SEM)) were directly achieved as a result of electro-renucleation (Figure 17c,d).²⁰⁴

There are also reports on using certain catalysts to directly grow s-SWCNTs.^{206–209} However, the mechanism for the selective formation of s-SWCNTs, which is critical for further improving the purity, still remains unclear.

As discussed above, the etching reaction is both metallic and small diameter selective. This brings complexity in the preferential growth of s-SWCNTs with the etching strategy. Additionally, these etching strategies severely reduced the yield of nanotubes, resulting in sparse SWCNTs on substrates. Well-aligned s-SWCNT arrays with high densities are considered the ideal materials for nanoelectronics, especially for high-perfor-

mance integrated circuits. Therefore, direct synthesis of s-SWCNT arrays with both high purity and high density are highly demanded for advanced applications.²¹⁰ By multiple growth procedures, the density of s-SWCNTs was remarkably improved to $\sim 10 \text{ tubes} \cdot \mu\text{m}^{-1}$.^{211,212} Using water vapor as etchant has additional advantages. For instance, it can etch away tangled tubes randomly grown near the catalyst region to improve the growth efficiency of aligned tubes and thus the density of the tube arrays. It can also remove amorphous carbon on the tubes to improve the alignment of the arrays.²¹²

Zhang et al. designed a so-called Trojan catalyst to grow extremely dense SWCNT arrays.²¹³ Fe and Mo atoms were incorporated into the sapphire substrates, and iron nanoparticles continuously formed on the surface of the substrates during the CVD process to catalyze the tube growth. With this strategy, they achieved an ultrahigh density of $160 \text{ tubes} \cdot \mu\text{m}^{-1}$, which is the highest reported density by CVD growth. The tube density

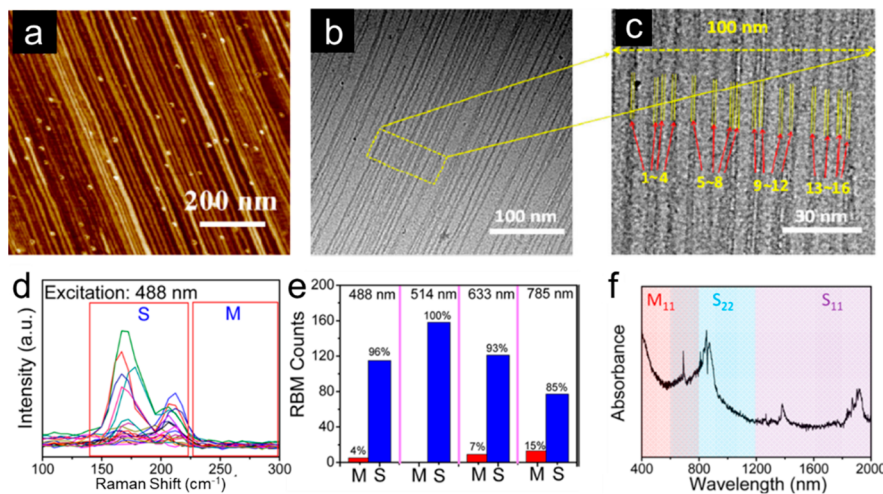


Figure 18. (a–c) AFM image of as grown SWCNT arrays with ultrahigh density (a), TEM images of transferred SWCNTs (b, c). Reproduced with permission from ref 213. Copyright 2015 Springer. (d–f) Raman RBM spectra with 488 nm excitation (d), statistics of m- and s-SWCNTs based on the multiwavelength laser Raman measurements (e), and UV–vis–NIR spectrum after background subtraction (f). Reproduced from ref 207. Copyright 2016 American Chemical Society.

was derived from TEM images. But the uniformity needs to be further examined (Figure 18a–c). The addition of Mo can stabilize the Trojan catalyst (Fe) and thus improve the efficiency of the catalysts. They further modulated the growth conditions by using ethanol and methane as mixed carbon sources and obtained arrays containing over 91% s-SWCNTs with a density over $100 \text{ tubes} \cdot \mu\text{m}^{-1}$ (Figure 18d–f).²⁰⁷ Though some progress has been made in increasing both the density and purity of the SWCNT arrays, the target of density higher than $125 \text{ tubes} \cdot \mu\text{m}^{-1}$ and purity of s-SWCNTs over 99.9999% required for high performance integrated circuits²¹⁰ is still far beyond the present capabilities of synthesis. Some revolutionary strategies may be needed to reach the target.

2.3. Chirality Controlled Growth of SWCNTs from Catalysts

2.3.1. Catalyst Design. Bimetallic Catalysts. The prologue of selective growth of chirality-enriched SWCNTs started from 2003, when Resasco et al.⁴⁸ demonstrated the growth of SWCNTs enriched with (6,5)/(7,5) chirality on bimetallic CoMo catalysts. By further optimizing the synthesis process, they improved the selectivity toward (6,5) SWCNTs to 55% with silica-supported CoMo catalysts. The mechanism proposed is that the MoO_x disperses and stabilizes metallic cobalt to form uniform catalyst nanoparticles of small diameter (Figure 19a).^{48,49} This mechanism was verified by the observation that the average tube diameter decreased from 2 to 1.4 nm when the concentration of Mo was increased or that of Co was decreased in the catalysts.²¹⁴ Several ETEM studies on $\text{Co}_x\text{Mo}_{1-x}/\text{MgO}$ catalyst showed that only Co species nucleated SWCNTs and Mo was not found within the catalyst nanoparticles.^{103,110} The enrichment of (6,5), (7,5), and (7,6) tubes was also obtained with bimetallic CoMn,¹⁸⁰ CoCr,¹⁸¹ FeRu (Figure 19b),⁵⁰ FeCo,^{215,216} FeCr,²¹⁷ FeMn,²¹⁸ FeCu,^{52,219} and CoCu¹⁸⁶ catalysts. There are many discussions on the roles of each component in the bimetallic catalysts. In the study of FeCu catalysts, it was found that the aggregation of Fe nanoparticles was effectively suppressed owing to the strong interaction between the binary components. ETEM study showed that the Cu phase anchored the Fe nanocrystals and inhibited their sintering. The small Fe nanoparticles were only observed on the Cu particles. Thus, the Cu-stabilized Fe nanoparticles of small

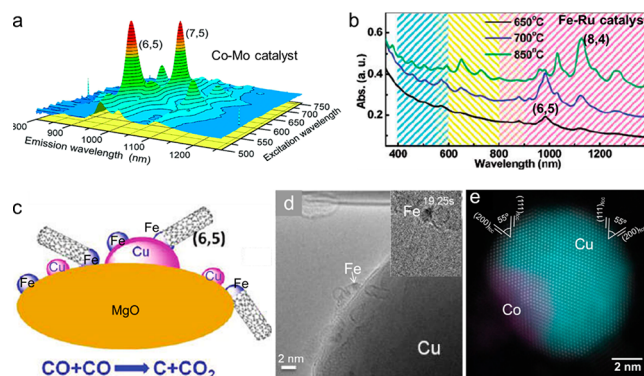


Figure 19. (a) Normalized fluorescence intensities for the Co–Mo catalyzed SWCNTs. Reproduced from ref 48. Copyright 2003 American Chemical Society. (b) UV–vis–NIR spectra of SWCNTs grown from FeRu catalyst at different temperatures. Reproduced from ref 50. Copyright 2007 American Chemical Society. (c, d) Scheme of SWCNT growth on the FeCu/MgO catalyst (c) and TEM image (d). Inset, ETEM image of a SWCNT nucleating from Cu-supported Fe nanoparticle. Reproduced from ref 185. Copyright 2012 American Chemical Society. (e) Energy dispersive X-ray scanning TEM image showing Co-anchored by Cu. Reproduced with permission from ref 186. Copyright 2015 Royal Society of Chemistry.

diameters catalyzed the enriched growth of (6,5) tubes (Figure 19c, d).¹⁸⁵ A similar mechanism was also evidenced in bimetallic CoCu catalysts with Co nanoparticles anchored on Cu (Figure 19e).¹⁸⁶

In addition to supported bimetallic catalysts, alloying is also an effective approach to improve the catalyst stability and ensure a narrower chirality distribution of the resultant SWCNTs. Chiang et al. found that the chirality distribution of SWCNTs varies with the compositional ratio of Ni/Fe in $\text{Ni}_x\text{Fe}_{1-x}$ and (8,4) SWCNTs were enriched with $\text{Ni}_{0.27}\text{Fe}_{0.73}$ catalysts (Figure 20a,c).⁵¹ The lattice expansion of Ni nanocrystals induced by the incorporation of Fe was observed from XRD, which is assumed to be responsible for the evolution of chirality distribution (Figure 20c). DFT simulations further confirmed that the cap of (8,4) SWCNTa is more stable on the surface of $\text{Ni}_{0.27}\text{Fe}_{0.73}$ crystal with an epitaxial relationship, which is in

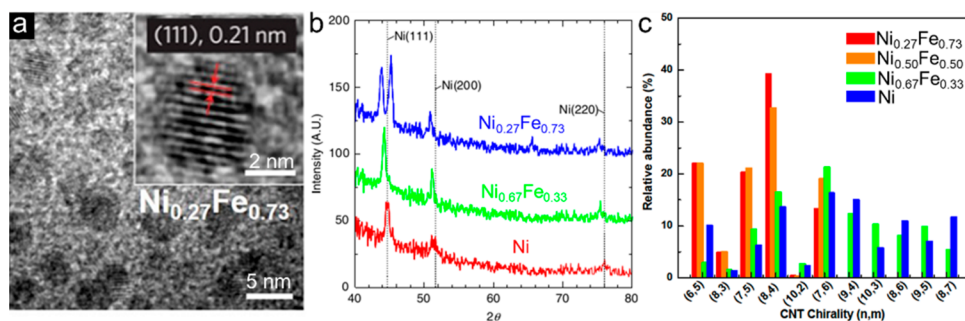


Figure 20. (a) HRTEM image of $\text{Ni}_{0.27}\text{Fe}_{0.73}$ nanoparticles. Reproduced with permission from ref 51. Copyright 2009 Nature Publishing Group. (b) XRD patterns of $\text{Ni}_x\text{Fe}_{1-x}$. (c) Relative (n,m) abundances of SWCNTs grown on $\text{Ni}_x\text{Fe}_{1-x}$ catalysts. Reproduced with permission from ref 129. Copyright 2012 Elsevier.

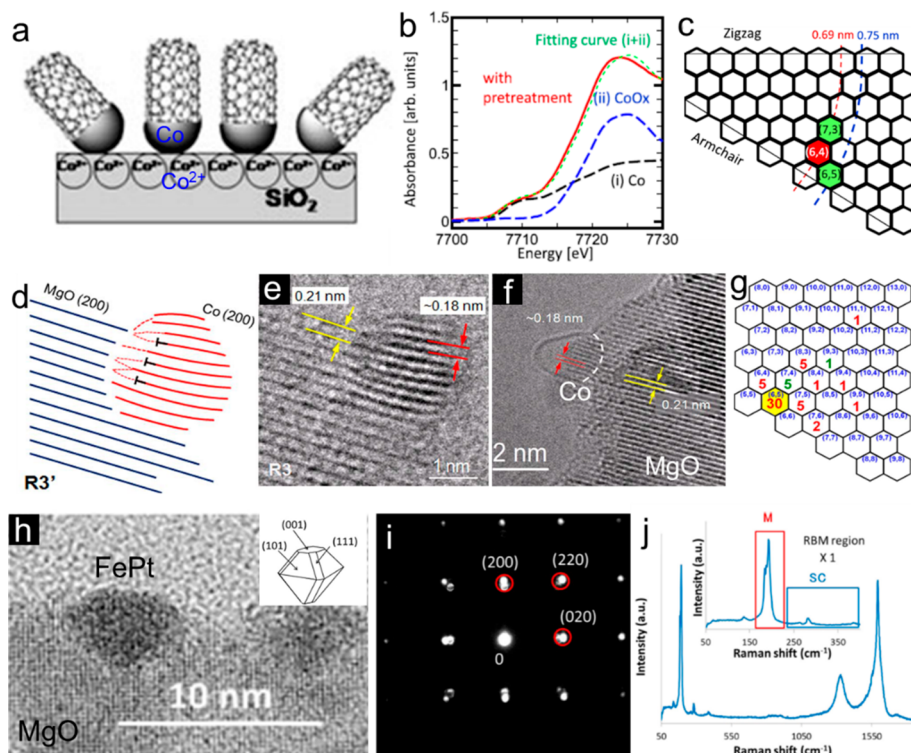


Figure 21. (a) Scheme showing the growth SWCNTs from partially reduced $\text{Co}/\text{Co}^{2+}/\text{SiO}_2$ catalyst. Reproduced with permission from ref 223. Copyright 2011 Royal Society of Chemistry. (b, c) Synchrotron X-ray absorption near-edge spectroscopy of partially oxidized Co catalyst (b) and corresponding chirality map of as-grown SWCNTs (c). Reproduced with permission from ref 224. Copyright 2017 Nature Publishing Group. (d–g) Scheme showing the lattice mismatch between Co and MgO (d), ETEM image showing epitaxial structure between Co and MgO (e), carbon cap growing on Co/MgO (f), and ED result of SWCNTs (g). Reproduced with permission from ref 75. Copyright 2013 Nature Publishing Group. (h–j) Cross-sectional TEM image (h) and corresponding selected area electron diffraction pattern (i) showing the epitaxial relation between MgO substrate and FePt catalyst; Raman spectra (excitation 633 nm) of as-grown SWCNTs (j). Reproduced with permission from ref 229. Copyright 2015 Elsevier.

agreement with previous experimental results.¹²⁹ The formation of alloys was also speculated to be responsible for the controlled growth of SWCNTs enriched with (6,5) chirality on other bimetallic catalysts such as Fe–Ru⁵⁰ and Co–Pt.⁵⁴ However, DFT-based MD simulations by Qiu and Ding showed that the CNT tends to preferentially bond to the more active element in an alloy catalyst during the nucleation. This induces phase segregation in alloy nanoparticles.²²⁰ Maruyama et al. identified an intermediate phase of $\text{Co}_6\text{W}_6\text{C}$ in sputtered Co and W thin films, which were proposed to associate with the selective growth of 50–70% (12,6) SWCNTs.²²¹ However, W disappeared after 5 min of low-pressure CVD growth, and Co is believed to be the catalyst for nanotube growth.²²²

Catalyst Support. The main function of catalyst supports is to anchor the catalyst nanoparticles and constrain their size and structure for chirality-enriched growth of SWCNTs. Mesoporous materials and high surface area oxides have been widely used to support metal nanoparticles and constrain their size, which has been effective not only in diameter-controlled growth but also in controlling the chirality. Manipulating the interaction between the catalysts and substrates is very important in such processes. Partially reduced metal/metal oxide, such as Co/Co^{2+} and Ni/Ni^{2+} , was used in controlled growth of SWCNTs (Figure 21a).^{223–225} By decrease of the reduction temperature or precise tuning of the oxidation degree of the catalyst using water vapor, sub-nanometer metal nanoparticles were anchored by their oxides as shown by XAS measurements (Figure 21b). Then the

resultant sub-nanometer metallic nanoparticles catalyzed the growth of SWCNTs with a narrow chirality distribution (Figure 21c). Similar mechanisms to anchor Fe nanoparticles by iron silicide (FeSi)²²⁶ were also reported.

In addition to the strong interaction, the oxidative supports can also stabilize the solid state catalyst by lattice match or epitaxy. This effect is also beneficial for maintaining the crystal structure of the nanocatalysts during the CVD process, which is crucial in controlling the structure of SWCNTs grown. He et al. adopted $\text{Co}_x\text{Mg}_{1-x}\text{O}$ solid solution catalyst precursors to prepare MgO-supported Co catalysts.^{75,227} They performed a TEM study under the reactive environment and observed the lattice mismatch between Co (200) and MgO (200) planes. The epitaxial interface stabilized Co on MgO to form well-dispersed catalyst nanoparticles with small diameters. Statistical analysis from electron diffraction (ED) confirmed the selectivity of ~53% for (6,5) tubes (Figure 21d–g). The substrate may also affect the catalyst morphology. When solid solution of $\text{Co}_x\text{Mg}_{1-x}\text{O}$ was prepared from a single-crystal MgO wafer instead of powders, the anchored Co catalysts yielded nanotubes with diameters shifted to ~1.23 nm.²²⁸ Partially faceted FePt{111}-nanoparticles were epitaxially formed on single-crystal MgO substrate (Figure 21h,i). These FePt nanoparticles half-buried into MgO showed superior thermal stability. These catalysts were used to grow vertically aligned SWCNTs enriched with metallic species (Figure 21j). Ago et al. found that CoMo catalysts on the (1120) plane of sapphire induced preferential growth of (16,2) SWCNTs, while near-armchair SWCNTs dominated on the (1102) plane. They speculated that the different atomic structures of the sapphire surfaces induced different morphologies and orientations of the catalysts, which then influenced the chirality of SWCNTs formed.²³⁰

Adjusting the Catalyst Structure by Additives. Introducing additives, such as water vapor, ammonia, and sulfur, during the stage of catalyst formation is effective to modulate the catalyst morphology and structure, which further affect the chirality distribution of SWCNTs.^{231–236} For instance, Fe nanocrystals preferentially exposing {111} facets were observed when helium with a trace amount of water vapor was introduced to treat the catalyst. These Fe catalysts were effective for the growth of 91% m-SWCNTs enriched with (9,9), (10,10), and (11,8) tubes (Figure 22a, b).²³¹ Hata et al. used H_2O vapor in H_2 to treat the Fe catalyst, but this time s-SWCNTs were obtained with purity of ~98%.²⁰⁹

The addition of sulfur into the catalysts may induce strong interaction with metal particles and segregate the metal particles.^{237–239} Windle et al. used sulfur containing Fe floating catalysts to grow SWCNTs enriched with armchair species.²³⁷ They assumed that iron particles coated with sulfur, where the iron–sulfur bond is comparatively strong, present more resistance to coalescence. Thus, the presence of sulfur in the reaction stream effectively arrests continued growth of the iron particles, preserving them at small dimensions for SWCNT nucleation. Chen et al. systematically studied the presence of sulfur species on SiO_2 supported Co catalysts in the controlled growth of SWCNTs.^{234,238,240} The application of cobalt sulfate rather than other types of cobalt salts is necessary for improving selectivity. They assumed that SO_4^{2-} bonded with Co may restrain the aggregation of Co nanoparticles on the SiO_2 surface (Figure 22c). Later on, they used $\text{H}_2\text{S}/\text{H}_2$ to treat the catalysts and showed that the formation of Co_9S_8 intermediates was helpful for the formation of Co nanoparticles with uniform size (Figure 22d). This preferential growth of (9,8) SWCNTs is

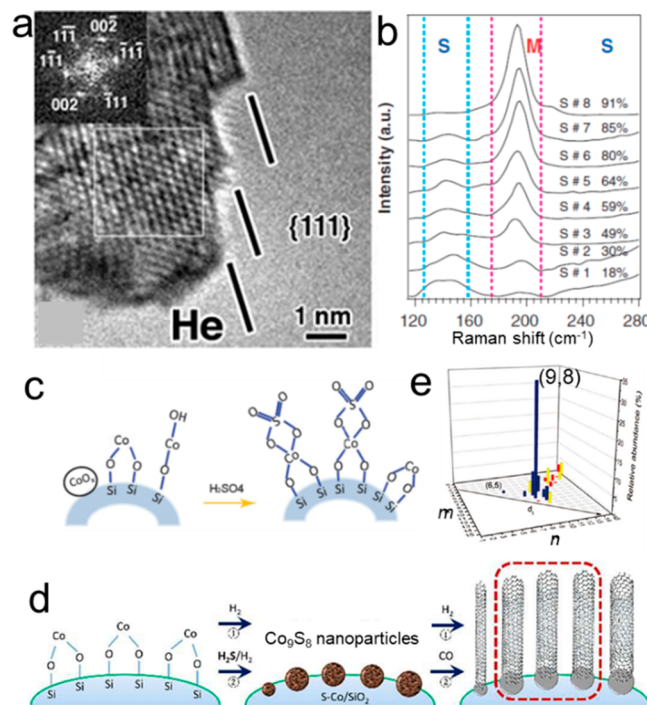


Figure 22. (a, b) ETEM image of {111} facets of Fe under 500 mTorr He and 10^{-2} mtorr H_2O at 500 °C. Evolution of RBMs for m-/s-SWCNTs, depending on the annealing ambient and duration. The estimated percentage of metallic tubes in each sample is shown (b). Reproduced with permission from ref 231. Copyright 2009 American Association for the Advancement of Science. (c, d) Scheme showing the evolution of Co catalysts by sulfur treatment: H_2SO_4 (c) and $\text{H}_2\text{S}/\text{H}_2$ (d). Reproduced with permission from refs 233 and 234. Copyright 2013 and 2016 Royal Society of Chemistry. (e) Chirality distribution map of SWCNTs grown on S-Co/ SiO_2 catalyst. Reproduced from ref 238. Copyright 2013 American Chemical Society.

proposed to relate to the stability of (9,8) caps on Co nanoparticles with suitable size (Figure 22e).

Intermetallic Catalysts with Unique Structure. It was proposed by both simulation and TEM observation that there is a relation between a SWCNT of defined chirality and its seeding catalyst in solid state.^{126,130} The solid catalyst was proposed to act as the structural template for SWCNT growth. This indicates that VSS routes should be superior to the VLS process in selectively growing SWCNTs of certain chirality. However, conventional metal nanoparticles such as Fe and Co with relatively low melting point are often molten in high-temperature processes, which are not applicable for the epitaxial model. As discussed above, the catalyst support has shown to be able to stabilize the metal nanoparticles, resulting better chirality selectivity.⁷⁵ Choosing metals with higher melting points²⁴¹ as catalysts or growing nanotubes at lower temperature can ensure the VSS growth of SWCNTs. Many nonmetallic catalysts including Al_2O_3 ,²⁴² SiO_x ,⁶⁹ SiC, BN,²⁴³ and diamond²⁴⁴ with much higher melting points have also been explored. However, none of these attempts achieved chiral selectivity higher than Co/MgO catalyst, which is 53%.⁷⁵

The failure to obtain SWCNTs with high chiral purity in various trials using solid state catalysts indicates that there must be additional crucial factors beyond solid state in catalyst design. Inspired by the high selectivity of enzyme catalyzed reactions enabled by the molecular recognition between enzymes and substrates, Li et al.¹⁵ realized that the unique structure of

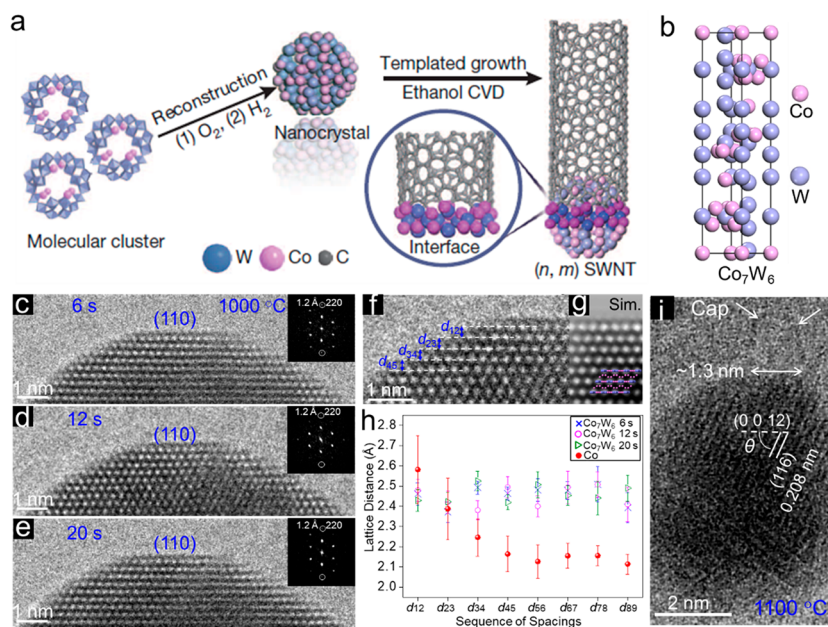


Figure 23. (a) Scheme of the synthesis of the intermetallic Co_7W_6 catalyst and templated growth of a specific (n,m) SWCNT. Reproduced with permission from ref 15. Copyright 2014 Nature Publishing Group. (b) Rhombohedral structure of intermetallic compound Co_7W_6 unit cell. (c–h) Time-sequenced ETEM images of Co_7W_6 nanoparticle at 1000°C in CO (c–e). Determination of the position of individual atomic columns by 2D Gaussian fitting (f). TEM simulation based on Co_7W_6 [10 10 1] (g). The Co_7W_6 (110) lattice spacings at different exposure time to CO at 1000°C . The (111) lattice spacings of fcc-Co at 700°C in CH_4/H_2 were included for comparison (h). Reproduced from ref 100. Copyright 2019 American Chemical Society. (j) Single shot *in situ* HRTEM image of a carbon cap growing from Co_7W_6 (0 0 12). Reproduced from ref 64. Copyright 2016 American Chemical Society.

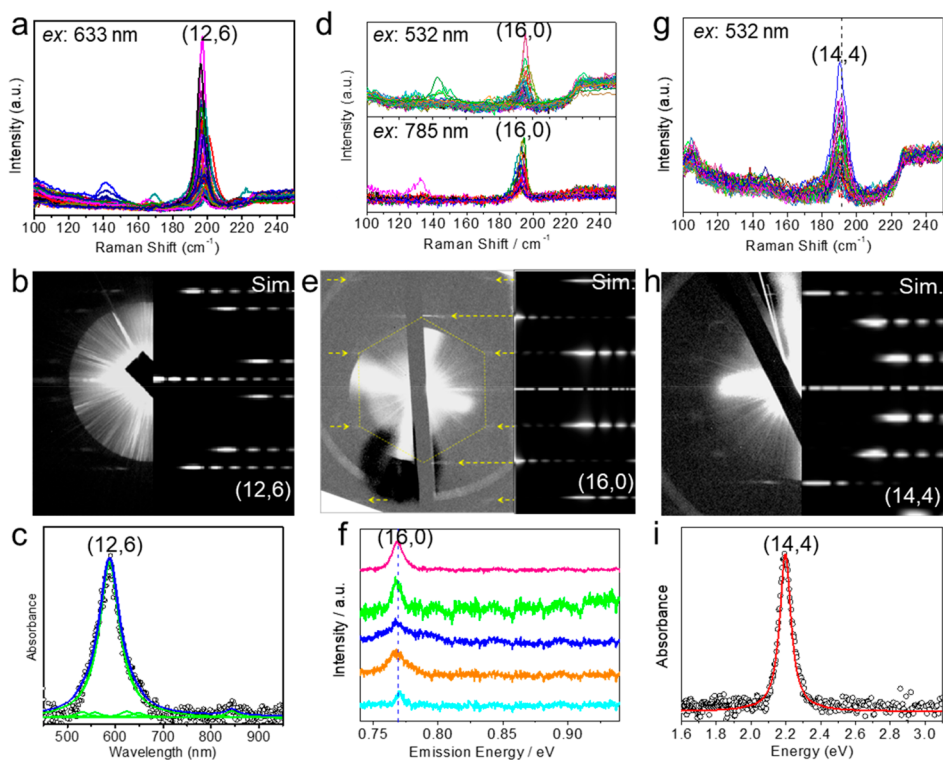


Figure 24. Characterizations of (12,6) (a–c), (16,0) (d–f), and (14,4) (g–i) SWCNTs. Panels a–c reproduced with permission from ref 15. Copyright 2014 Nature Publishing Group. Panels d–f reproduced from ref 145. Copyright 2015 American Chemical Society. Panels g–i reproduced from ref 59. Copyright 2017 American Chemical Society.

catalysts is essential to realize the “recognition” between catalysts and nanotubes. Therefore, catalysts with both high melting point and unique atomic arrangements (i.e., lower

crystalline symmetry) are needed for the chirality-selective synthesis of SWCNTs (Figure 23a). They proposed tungsten-based intermetallic compounds as the choice. Indeed, such a

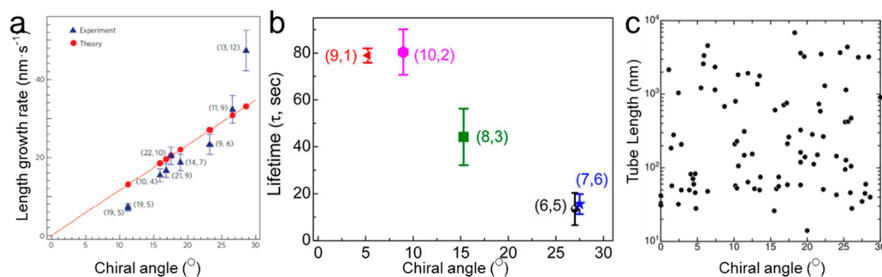


Figure 25. Chiral angle as a function of growth rate (a), lifetime (b), and length (c) of SWCNTs. Panel a adapted with permission from ref 123. Copyright 2012 Nature Publishing Group. Panel b adapted from ref 140. Copyright 2013 American Chemical Society. Panel c adapted with permission from ref 189. Copyright 2017 Elsevier.

new type of catalyst is an ideal choice. Co₇W₆ possess a rhombohedral crystal structure with lower lattice symmetry to offer a unique atomic arrangements (Figure 23b); meanwhile the presence of tungsten ensures a high melting point.

Since Co is very efficient in catalyzing SWCNT growth, the preparation of Co₇W₆ catalysts without Co residues is crucial for achieving high chiral selectivity. Thus, the selection of catalyst precursor is important. When salts of tungsten and cobalt were used as catalyst precursor, it was found that the selectivity was not very high due to the presence of residual Co.²⁴⁵ Polyoxometalate molecular clusters containing W and Co are superior precursors for Co₇W₆ nanocrystals with three obvious advantages: the clusters are nanosized, W and Co are atomically mixed within the clusters, and the ratio of W to Co is high enough. These advantages benefit the preparation of Co₇W₆ nanocrystals without free Co species under milder conditions (Figure 23a).¹⁵

The Co₇W₆ nanocrystals present high stability at 700–1100 °C under the carbon feeding conditions, which was confirmed by atomic level evidence from *in situ* aberration-corrected ETEM and overall observation by *in situ* XAS. No structural changes induced by carbon dissolution were observed when carbon was fed at 1000 °C (Figure 23c–h).¹⁰⁰ From *in situ* TEM at 1100 °C, a SWCNT cap was also found to grow from the (0 0 12) plane of the Co₇W₆ nanocrystal (Figure 23i). These *in situ* observations verify that Co₇W₆ nanocrystals are stable under carbon feeding at the CVD temperature, acting as the templates for nanotube growth.

Using the Co₇W₆ nanoparticles prepared at 1030 °C as catalysts, Li et al. achieved a preferential growth of (12,6) SWCNTs with the proper ethanol/hydrogen supply. They demonstrated that the purity of (12,6) species is over 92% by using three methods, Raman spectroscopy, UV-vis-NIR absorption, and AFM combined with Raman mapping (Figure 24a–c).¹⁵ HRTEM imaging of catalyst–tube interface confirmed (12,6) tubes grown perpendicularly to the (0 0 12) planes of Co₇W₆ (Figure 24g,h).⁶⁴ This strategy showed its validity for the selective growth of tubes of other specific chiralities. Zigzag (16,0) SWCNTs and (14,4) SWCNTs were synthesized with a selectivity of 79% and 97%, respectively, using (1 1 6) and (1 0 10) planes of Co₇W₆ as the structural templates under the optimized growth conditions (Figure 24d–i).¹⁴⁵ For the (14,4) samples, the chiral purity was further improved to 98.6% with a high s-SWCNT content of 99.8% by treatment with water.⁵⁹

3.3.2. Kinetic Control. Kinetics is always important in all chemical processes, including the CVD growth of SWCNTs. Kinetic processes such as carbon diffusion and tube growth depend on the states and properties of catalysts and hence vary

significantly from liquid to solid catalysts and also change with the composition and structure of catalysts. On the other hand, the intrinsic kinetic difference in growth among tubes of different chiralities will unavoidably contribute to the chirality distribution of SWCNTs in the CVD products. We will discuss the kinetic control in chirality-controlled growth of SWCNTs by VLS and VSS processes.

Kinetic Control in VLS Growth of SWCNTs with Enriched Chirality. It has been known for a while that growth rate of SWCNTs is positively proportional to the chiral angle. This tendency was found in both theoretical simulations^{90,136,246} and some experimental observations.¹²³ Maruyama et al. employed *in situ* Raman to track the growth of SWCNTs from Fe catalyst. They found a linear positive correlation between chiral angle and growth rate (Figure 25a).¹²³ People believed that the chirality enrichment of (6,5), (7,5), (7,6), and (9,8) tubes^{49,52,53} with large chiral angles originated from their higher growth rates. On the contrary, the lifetime (or termination time) as a function of chiral angle presented a negative correlation in metal-free growth (Figure 25b).¹⁴⁰ The tube length can be seen as a product of the growth rate and lifetime. Therefore, the relation between chiral angle and tube length is complex. He et al. demonstrated by statistical analysis of TEM measurements that the tube length and chiral angle are uncorrelated (Figure 25c).¹⁸⁹ Most recently, Wei's group found a nearly 10-fold faster decay rate of metallic CNTs than semiconducting CNTs and realized a spontaneous purification of predicted 99.9999% ultralong (>100 mm) semiconducting tubes.²⁴⁷

Carbon feeding rate, which is determined by the CVD conditions, affects the tube growth rate. The effect of CVD conditions such as temperature,^{49,52,146,248} type,^{249–251} and composition of carbon feed stocks,^{249–251} pressure,^{252,253} and plasma treatment^{254–256} on the chirality distribution of SWCNTs has been intensively studied (Figure 27). Much empirical knowledge has been accumulated, but a general rule to guide the selection of carbon feeding conditions is still absent. Hydrocarbons (such as, methane, ethane, ethylene, acetylene, and toluene), alcohols (methanol, ethanol, and propanol), and carbon monoxide are the most widely used carbon feedstocks. Different carbon precursors decompose via different pathways at different conditions. Since the disproportionation of CO is an exothermic and entropy-decreasing reaction, the CVD synthesis of SWCNTs from CO is generally carried out under high pressure via a so-called HiPco process.²⁵⁷ The decomposition of hydrocarbons and alcohols is endothermic and entropy-increasing; therefore such carbon stocks are normally used in atmospheric or lower pressure. Ethylene, acetylene, and ethanol are generally easier to decompose than methane. The by-products also affect nanotube growth. Radicals of •CH₃, •H, and

\bullet OH generated from the decomposition of hydrocarbons and alcohols are all very reactive. All these factors will affect the chiral distribution of final product.^{197,249,258}

CO often presents higher chiral selectivity than CH₄ in CVD processes (Figure 26a).^{49,97,249,250} An *in situ* TEM study showed

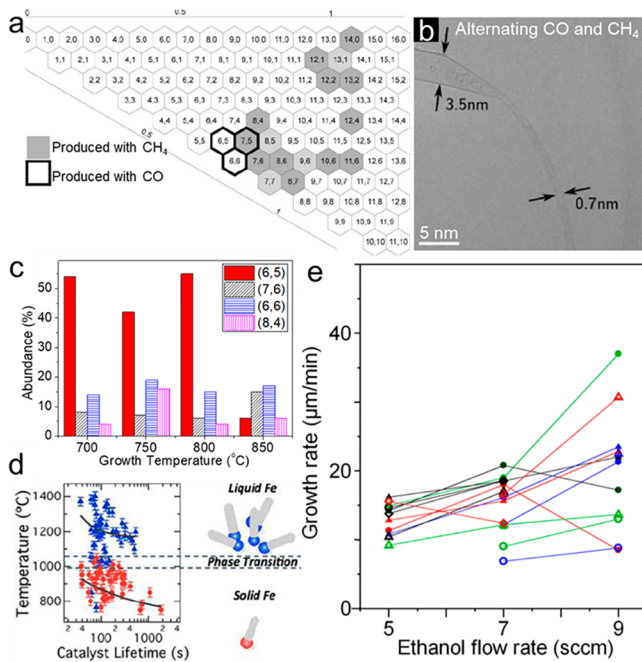


Figure 26. (a–c) Effects of type of carbon precursor (a, b) and temperature (c, d) on the growth of SWCNTs. Panels a and c Adapted from ref 49. Copyright 2006 American Chemical Society. Panel b adapted with permission from ref 97. Copyright 2018 Royal Society of Chemistry. Panel d reproduced from ref 262. Copyright 2013 American Chemical Society. (e) Growth rate of individual SWCNTs as a function of ethanol flow rate. Adapted from ref 264. Copyright 2018 American Chemical Society.

an obvious change of SWCNT diameter when the carbon feedstock was alternated from CO to CH₄ (Figure 26b).⁹⁷ This gives direct evidence of the effect of carbon feedstock on tube growth. Various carbon feedstocks produce different carbon contents inside the catalysts, resulting in different wettability of the catalysts to the wall of nanotubes. The difference in wettability may lead to different growth modes of the tubes, either tangential or perpendicular. On the other hand, precursors may affect the reaction pathways and the kinetics of structure healing of the tubes, resulting in precursor-dependent effects on chirality distributions.²⁵⁹ Hydrogen, a common component in the reaction mixture in CVD systems, also plays important roles. It may adsorb on the catalyst surface, affecting the catalytic behavior. Meanwhile, H₂ may also etch carbon species including amorphous and graphitic carbon. The disproportionation of CO generates CO₂. Hence, adding CO₂ to the CVD system will affect the disproportionation reaction and influence the formation of SWCNTs. Kauppinen et al. obtained colorful SWCNT thin films by introducing CO₂ into the system during the floating-catalyst CVD process using CO as carbon feedstock.²⁶⁰ The color of the SWCNT thin film evolved from gray to green and brown to gray again with the concentration of CO₂. They believed that the colors originated from the different diameter distributions of nanotubes resulting from the different concentrations of CO₂ in the CVD system.

The presence of components other than the carbon source may also influence the behavior of the catalysts. For example, trace oxygen in the carbon feedstock can effectively improve the catalyst activity and prolong the catalyst lifetime during the growth of SWCNTs.²⁶¹

The feedstock pressure and flow rate directly affect the carbon concentrations, thus affecting carbon supply for growing SWCNTs. Chen et al. found that the ratio of (6,5)/(7,5) increases with increased CO pressure from 2 to 18 bar.²⁵²

Growth temperature is a distinct impact factor on the chirality distribution of SWCNTs. It not only affects the decomposition of carbon feed stock but also remarkably influences the structure and property of catalysts. It is natural that the temperature determines the phase state. An *in situ* Raman study by Maruyama et al. showed that lifetime and efficiency of Fe catalyst undergo sharp improvement at ~1000 °C due to the solid-to-liquid phase transition of catalysts (Figure 26d).²⁶² Resasco et al. performed the growth of SWCNTs using CoMo catalyst at 700–850 °C. The highest selectivity of 55% (6,5) SWCNTs was achieved at 800 °C, but it sharply decreased to 6% upon further increase of the temperature to 850 °C (Figure 26c).⁴⁹ This is possibly caused by the phase change of catalysts from solid to liquid. A low temperature preference for selective growth of SWCNTs has been reported for FeRu,⁵⁰ FeCu,⁵² CoPt,⁵⁴ FeMn,²¹⁸ and CoMn²⁶³ catalysts. It was speculated that catalyst size is sensitive to the temperature. At lower temperature, catalyst size remains small and uniform. Higher selectivity and smaller diameter of nanotubes were often observed at lower temperature.

Temperature may also play more complex roles. Zhang et al. proposed a “tandem plate” CVD process by periodically changing growth temperature to obtain near-zigzag SWCNTs.²⁴⁸ It was proposed that temperature induced variation of interfacial energy between tube and catalyst led to the reconstruction of nanotube ends attached on Fe catalyst. As a result, SWCNTs with large chiral angle tend to convert to near-zigzag species step by step upon varying the temperature multiple times.

It is still a challenge to give a visualized insight into the relation between CVD condition and growth result. Indeed, it is difficult to directly trace the decomposition of carbon precursors in CVD processes. Although some researchers tried to monitor the possible species in the exhaust port of the CVD system by using gas chromatography and mass spectrometry,^{197,208} intermediates at high temperature are still unknown because they are unstable and easily transform to stable ones. There are also efforts on *ex situ* characterizations to capture the influence of CVD conditions.¹⁴⁶ Maruyama’s group adopted a feasible method to trace the growth process of individual SWCNTs using isotopically labeled ¹³C-ethanol as carbon precursor.²⁶⁵ They found that the two carbon atoms in ethanol do not contributed equally to the growth of SWCNTs. The carbon atom away from the –OH group is preferentially inserted into the tube, and this tendency depends on the temperature. This result indicates that temperature indeed affects the pathway of carbon precursor decomposition. They also found that the growth rates of most SWCNTs increase with the flow rate of ethanol, but some other SWCNTs exhibited a negative correlation (Figure 26d).²⁶⁴

Obviously, regulation of the CVD conditions is very complex. It influences both the catalyst activity and carbon feeding rate, leading to variations of the nucleation probability, lifetime, and growth rate of SWCNTs. All these variations are (*n,m*)

dependent. As a result, the number and length of each type of (n,m) SWCNTs are disparate. The abundance of a certain (n,m) species in final products can be seen as a cofunction of their number and lengths (Figure 27). Therefore, these factors should be optimized simultaneously to achieve the highest (n,m) selectivity.

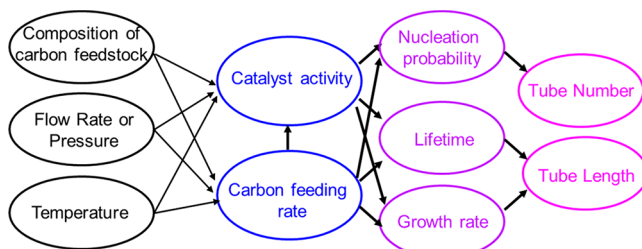


Figure 27. Relation between CVD parameters and the growth of SWCNTs.

Kinetic Control in VSS Growth of $(2m,m)$ and $(n,n - 1)$ SWCNTs. Kinetic effect on the controlled growth of SWCNTs via VSS is different from the case of VLS. Zhang's group proposed a symmetry matching model based on solid metal carbides as catalyst (Figure 11b).¹⁸ They found that $(2m,m)$ tubes ($\theta = 19.1^\circ$) grown from Mo₂C catalyst in a hydrogen-free atmosphere (pure ethanol) are much longer than other species, and the $(12,6)$ tubes are the longest ones (Figure 28a). This

by the kinetically favorable growth of $(2m,m)$ tubes with high carbon feeding.

Zhang et al. also reported the kinetically controlled synthesis of $(8,4)$ tubes on solid Mo₂C catalyst with CO as the carbon source.²⁶⁶ Lower feeding rate of CO benefits higher selectivity. A SWCNT sample containing 46.6% $(8,4)$ tubes was synthesized under optimized conditions. When Co catalyst was used, they found the preferential growth of $(n,n - 1)$ SWCNTs ($25^\circ < \theta < 30^\circ$) at a lower carbon feeding rate (lower carbon/hydrogen or C/H ratio) (Figure 28c). They claimed that Co nanoparticles maintain the solid state at the CVD temperature of 850 °C. They proposed based on DFT calculations that (n,n) tubes tend to convert to $(n,n - 1)$ or $(n + 1,n)$ by kinetically incorporating an energetically preferred pentagon–heptagon pair at the tube–catalyst interface. By precise control of the size of the Co catalyst at 1.4 ± 0.25 nm and lowering of the C/H ratio to 1/40, $(10,9)$ SWCNTs with purity higher than 80% were obtained (Figure 28d).²⁶⁷ However, there are at least six possibilities of (n,m) switching, including $(n,m \pm 1)$, $(n \pm 1,m)$, $(n + 1,m - 1)$, and $(n - 1,m + 1)$, when an adjacent pair of pentagon–heptagon is incorporated in a tube.²⁶⁸ A recent MD simulation by Maruyama et al. showed that an adjacent pair of pentagon–heptagon changes the chirality to $(0,\pm 1)$, $(\pm 1,0)$, $(-1,1)$, or $(1,-1)$.²⁶⁹ The chirality change will be greater, $(0,\pm 2)$, $(0,\pm 3)$, and so on, if the pentagon is away from heptagon. How to achieve a single dominant $(n,n - 1)$ species is still a mystery because it is very difficult to control the number of pentagon–heptagon pairs and their locations. Kinetic modulation has shown some success in controlling the chirality. However, the chiral purity is still far from satisfactory.

Kinetic Control in Chirality-Specific Growth of SWCNTs from Co₇W₆ Catalysts. The adoption of Co₇W₆ as catalysts of unique structure brings huge advantage to the chirality-specified growth of SWCNTs. However, the optimization of kinetic growth conditions is still necessary. For zigzag SWCNTs ($\theta = 0^\circ$), which are known to be kinetically unfavorable,^{136,232} the careful tuning of growth conditions is even more important. The kinetic unfavorability of $(16,0)$ tubes is evident from the facts that the mean length of $(16,0)$ tubes is obviously shorter than other species and the purity of $(16,0)$ tubes is higher for shorter growth time (Figure 29b,c). Hydrogen can adsorb on the surface of catalysts and also etch carbon species, thus increasing the concentration of H₂ will decrease the nucleation rate of all (n,m) species and lower the diffusion rate of carbon species.^{49,270} As a result, the weakness of zigzag tubes in growth kinetics is partially relieved. Then, with the help of template effect of Co₇W₆ (116) plane, zigzag $(16,0)$ SWCNTs of 79% purity were synthesized under larger H₂ supply (Figure 29a).¹⁴⁵ In contrast, higher C/H ratio and carbon feeding benefits selectivity toward $(12,6)$ tubes (Figure 29d–f). Obviously, for the structure-templated growth from Co₇W₆ catalysts, each (n,m) species has its favorite carbon feeding and kinetic conditions. Optimizing the carbon feeding by tuning the temperature and the composition of carbon stock together, Li et al. successfully realized the synthesis of $(14,4)$ tubes with purity of 88–96% at 800–1050 °C (Table 2).⁵⁹

2.3.3. Strategy for Chirality-Specific Growth of SWCNTs. The selection of catalysts is the most important issue in the chirality-specific growth of SWCNTs. The catalyst nanoparticles should maintain crystallized structures during the CVD process. But this is not enough. Lower structural symmetry with unique atomic arrangement of the catalysts is also essential to ensure the specific structural matching between the catalyst crystals and the tubes. Monocomponent metal catalysts often

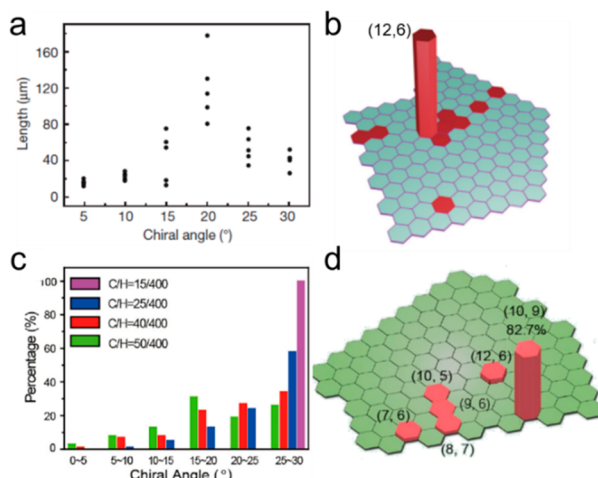


Figure 28. (a) Chiral angle as a function of tube length. (b) Chirality map of SWCNTs grown from Mo₂C catalyst. Reproduced with permission from ref 18. Copyright 2017 Nature Publishing Group. (c) Chiral angle as a function of its percentage. (d) Chirality map of SWCNTs grown from Co catalyst. Adapted with permission from ref 267. Copyright 2019 Elsevier.

kinetic favorability of $(2m,m)$ is in agreement with the previous simulation. They also speculated that hydrogen can weaken the kinetic growth rate. By increase of the concentration of ethanol to reach a maximum growth rate, SWCNT arrays containing 90% $(12,6)$ tubes and 80% $(8,4)$ tubes were synthesized with Mo₂C and WC catalyst, respectively (Figure 28b). There is another report on the preferential growth of $(12,6)$.²²¹ They used Co₆W₆C as catalyst and pure ethanol without hydrogen as carbon precursor in a low pressure CVD process and found that the catalysts converted to Co after 5 min of CVD. It is likely that the selective growth of $(12,6)$ SWCNTs on Co catalyst is caused

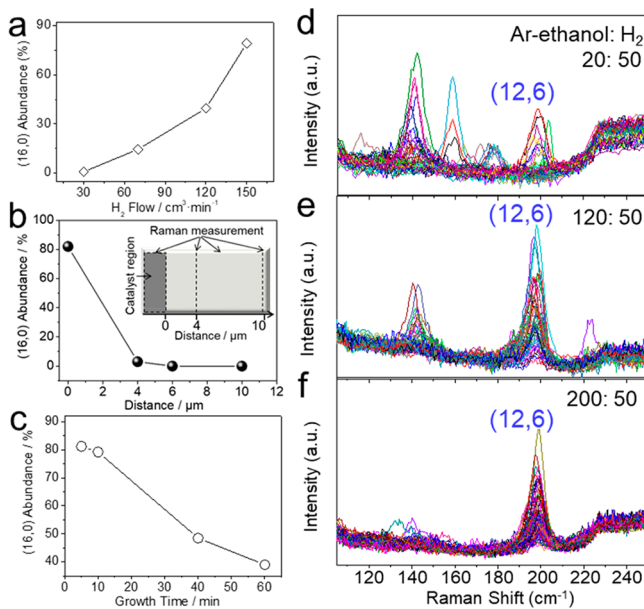


Figure 29. (a–c) Effect of H₂ flow rate (a) and growth time (c) on the selectivity of (16,0) tubes and content of (16,0) tube at different distances from the catalyst region (b). Reproduced from ref 145. Copyright 2015 American Chemical Society. (d–f) Effect of Ar supported ethanol flow rate on the selectivity of (12,6) tubes. Reproduced from ref 64. Copyright 2016 American Chemical Society.

exhibit higher crystal symmetry and atomic homogeneity, tolerating the formation of SWCNTs with different chiralities. Normal alloys have disordered atomic structures. Therefore, neither simple metallic catalysts nor normal alloyed catalysts work well for chirality-selective synthesis of SWCNTs. Tungsten based intermetallic compounds meet the criteria of both high melting point and unique atomic arrangements and hence are ideal catalysts to achieve the synthesis of SWCNTs with specified structures.

Optimizing the growth conditions is also crucial to improve the chiral selectivity. A Co₇W₆ nanocrystal presents various crystal planes. Though the unique atomic arrangements of each plane obviously reduce the total number of possible chiralities nucleated, the growth of only one type of SWCNT is still unattainable. Fortunately, it has been observed that the nucleation of nanotubes with certain diameters has an optimized carbon feeding rate.⁶⁸ Experiments on Co₇W₆ catalysts also present referential growth conditions of different SWCNTs with different chiralities as discussed previously. Therefore, kinetic conditions are another fulcrum for chirality-specified synthesis of SWCNTs. However, the tube growth process is quite complex, and the stages of nucleation and growth may require different kinetic conditions. It was found that the nucleation, a very short process, requires a higher carbon feeding rate than the growth stage.²⁷¹ Hence, we need to optimize the kinetics of these two stages separately to control the nucleation probability and growth rate of each (n,m) SWCNT.

The chirality-specific growth of SWCNTs can only be realized by the collaboration of the template effect of the catalysts and the manipulation of the growth conditions (Figure 30). The

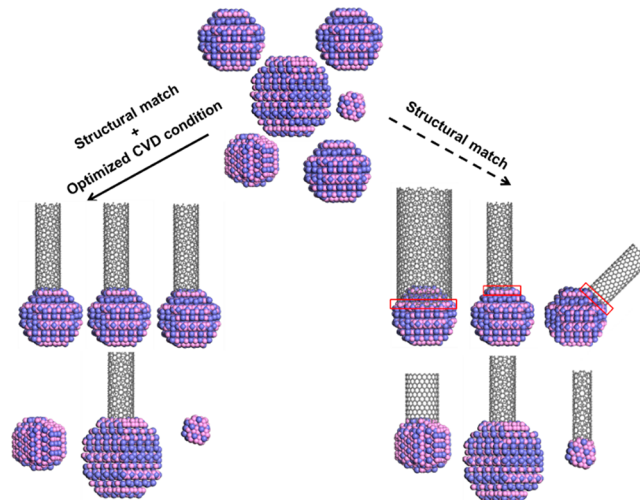


Figure 30. Schematic representation of the cooperative functions of thermodynamics and growth kinetics.

structural recognition between a SWCNT of a specific (n,m) type and a certain catalyst facet represents thermodynamic ascendancy, and the CVD conditions bring different growth kinetics of the nanotubes.

2.4. SWCNTs Initiated by Predesigned Nanocarbon Segments

Predesigned segments of nanotubes can also act as the starting materials and structure templates for the formation of SWCNTs with controlled chiralities. The idea of amplifying SWCNTs was invented in 2005 by Smalley.²⁷² Later on, short nanotubes,^{13,272–275} fullerene based structures,^{276–279} carbon nanorings,²⁸⁰ graphene nanoribbons,²⁸¹ and polycyclic aromatic hydrocarbons¹⁶ have been used as the starting segments to further grow into SWCNTs as summarized in Figure 3b. In this part, we will first introduce the formation of SWCNTs from nanocarbon segments and then summarize the methods for the preparation of chirality-specified SWCNTs.

2.4.1. Synthesis of SWCNTs from Nanocarbon Segments. *Short Tubes.* Amplifying a short nanotube into a longer tube is a straightforward route to elongate its length and retain its chiral structure. In this process, the initiating segments serve as the structural templates for further growth of the nanotubes. Smalley et al. attached metal nanoparticles onto the open ends of SWCNTs and first realized the regrowth of SWCNTs. The amplified SWCNTs were expected to inherit the chirality of the original short tubes (Figure 31a).^{272,273} However, the yield was only 3%, and solid proof of fixed chirality after amplification was absent. Obviously, it is not possible to guarantee that all the catalysts are attached to the open end of the tubes. Other new tubes will grow from those undocked catalysts.

Table 2. Optimized CVD Conditions for Growing (14,4) SWCNTs with Co₇W₆ Catalyst

CVD conditions	temperature (°C)	800	850	900	950	1000	1050
Ar–ethanol/H ₂ (cm ³ ·min ⁻¹)	300/20	300/25	300/30	240/30	200/35	200/30	
(14,4) abundance	88.3%	87.7%	92%	93%	93.4%	96%	

Adapted from ref 59. Copyright 2017 American Chemical Society

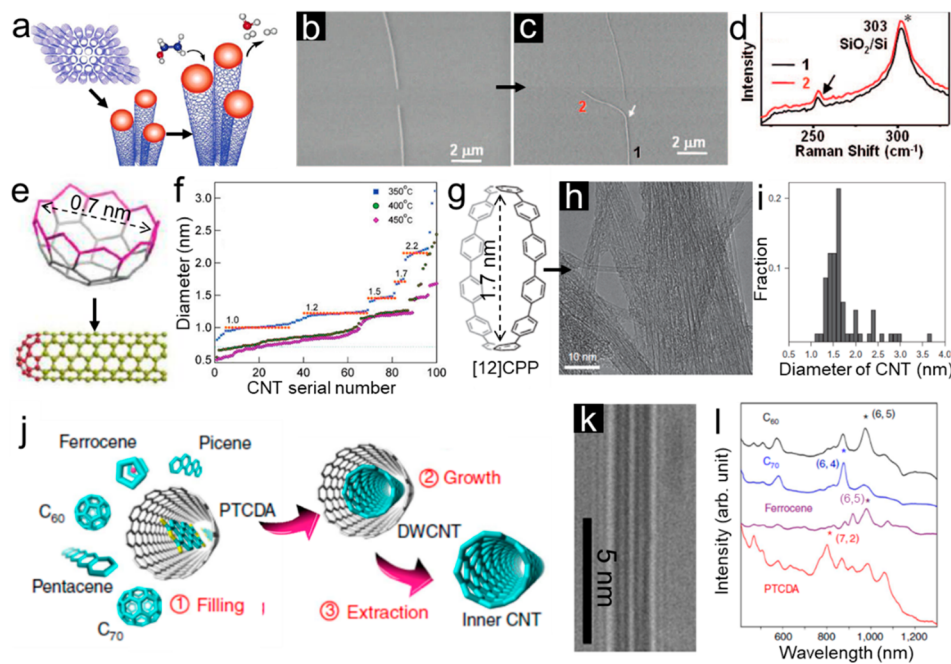


Figure 31. (a) Schematic showing the amplification of SWCNTs with metal nanoparticles docked in the open ends of tubes. Reproduced from ref 272. Copyright 2005 American Chemical Society. (b–d) SEM images (b, c) and Raman spectra (d) of SWCNTs before and after cloning growth. Reproduced from ref 275. Copyright 2009 American Chemical Society. (e, f) Illustration of growing SWCNT using opened C_60 as a cap (e) and diameter distribution of as-cloned SWCNTs (f). Reproduced from ref 276. Copyright 2010 American Chemical Society. (g–i) CPP molecule (g), TEM image of SWCNTs synthesized from [12]CPP (h), and diameter distribution histograms (i). Reproduced with permission from ref 280. Copyright 2013 Nature Publishing Group. (j–l) Schematic showing the formation of SWCNT within a parent-tube template (j), TEM image (k), and UV–NIR–vis spectra of the inner tube (l). Reproduced with permission from ref 281. Copyright 2013 Nature Publishing Group.

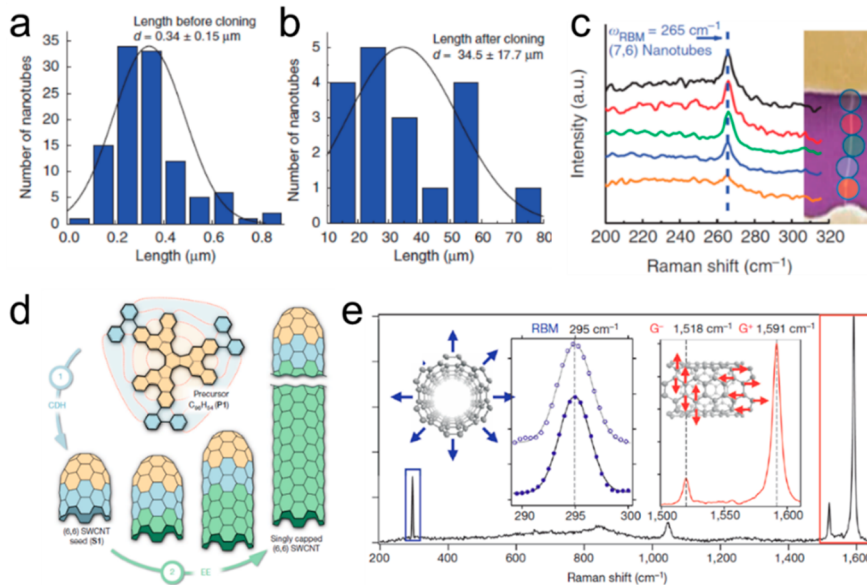


Figure 32. (a, b) Length distributions of SWCNTs before (a) and after (b) the VPE growth. (c) Raman RBM spectra along a SWCNT confirming the same chirality after cloning. Reproduced with permission from ref 13. Copyright 2012 Nature Publishing Group. (d) Schematic showing the growth of a (6,6) SWCNT from predesigned polycyclic hydrocarbon molecule. (e) Raman spectrum of a (6,6) SWCNT. Reproduced with permission from ref 16. Copyright 2014 Nature Publishing Group.

Later on, Liu et al. proposed “cloning” growth, the idea that the nanotube itself can be elongated without catalyst. The elongated SWCNTs inherit the chirality of the parent segments as confirmed by SEM and Raman measurements (Figure 31b–d).²⁷⁵ The yield of “cloning” on a SiO_2 surface was 9%, but it was increased to 40% on a quartz substrate. They further employed a microwave-assisted pathway to regenerate SWCNTs from

carbon fragments on a SiO_2/Si substrate. They assumed that microwave irradiation provides fast heating to remove polar groups bonded to nanotubes and reduce the spontaneous closure of open ends of tubes. With this strategy, the efficiency of regeneration can reach 100%, and the regenerated SWCNTs fully retain the original chirality.²⁸²

Fullerenes. Opened fullerene was used as a cap to initiate a nanotube. However, the tubes generated showed broad diameter distributions (Figure 31e,f).²⁷⁶

Graphene Nanoribbons. Shinohara et al. encapsulated the graphene nanoribbons into SWCNTs with diameters of 1.4 nm. The encapsulated graphene was transformed into nanotubes by self-intertwining upon annealing at 1200 °C. The inner tubes presented an enrichment of (7,2) and (8,1) chiralities attributed to the template effect of the outer tubes (Figure 31j–l).²⁸¹

Carbon Nanostructures from Hydrocarbons. Atomically precise synthesis of SWCNTs from aromatic hydrocarbons, namely, “bottom-up” synthesis,^{283–286} has attracted the interests of organic chemists. However, only finite models such as carbon nanorings and nanocaps were obtained. Later on, researchers combined these aromatic hydrocarbons with CVD method and tried to grow by epitaxy SWCNTs with defined chirality. For example, cycloparaphenylen (CPP) was used to initiate the growth of SWCNTs using ethanol as carbon source at 500 °C.²⁸⁰ Although some tubes presented diameters similar to the size of CPP, precise chirality control was still unsuccessful (Figure 31g–i). C₅₀H₁₀ molecules were used as a predesigned cap of (5,5) tube and were also proposed to epitaxially grow (5,5) SWCNTs. However, Raman measurements showed that none of the resultant SWCNTs are (5,5).²⁷⁷

2.4.2. Chirality-Specified SWCNTs by Elongation of Nanocarbon Segments. There are two strategies reported in growing SWCNTs with designed chirality from nanocarbon segments.^{13,16} One is the cloning growth of SWCNTs by using presorted single-chirality SWCNTs as seeds via catalyst-free vapor-phase epitaxy (VPE).¹³ Activation of seeds in air or water vapor is important in improving the efficiency of cloning. It was proposed that certain functional groups at the open ends of tubes formed in the pretreatment are crucial for incorporating carbon (Figure 32a–c). Ethylene presented the highest efficiency in cloning growth among the tested carbon stocks including methane, ethanol, and ethylene.¹⁴⁰ Homma et al. also realized the cloning growth with both hot- and cold-wall CVD. They suggested a Diels–Alder cycloaddition mechanism when using C₂H₂ as carbon source.²⁸⁷

The other example is the synthesis of (6,6) tubes by using the seeds obtained from the predesigned polycyclic hydrocarbon C₉₆H₅₄ molecules. The key to this success is the choice of the Pt(111) surface, which can stabilize the aromatic C₉₆H₅₄ molecule and catalyze its transformation to a (6,6) cap at 770 K by cyclodehydrogenation (CDH) reaction. Around half of the molecules transformed into caps detected by scanning tunneling microscopy (STM). The (6,6) caps were epitaxially elongated to form nanotubes of ~200 nm by ethanol CVD at 670 K (Figure 32d,e).¹⁶ However, the chirality identification and quantification need to be further examined.^{288–292} This method resembles closely a proposal reported by Jansen et al.^{293,294} The efficiency of this method is sensitive to the substrates and the type of the cap precursors. When Rh(111) surface was used instead of Pt(111) and C₆₀H₃₀ precursor, a full conversion into (6,6) caps was achieved. However, the information on subsequent tube growth is unknown.²⁹⁵

The advantage of the amplification of nanocarbon segments into SWCNTs is that the process is predesignable. However, this approach still faces many challenges. For example, the activation of the segments is very tricky because the activation should not damage the structure of the seeds and the ends of seeds should match the growth conditions. The uniformity of the precursors needs to be further improved. The stability of the nanocarbon

seeds at high temperature is another issue. It is normally not easy for such tiny structures to maintain their structure at the temperatures required to form well-graphitized nanotubes. The nucleation of new nanotubes is always difficult to prevent. The statistical information on chiral purity of cloned tubes grown by VPE or CDH methods is not reported yet. From all of above observations, the efficiency, the purity, the precise control of the tube structure, and the seed supply are the main challenges for this method.

2.5. Open Questions and Challenges in Chirality-Controlled Growth of SWCNTs

2.5.1. Understanding the Growth Mechanism. Rational design of the chirality-specified synthesis of SWCNTs must be based on a full understanding of the mechanism of tube growth. Both theoretical and experimental results have revealed the effect of catalysts on the chirality of SWCNTs grown, but how the chirality of a tube is determined during the growth remains a mystery.

One assumption is that the chirality is fixed during the nucleation and the chirality of the tube is defined by the cap.^{76,126} If this is the case, then how the structure of a cap is controlled becomes crucial. Till now, we still lack experimental evidence on this issue. Simulations by Ding et al. suggested that the probability of nucleating any cap is the same on the liquid catalyst but can be different on solid catalyst.⁸⁷ However, even if the structure of the cap can be controlled, it is obvious that any defects in a SWCNT will change the tube’s chirality.^{88,296} Defect healing may happen during the growth process.⁸⁹ But defect healing does not necessarily bring the structure of the tube back exactly to the original. Chirality change of SWCNTs was verified by *in situ* Raman²⁹⁷ and isotope labeling experiments.²⁶⁴

There is an argument that the tube wall other than the cap plays dominant role in deciding the growth behavior.^{143,298} This is also possible considering the tremendously larger number of atoms in the wall than in a cap.

The above discussion is mainly based on thermodynamic considerations. How the kinetics in the nucleation and growth stages affects the chiral selectivity is also an open question. Some theoretical models were proposed that carbon incorporation, also described as the kink-running process, is the rate-determining step,^{87,139} which was supported by experiments of positive correlation between the tube growth rate and its chiral angle.¹²³ Yakobson et al. combined the thermodynamic and kinetic factors together in their simulation and gave a prediction on the preferential growth of tubes with each chirality.¹³⁵ More experimental facts are needed to verify its general validity.

In summary, there are still many challenges in rational design for the synthesis of chirality-pure SWCNTs. An atomic level model on the growth mechanism is needed. A full exploration of how the thermodynamic and kinetic factors influence the chirality distribution is also necessary. Besides progress in the theoretical studies, recent developments in *in situ* techniques will be able to offer new insight into the mechanism of chirality-controlled growth of SWCNTs.

2.5.2. How Far Can Selective Growth Practically Go? It is great progress in SWCNT growth from 55% (6,5) tubes⁴⁹ to 97% (14,4) tubes.⁵⁹ However, this purity is still far below the requirements of high end applications. How then can we further increase the purity of the products and what purity can we reach?

According to our current understanding, catalyst may act as the structural template for SWCNT growth.^{15,127} This means that the uniformity of the catalyst nanocrystals is one of the key

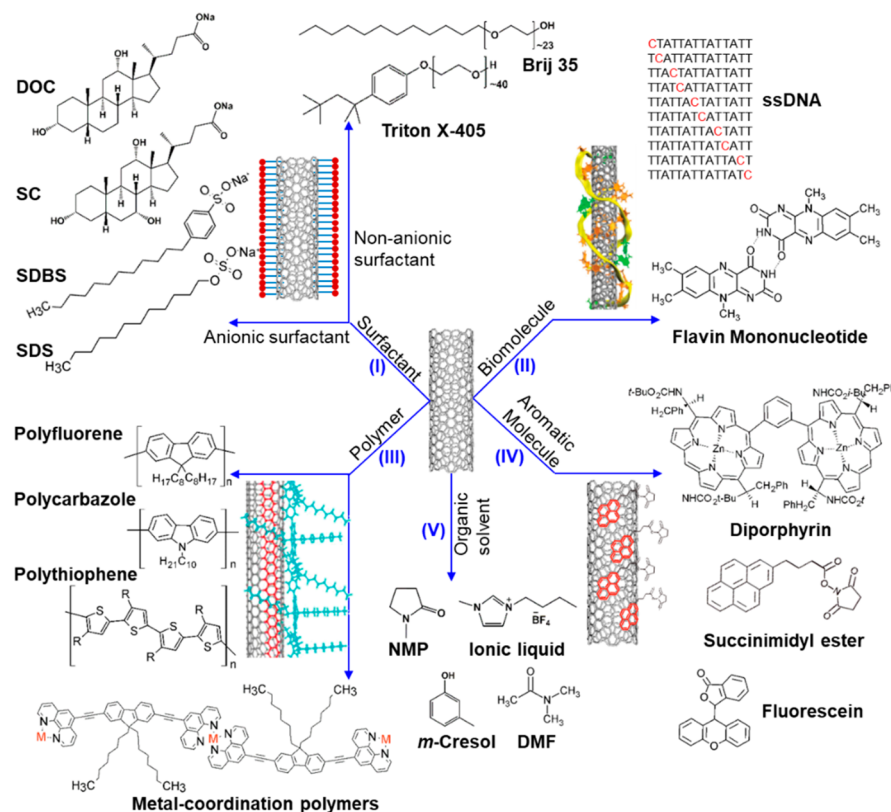


Figure 33. Summary of dispersing agents and solvents used for noncovalent SWCNT dispersion. Part II reproduced with permission from ref 11. Copyright 2009 Nature Publishing Group. Part III reproduced from ref 318. Copyright 2011 American Chemical Society.

factors in improving the chiral purity of SWCNTs, and nanocrystals with identical composition, size, morphology, and structure are ideal. Therefore, great efforts are needed to improve the preparation of catalyst particles, loading on catalyst support, and stability. CVD conditions are another factor that needs to be carefully tuned to avoid any unfavorable nucleation of SWCNTs. After all these efforts, the chiral purity will be further improved under the optimized growth condition. We expect the abundance of ~99% for a single chirality species is possible to reach. Yet we still do not know the highest purity that we can eventually realize.

The current strategy relies very much on the kinetic growth conditions, especially the carbon feeding conditions.^{64,135} So the homogeneity of the carbon decomposition and diffusion at the catalyst surface is of crucial importance for reaching high chiral selectivity. This indicates that the scaling up of the synthesis is very challenging. Currently, successful attempts reported are all surface growth processes on flat substrates. Surface grown SWCNTs are convenient for some applications such as FETs. Bulk synthesis of chirality-enriched SWCNTs with reasonable selectivity has not been realized yet. But we believe the bulk synthesis of chirality-pure SWCNTs can still be expected with the careful design of catalysts, reactors, and CVD procedures.

3. SORTING SWCNTS

Sorting SWCNTs by their atomic structures in liquid medium is an alternative approach to achieve single (n,m) species. Over the years, sorting SWCNTs by length, diameter, conductivity, chirality, and handedness has been intensively studied and is possible now by a number of techniques. These can be found in some reviews,^{299–305} but information about the most recent advances is lacking. Here we will provide comprehensive

coverage of progress in sorting SWCNTs. We begin by defining the challenges in this area. After an account of SWCNT dispersion, sorting methodologies, and mechanisms, we will delve into the main scope of sorting SWCNTs. These discussions are divided into five parts: length, diameter, conductivity, atomic-structure-based chirality, and enantiomer sorting. Some open questions in this field are also discussed in the end.

3.1. A Brief Account of Sorting SWCNTs in Solution

3.1.1. Challenges in SWCNT Sorting. Significant progress has been made in sorting SWCNTs with controlled electronic type and chirality. However, challenges existing in this field should not be underestimated.

First, attaining nondefective, long length, high concentration individual SWCNTs in liquid media is highly demanded for subsequent sorting and further applications. Because of the poor solubility and low dispersibility of the SWCNTs in either aqueous or organic media, extensive ultrasonication and subsequent centrifugation are indispensable procedures, which may cause uncontrolled damage of the nanotube structure and therefore compromised intrinsic properties. In addition, another problem is how to efficiently remove the dispersants from the SWCNT sidewalls after the separation.

Second, the purity, yield, and species of the separated SWCNTs is still far from satisfactory. Most chirality sorting strategies work well only for small diameter (<1 nm) SWCNTs. Chirality separation of larger diameter tubes needs to be developed.³⁰⁶ The chiral purity of sorted SWCNTs needs to be further improved. An atomic level understanding for the selectivity between SWCNTs and dispersants, as well as the

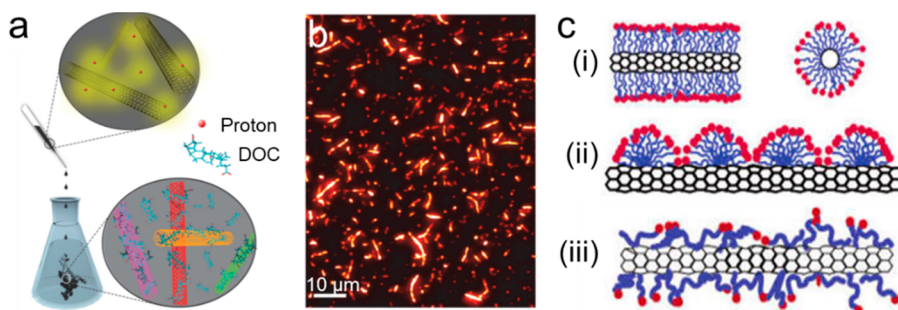


Figure 34. (a, b) Scheme showing the neutralization of a SWCNT–superacid suspension with NaOH aqueous solution in the presence of DOC (a) and bright NIR-photoluminescence image of long individual SWCNTs (b). Reproduced from ref 321. Copyright 2017 American Chemical Society. (c) Schematic showing the mechanisms for dispersing SWCNTs by surfactants: SWCNT–dispersant micelle. Reproduced from ref 319. Copyright 2004 American Chemical Society.

thermodynamic and kinetic control are required for the further improvement of the chiral purity.

Third, and the most important for practical applications, a number of sorting methods are still limited to laboratory studies with limited total quantities and high costs. The challenge lies in efficiently extracting each single (*n,m*) species from their mixtures with low cost. The long operation time and complicated operation steps in some methods limit the utilization in large-scale industrial applications.

3.1.2. Strategies for Dispersion of SWCNTs. The solution-based separation methods require SWCNTs individually dispersed and soluble in liquid medium, such as water and organic solvents. Unfortunately, the raw SWCNTs are always bundled due to the strong van der Waals intertube interactions (\sim eV/nm). A long-standing challenge lies in the poor solubility and low dispersibility of the SWCNTs in both aqueous and organic media due to the hydrophobic nature of the SWCNT sidewall. To resolve this problem, dispersant agents are necessary for surface modification of SWCNTs assisted by stirring, grinding, and ultrasonication. The modification with dispersant agent is generally classified into covalent and noncovalent approaches.

In the early stages, the approaches for SWCNT dispersion focused on covalent functionalization of SWCNTs by incorporating functional groups, to improve the hydrophilicity, solubility, and stability of the SWCNTs to some extent.^{307–310} However, covalent binding decreases the inherent physical and mechanical performance of SWCNTs, owing to structural damage during chemical reaction. Alternatively, noncovalent approaches through either surfactant absorption^{311–314} or π – π stacking with aromatic small molecules^{315–317} or DNA⁶² or polymer^{60,318} wrapping that can help preserve the intrinsic properties of SWCNTs have been more commonly used. Here, we will mainly elaborate on the dispersion of SWCNTs via the noncovalent approaches, classifying them into two categories: aqueous and the nonaqueous systems (Figure 33).

Surfactant. Quite a few ionic (anionic, cationic, and zwitterionic) and nonionic surfactants have been proven effective for dispersing SWCNTs (I, Figure 33), but the mechanisms vary greatly. For ionic surfactants, sodium dodecyl sulfonate (SDS) was the earliest reported for SWCNT dispersion.³¹⁴ Later on, a number of surfactant molecules such as sodium cholate (SC), sodium dodecylbenzenesulfonate (SDBS),³²⁰ and sodium deoxycholate (DOC) have been widely investigated for SWCNT dispersion. A model of “unzipping” was proposed by Smalley et al.^{311,312} to describe the nanotube isolation from the bundle. In this model, the surfactant

molecules intrude in the small spaces of bundles between individual tubes and separate them. Accordingly, surfactants with too bulky hydrophobic groups less easily penetrate the intertube or interplatelet region and show reduced debundling efficiency. Nonionic molecules, such as Triton and Brij,^{312,313} were also found to efficiently disperse SWCNTs in water. Lacking Coulomb repulsion to prevent SWCNTs from aggregating, the nonionic surfactant’s ability to disperse SWCNTs appears to be mainly due to the long or branched disordered polar chains. Surfactants of larger molecular weights disperse more nanotubes due to the improved steric stabilization by longer polymeric chains.³¹²

In general, a SWCNT dispersion is more like a colloidal solution. The solution composition, polarity, and pH can modulate the double-layer structure of the SWCNT micelles and consequently affect the dispersing efficiency. Instead of using ultrasonication and ultracentrifugation to prepare well-dispersed nanotubes, SWCNTs can be easily dispersed in superacid—chlorosulfonic acid. Then by neutralization of the superacid with NaOH/DOC, DOC-dispersed SWCNTs were obtained.³²¹ This is a nondestructive dispersion method. The average tube length is more than 350% longer than that with the sonicated methods (Figure 34a,b). The nondestructive nature of this method resulting in these long individual SWCNTs is a big advantage in many applications. In addition, the concentration of surfactant should be larger than that of the critical micelle and exceed the concentration of nanotubes. Surfactant concentration was found to affect the self-assembled structures of surfactants on the nanotube surface. Several possible models were postulated that SWCNTs form the core of cylindrical micelles of surfactants³²² or are coated by adsorbed hemimicellar surfactants³²⁰ or are randomly coated by surfactants under different concentrations of surfactant (Figure 34c).³¹⁹

Although most of surfactants can achieve monodispersed SWCNTs in aqueous solution with concentration as high as \sim 1 mg·mL⁻¹, they show little preference to specific SWCNTs.³²³ Therefore, atomic-structure-based sorting with surfactant dispersed SWCNTs is always assisted by other methods such as size exclusion chromatography (SEC), IEX, DGU, GCC, and ATP extraction.

Biomolecules. Biomolecules such as DNA,^{62,324–326} nucleotides,³²⁷ polyarginine,³²⁸ and peptides,^{329,330} are another choice of dispersants used in aqueous media and are more versatile and complicated than surfactants (II, Figure 33). Among these biomolecules, DNA is of great importance. In 2003, Zheng et al. first reported the well-dispersed SWCNTs by single-stranded DNA (ssDNA) in aqueous solution.⁶² They proposed that two-

dimensional sheets of the periodic purine–pyrimidines linked by hydrogen bonds can selectively wrap certain nanotubes (Figure 35). With this strategy, further separation of SWCNTs with desired structures was realized assisted by techniques of IEX, DGU, and ATP extraction.

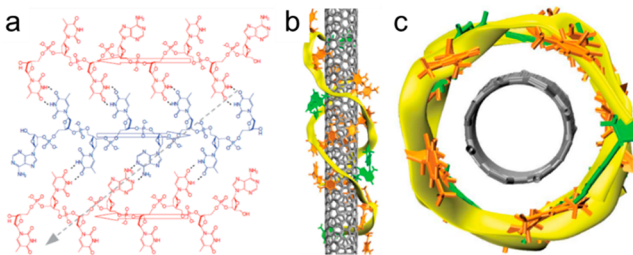


Figure 35. (a) 2D DNA sheet. (b, c) Side (b) and vertical (c) views of a DNA barrel on an (8,4) nanotube formed by wrapping a 2D DNA sheet. Reproduced with permission from ref 11. Copyright 2009 Nature Publishing Group.

Other biomolecules such as nucleotides,³²⁷ polyarginine,³²⁸ and peptides^{330,331} can be also used for the dispersion of SWCNTs in water. These biomolecules with their aromatic and hydrophobic side chains can form hydrophobic and π – π interactions with SWCNTs.³³² For example, the flavin mononucleotide can self-assemble to form a two-dimensional ribbon and wrap nanotubes with coaxial π – π interactions, resulting the dispersion of SWCNTs.³²⁷ However, most of these macromolecular systems did not realize the subsequent structure-controlled sorting of SWCNTs.

Conjugated Polymers. In organic solvents, some conjugated polymers, such as polyfluorene (PFO), regio-regular polythiophene, and polycarbazole, have been found to be powerful agents to debundle and disperse SWCNTs by wrapping around nanotubes through noncovalent π – π interactions (III, Figure 33).⁶⁰ Additionally, the conjugated polymer dispersed SWCNTs usually have simultaneous enrichment of s-SWCNTs. This aspect will be discussed in a later section in detail.

Small Aromatic Molecules. Small aromatic molecules, such as pyrene-carrying ammonium ion, polycyclic aromatic ammonium amphiphiles, rhodamine B, fluorescein, and diporphyrin, have been used to disperse SWCNTs via π – π interaction (IV, Figure 33).^{315–317,333,334} In addition, other π – π conjugated systems such as small pieces of graphene and graphene oxides also proved effective for dispersing SWCNTs.^{335,336} Among these aromatic compounds, rhodamine B and fluorescein can disperse SWCNTs in aqueous solution as they hold both hydrophilic and hydrophobic moieties, similar to surfactants. Dispersing SWCNTs by fluorophore or dye

molecules was reported to be a kinetic behavior, which is not related to thermodynamic stability of their complex.³¹⁷ The efficiency of dispersion may be determined by the on-rate of these molecules to the SWCNT surface instead of the off-rate. When chiral centers are present in aromatic molecules (for example, chiral diporphyrin), they can separate enantiomers of SWCNTs owing to their different affinities to left- and right-handed nanotubes.³¹⁶

Direct Dispersion of SWCNTs in Organic Solvent. In addition to the dispersing agents, organic solvents such as ionic liquids,³³⁷ N-methyl-2-pyrrolidone (NMP),³³⁸ *m*-cresol,³³⁹ and *N,N*-dimethylformamide (DMF) can also disperse SWCNTs (V, Figure 33). For instance, SWCNTs were found to easily disperse in the imidazolium-based ionic liquid to form a thermally stable gel just by mechanical milling. The SWCNT content can be as high as 1%.³³⁷ The imidazolium ions were proposed to interact with the tube wall through “cation– π ” interaction and thus exfoliate the nanotube bundles.³⁴⁰ Further spectroscopic and molecular modeling studies demonstrated that SWCNTs interact with ionic liquid through weak van der Waals interactions other than the cation– π interaction.³³⁹ However, none of these organic solvents can be used alone to realize the subsequent separation of SWCNTs.

In summary, dispersing SWCNTs via the noncovalent approach is mainly through van der Waals interactions, π – π stacking, and hydrophobic interactions. The dispersibility of SWCNTs in nonaqueous solution is generally lower than that in the aqueous systems. Although it can be significantly improved by choosing appropriate organic solvents and regulating the polymers (polymer backbone, side-chain, molecular weight, and interaction mode), the difficulty of removing polymer wrapped on tube walls still limits their applications.

3.1.3. Methodologies and Mechanisms of Sorting SWCNTs.

Solution based approaches have proven to be effective for sorting SWCNTs dispersed by noncovalent wrapping. Reported sorting methods include (di-)electrophoresis,^{61,341} DGU,³⁴² IEX,³²⁴ SEC,^{343,344} GCC,^{345,346} polymer or small molecular extraction,^{60,347} and ATP extraction (Figure 4).³⁴⁸ We will briefly describe the mechanisms for sorting SWCNTs.

Dielectrophoresis. Alternating current dielectrophoresis, first proposed by Krupke et al. in 2003, is based on different mobilities of SWCNTs in medium when an external electric field is introduced.⁶¹ Due to the striking difference in the dielectric constants of the m- and s-SWCNTs, the m-SWCNTs with larger dipole moments move faster toward the electrode than s-SWCNTs (Figure 36). This method can be also used to selectively manipulate and deposit the SWCNTs in solution into an array of uniform electronic type. Due to the limitations to

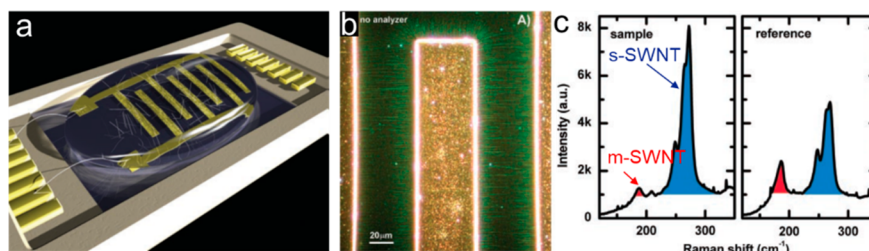


Figure 36. (a) Illustration of dielectrophoresis. (b) Rayleigh scattered light from the dielectrophoretically deposited SWCNTs and the electrodes. (c) Raman spectra of SWCNTs (excitation 514.5 nm). Reproduced with permission from ref 61. Copyright 2003 American Association for the Advancement of Science.

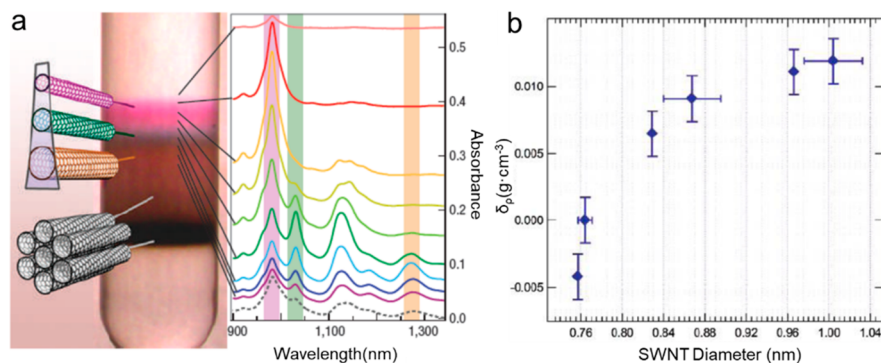


Figure 37. (a) Photograph showing the discrete bands of SWCNTs separated by DGU and corresponding absorption spectra of each band. Reproduced with permission from ref 14. Copyright 2006 Nature Publishing Group. (b) SWCNT diameter as a function of buoyant density. Reproduced from ref 342. Copyright 2005 American Chemical Society.

achieving single-chirality species and large-scale separation, as well as complicated separation processes and low separation efficiency, this method did not receive much attention later.

Ion Exchange Chromatography. In 2003, IEX was first reported by Zheng et al. to separate DNA-wrapped SWCNTs (DNA-SWCNTs). Initially, SWCNTs with narrow diameter distribution and defined electric type were separated with IEX on the basis of different adsorption and desorption of SWCNT–DNA hybrids on functionalized resins (Figure 4).³²⁴ Later on, they systematically studied the effects of DNA wrapping configuration and tube dielectric properties and found that the charge density of the DNA–SWCNT is most important for separation, indicating an electrostatic interaction-based mechanism.³⁴⁹ However, further investigation on sorting SWCNTs of single-chirality with DNA suggested another possible mechanism. The structure of SWCNT–DNA hybrids is determined by the ssDNA sequence and tube chirality, which in turn affects the adsorption and retention of various (n,m) SWCNTs on the stationary phase.^{11,62,324,350} Understanding the relationships between a tube's chirality, DNA–SWCNT configuration, and interactions between hybrid and resin are important in IEX based separation.

Density Gradient Ultracentrifugation. Inspired by biochemical separation methodologies, Hersam's group first demonstrated the sorting of DNA–SWCNTs by DGU with selective diameter and conductivity separation,^{14,342} which is a big breakthrough in the field of nanotube sorting. Surfactant–SWCNTs with their buoyant densities determined by tube diameter and electronic type were separated in a density gradient medium under high centrifugal force. The measured density of SWCNTs was found to increase with increasing nanotube diameter (Figure 37). Additionally, other factors including the surface coating by surfactants, hydration layer, and charge distribution can also affect the buoyant density.³⁵¹ These factors vary the density of SWCNTs and enable their separation by ultracentrifugation in a density gradient. Although DGU technique appears to be a powerful approach for SWCNT sorting, it still suffers from the disadvantages of multistep centrifugation, high-cost equipment, and long-time operation, thus limiting its practical application to some extent.

Gel Column Chromatography. Around the year 2009, two groups from Japan and Germany reported chromatography-based separation of SWCNTs.^{345,346,352} This technique was based on the differential partition of SWCNTs between the mobile and stationary phases. Upon injection of the surfactant-wrapped SWCNTs into the agarose gel, s-SWCNTs present

stronger interaction with gels than m-SWCNTs, which allows the simple extraction of s-SWCNTs (Figure 38). Kataura's

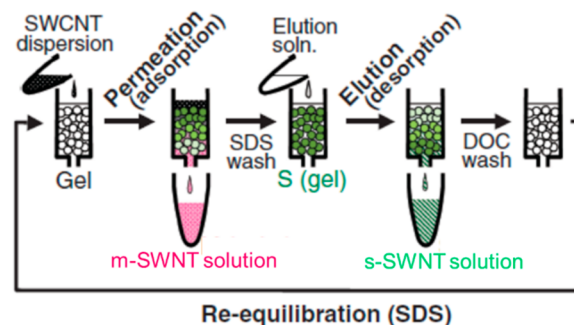


Figure 38. Schematic diagram of m- and s-SWCNT separation using a column filled with agarose gel beads. Reproduced with permission from ref 346. Copyright 2009 Japan Society of Applied Physics.

group further demonstrated the diameter and chirality based separation of SWCNTs with the rational choice of surfactant composition to modulate the hydrogel/tube interaction. This method allows chirality¹² and handedness³⁵³ separations but is still limited to separation of semiconducting (n,m) species.

Selective Dispersion and Extraction by Polymers. Dispersion of SWCNTs by certain polymers shows surprisingly high selectivity toward the s-SWCNTs, which was first demonstrated by Nicholas et al. in 2007 by using the simplest PFO.⁶⁰ This technique only involves (1) sonication of SWCNT and polymer mixtures in organic solvents for around 30 min to disperse SWCNTs, (2) centrifugation of polymer wrapped SWCNT solution for 1–2 h to sediment the SWCNT aggregates and m-SWCNTs, and (3) collection of the s-SWCNT supernatants, which are ready for use.⁶⁰ To realize single-chirality or enantiomer sorting, chiral groups on either the polymer side chain or the polymer backbone have been introduced in PFO derivatives.^{318,354} Molecular modeling indicates that single chirality selectivity might be due to a cooperative effect between the chiral groups and polymer wrapping conformations.³¹⁸

For the family of polythiophenes, another group of widely used conjugated polymers to selectively disperse s-SWCNTs, a polarizability-based mechanism was suggested by DFT calculations.³⁵⁵ Compared to s-SWCNTs, m-SWCNTs exhibit 10^3 larger polarizability due to their higher carrier concentrations. Due to the strong polarizability of m-SWCNTs, theoretical

studies indicate that m-SWCNT/polymer complexes possess stronger charge transfer interactions than s-SWCNT/polymer complexes. The more polar m-SWCNT/polymer complexes therefore tend to aggregate or bundle in nonpolar solvents, forming a sediment after centrifugation, while polymer wrapped s-SWCNTs remained in the supernatant.³⁵⁵ This mechanism has been supported by some experimental results including solvent, polymer backbone, and side chain effects.³⁵⁶ For instance, nonpolar solvents (e.g., toluene, *m*-xylene) usually show better selectivity to s-SWCNTs than a polar solvent (e.g., tetrahydrofuran).^{356,357}

Aqueous Two-Phase Extraction. Sorting SWCNTs with ATP extraction was first reported by Zheng et al. in 2013.³⁴⁸ This was realized by mixing polyethylene glycol (PEG) and dextran to form two immiscible aqueous phases and allowing nanotubes to selectively partition between dextran-rich and PEG-rich phases according to tube structure (Figure 39). This

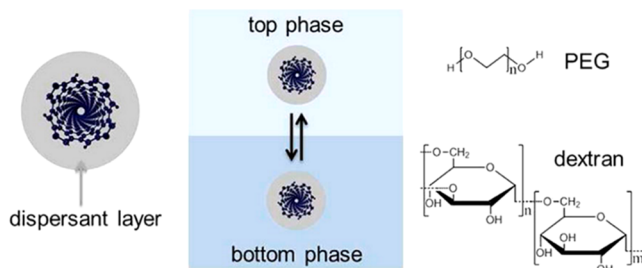


Figure 39. Spontaneous partition of SWCNTs in PEG/dextran two-phase system. Top phase is PEG-rich, and bottom phase is dextran-rich. Reproduced from ref 348. Copyright 2013 American Chemical Society.

chirality selective partition is caused by the difference in nanotube's intrinsic hydrophobicity and the resultant solvation energy. The technique is promising with advantages such as low equipment requirement, simple operation, short separation time, and good scalability.

According to the practical requirements and sorting conditions, separation of SWCNTs can be achieved in five different areas, that is, length, diameter, conductivity, chirality, and enantiomers (Figure 4). However, it is important to keep in mind that the separation of SWCNTs is usually accomplished simultaneously in those different areas. For example, most of the diameter dependent separation is the result of enrichment of several (*n,m*) species, accompanied additionally by conductivity enrichment. Therefore, to avoid repetition, we will briefly introduce various methods used in the length, diameter, and conductivity separation of SWCNTs in next section. In chirality (section 3.3) and enantiomer sorting (section 3.4) sections, specific examples will be discussed in detail.

3.2. Length, Diameter, and Conductivity Based Sorting of SWCNTs

3.2.1. Length-Based Sorting of SWCNTs. The widely used ultrasonication and ultracentrifugation approaches always cut nanotube into short species with a broad range of length distribution, ranging from several nanometers to micrometers. Sorting SWCNTs to achieve uniform length has been extensively explored for various applications, such as quantum confinement³⁵⁸ and bioimaging.³⁵⁹ A uniform distribution of length is also beneficial for improving the chirality sorting. Several strategies for SWCNT length fractionation have been demonstrated, including SEC,^{343,360,361} field flow fractionation,^{362,363} DGU,^{364,365} cross-flow filtration,³⁶⁶ and selective

precipitation.^{367,368} Among these approaches, the hydrodynamic radius-based SEC method has been used in sorting SWCNTs with uniform length.^{343,360,361,365,369} SWCNT samples with different lengths stay in the mobile phase in SEC, and the mobility of SWCNTs is inversely proportional to the tube length.³⁶⁰ Zheng et al. demonstrated the separation of DNA-wrapped SWCNTs with precisely controlled length by SEC.³⁶⁷ They further extended this technique to the more commonly used surfactant-dispersed SWCNT systems by using porous silica and bile salt solution as stationary and mobile phases, respectively (Figure 40a).³⁶⁹ This method can reduce

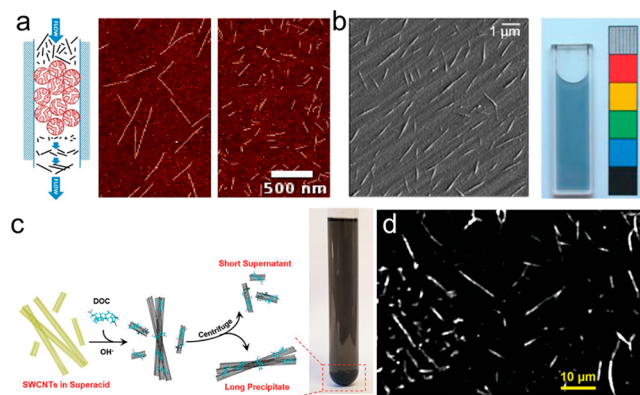


Figure 40. (a) Schematic of length sorting of SWCNTs with SEC and representative AFM images. Reproduced from ref 369. Copyright 2013 American Chemical Society. (b) AFM image of nanotubes with averaged length of 960 nm and photograph showing the color of the solution for the spectra shown. Reproduced with permission from ref 365. Copyright 2008 Wiley. (c) Scheme of the self-sorting process of ultralong SWCNTs. (d) PL image of the sorted ultralong s-SWCNTs. Reproduced with permission from ref 374. Copyright 2019 Wiley.

the tube length variation to 10% in sorted fractions and are scalable in principle. Zheng et al. developed a simple method to separate SWCNTs with fractionated length by tuning PEG concentration.³⁷⁰ Shorter SWCNTs tend to assemble into a reversible cluster at higher PEG concentration, which was then separated by gentle centrifugation. Although the length uniformity is lower than that obtained from the SEC method, the selective precipitation method is far more facile and scalable since it does not require elaborate equipment. Other methods such as modification of SWCNTs^{362,371,372} and truncation of SWCNTs by acid treatment³⁷³ were also developed to achieve length separation but with poor length uniformity.

Dispersing individual SWCNTs with long length in solution is another long-standing challenge. Nanotube length is generally less than 1 μm by the above methods. Fagan et al. achieved length fractionated SWCNTs in excess of 1 μm by ultracentrifugation (Figure 40b).³⁶⁵ They suggested that the length separation is allowed by the differences in the scaling of the buoyancy and frictional forces, and thus longer SWCNTs move at a larger rate in opposition to the applied acceleration. Recently, tube length was extended to $\sim 10 \mu\text{m}$ by using a so-called "self-sorting" method, proposed by Wang et al.³⁷⁴ The short SWCNTs dispersed by neutralizing chlorosulfonic acid tend to stay as an isotropic phase due to the weak interaction. Long tubes tend to self-align as bundles and precipitate at the bottom of the solution and thus can be separated by centrifugation (Figure 40c,d). This chlorosulfonic acid-based

dispersion combined with self-sorting method has potential in fabricating ultralong single-chirality SWCNT arrays.

3.2.2. Diameter-Based Sorting of SWCNTs. The diameter separation of SWCNTs appears to be partial or incomplete chirality sorting, which was extensively explored in the early years.^{62,324,341} In 2003, Zheng et al. first demonstrated the diameter separation of DNA-dispersed SWCNTs followed by IEX to yield nanotubes with narrow diameter distribution.³²⁴ Each fraction of these separated SWCNTs showed the same chemical environment without doping.³⁷⁵ Arnold et al. demonstrated the diameter separation of DNA-dispersed SWCNTs in aqueous density gradients by DGU.³⁴² They separated SWCNTs of different diameters in the density gradients of iodixanol with different buoyant densities. The measured density of SWCNTs was found to increase with increasing nanotube diameter (Figure 37a,b). The DGU method was further utilized to separate water-filled SWCNTs from empty ones.³⁷⁶ Kataura et al. also developed diameter separation of SWCNTs by agarose gel chromatography.³⁷⁷ The m-SWCNTs were eluted with SDS solution first. Subsequently, the s-SWCNTs that remained in the gel column were collected with DOC solution as the eluant. By gradually increasing the concentrations of DOC eluant at each fraction, small diameter tubes were eluted first at the lower concentration DOC and then large diameter tubes were eluted with the higher DOC concentration (Figure 41). Conjugated polymer extraction is

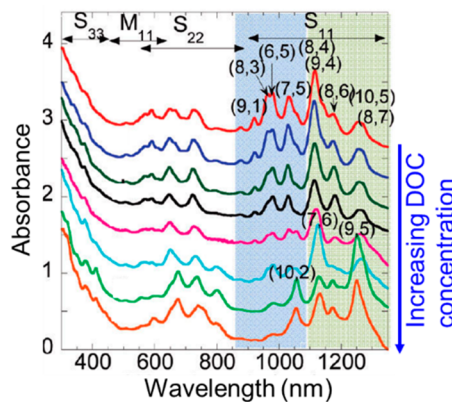


Figure 41. Absorption spectra of the s-SWCNTs with different diameter distributions by gradually increasing the DOC concentration. Reproduced from ref 377. Copyright 2010 American Chemical Society.

another effective way to separate SWCNTs with narrow diameter distribution.³⁷⁸ By designing conjugated polymers with different structures, larger diameter ($d_t > 1.3$ nm) SWCNTs with narrow distribution can also be realized from arc-discharge SWCNT samples.³⁷⁹

3.2.3. Conductivity-Based Sorting of SWCNTs. In this section, we provide a comprehensive summary of the strategies for sorting m- and s-SWCNTs by noncovalent interactions with various dispersants.

Conductivity-Based Separation of Surfactant Dispersed SWCNTs. Prior to 2006, a number of reports on metal and semiconducting SWCNT separation with varying degrees of success appeared in the literature.³⁰⁰ In 2006, the pioneering work on the m- and s-SWCNT separation via DGU was reported by Arnold et al. The choice of competing cosurfactants to disperse nanotubes resulted in subtle differences in buoyant densities of m- and s-SWCNTs (Figure 37a).¹⁴ Later, Yanagi et al. modified DGU by using sucrose instead of iodixanol as

density gradient medium. They achieved high-purity s- and m-SWCNT sorting by lowering the temperature and increasing the surfactant concentration with improved separation capability.³⁸⁰

GCC, first reported by Kappes et al.,³⁵² is an especially simple, effective, and scalable method for sorting SWCNTs. The procedure initially involves sonicating the SWCNTs in an aqueous SDS solution. The m-SWCNTs pass through the Sephadryl-200 packed column, while the s-SWCNTs are retained at the top of the column. The s-SWCNTs are then eluted via the addition of a second surfactant (typically sodium cholate).³⁵² Around the same time, Kataura's group demonstrated the success of using agarose gel beads as column media (Figure 42a,b).³⁴⁶ Several studies since then have shown that the

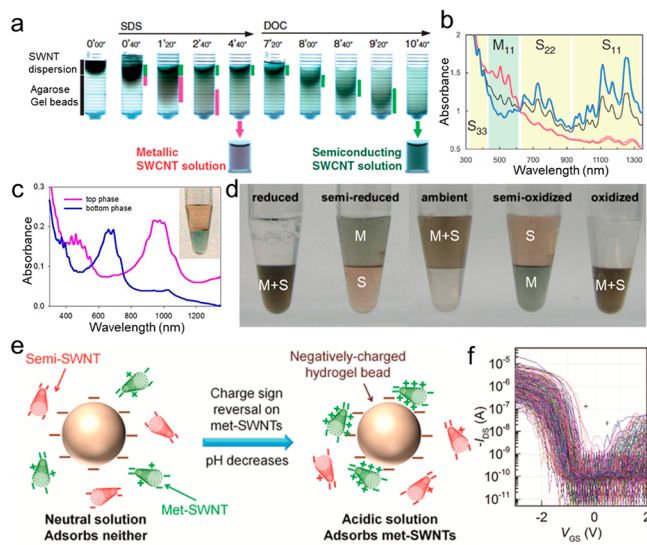


Figure 42. (a, b) Sequential photographs showing the progress of sorting m- and s-SWCNTs in an agarose gel packed column (a) and absorption spectra (b). Reproduced with permission from ref 346. Copyright 2009 Japan Society of Applied Physics. (c) Absorption spectra. Reproduced from ref 348. Copyright 2013 American Chemical Society. (d) Redox-governed m- and s-SWCNT partition in a PEG/dextran two-phase system. Reproduced from ref 389. Copyright 2015 American Chemical Society. (e, f) Schematic of the charge sign reversal chromatographic sorting process (e) and transfer characteristics of 320 devices (f). Reproduced from ref 390. Copyright 2016 American Chemical Society.

mechanism is likely dominated by selective adsorption of the s-SWCNTs to the column media.^{381,382} They further impressively demonstrated high purity and yield of m- and s-SWCNT separation by optimizing the components and concentration of eluate, as well as the process parameters, such as column type, column length, temperature, and pH.^{12,377,383,384} The purity of s-SWCNTs was further improved to 99.9% by Tulevski et al. using iterative GCC. They fabricated 4212 FETs with these separated tubes, in which only 6 devices displayed metallic behavior.³⁸⁵

The ATP extraction provided a new solution to separate m- and s-SWCNTs in two phases containing PEG/dextran with different hydrophilicity (Figure 42c).³⁴⁸ s-SWCNTs are more hydrophobic due to their lower polarizability and m-SWCNTs are more hydrophilic; thus s- and m-SWCNTs selectively partition in two phases. This method was also able to sequentially separate double-walled CNTs (DWCNTs) by electronic type and diameter.³⁸⁶ The tube–surfactant hydration is the key factor for ATP extraction. ATP extraction can also be

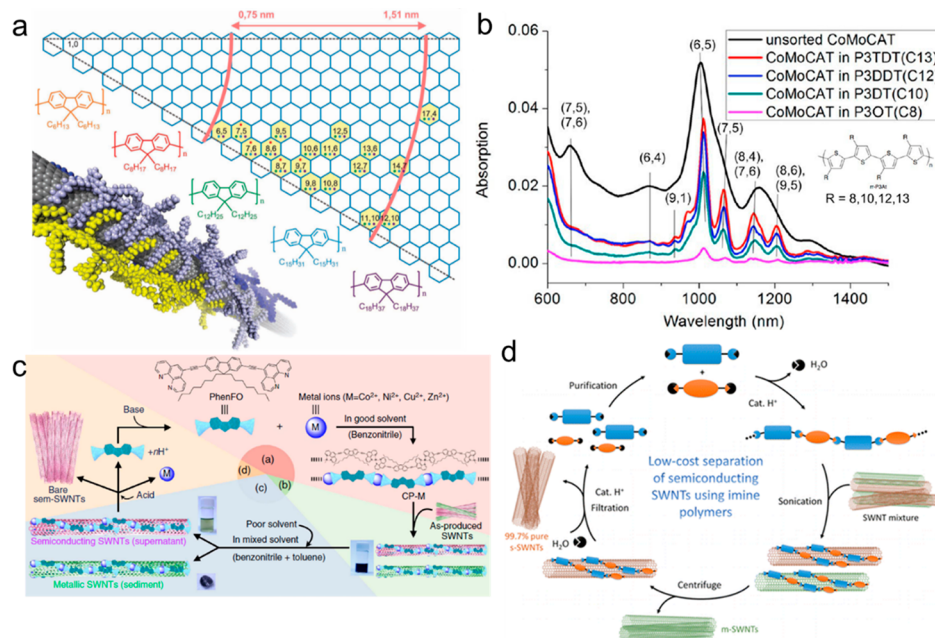


Figure 43. (a) Chirality map of different diameter distributions of s-SWCNTs selected by PFO derivatives with different length of side chains. Reproduced with permission from ref 379. Copyright 2013 Wiley. (b) Absorption spectra for polythiophene-sorted SWCNTs in toluene. Reproduced from ref 400. Copyright 2014 American Chemical Society. (c) Method for s-SWCNT sorting using removable solubilizers. Reproduced with permission from ref 408. Copyright 2014 Nature Publishing Group. (d) Proposed separation cycle of pure s-SWCNTs using imine polymers. Reproduced from ref 413. Copyright 2016 American Chemical Society.

improved by lowering the temperature and multiple-cycle extracting.^{387,388}

Zheng et al. further found that redox reactions play very important roles in the conductivity separation via ATP extraction.³⁸⁹ They used NaBH₄ as reductant and NaClO as oxidant and tried to configure the surfactant coating layer on SWCNTs by tuning the electron-transfer between redox molecule and tube (Figure 42d). The highest purity of purified s-SWCNTs was reported to be $99.94 \pm 0.04\%$ by Chan-Park et al.³⁹⁰ When the pH was tuned to set the redox potential of the O₂/H₂O couple at certain value, the surface charge of m-SWCNTs was inverted to cationic, whereas s-SWCNTs remained anionic. Then the cationic SWCNTs were preferentially attracted by anionic agarose chromatography beads; thus ultrahigh purity s-SWCNTs were achieved in a single chromatography pass (Figure 42e,f). This method closely resembles a 2005 report by Jagota et al.³⁹¹

Conductivity-Based Separation of Polymer Wrapped SWCNTs. Conjugated polymers have been proven to be an effective method to dissolve and extract only s-SWCNTs in organic solvents. After the first report of using PFO to extract s-SWCNTs from CoMoCAT samples by Nicholas et al.,⁶⁰ a large amount of extractants such as PFO derivatives, thiophene- and carbazole-based polymers, and their copolymers have been widely adopted and further developed by several groups.^{302,305,347,392} The polymer structure including backbone structure, side chain length, and molecular weight were found to affect the diameter or chirality distributions of extracted s-SWCNTs.^{354,378,379,393–400} It was consistently found that, within a given polymer series, increasing the aromatic surface area of repeat units within the backbone is correlated with the dispersion of larger-diameter s-SWCNTs (Figure 43a).^{379,392,401–404} A library of 23 types of fluorene- and carbazole-based polymers with different backbone structures was investigated by Mayor et al. It was found that 2,7-linked

conjugated polymers produce more stable SWCNT dispersions than the 3,6-linked analogs.³⁹⁶ Besides the structural factors, the solvent types (density, viscosity, polarity, aromaticity, and solvent architecture) and treatment conditions (temperature, sonication, and precipitation during the process) were also extensively explored to improve the selectivity toward s-SWCNTs.^{356,392,393,405–412}

For the practical application of sorted s-SWCNTs, there are several serious problems when using polymer extraction, that is, low extraction efficiency and difficulty in removal of wrapped polymers from SWCNT/polymer composite.

To improve the yield, longer alkyl chains in the polymer proved effective,^{396,400} and some polymers with a higher molecular weight tended to solubilize nanotubes with a higher concentration. For instance, Bao et al. found that yield of the s-SWCNTs extracted from a CoMoCAT sample is significantly increased when the side-chain length of polythiophene extractants is increased (Figure 43b). MD simulations including explicit toluene molecules demonstrated that the improved yield is due to the increased surface contact area between the SWCNTs and the longer side chain of polymers.⁴⁰⁰

To remove polymer from SWCNT/polymer composites after extraction, polymer backbones that are degradable and recyclable and that selectively disperse s-SWCNTs have been developed, with removal mechanisms including supramolecular complex chemistry,⁴⁰⁸ hydrogen bond disruption,⁴¹⁴ and imine hydrolysis.⁴¹³ An impressive strategy was reported by Toshimitsu and Nakashima⁴⁰⁸ in 2014. They developed a kind of PFO-like polymer coordinated by metal ions that can separate s-SWCNTs. Then this polymer on the SWCNTs was efficiently depolymerized into monomer components by adding protic acid (Figure 43c).⁴⁰⁸ Later on, imine-based conjugated copolymers also proved effective for reversibly attracting and releasing s-SWCNTs. This kind of polymer can be depolymerized into

monomers by breaking imine bonds at mildly acidic conditions, yielding polymer-free s-SWCNTs (Figure 43d).⁴¹³

In general, enrichment or even separation of SWCNTs with different conductivity or different structures can be realized using surfactants as dispersing agents in aqueous systems. The disadvantages lie in the large amount of surfactants required, the time-consuming ultrasonication, and the resulting increased defects on SWCNTs. How to achieve massive m- and s-SWCNT samples with higher purity, fewer defects, and longer lengths to meet the requirements by nanoelectronics is still a challenge in this field.

3.3. Sorting SWCNTs by Chirality

At present, in addition to CVD growth, solution-based separation has become another effective way to achieve single (*n,m*) SWCNTs. To date, there have been 40 kinds of enriched or high-purity (*n,m*) species and their enantiomers in the diameter range of 0.6–1.5 nm achieved by different separation methods (Figure 44). We will introduce the progress on separation development for SWCNTs based on the different systems.

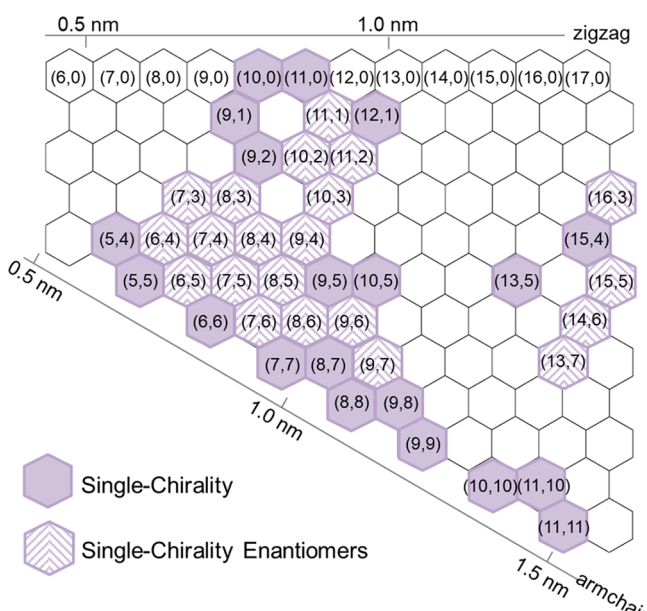


Figure 44. Summary of (*n,m*) species of SWCNTs and their enantiomers achieved by sorting.

3.3.1. Sorting SWCNTs Dispersed by Surfactants. The surfactant dispersion system is the most widely used and mature system in the field of SWCNT chirality sorting, which has been proven to be valid for DGU, GCC, and ATP extraction methods.

Density Gradient Ultracentrifugation. On the basis of diameter sorting, the realization of single-chirality sorting by DGU relies on enhancing the density difference among SWCNTs with different (*n,m*) species so that the separation of specific chirality SWCNTs can be achieved by means of ultracentrifugation. There are generally two strategies to amplify the density difference. One is the modification of the density gradient medium. Weisman et al. made a breakthrough by introducing nonlinear DGU and successfully obtained ten enriched (*n,m*) species and even their enantiomers,⁴¹⁵ which will be discussed in section 3.4.1. Another work of Green and Hersam showed that (6,5) SWCNTs with abundance of 84% are produced via orthogonal iterative DGU.⁴¹⁶ Another strategy is

the modification of the surfactant. The adsorption of a surfactant on a tube with a specific structure is different, and the density of the surfactant–SWCNT composite formed therefore changed. For example, cosurfactants of SDS and DOC were proposed to form a DOC-enriched SDS–DOC co-wrapped SWCNT configuration, which results in chirality redistribution by DGU and 97% pure isolation of (6,5) nanotubes.⁴¹⁷ Other techniques such as selective encapsulation of water³⁷⁶ or organic molecules⁴¹⁸ into the inner wall of tube were also developed to amplify the density differences and therefore achieve (*n,m*) species enrichment by DGU.

Gel Column Chromatography. In 2011, Kataura's group first reported the large-scale separation of SWCNTs with 13 types of (*n,m*) species by GCC,¹² and they further realized milligram-scale throughput in 2016 (Figure 45).⁴¹⁹ This achievement is the result of the chirality-dependent interaction strength of tubes with allyl dextran-based gel. Thus, the SWCNTs with different bonding interactions will be adsorbed in different adsorption sites of the column, resulting in the chirality separations of SWCNTs by sequential elution. The initial separation can be repeated to improve the chiral purity. However, the efficiency and yield will be decreased. GCC technique was further modified to efficiently amplify the interactions between SWCNTs and the gel by ethanol,⁴²⁰ temperature,³⁸⁴ pH,^{421–423} and salts;⁴²⁴ chirality separation and yields were then improved greatly. For example, by accurately optimizing pH (accuracy ~0.1) of the surfactant solution with CO₂ bubbling, Yanagi et al. achieved a high purity (>99%) of the single-chirality (6,5) samples without residual m-SWCNTs.⁴²¹ However, there have been fewer works reported for separating metallic (*n,m*) species with GCC. Only metallic (10,4)-enriched SWCNTs were achieved by Kataura et al., which was conducted at a low SDS concentration to increase the interaction between the gel and the m-SWCNTs.⁴²⁵ The purity of metallic (*n,m*) species may be improved by repeated separations or utilizing a longer column or columns connected in series.

Aqueous-Two Phase Extraction. On the basis of ATP extraction developed by Zheng et al. in 2013, Fagan et al. further improved the sorting resolution of single (*n,m*) species by carefully regulating the surfactant concentrations in two phases.⁶³ They found that SWCNTs selectively partition from bottom (dextran enriched phase) to top (PEG enriched phase) upon gradually increased of the concentration of SDS or DOC. This preferential partition for each (*n,m*) is monotonic to the SDS concentration, which enables sequential separation (Figure 46). Multiple (*n,m*) species were isolated in 3–10 steps with this method, and each step requires <5 min.⁶³ This technique was further proven to be valid for separation of large-diameter (*n,m*) species ($d_t \approx 1.4$ nm).^{306,426} Duque et al. further studied the mechanism of ATP extraction of surfactant dispersed SWCNTs.⁴²⁷ They proved that the main driving force of nanotubes in two phases is the hydrophilicity of the surfactant adsorbed on the nanotube surface but not the intrinsic nanotube hydrophobicity. Specifically, the DOC-coated SWCNTs are more hydrophilic than the SDS-coated ones. The addition of salts, such as NaCl and NaSCN, may cause structural reorganization of the surfactant adsorbed on the tube surface, which in turn affects its hydrophilicity. They combined multiple surfactants in suitable concentration ratios and then tuned them with appropriate salts, finally obtained highly enriched (6,5) and (7,5) nanotubes in just 1 or 2 steps, thereby improving chiral separation of SWCNTs. Most recently, Flavel et al. showed that by using pH tuning, 11 different single chirality SWCNTs can be

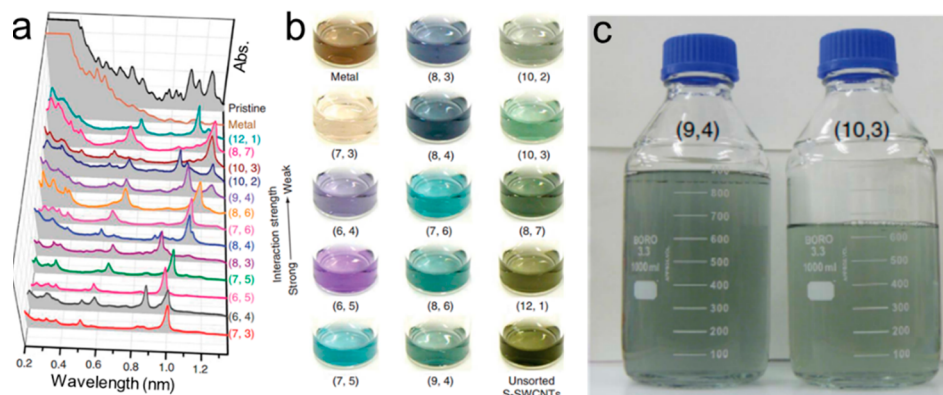


Figure 45. (a, b) Optical absorption spectra (a) and photographs of 13 (n,m) SWCNTs with distinct colors (b). Reproduced with permission from ref 12. Copyright 2011 Nature Publishing Group. (c) Photographs of (9,4) (900 mL) and (10,3) (600 mL) SWCNT dispersions. Reproduced with permission from ref 419. Copyright 2016 Nature Publishing Group.

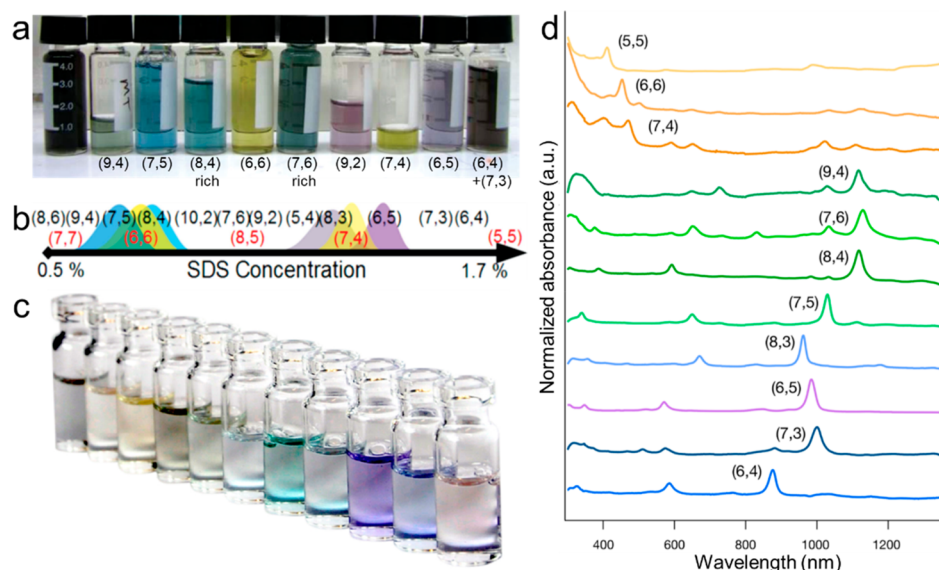


Figure 46. (a) Photograph showing ATP extracted SWCNT enriched or single (n,m) species. (b) Approximate order of partition to the top phase with increasing SDS concentration at fixed DOC concentration. Reproduced with permission from ref 63. Copyright 2014 Wiley. (c) Photograph showing ATP extracted 11 different single-chirality SWCNTs. (d) Absorption spectra of the isolated (n,m) fractions. Reproduced from ref 428. Copyright 2019 American Chemical Society.

purified in no more than three steps by ATP (Figure 46c,d).⁴²⁸ This finding greatly simplifies the technique and has potential to be applied to the purification of larger diameter single-chirality nanotubes.

The above results with ATP separation are obtained with surfactant dispersions of SWCNTs. Zheng's group further extended the ATP extraction to sorting SWCNTs dispersed by DNA,⁴²⁹ which will be discussed in next section.

Separation of surfactant dispersed SWCNTs provides a convenient way to obtain single-chirality SWCNTs. However, there are still some challenges in the surfactant system: (1) surfactants absorbed on SWCNTs are not easily removed, which greatly reduces the electrical properties of SWCNTs; (2) ultrasonic operation during dispersion shortens the length of the SWCNTs, mostly less than 1 μm ; (3) the cost of consumables and equipment used is high, and the operation process is difficult to master, making it difficult to promote and be used at large-scale.

3.3.2. Sorting SWCNTs Dispersed by DNA.

DNA proved to be very promising for sorting single-chirality SWCNTs.

However, the yields and the types of (n,m) SWCNTs are very limited in early works.^{350,430,431} In 2009, Zheng et al. reported that IEX sorting of DNA-wrapping of SWCNTs yields 12 major single-chirality semiconducting species¹¹ and further achiral (6,6) and (7,7) tubes.²⁹⁰ Special DNA/SWCNT pairs were selectively extracted with IEX owing to their weak electrostatic interaction with resin (Figure 47a). Although IEX-based sorting realized the atomic-scale recognition of DNA and nanotube, it still faces some problems. Searching specific DNA sequences from a vast database is time-consuming and expensive, and DNA is more costly than small-molecule surfactants.

To improve the efficiency of separation, Zheng's group⁴²⁹ combined the highly specific DNA recognition with the ATP extraction. Partition of the SWCNTs in a polymer-modified two phase system was found to be sensitive to DNA sequence, which is possibly related to the solvation energy. With rational choice of DNA sequence, polymer composition (poly(vinylpyrrolidone), polyacrylamide or poly(ethylene glycol) diamine) in two-phase systems, and partition modulators, 15 kinds of single-chirality nanotubes were separated (Figure

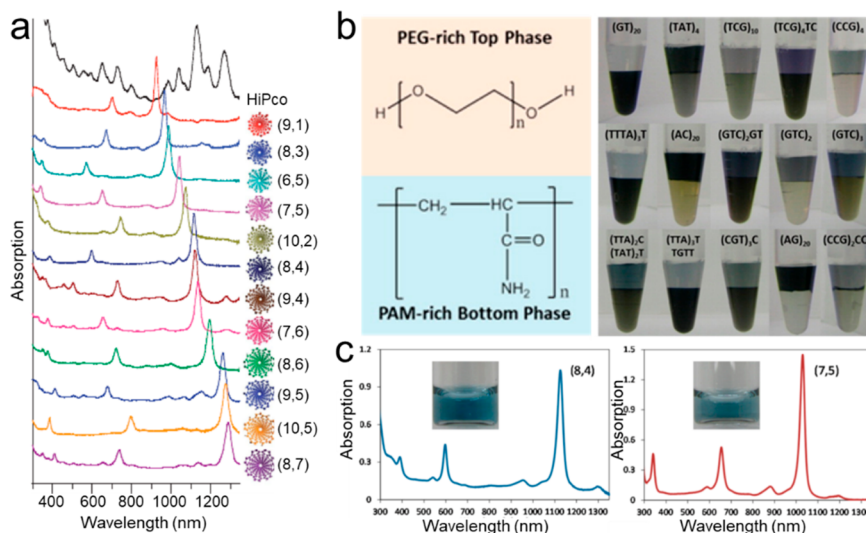


Figure 47. (a) Absorption spectra of 12 kinds of single-chirality SWCNTs. Reproduced with permission from ref 11. Copyright 2009 Nature Publishing Group. (b, c) Sequence-dependent partition of DNA–SWCNTs in the PEG/polyacrylamide (PAM) system (b) and absorption spectra of (8,4) and (7,5) species (c). Reproduced from ref 429. Copyright 2014 American Chemical Society.

47b,c).⁴²⁹ In 2016, more than 20 distinct (n,m) species and their enantiomers were further purified, which will be discussed in next section.⁴³² Most recently, Zheng et al. developed a new ATP system of PEG/DX and realized the chirality sorting of DNA-SWCNTs including zigzag (10,0) species (Figure 48).⁴³³

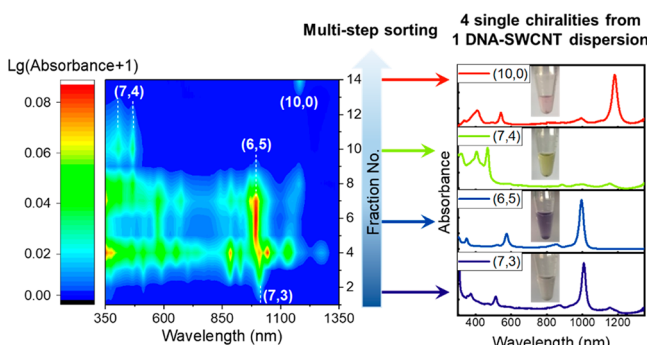


Figure 48. Multistep sorting single-chirality of DNA/SWCNTs by ATP system. Reproduced from ref 433. Copyright 2019 American Chemical Society.

The wide selection of polymer phases and the availability of a practically unlimited number of DNA sequences therefore suggest that there is tremendous potential for further improvement in SWCNT separation by this methodology. However, the polymer used in this method is relatively expensive, and the final separation result can be affected by the temperature and redox conditions in the separation process. If a suitable low-cost ATP system is combined with the advantages of short separation time, simple equipment, and convenient operation, the ATP method can have wide application prospects for realizing large-scale separation of SWCNTs.

3.3.3. Sorting SWCNTs Dispersed by Polymers. In addition to the surfactant and DNA systems in aqueous media, selective conjugated polymer extraction in organic solvent is another method to achieve the enrichment of (n,m) species. As a rule, the separation level achieved by the conjugated polymer extraction method for SWCNTs is mainly diameter separation and high purity semiconductor separation; moreover, the

enrichment of a single chiral SWCNTs can be obtained under suitable separation conditions. Since Nicholas et al. first reported that PFO can selectively disperse s-SWCNTs in toluene,⁶⁰ a family of PFO based polymers were extensively used in sorting chirality-enriched SWCNTs in organic solvents.^{378,393,434,435} In addition, the concentration of the polymer, molecular structure, and the solvent also affect the selectivity. For instance, Kappes et al. achieved the near single-chiral separation of (7,5), (7,6), (10,5), and (9,7) species with respective enrichments up to ~90% by tuning the concentration ratio of polymer to SWCNTs, only in a single sonication and centrifugation step.³⁹⁴ This work also for the first time demonstrated DGU sorting of SWCNT polymer suspensions in organic solvents. They have succeeded in extracting large-diameter ($d_t > 1.3$ nm) (15,4) SWCNTs owing to the strong interaction between poly(9,9-diethylfluorene-*alt*-benzothiadiazole) and (15,4) nanotubes. The polymer based extraction of species with single chirality will be very simple if a suitable polymer and solvent can be found. For example, 96–97% enriched (6,5)-SWCNTs were achieved with only one-step extraction and simple sonication when using bipyridine and 9,9-diethylfluorenyl-2,7-diyl as extractant and *m*-xylene and *p*-xylene as solvents.⁴³⁶

In general, the chiral purity of conjugated polymer separated SWCNTs is not as high as that using surfactant or DNA as a dispersing agent in aqueous phase systems. Additionally, rational design of the specific polymer is still a critical issue in the separation of SWCNTs. So far, the mechanisms of the interaction between polymers and SWCNTs of specific chirality are still unclear.

3.4. Enantiomer-Based Sorting of SWCNTs

Sorting single-chirality enantiomers is the summit of structure-controlled separation. Compared with well-studied conductivity and chirality separation, single-chirality enantiomer separation requires more precise techniques to achieve chirality and handedness control simultaneously. The enantiomers of chiral SWCNTs have been found to have almost identical properties except for optical activity, which increases the difficulty in selective separation and purification. Analogous to the organic chiral molecular separation strategy, the enantiomeric separa-

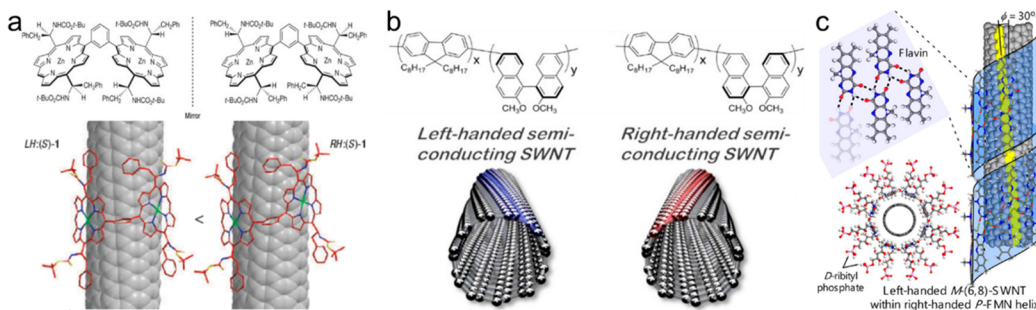


Figure 49. (a–c) SWCNT enantiomers separated by chiral diporphyrin (a), PFO based polymers (b), and flavin mononucleotide (c). Panel a reproduced with permission from ref 316. Copyright 2007 Nature Publishing Group. Panel b reproduced from ref 354. Copyright 2012 American Chemical Society. Panel c reproduced from ref 327. Copyright 2012 American Chemical Society.

tion process can be achieved by means of dispersion with a suitable chiral dispersant and then utilizing different separation methods. The chiral dispersant used involves small molecules,^{316,327,437–442} DNA,⁴³² and polymers,³⁵⁴ which based on structural matching lead to differences in density or hydrophilicity of enantiomeric SWCNTs.

3.4.1. Chirality-Enriched Enantiomer of SWCNTs. In 2007, Komatsu's group designed and synthesized a chiral zinc diporphyrin with phenyl as a bridging group, namely, nanotweezers, and realized the enantiomeric separation of SWCNTs for the first time (Figure 49a).³¹⁶ The difference in the binding energy of chiral diporphyrins and the enantiomers of SWCNTs is the basis for the separation of SWCNTs enantiomers. After that, a series of diporphyrin based derivatives were designed by changing the spacer and bridging groups to separate enantiomers with different diameters^{441,443} and even specific chirality.^{438,440} For instance, Komatsu et al. achieved optically active SWCNTs with $d_t > 1.0$ nm and enriched m-SWCNTs by a synthesized chiral diporphyrin with a much larger cavity, namely, nanocalipers.⁴⁴⁴ When phenanthrene was used as a bridging group, a single enantiomer of (6,5)-SWCNTs with enantiomeric excess of 67% was enriched through the molecular recognition.⁴⁴⁰ The usage of diporphyrins as chiral recognition molecules provides guidance for the separation of SWCNTs enantiomers, but only a mixture of many different (n,m) species was achieved.

The adsorption and entanglement of a polymer on the surface of the SWCNTs is more stable and can be used to separate SWCNT enantiomers. Chiral binaphthol modified PFO copolymer was found to effectively extract enantiomeric (6,5) and (7,5) tubes. In this system, chiral binaphthol was regarded as a center for enantiomeric attraction and PFO with long alkyl chains was believed to disperse s-SWCNTs (Figure 49b).³⁵⁴

The enantiomeric separation of SWCNTs can also be achieved by water-soluble chiral small molecules. For example, flavin mononucleotide containing a chiral D-ribityl phosphate chain with a right-handed helix attracted the right-handed tubes.³²⁷ This enantioselectivity originates from the sp^3 nitrogen atom linking the sugar moiety to the flavin ring, resulting in two flavin mononucleotide configurations (Figure 49c). The chiral surfactant sodium cholate was also found to recognize the left- and right-handed nanotubes owing to the subtle differences in their buoyant densities.⁴³⁹ On the other hand, sorting single-handed enantiomeric SWCNTs in a cosurfactant system was also realized with nonlinear DGU (Figure 50).^{415,445}

Chiral organic molecules as isomer selectors in the aforementioned methods have been proven effective for enantiomeric sorting, but only a complicated enantiomer

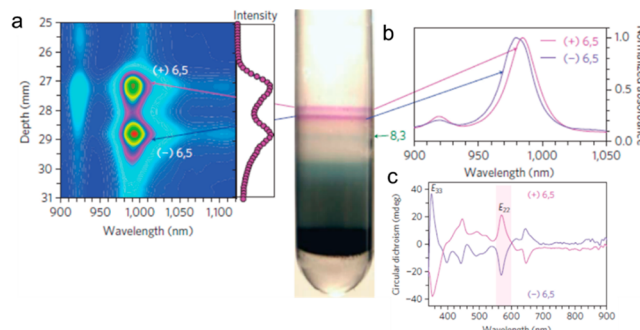


Figure 50. (a–c) PL map (a), UV-vis–NIR absorption (b), and CD (c) spectra of enantiomeric SWCNTs separated by nonlinear DGU. Reproduced with permission from ref 415. Copyright 2010 Nature Publishing Group.

mixture of many different (n,m) species was achieved. Moreover, the separation yield was insufficient because of the limited production and high cost of the synthetic chiral molecules. The DGU method is complex and requires a long separation process. The separated species contain a density medium, such as iodixanol, which is very expensive. These disadvantages preclude the large-scale production and practical applications of single isomer species.

3.4.2. Single-Chirality Enantiomers of SWCNTs. Kataura et al. developed a feasible, low-cost, and highly efficient method for separating 9 distinct single-chirality enantiomeric SWCNTs using GCC.³⁵³ The chiral center of the allyl dextran-based gel has different interaction with left- and right-handed nanotubes, which leads to the enantiomeric separation (Figure 51a). By using m-SWCNT mixtures as starting materials, they also achieved the enantiomer separation of m-SWCNTs for the first time.⁴²⁵ To improve the purity of single-chirality enantiomers, a combination of the overloading selective adsorption and stepwise elution was developed by Kataura et al.⁴⁴⁶ More types of single-chirality s-SWCNT isomers were then sorted using the optically active dextran packed column. These single-chirality enantiomers with the highest reported purity can be utilized in circular dichroism (CD) studies (Figure 51b).

In 2006, Brus et al. first discovered that DNA–SWCNT complexes can exhibit strong CD signals, with prominent sharp peaks corresponding to the excitonic transitions in the absorption spectrum.⁴⁴⁷ In 2009, Zheng et al. further realized the separation of single-chirality SWCNTs with IEX.¹¹ However, they did not perform the CD spectroscopy to characterize the enantiomer. In 2016, 20 types of single-chirality enantiomeric SWCNTs covering achiral and chiral species were

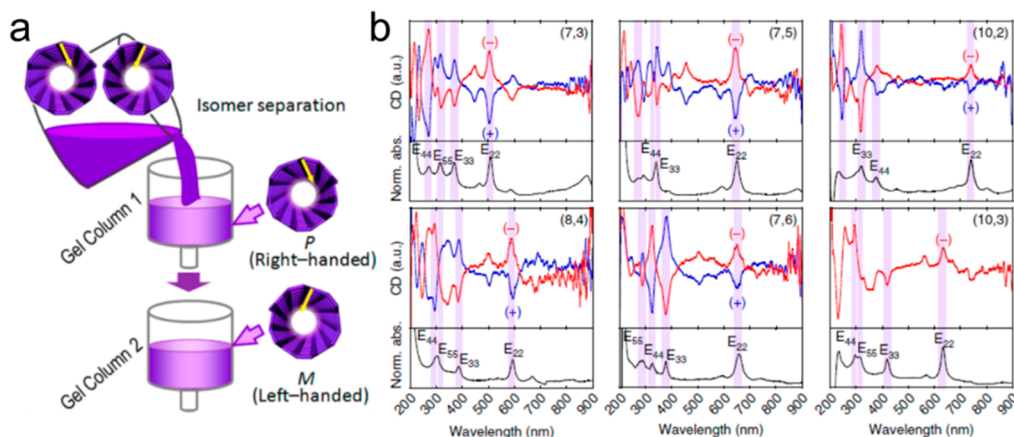


Figure 51. (a) GCC method for easily separating the optical isomers. Reproduced from ref 353. Copyright 2014 American Chemical Society. (b) CD spectra of single-chirality enantiomers. Reproduced with permission from ref 446. Copyright 2016 Nature Publishing Group.

successfully separated with ATP extraction in a DNA system (Figure 52).⁴³² Two different conformations of DNA wrapped

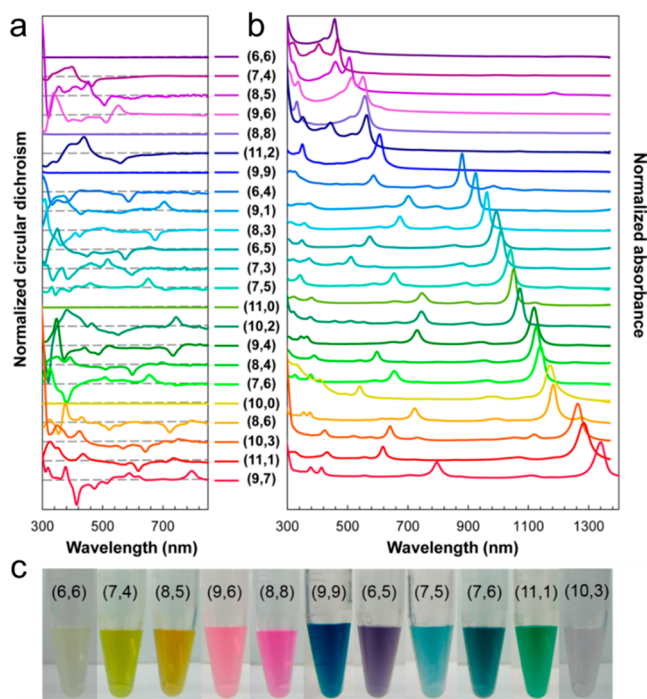


Figure 52. (a, b) CD (a) and absorption (b) spectra of the selected (n, m) species. (c) Photographs of enantiomeric single-chirality SWCNTs. Reproduced from ref 432. Copyright 2016 American Chemical Society.

left- and right-handed nanotubes leading to different chemical reactivity. For example, (+)-(6,5) tubes were more strongly oxidized by NaClO than the (-)-(6,5) tubes; thus the latter one is much more tightly contacted with DNA. Later on, a similar method was developed by exchanging strong binding bile salt surfactant with DNA; the yield of enantiomers is nearly 100%.⁴⁴⁸

Overall, although researchers have a certain understanding of the enantiomeric separation of SWCNTs, the intrinsic mechanism of the separation process still needs in-depth research, and the application of SWCNT enantiomers has not been demonstrated, which slows the development of enantiomeric separation.

3.5. Other Purification Techniques

Selective poststretching is also a promising way to obtain SWCNTs with conducting selectivity. The general driving force is that m-SWCNTs are more easily oxidized than the s-SWCNTs. Techniques based on optical,^{449,450} electrical,^{31,451–453} plasma,⁴⁵⁴ microwave,⁴⁵⁵ or chemical^{456–463} effects face some problems, for example, incomplete removal of the m-SWCNTs and partial removal or degradation of the s-SWCNTs. However, none of these methods is able to obtain single-chirality SWCNTs or m-SWCNTs.

3.5.1. Electrical Break Down. The electrical break down approach is based on the electrical properties of m- and s-SWCNTs, in which the metallic tubes are selectively broken down with Joule heating, while the semiconducting ones are preserved by controlling the gate voltage.⁴⁵¹ This scheme, however, has two critical disadvantages. First, there are some undesirable results such as band-to-band tunneling, heat sinking at the contacts, and failure in gate dielectrics,⁴⁶⁴ all of which can prevent proper operation of the process. It is worth noting that the random appearance of a narrow gap (~ 100 nm) m-SWCNT is not well controlled. Numerous residual m-SWCNTs still exist in the sample, as schematically shown in Figure 53a,b,⁴⁶⁵ thereby preventing generalized use in subsequently fabricated devices. The thermocapillary-induced full length removal m-SWCNTs proposed by Rogers et al. is quite promising.⁴⁶⁶ The local Joule heating on m-SWCNTs induced by the current injection increases the temperature (a few degrees). Then the temperature gradients drive thermocapillary flow in an overcoat of the thermocapillary resist. The coated resist on m-SWCNTs was selectively opened by thermocapillary flow, and m-SWCNTs were then completely eliminated by ion etching (Figure 53e). Although this method nondestructively yields s-SWCNTs with high purity, it still has some limitations for practical application. The multiple steps of fabricating devices and coating and removing resist are costly and time-consuming. The contact with electrode will affect the current injection and the follow-up steps. The residuals on s-SWCNTs after removing resist may also degrade their properties. The space resolution of this method is restricted by the capillary length scale, which is not applicable for highly dense SWCNT arrays. Maruyama et al. proposed an organic film (molecular glass or PMMA)-assisted electrical breakdown method to achieve pure s-SWCNT arrays, which can be used for a number of FET channels. This method achieves high selectivity toward s-SWCNTs with high space

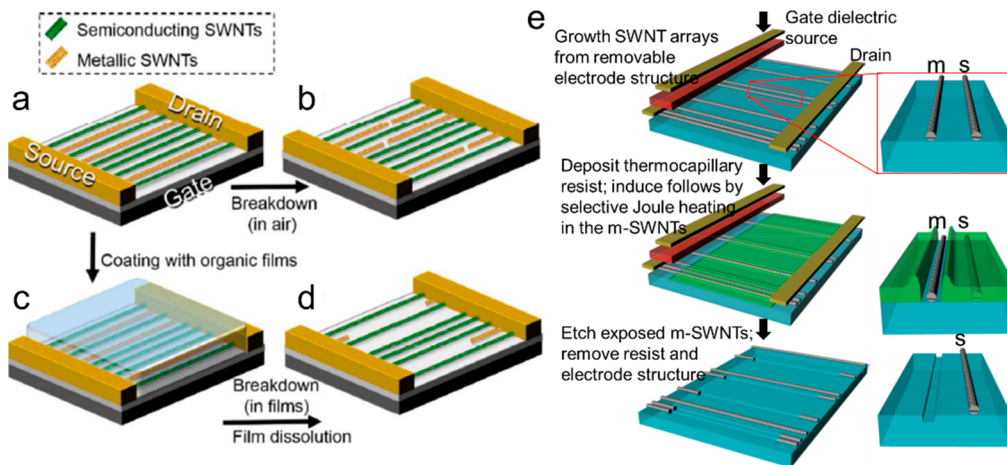


Figure 53. (a–d) Schematic illustrations of electrical breakdown in air (a, b) and coated with organic film (c, d). Reproduced with permission from ref 452. Copyright 2014 Royal Society of Chemistry. (e) Process for selective etching m-SWCNTs induced by thermocapillary flow. Reproduced with permission from ref 466. Copyright 2013 Nature Publishing Group.

resolution of 55 nm, similar to in-air breakdown (Figure 53a–d).⁴⁵²

3.5.2. Selective Chemical Reaction. Direct gas-phase chemical etching is very simple and scalable. Numerous methods have been developed to destroy m-SWCNTs in gas-phase, such as oxidation (O_2 ,^{457,458,467 O_3 ,⁴⁶² H_2O ,⁴⁵⁶ SO_3 ,⁴⁶⁸ NO_2 ,⁴⁶⁰)⁴⁶⁹, hydrogen or methane plasma,^{454,469} fluorine gas,⁴⁷⁰ and metal-assisted catalytic reaction.^{461,463} Dai et al. proposed a methane-plasma enhanced gas-phase hydrocarbonation reaction to preferentially etch m-SWCNTs; 100% s-SWCNTs with little damage were retained (Figure 54a). The reactivity of}

systems via $\pi-\pi$ stacking. Unlike the other techniques discussed above, these approaches can be applied to long SWCNT systems without introducing damage, while the SWCNT formation is perfectly maintained.

3.6. Future Perspectives on SWCNT Sorting

Research on sorting SWCNTs has made tremendous progress since its humble beginning in 2002. At this point, we have sorting methods that can control every single structural aspect of a SWCNT for small-diameter (≤ 1 nm) tubes. Along with the development of sorting, various methods of noncovalent modification and solution chemistry of SWCNTs have also been revealed, providing foundations for future chemistry of SWCNTs. Understanding molecular mechanisms of SWCNT sorting and discovery and invention of more effective and simpler sorting methods are two related tasks that will occupy the central stage of future SWCNT sorting research. In practice, the current scale of chirality or enantiomer sorting is still too low to meet the needs of many fundamental studies and technological applications. However, we are optimistic that this issue can be solved by combined improvement in controlled SWCNT synthesis and sorting methods.

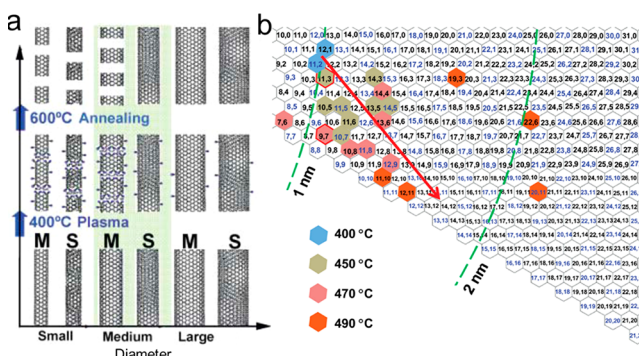


Figure 54. (a) Evolutions of SWCNT diameter and metallicity with methane-plasma treatment. Reproduced with permission from ref 454. Copyright 2006 American Association for the Advancement of Science. (b) Chirality map of reactivity of SWCNT at different temperatures with a red arrow indicating toward the large chiral angle and large tube diameter direction. Reproduced with permission from ref 458. Copyright 2013 Wiley.

nanotube depends on not only metallicity but also on diameter and chiral angle (Figure 54b).⁴⁵⁸ Gas-phase etching has potential application because the purified s-SWCNTs maintain their intrinsic properties without residues. However, one drawback of gas-phase etching is that all SWCNTs are destroyed to some extent.

Selective adsorption of chemicals on SWCNTs is another strategy to remove either s- or m-SWCNTs.^{471–473} The selectivity is attributed to the fact that SWCNTs are extended π -electron systems that can interact with other π -electron

4. CHIRALITY ASSIGNMENT AND QUANTIFICATION OF SWCNTs

The characterization of SWCNTs including chirality assignment and quantification is essential in chirality-selective preparations and sorting. It can tell us the composition and purity of the products and provides feedback to further guide controlled preparation and sorting. In this part, we will review the optical and nonoptical methods for chirality assignment and the quantification of the ensemble and the surface-grown SWCNTs. We will consider the applicability of different methods with respect to different SWCNT samples and also discuss reliable methodology based on the combination of different techniques.

4.1. Chirality Assignment

4.1.1. Basic Principles. The current approaches for SWCNT chirality assignments can be classified into optical and nonoptical techniques (Figure 55). The optical spectroscopic methods include resonant Raman scattering, absorption, photoluminescence (PL), resonant Rayleigh scattering (RRS), and circular dichroism (CD) spectroscopies, in which the

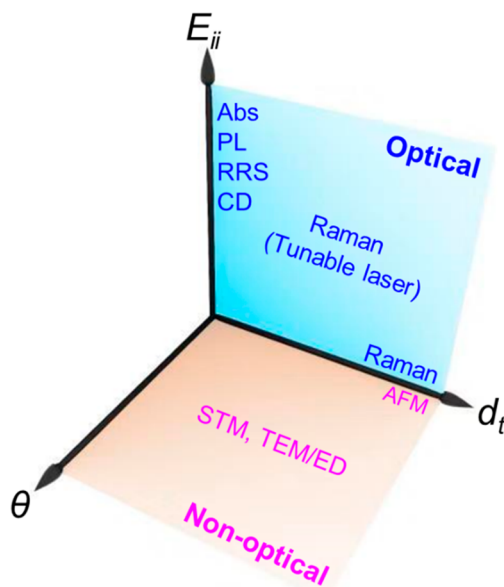


Figure 55. Summary of the (*n,m*) assignment of SWCNTs based on E_{ii} , d_t , and θ by using optical and nonoptical methods. (Abs, absorption; PL, photoluminescence; RRS, resonance Rayleigh scattering; CD, circular dichroism; STM, scanning tunneling microscopy; ED, electron diffraction).

chiralities are assigned based on the characteristic E_{ii} (in absorption, PL, Rayleigh, Raman, CD) and d_t (in Raman).⁴⁷⁴ In nonoptical methods, the (*n,m*) are identified by using d_t and θ obtained from STM^{475,476} or TEM/ED.^{296,477,478} In this section, we will introduce the theory and methodology of these methods and discuss their practicability and limitations in the application of chirality-controlled preparation.

Before going into the detailed methodology of the spectroscopic methods for chirality assignment, we first briefly discuss the five photophysical processes of absorption, Raman scattering, Rayleigh scattering, and PL for identifying the chiral index of SWCNTs. Figure 56a shows an absorption process of a

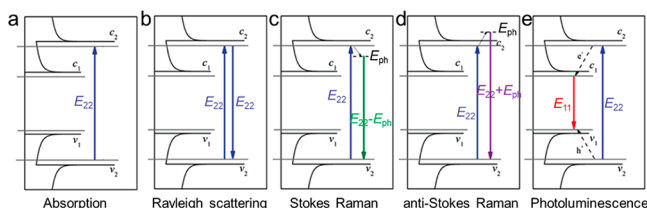


Figure 56. DOS of a s-SWCNT showing the allowed basic photophysical processes: (a) absorption; (b) Rayleigh scattering; (c) Stokes Raman scattering; (d) anti-Stokes Raman scattering; (e) PL. Panels b–e adapted with permission from ref 474. Copyright 2013 Wiley.

s-SWCNT. If the incident photon energy (E_{ph}) matches with the excitonic E_{22} of this tube, the photon is absorbed by the tube, and thus an exciton is produced. The Rayleigh scattering is an elastic process when the exciton recombines in a radiative way without change of energy (Figure 56b). In contrast, Stokes Raman (Figure 56c) and anti-Stokes Raman (Figure 56d) are inelastic processes when the exciton recombines with a slightly lower ($E_{22} - E_{ph}$) or higher energy ($E_{22} + E_{ph}$) than E_{ph} . PL occurs when the exciton relaxes to the lowest excitonic state, and thus the exciton recombines with a lower energy (E_{11}) than E_{ph}

(Figure 56e). However, PL cannot happen in m-SWCNTs due to the nonradiative recombination of the exciton by the continuous DOS at the Fermi level.

The method to distinguish the (*n,m*) of SWCNTs by spectroscopies is to directly compare the E_{ii} and d_t values in a Kataura plot, which was named after H. Kataura who first used an $E_{ii}-d_t$ plot to illustrate the Raman and absorption spectra of SWCNTs in 1999.⁴⁷⁹ Figure 57a represents a typical Kataura plot for all types of SWCNTs covering d_t of 0.5–2.0 nm and E_{ii} of 0–3 eV. The E_{ii} values of the SWCNTs were calculated by zone folding of the graphene electronic structure, as obtained from a nearest-neighbor TB model, with d_t obtained from eq 1 of ref 479. Later, Kataura's group reported an extended Kataura plot showing by CD analysis that E_{ij} is a function of $1/d_t$ (Figure 57b,c).⁴⁸⁰ The asymmetric excitonic band structures of 12 SWCNTs of different (*n,m*) with high enantiomeric purity were successfully determined based on the obtained E_{ii} and E_{ij} energies.

In the Kataura plot, E_{ii} is a key issue; in addition to (*n,m*), their values depend strongly on the environment.^{481–484} Several sets of E_{ii} values have been experimentally measured for SWCNTs in suspensions, on substrates, in freestanding forests, or suspended over trenches. Within these sample, suspended SWCNTs with gas molecules desorbed by treatment in vacuum present the highest E_{ii} values. The interactions between SWCNTs and the environment usually cause red shifts up to 100 meV in E_{ii} due to the dielectric screening effect. The E_{ii} values obtained from different approaches (e.g., Raman, PL, RRS) are also different from each other because of the difference in the states of the excitons. These differences in E_{ii} lead to large uncertainty in chirality determination under complex environments using the Kataura plot. Resonant Raman spectroscopy shows relatively high inaccuracy because the shifts in E_{ii} from the influence of the environment will significantly change the resonance conditions of various chiralities.⁴⁸⁵ To precisely identify the (*n,m*), we need first to consider the SWCNT environment and then choose a Kataura plot with E_{ii} values obtained in the same or similar tube environments. If such a Kataura plot is unavailable in the literature, we can form one by shifting the E_{ii} with an estimated value from those well-established Kataura plots, for example, the well-known Kataura plot of supergrowth SWCNTs.⁴⁸⁶

Recently, Yang et al. reported a series of bilayer plots to accurately determine the (*n,m*) of SWCNTs under complex environments by taking into account the interactions of the SWCNT and its local environment.⁴⁸⁷ In the bilayer plots, the y coordinate is the difference in E_{ii} (ΔE_{ii}), and the x coordinate is the corresponding E_{ii} average in one layer and the corresponding ω_{RBM} in the other layer (Figure 58). They showed that under complex environments, the ΔE_{ii} remains nearly unchanged. Therefore, only the shifts in the x coordinates between the two layers, that is, between the measured and expected values of E_{ii} and ω_{RBM} , need to be considered. In general, the bilayer plots contain all the information provided in the corresponding Kataura plot but show less data overlapping. Moreover, the bilayer plots provide additional information on the degree of interactions between the SWCNTs and the environments. The disadvantage of the bilayer plots, however, is that instead of one Kataura plot, a series of bilayer plots are required when multiple E_{ii} values are needed. Yang et al. also provided an online program⁴⁸⁸ to make accurate and convenient (*n,m*) assignments for various SWCNT samples based on the bilayer plots.

4.1.2. Resonant Raman Spectroscopy. Among a number of spectroscopic methods, Raman is a nondestructive method

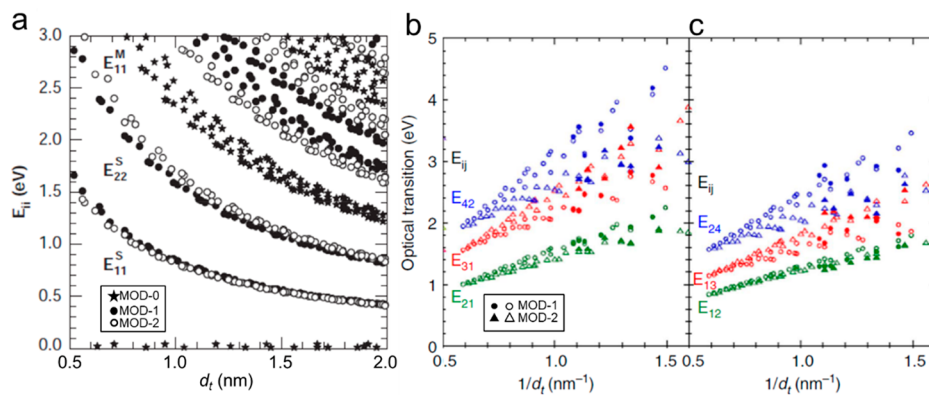


Figure 57. (a) E_{ii} – d_t plot. Reproduced with permission from ref 20. Copyright 2005 Elsevier. (b, c) E_{ij} – $1/d_t$ plot. Solid and open symbols indicate the experimental and calculated results, respectively. Reproduced with permission from ref 480. Copyright 2016 Nature Publishing Group.

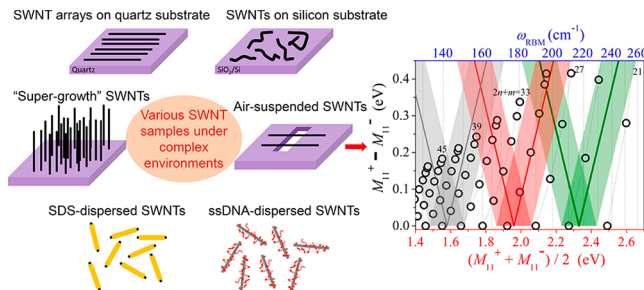


Figure 58. Schematic illustration of SWCNTs in different environments. Bilayer plot for the E_{11}^M of air-suspended m-SWCNTs. Reproduced from ref 487. Copyright 2017 American Chemical Society.

and is the most intensively used method for SWCNT structure assignment. The technique employs standard commercial micro-Raman spectrometers and lasers and requires minimal sample preparation. Different types of SWCNT samples, such as grown or dispersed on a substrate, vertically aligned arrays, surfactant dispersed solution, and freely suspended tubes, are all satisfactory for Raman measurements. Figure 59 shows a typical

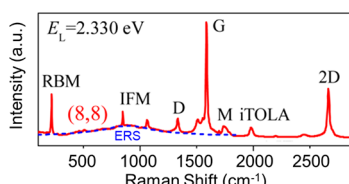


Figure 59. Background subtracted Raman spectra of DNA-sorted (8,8) SWCNTs with 2.33 eV excitation. Reproduced from ref 491. Copyright 2016 American Chemical Society.

resonant Raman spectrum of the DNA-sorted (8,8) SWCNTs deposited on sapphire. Two dominant peaks of RBM (~ 100 – 400 cm⁻¹) and the tangential vibrational mode (G band) (1550 – 1600 cm⁻¹) confirm the existence of the SWCNTs and are both first-order Raman modes. Other weak features, such as the intermediate frequency modes (IFM) (600 – 1000 cm⁻¹), the defect-induced D band (~ 1350 cm⁻¹), the M band (~ 1750 cm⁻¹), and the iTOLA band (~ 1950 cm⁻¹, combinational mode of in-plane transverse optic (iTO) and longitudinal acoustic (LA)) are higher order Raman modes. A broad electronic Raman scattering (ERS) feature was also found in m-SWCNTs.^{489,490} Using Raman spectroscopy to figure out the structures and electronic and phonon properties of SWCNTs

has been reviewed comprehensively by Dresselhaus et al.²⁰ Here, the main focus of this section is on chirality assignments by the features of RBM, G-band, and ERS features.

ω_{RBM} – d_t Relationship. Since the Raman signals of SWCNTs are only observable under resonance, the Raman intensity can be somehow calculated by considering the difference between E_L and E_{ii} as well as the electron–phonon and phonon–phonon interactions. According to such an idea, by assignment of the (n,m) using one single laser line, the first relation between the RBM frequency and d_t of SWCNTs on silicon substrates, that is, $\omega_{RBM} = 248/d_t$, was established by Dresselhaus et al.⁴⁹² A more general relation writes as

$$\omega_{RBM} = A/d_t + B \quad (1)$$

The parameter A is associated with the vibrational force constant of the sp² C–C bond, and the parameter B is related to the environmental effects, accounting for tube bundling,^{491,493} substrate–tube interactions,⁴⁸⁵ amorphous carbon coating,⁴⁹⁴ molecules adsorbed onto the tube sidewalls,⁴⁹⁵ interaction between the tube and the dispersants in solution,⁴⁹⁶ static pressure difference,⁴⁹⁷ etc. For suspended SWCNTs in vacuum, which are free of various interactions, the parameter B is expected to be zero.⁴⁸⁶ A variety of ω_{RBM} – d_t relationships were reported, including relationships for vertically aligned SWCNT forests on silicon and quartz substrates,⁴⁸⁶ suspended SWCNTs,^{288,498} surfactant-dispersed SWCNTs,⁴⁸¹ and random SWCNTs grown on the SiO₂/Si substrate,⁴⁸⁵ which are summarized in Table 3. With the d_t values calculated from ω_{RBM} and the resonance condition of $E_{ii} \approx E_L$ (n,m) assignments for individually isolated SWCNTs can be made from the RBM feature based on the Kataura plot (Figure 57). However, it is obvious that the E_{ii} obtained by this method is not precise, with an estimated resonance window of ± 100 meV. It usually cannot be used to precisely identify the chirality of SWCNTs.

For a more accurate (n,m) assignment, the tunable laser Raman spectroscopy is applied to give ω_{RBM} and E_{ii} with high accuracy simultaneously; thus (n,m) can be distinguished by comparing with the Kataura plot. Fantini et al. used a tunable Raman system, which allows E_L to be changed almost continuously from 1.52 to 2.71 eV (altogether 76 E_L values), to provide the evolution of ω_{RBM} as a function of E_L (Figure 60a).⁴⁸¹ Each RBM peak in 3D Raman excitation spectra represents a SWCNT with E_{ii} resonance (Figure 60b,c).⁴⁸³ Then a resonance profile with several characteristic peaks representing the E_{ii} values was obtained. However, the resonance profile is sensitive to the form of existence of the

Table 3. $\omega_{\text{RBM}} - d_t$ Relations for Different Types of SWCNT Samples

samples	method	$\omega_{\text{RBM}} = A/d_t + B$	ref
SWCNTs grown on SiO ₂ /Si substrates	Raman	$\omega_{\text{RBM}} = 245/d_t^{\text{a}}$	492
	Raman	$\omega_{\text{RBM}} = 214/d_t + 19$	499
	Raman	$\omega_{\text{RBM}} = 235.9/d_t + 5.5$	485
transferred isolated SWCNTs on SiO ₂ /Si substrates	Raman	$\omega_{\text{RBM}} = 222/d_t + 8$	500
vertically aligned SWCNT forests on silicon and quartz substrates	tunable laser Raman	$\omega_{\text{RBM}} = 217/d_t + 15$	501
air-suspended SWCNTs	Raman	$\omega_{\text{RBM}} = 227/d_t + 0.3$	486
	Raman + ED	$\omega_{\text{RBM}} = 228/d_t$	498
	Raman	$\omega_{\text{RBM}} = 204/d_t + 27$	288
	Raman	$\omega_{\text{RBM}} = 200/d_t + 26$	491
surfactant-dispersed SWCNTs	tunable laser Raman	$\omega_{\text{RBM}}^{(\text{s})} = 223/d_t + 10$	481
		$\omega_{\text{RBM}}^{(\text{m})} = 218/d_t + 17$	
	tunable laser Raman	$\omega_{\text{RBM}}^{(\text{s})} = 227/d_t + 7.3$	502
		$\omega_{\text{RBM}}^{(\text{m})} = 227/d_t + 11.8$	
	Raman + PL	$\omega_{\text{RBM}} = 223.5/d_t + 12.5$	503
	tunable laser Raman	$\omega_{\text{RBM}} = 215/d_t + 18$	483
	tunable laser Raman	$\omega_{\text{RBM}} = 214.4/d_t + 18.7$	504

^aThe sp² C–C bond length $a_{\text{C-C}} = 1.42 \text{ \AA}$ instead of 1.44 Å (ref 492) was used in this review to obtain $A = 245 \text{ nm}\cdot\text{cm}^{-1}$.

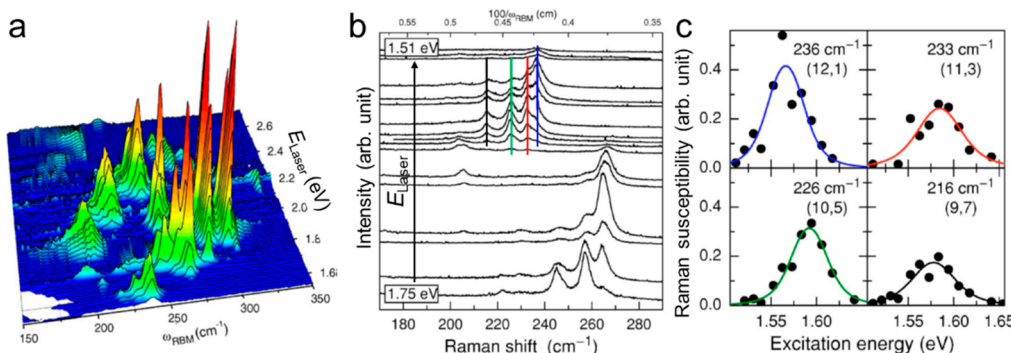


Figure 60. (a) 3D color map of SDS dispersed HiPco SWCNTs showing Raman RBM evolution as a function of 76 different E_L values. Reproduced with permission from ref 481. Copyright 2004 American Physical Society. (b) Raman RBM of SWCNTs at different E_L from 1.51 to 1.75 eV. (c) Resonant profiles for the peaks marked in panel b by vertical lines. Reproduced with permission from ref 483. Copyright 2005 American Physical Society.

SWCNT and its environment, such as freestanding, on the surface of substrate, and dispersed in aqueous or organic solution with different wrapping agents. The Raman intensity at different laser energy requires careful calibration for accurate (n,m) assignment. The limitation is that the tunable laser is very expensive and there is still no commercialized spectrometer, which brings more complexity to experiments.

Due to the limitation of resonance windows, most the SWCNTs are in resonance and detected using one or several Raman excitation lasers, especially for the surface-grown SWCNTs. For a given excitation laser line, the resonance window width for E_{ii} was often estimated to $\pm 100 \text{ meV}$. The d_t is usually calculated with an uncertainty of $\pm 0.02 \text{ nm}$ according to the experimental $\omega_{\text{RBM}} - d_t$ relationships. The uncertainties of d_t and E_{ii} provide several possible (n,m) assignments; however it is still difficult in most cases to result in a certain (n,m) assignment. Surface-enhanced Raman spectroscopy (SERS) resulting from the strong surface plasmonic resonance of certain metal nanoparticles has been utilized in characterizing each SWCNT in an ensemble form or grown on a surface with only one laser wavelength.^{505–507} However, SERS overwrites the information on E_{ii} and thus is not favorable for the identification of (n,m).

G-Band. The G-band including higher frequency G⁺ and lower frequency G⁻ is the most commonly used Raman feature

to distinguish several specific types of individual SWCNTs, especially for m- and s-SWCNTs. The G⁻ component in m-SWCNTs always presents an asymmetric Breit–Wigner–Fano (BWF) line shape,⁵⁰⁸ whereas the G⁻ in a s-SWCNT shows a symmetric Lorentzian line shape (Figure 61a). The sharp of G peak was also used to discriminate chiral and achiral SWCNTs. Chiral SWCNTs present both G⁺ and G⁻ components, whereas achiral SWCNTs only present a single G⁺ or G⁻ peak. For example, (25,0) zigzag s-SWCNTs and (10,10) armchair m-SWCNTs only show a narrow G⁺ peak, whereas (24,0) zigzag m-SWCNTs only show a single broad BWF shaped G⁻ peak (Figure 61b).⁵⁰⁹ The lack of G⁻ mode was also observed in other enriched armchair or zigzag tube samples.^{145,510} However, other factors such as the substrate effect,⁵¹¹ misalignment and defects of SWCNTs, bundling,⁵¹² and bending⁵¹³ were found to result in multiple G bands, bringing more difficult to identify achiral SWCNTs by G features only. Normally, Raman intensity of the G⁻ band is lower than that of G⁺ in SWCNTs, which can be violated in some small diameter MOD-1 SWCNTs when in resonance with E_{33} and E_{44} .

G⁻ band frequency strongly depends on d_t with a relation of $\omega_{\text{G}} = A - B/d_t^C$ (Figure 61c, Table 4).^{514–516} G⁺ band frequency is also related to d_t , but not as much as G⁻. The intensity ratio of G⁻/G⁺ is also found to be depend on θ (Figure

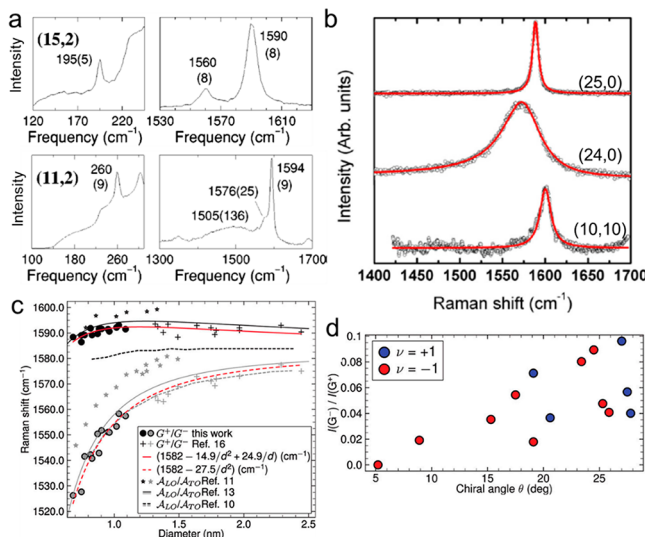


Figure 61. (a, b) Intrinsic Raman RBM and G-mode ranges of chiral (a) and achiral SWCNT (b). The chiralities are determined based on Raman and ED. Reproduced with permission from ref 514 and ref 288. Copyright 2002 and 2009 American Physical Society. (c) $1/d_t$ as a function of G band frequency (G^- and G^+) from isolated SWCNTs. (d) Intensity ratio of G^-/G^+ as a function of θ . Reproduced from ref 515. Copyright 2012 American Chemical Society.

Table 4. $\omega_G - d_t$ Relations for Different Types of SWCNTs

samples	$\omega_G = A - B/d_t^C$	ref
SWCNTs grown on SiO ₂ /Si substrates	$\omega_{G^-}^{(m)} = 1591 - 79.5/d_t^2$	514
	$\omega_{G^-}^{(s)} = 1591 - 47.7/d_t^2$	
	$\omega_{G^-} = 1592 - 41.4/d_t^{1.4}$	517
s-SWCNT suspensions ($d_t \leq 1$ nm)	$\omega_{G^-} = 1582 - 27.5/d_t^2$	515
	$\omega_{G^+} = 1582 - 14.9/d_t^2 + 24.9/d_t$	
m-SWCNTs (calculated from nonorthogonal TB model)	$\omega_{G^-} = 1582 - 38.8/d_t^2$	518

61d).⁵¹⁵ This allowed the successful chirality assignment of purified SWCNTs with $d_t \leq 1.1$ nm.

It is more accurate to estimate d_t from the $\omega_G - d_t$ relationship than from the $\omega_{RBM} - d_t$ relationship because the resonance window of G band is wider than that of RBM. However, the disadvantage of this method lies in the significant peak overlap for large diameter tubes leading to inaccurate chirality assignment.

ERS Feature. ERS, first observed by Kong et al. on m-SWCNTs,⁴⁸⁹ is a resonance enhancement process that appears when the scattered photon energy matches the corresponding E_{ii}^M . ERS features are always centered at E_{ii}^M , and the energy of the scattered photons of ERS is independent of E_L . Li et al. reported an accurate method that can be used to make chirality assignment for all m-SWCNTs based on the ERS features (Figure 62).^{490,491} By use of a single laser line, the paired E_{ii}^{M+} and E_{ii}^{M-} can be observed simultaneously. With these two energy levels and the d_t derived from RBM, the chiral index can be accurately identified based on the Kataura plot or the bilayer plot. A single ERS signal at E_{ii}^M was observed as no E_{ii}^M splitting occurs for armchair SWCNTs. Based on the ERS feature, the E_{ii}^M can be precisely determined to be about ± 1 meV for a single detection and to be about ± 10 meV when taking into account the environmental effects, leading to accurate assignment of the (n,m).

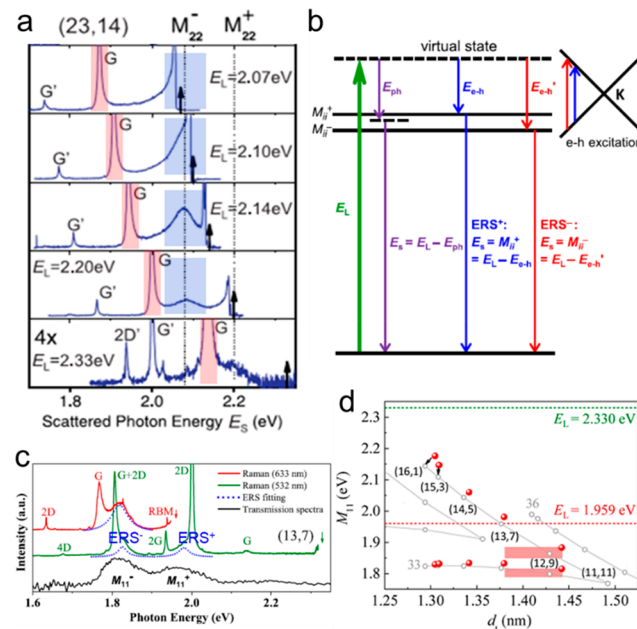


Figure 62. (a) Raman spectra of a (23,14) m-SWCNT as a function of the scattered photon energy. Reproduced with permission from ref 489. Copyright 2011 American Physical Society. (b, c) Schematic showing the resonantly enhanced ERS⁺ and ERS⁻ processes in a m-SWCNT, compared to a typical resonant Raman process. E_{ph} and E_{e-h} are phonon mode and electron–hole pair energy, respectively (b); Raman and transmission polarized absorption spectra of a suspended (13,7) m-SWCNT (c). Reproduced with permission from ref 490. Copyright 2016 American Physical Society. (d) Chirality assignment of m-SWCNTs in the branch of $(2n + m) = 33$ at 1.959 and 2.330 eV excitations in Kataura plot. Reproduced from ref 491. Copyright 2016 American Chemical Society.

Other Raman features of IFM^{500,519} and 2D bands were also used to distinguish different types of individual SWCNTs. The IFM band involves two dispersive IFM⁻ and IFM⁺ features and a nondispersive out-of-plane transverse optic (oTO) feature (600–1100 cm⁻¹). The 2D band, twice frequency of the D band, originates from a two-phonon process. Most of the individual SWCNTs usually exhibit a symmetric 2D band, whereas only MOD-1 s-SWCNTs and non-armchair m-SWCNTs show split 2D bands.^{520,521} However, these features cannot be used to precisely identify a certain (n,m) SWCNT.

4.1.3. Photoluminescence Spectroscopy. PL spectroscopy also directly provides E_{ii} values for s-SWCNTs dispersed in solutions and individually suspended across slits. In 2002, PL experiments were first carried out on SWCNTs well dispersed in surfactants by Weisman et al. (Figure 63a).⁵⁰³ Both excitation (E_{22} or higher E_{ii}) and emission energies (E_{11}) were used to determine (n,m). The (n,m) index of individually suspended and substrate-supported SWCNTs can be assigned when using tunable lasers to detect E_{11} . A simultaneous PL and Raman spectrometer provides a more accurate (n,m) assignment with E_{ii} obtained from PL and d_t derived from RBM frequency (Figure 63b,c).^{522–525} However, PL signal can be strongly decayed or quenched due to the interaction between tube and substrate.^{525–527} This can be resolved by putting SWCNTs over the trenches or transferring SWCNTs to a new substrate such as clean glass or quartz to decrease the interaction strength between tube and substrate.⁵²⁸

PL was also used to investigate two enantiomers, left- and right-handed (6,5) SWCNTs, separated by DNA.⁴³² From the

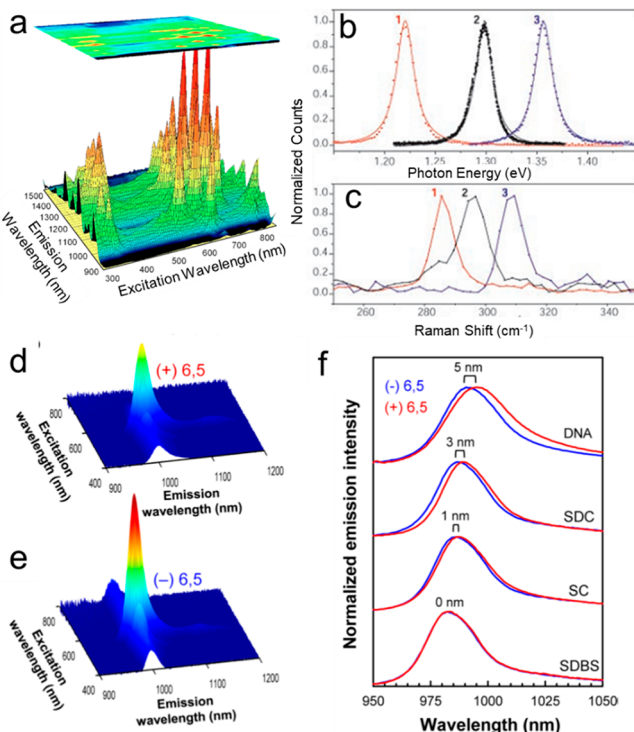


Figure 63. (a) 3D PL map of SDS–SWCNT dispersion. Reproduced with permission from ref 503. Copyright 2002 American Association for the Advancement of Science. (b, c) PL emission spectra of three different individual SWCNTs, labeled 1 to 3 (b) and corresponding RBM frequency (c). Reproduced with permission from ref 522. Copyright 2003 American Association for the Advancement of Science. (d–f) 3D PL maps of the (+)-(6,5) (d) and (−)-(6,5) (e) enantiomers. Comparison of PL spectra normalized by the peak emission intensity for the (−)-(6,5) and (+)-(6,5) enantiomers (f). Reproduced from ref 432. Copyright 2016 American Chemical Society.

E_{11} emission peak, it was observed that the (−)-(6,5) enantiomer exhibits a 1.7 times higher brightness than that of the (+)-(6,5) enantiomer, and the peak of the former one was blue shift by 5 nm and was 6 nm narrower relative to the latter (Figure 63d–f). This phenomenon shows the possibility to identify and distinguish between a pair of enantiomers using PL.

4.1.4. Absorption Spectroscopy. UV–vis–NIR absorption is also an easily accessible way to determine the chirality of SWCNTs well-dispersed in suspensions. It has been widely employed since it reveals some d_t -dependent absorption bands in the ultraviolet, visible, and near-infrared wavelength, corresponding to the characteristic E_{ii} of SWCNTs (Figure 64).⁵²⁹ For s-SWCNTs, four interband transition peaks (E_{11} , E_{22} , E_{33} , E_{44}) usually appear in the UV–vis–NIR spectrum in wavelengths of 400–1600 nm, whereas one interband transition (E_{11}) appears with other transitions outside this range. However, an overlap between the contributions of different (n,m) SWCNTs to the absorption spectra gives this technique a lack of specificity for characterizing SWCNT species.

Recently, some new optical methods were developed to directly measure the SWCNT absorption spectrum on substrate. Fatti et al. developed spatial modulation spectroscopy (SMS) in a double microscope system, over a broad optical spectral range to measure the absolute absorption cross-section of individual SWCNTs.⁵³⁰ Transmitted or reflected light energy can be obtained when moving a single nano-object under a polarized light beam. It directly provides the absolute absorption cross-

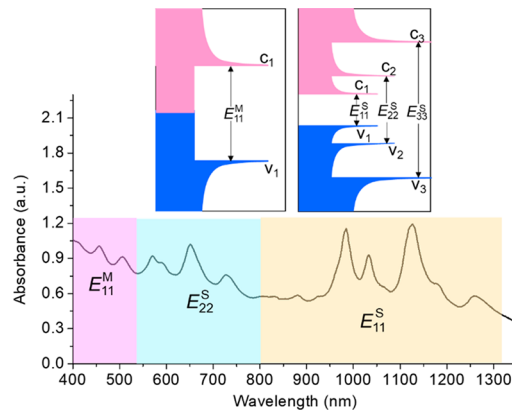


Figure 64. UV–vis–NIR absorption spectrum of CoMoCAT SDS–SWCNT dispersion. Different electronic transitions are labeled. Inset shows the DOS plots and corresponding E_{ii} of m-SWCNTs (left) and s-SWCNTs (right).

section at the incident light wavelength of the SWCNT (Figure 65a–c). Wang et al. developed another new optical absorption

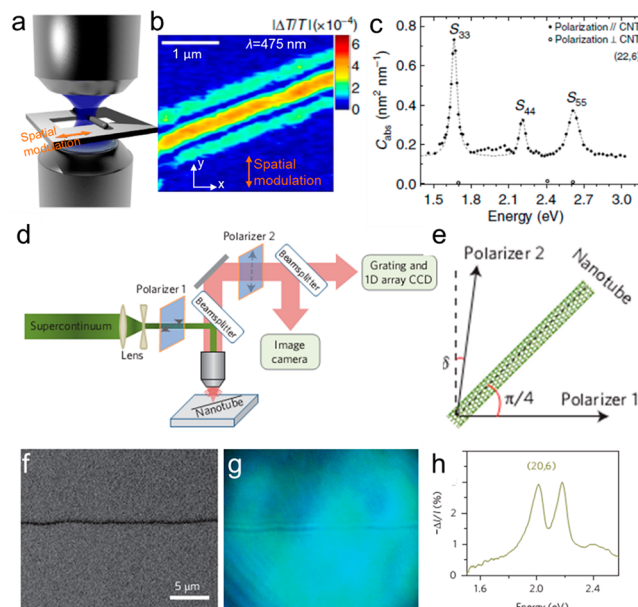


Figure 65. (a–c) Sketch of the SMS technique (a), transmission SMS image of suspended segment of a (22,6) SWCNT (b), and corresponding absolute absorption cross-section spectrum (c). Reproduced with permission from ref 530. Copyright 2013 Nature Publishing Group. (d–h) Integration of the high-contrast polarization microscopy for imaging and chirality assignment of SWCNTs (d), configuration of incident polarizer 1, outgoing polarizer 2, and a SWCNT (e), SEM (f), direct optical images of an individual nanotube (g), and reflective spectrum of this SWCNT (h). Reproduced with permission from ref 531. Copyright 2013 Nature Publishing Group.

method by using a combination of polarization-based microscopy and supercontinuum laser illumination. They established real-time high-throughput optical imaging assisted with broadband spectroscopy to determine the E_{ii} of individual SWCNTs on various substrates.⁵³¹ A nanotube oriented at 45° was illuminated by the incident light with horizontal polarization after the polarizer 1. The electrical field scattered by the nanotube is polarized along the nanotube axis because the light perpendicularly polarized to the nanotube endures a strong

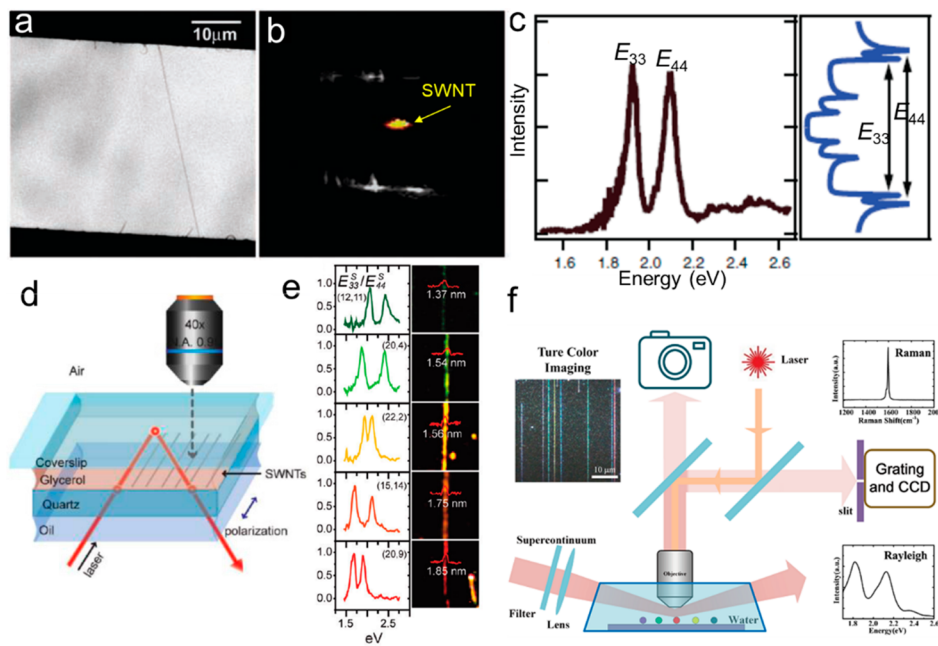


Figure 66. (a–c) SEM image of an isolated SWCNT that spans the slit (a), Rayleigh scattering of this tube imaged on a CCD camera (b), Rayleigh scattering spectrum of an isolated s-SWCNT and the DOS of a similar s-SWCNT (c). Reproduced with permission from ref 533. Copyright 2004 American Association for the Advancement of Science. (d) Scheme of optical setup of an on-chip Rayleigh image. (e) Color Rayleigh images of SWCNTs, along with their corresponding optical spectra and AFM height traces (shown in red). Reproduced from ref 538. Copyright 2011 American Chemical Society. (f) Integration of Rayleigh imaging and optical spectroscopy for true-color real-time imaging and chirality assignment of SWCNTs. Reproduced with permission from ref 539. Copyright 2015 Springer.

depolarization effect, whereas the reflection from the substrate retains the horizontal polarization. Since polarizer 2 is placed in a nearly vertical direction (with δ deviation), the substrate-reflected field reduces strongly by $\sin(\delta)$ but the field scattered by the nanotube remains. Therefore, the contrast of the nanotube is greatly enhanced, enabling the direct visualization of nanotubes on a growth substrate and fast assignment the (n,m) of each individual SWCNT (Figure 65d–h). The elliptical polarization-based optical method was further used to determine the real and imaginary susceptibility of individual SWCNTs with defined (n,m) in the E_{ii} range of 1.6–2.7 eV.⁵³² Above optical methods work well for individual substrate-supported nanotubes and suspended nanotubes. Very clean substrates and well-aligned, long enough ($>5 \mu\text{m}$), and low density ($<0.2 \text{ tube}\cdot\mu\text{m}^{-1}$) SWCNTs are required.

4.1.5. Rayleigh Scattering Spectroscopy. Compared to conventional measurements, Rayleigh spectroscopy presents many advantages in characterizing the chirality of SWCNTs. It relies on elastic scattering, which can be applied to both s- and m-SWCNTs, and allows visible wavelength excitation and detection for better spatial resolution and detection sensitivity. Rayleigh scattering peaks of individual SWCNTs can be detected by using a supercontinuum white laser, which corresponds to the van Hove singularities in the DOS of SWCNTs and enables chirality assignment (Figure 66a–c).^{533–535} The chirality can be determined precisely when Rayleigh scattering spectra (to obtain E_{ii}) are combined with Raman (to obtain d_i).⁵³⁶ An “atlas” for the optical transitions of SWCNTs was established by Wang et al. based on determination of 522 E_{ii} values from 206 individual air-suspended SWCNTs covering diameters from 1.3 to 4.7 nm.⁵³⁷ In this work, simultaneous Rayleigh scattering and ED measurements on the same tube enabled accurate assignment of (n,m) . The basic method to identify the chiral index of

suspended SWCNTs by various optical approaches is to compare only E_{ii} with the atlas. Rayleigh spectroscopy used in this work employs high-brightness supercontinuum white light on suspended nanotubes to determine the optical resonances for individual nanotubes with an uncertainty of less than 20 meV. However, a significant source of the uncertainty is the difficult-to-control environmental effects, where unintentional mechanical strain, charge doping, and gas adsorption can shift the E_{ii} by more than 10 meV.

The SWCNTs are colored because the resonance Rayleigh scattering peaks of SWCNTs are located in the visible range. In turn, this could facilitate the chirality assignment of individual SWCNTs. For air-suspended SWCNTs, it is effective to increase the excitation light intensity by using a supercontinuum white laser (Figure 66b).⁵³³ However, it is difficult to achieve real color imaging for SWCNTs on substrates due to the strong background scattering and the extremely low scattering intensity of SWCNTs. To overcome this problem, Park et al. developed a broadband laser-induced dark-field microscope to minimize the background scattering, allowing Rayleigh imaging of SWCNTs on substrate for the first time.⁵³⁸ In Figure 66d, a quartz substrate with SWCNTs was coated with glycerol, serving as an index-matching medium to weaken the background scattering effect. Additionally, the laser excitation geometry prevented incident light from being collected by the detection optics. The SWCNTs show distinct colors, and chiral indices were assigned simultaneously by combining Rayleigh scattering spectrum (to obtain E_{ii}) and AFM (to obtain d_i) (Figure 66e).

The intensity of Rayleigh scattering can be significantly improved owing to the enhanced interface dipole effect, which enables the imaging of the colors of SWCNTs on substrate by using a supercontinuum white laser illumination source.⁵³⁹ During imaging, different (n,m) SWCNTs display different colors, which provides general structural information on

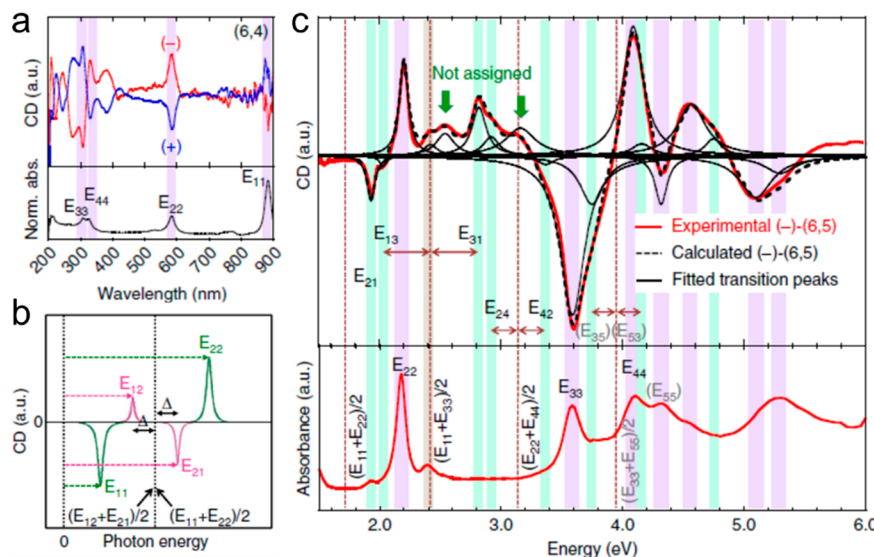


Figure 67. (a) CD spectra and absorption spectrum of the purified (6,4) SWCNTs. (b) Schematic showing a CD spectrum of a (−)-enantiomer with the asymmetric band structure. (c) CD and absorption spectra of the purified (−)-(6,5) SWCNTs. Reproduced with permission from ref 480. Copyright 2016 Nature Publishing Group.

SWCNTs. This imaging system can also provide a pair of (ω_{RBM} , E_{ii}) or (d_t , E_{ii}) simultaneously when combined with Raman and Rayleigh spectroscopies (Figure 66f). Unlike other techniques, this method has shown great promise for improving controlled growth as it is capable of quickly, reliably, and accurately determining both chiral index and abundance of SWCNTs simultaneously. However, it is also faced with the same problem as the polarized optical absorption method that very clean substrates and well-aligned, long SWCNTs are required.

4.1.6. Circular Dichroism Spectroscopy. Circular dichroism (CD) spectroscopy equipped with left- and right-handed circularly polarized light with respect to its wavelength reveals the difference in absorption. CD activity allows us to distinguish between SWCNT isomers with different chiralities.⁵⁴⁰ However, a mixture of SWCNTs with various chiralities is not applicable in CD spectroscopy due to the congestion of peaks in the CD spectra. In addition to single-chirality SWCNT samples with high purity, CD analysis also requires highly separated enantiomers. The high-purity single-chirality enantiomeric SWCNTs enable the assignment of E_{ii} and E_{ij} based on the optical transition selection rules (Figure 67a). Kataura et al. successfully determined the asymmetric excitonic band structures of 12 different single-chirality SWCNT enantiomers using the obtained E_{ii} and E_{ij} (Figure 67b, c).⁴⁸⁰ This is the first work that experimentally determines the asymmetric band structures of SWCNTs with different (n,m).

4.1.7. Scanning Tunneling Microscopy. The direct atom-resolved imaging technique of STM can directly characterize the d_t and chiral angle θ of a SWCNT.^{16,475,476} In an atomically resolved STM image, the black dots were attributed to the centers of hexagons. θ was determined from the angle between the hexagon rows and tube axis (Figure 68a).⁴⁷⁶ The d_t value was derived from the relative height between the nanotube and the surface after deconvoluting the tip contribution to the image. The accuracy of the STM measurement on a flat Au surface can be 0.05 nm at most. Zhang et al. reported a method to assign the (n,m) with the handedness, θ , d_t , and E_{ii} of SWCNTs. Handedness of SWCNTs can be also obtained by STM according to the chirality-dependent alignment of SWCNTs on a graphite surface.^{541,542} Taking the graphite trenches with

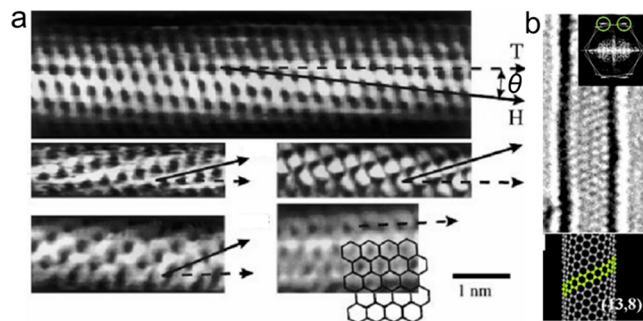


Figure 68. Direct imaging techniques to determine the (n,m) of SWCNTs. (a) Atomically resolved STM images showing tube axis (T) and direction of nearest-neighbor hexagon rows (H). Reproduced with permission from ref 476. Copyright 1998 Nature Publishing Group. (b) Moiré pattern and its Fourier transform. The best-fit model of the (13,8) SWCNT is also shown. Reproduced with permission from ref 296. Copyright 2004 Nature Publishing Group.

zigzag edges as necessary references, detailed formulas were summarized, and they are much more suitable to determine the handedness and θ of grown SWCNTs on graphite. In combination with the resonant Raman spectroscopy, the chiral index can be identified from the (d_t, θ) plot.

STM assisted spectroscopy (STS) directly reveals the major features in DOS for both s- and m-SWCNTs based on the $I-V$ data.⁴⁷⁶ However, this method has a significant error of 50–100 meV, which makes it unlikely to become a credible method in measuring electronic structures of SWCNTs.

4.1.8. Transmission Electron Microscopy. An atomically resolved AC-HRTEM image can also directly give the d_t and θ of a SWCNT.²⁹⁶ In an AC-HRTEM image, the moiré pattern originates from helically rolling up graphene layers. Fourier transform derived from the AC-HRTEM image shows two symmetric hexagons. These two hexagons with a mismatch angle (doubled θ) represent two graphene layers in the front or back of this nanotube. Therefore, the chiral index (n,m) can be determined from θ and d_t measured in the AC-HRTEM image and Fourier space (Figure 68b).²⁹⁶ However, the precision of θ

and d_t is limited by the resolution of the TEM image, leading to the assignment with pessimistic error bars.

ED was first introduced to characterize SWCNTs by Iijima and Ichihashi at the time of SWCNTs' discovery² and is obviously one of the most powerful methods for precisely identifying the chirality. Qin and Jiang et al. developed a series of ED methods to determine the structure of individual SWCNTs.^{478,543,544} An ED simulator was also launched on the Qin group Web site⁵⁴⁵ to assist the researchers in conveniently getting a standard ED pattern for a given (n,m) SWCNT. Figure 69a,b shows typical calculated and exper-

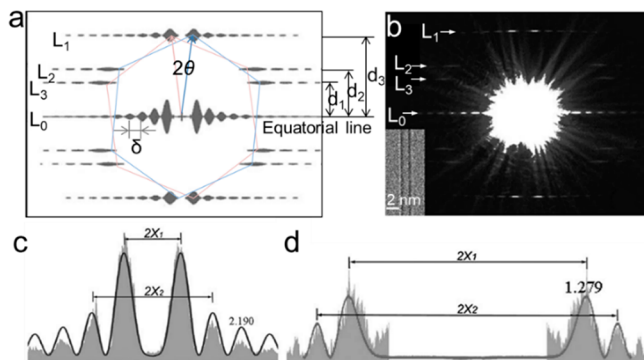


Figure 69. (a) Simulated ED pattern of a (17,2) SWCNT. The three principal layer lines (L_1 , L_2 , L_3) and layer-line spacings (d_1 , d_2 , d_3) are indicated. (b) ED pattern of a (17,2) SWCNT. Inset is a HRTEM image of a SWCNT. (c, d) Intensity profiles of principal layer line L_1 (c) and L_2 (d). Reproduced with permission from ref 546. Copyright 2005 Elsevier.

imental ED patterns of a (17,2) SWCNT. A high-quality ED pattern provides at least three solutions to identify the chiral index based on its layer-line intensity and spacing.^{199,200,544}

First, the n and m values can be directly determined from the order of the Bessel function, which is derived from the scattering intensity distribution of layer lines (L_1 , L_2 , L_3) (Figure 69c,d). However, this method has two major uncertainties originating from the low signal/noise ratio and low resolution of the intensity profile. It also has been proven by Jiang et al. that the tilt of the tube will strongly affect the intensity distribution of layer lines. The tilt angle between the near horizontal nanotube and the vertical electron beam is needed to correct the measurements.⁵⁴⁷ The second method is to calculate the ratio of n/m according to eq 2:

$$\begin{aligned} n/m &= (2d_3 - d_2)/(2d_2 - d_3); \\ n/m &= (d_1 + d_3)/(d_3 - 2d_1) \end{aligned} \quad (2)$$

where d_3 , d_2 , and d_1 are the layer line spacings of L_1 , L_2 , and L_3 , respectively, with a relationship of $d_3 = d_2 + d_1$ (Figure 69a). This method is more convenient and accurate because n/m ratio is independent of the CCD camera length and the tilt angle. Additionally, it sets less stringent constraints on signal/noise ratio of the ED pattern. However, this method cannot provide d_t because other (n,m) SWCNTs have the same ratio of n/m , for example, (6,3), (8,4), (10,5), etc. Fortunately, d_t can be acquired with other methods such as HRTEM image and RBM frequency or deduced from $d_t = 1/\delta$, where δ (nm^{-1}) is the period of radial oscillations of the equatorial line in the ED pattern (Figure 69a). The third method is to calculate θ according to eq 3,

$$\theta = \tan^{-1} \frac{2d_2 - d_3}{\sqrt{3}d_3} = \tan^{-1} \frac{d_2 - d_1}{\sqrt{3}d_3} \quad (3)$$

Although θ deduced from ED is independent of tube inclination,⁵⁴⁸ d_t is significantly affected by the tilt of the tube, which brings some uncertainty in the (n,m) assignment. SWCNTs with d_t over 5.1 nm are not suitable for microscopic or ED measurement because the tubes tend to be collapsed.⁵⁴⁹

4.1.9. Other Methods. In addition to the conventional characterization methods, some other techniques were also able to determine the structure of SWCNTs. Polarization-based photocurrent spectroscopy probes E_{11} and E_{22} in parallel polarization.⁵⁵⁰ This method is only applicable for individual suspended SWCNTs. Other methods such as FET,²⁰¹ SEM,^{551,552} electric force scanning probe microscopy,⁵⁵³ and infrared scattering-type scanning near-field optical microscopy⁵⁵⁴ are only applicable to distinguish m- and s-SWCNTs and are thus unable to identify their chirality.

4.1.10. Combination of Multiple Techniques. It is worth mentioning that despite the many advantages of optical and nonoptical techniques, there are limitations hindering the use of one technique alone to accurately determine the chiral index.

Uncertainty in Determining E_{ii} . E_{ii} values obtained by optical methods are always affected by tube environment. First, a bundling effect was often found in many types of samples,^{555,556} especially in suspended nanotubes.⁵⁵⁷ PL emission of suspended bundled SWCNTs shows a red shift of ~ 20 meV.⁵⁵⁷ Second, red shifts of E_{11} (7–60 meV) and E_{22} (5–60 meV) were observed in the on-substrate tubes compared to their suspended segments.^{530,558} It is also found that using E_{ii} obtained by optical methods to assign (n,m) works well for SWCNTs with relatively small diameter (normally $d_t < 1.5$ nm) but is inaccurate for large-diameter tubes (normally $d_t > 1.5$ nm) because large-diameter SWCNTs with similar d_t always exhibit similar E_{ii} ; for example, (17,15) and (18,14) tubes (Table 5).

Table 5. Comparison of Two Pairs of (n,m) SWCNTs

(n,m)	d_t (nm)	θ (deg)	E_{33}, E_{44} (eV)	conductivity
Pair 1				
(19,14)	2.25	25.0	1.69, 1.98	semiconducting
(20,15)	2.38	25.3	1.60, 1.89	semiconducting
Pair 2				
(17,15)	2.17	27.9	1.72, 2.06	semiconducting
(18,14)	2.17	25.9	1.69, 2.10	semiconducting

Uncertainty in Determining θ . The nonoptical approaches are very tedious for routine use. The main error in determining θ using STM comes from the determination of tube axis. It is very difficult to acquire atomic resolution TEM images because SWCNTs are not stable under the e-beam irradiation at a high magnification. For the ED method, it is applicable only for clean suspended individual SWCNTs. SWCNTs with very small θ normally cannot grow long. So information on such tubes may be lost due to the difficulties to put them across a gap for ED measurement. Besides, the values of both d_t and θ for large-diameter SWCNTs must be detected very accurately in order for unambiguous determination of (n,m) . It is also difficult to analyze the ED patterns from SWCNT bundles, bringing more uncertainty with ED method.

Based on the above discussion, the combination of optical and nonoptical techniques provides a more reliable way to precisely determine the chiral index. It is especially feasible for large-

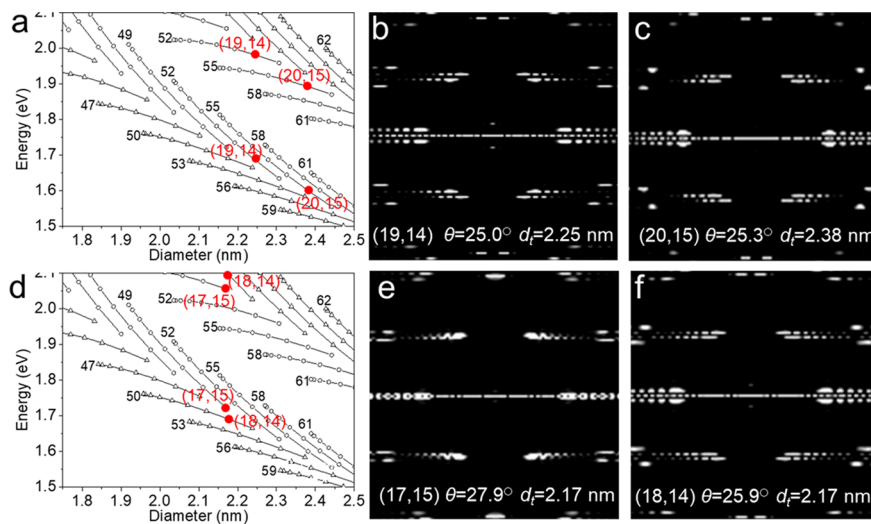


Figure 70. Chirality assignments using the combination of E_{ii} , d_t , and θ . (a, d) Expanded view of the Kataura plots for large diameter SWCNTs. The E_{ii} are from the atlas theoretical value.⁵³⁷ (b, c, e, f) Simulated ED patterns of (19,14) (b), (20,15) (c), (17,15) (e), and (18,14) (f) SWCNT.

diameter SWCNTs as well as DWCNTs.^{516,537,559,560} SWCNTs of large diameter (normally $d_t > 1.5$ nm) often exhibit similar d_t , θ , and E_{ii} , so they may show similar characteristics in TEM measurements. For instance, the ED pattern of a (19,14) tube is very similar to that of a (20,15) tube, because these two tubes have similar d_t and θ (Figure 70b,c, Table 5). A small error in either d_t or θ results in uncertainty in indexing the (n,m) of a SWCNT. Fortunately, the E_{33} and E_{44} of (19,14) and (20,15) tubes measured by optical methods are different (Figure 70a). In contrast, it is difficult to distinguish the (18,14) and (17,5) tubes with various optical methods because of their similar d_t , E_{33} , and E_{44} (Table 5). A slight error in either d_t or E_{ii} caused by the environment results in an ambiguity in indexing the (n,m) of a SWCNT. However, the ED patterns of them differ greatly, which can be used to easily discern them (Figure 70d–f). The above examples show that the combination of ED and spectroscopic methods enables an accurate assignment of large-diameter SWCNTs.

4.2. Chirality Quantification

Accurately quantifying the (n,m) species in a SWCNT ensemble is a key step in chirality controlled preparation and is also essential for high-end applications of SWCNTs. Unfortunately, currently there is no quantitative standard to accurately determine the (n,m) abundance, and there is still an absence of standard SWCNT samples with known (n,m) contents. The definition of chirality abundance can be divided into two categories (Figure 71). One is the SWCNT concentration abundance for a sample containing different (n,m) species, taking into consideration both the tube length and tube number. This is normally applicable for quantifying ensemble SWCNT samples, including SWCNT dispersions in solvent and SWCNT network films. The other is the SWCNT number abundance of each (n,m) species, regardless of the tube length, which is generally applicable for individual SWCNTs on a substrate. The counting-based methods such as Raman,¹⁵ polarized optical absorption,⁵³¹ Rayleigh scattering,⁵³⁹ and ED¹⁷³ are often used to statistically determine the population and number abundance of different (n,m) species.

4.2.1. Quantification of Ensemble SWCNTs. Ensemble form nanotubes are generally dispersed in a suspension for further optical measurements. Signal intensity based optical

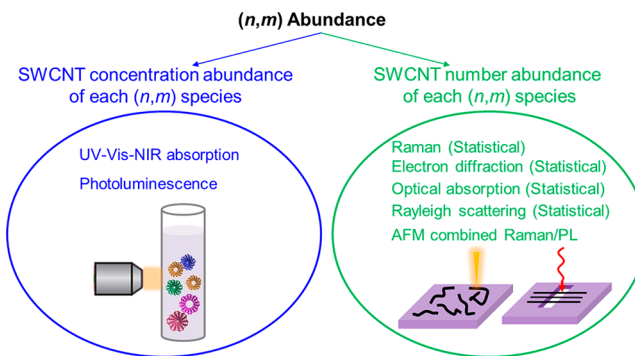


Figure 71. Two categories of (n,m) abundance and corresponding quantitative methodologies. Right part adapted from ref 487. Copyright 2017 American Chemical Society.

techniques such as Raman, UV–vis–NIR absorption, and PL are basic methods to this end. However, the signal intensity itself can give accurate quantitative estimation of neither the (n,m) concentration nor their relative abundance, because the information on chirality dependence of physical parameters, such as optical cross-sections and quantum yields, is missing.

Absorption. For quick characterization of SWCNT suspensions, UV–vis–NIR absorption spectroscopy has been widely employed and has worked for both semiconducting and metallic (n,m) species. The quantification for the carbon concentration of each (n,m) species of SWCNTs from UV–vis–NIR absorption spectra is based on the absorption band of each (n,m) SWCNT by integrating the absorption peak. But this approach is only applicable for well resolved spectra; meanwhile the absorption cross-section associated with a given chirality is known. However, the cross-section varies very much between (n,m) species, creating an extra difficulty in weighting correctly the absorption peaks.

Reported values for absorption cross-sections range from 10^{-18} to 10^{-17} eV·cm² per atom for E_{11} ^{561,562} and 10^{-19} to 10^{-17} eV·cm² per atom for E_{22} .^{563,564} These discrepancies clearly indicate the need for more accurate measurements of absorption cross-sections of various (n,m) species of SWCNTs. This is crucial for reliable quantitative analyses. Determining the absorption cross-section of a SWCNT species requires

combined measurements of optical attenuation and concentration of this (n,m) species. Weisman et al. measured the absolute cross-sections for the E_{11} and E_{22} absorption of 7 s-SWCNTs species in suspensions.⁵⁶⁵ Chirality-specific concentrations were calculated by using PL microscopy to directly count tubes. The cross-sections per atom were found to inversely relate to d_t (Figure 72a). Vialla et al. proved

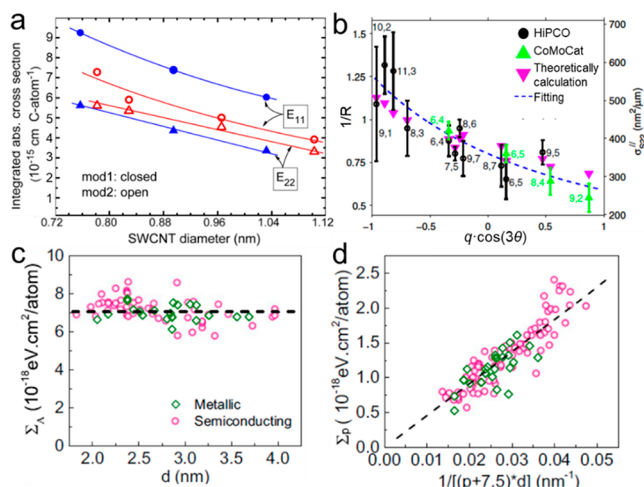


Figure 72. (a) Integrated E_{11} and E_{22} absorption cross-sections as a function of d_t . Reproduced from ref 565. Copyright 2014 American Chemical Society. (b) Inverse of the R ratio as a function of $q \cdot \cos(3\theta)$. Reproduced with permission from ref 566. Copyright 2013 American Physical Society. (c) Integrated absorption cross-section. (d) Tube-dependent exciton oscillator strength described by a law of $4.6 \times 10^{-24} / [(p+7.5)d]$ $\text{eV}\cdot\text{cm}^3/\text{atom}$ (dashed line). Reproduced with permission from ref 559. Copyright 2014 National Academy of Sciences of the USA.

experimentally that absolute absorption cross-section of s-SWCNTs at their E_{22} depends on their θ , and deduced a simple empirical expression, $\sigma E_{22} = 10^3 / [q \cdot \cos(3\theta) + 28]$, for the E_{22} absorption cross-section of a (n,m) species (Figure 72b).⁵⁶⁶

The above absorption measurements on nanotube ensembles only provided averaged behavior. It is still challenging to reliably determine the absorption cross-section at the single-tube level. Wang et al. demonstrated a high-throughput of polarized homodyne method to quantitatively measure the absorption cross-section of individual SWCNTs.⁵⁵⁹ In combination with ED measurements on the same tube, the absolute absorption cross-sections of an individual SWCNT with defined (n,m) can be determined. They noted that for all of over 50 individual SWCNTs, the averaged and integrated absorption cross-sections are $\sim 7.6 \times 10^{-18} \text{ eV}\cdot\text{cm}^2/\text{atom}$ and $7.1 \times 10^{-18} \text{ eV}\cdot\text{cm}^2/\text{atom}$, respectively, in the 1.55–2.48 eV spectral range (Figure 72c). The exciton oscillator strength has a relationship with d_t and transition order (p). Surprisingly, both m- and s-SWCNTs exhibit similar exciton oscillator strength despite their largely different electron–hole interactions (Figure 72d).

Another critical issue that hampers quantitative analysis is fitting of absorption spectra. The fitting-sensitive factors include the full width at half-maximum, the spectral line shape, the determination of spectral regions for m- or s-SWCNTs and (n,m) dependent on E_{ii} , the appropriate height or peak area ratio of E_{11}^S/E_{22}^S for each (n,m) species, electron–phonon sideband contributions to the main peaks, types of background subtraction, etc.⁵⁶⁷ For example, most work used empirical background that was subtracted at the peak minima to approximate the absorption from electronic transitions of SWCNTs.^{568–570} Such empirical background always cause a significant deviation in determining the absorption peak position and area, thus leading to a deviated analysis of (n,m) abundance. The absorption background of SWCNTs in dispersions varies significantly with external factors, including the types of surfactant, preparation process, and chemical doping.⁵⁶⁹ With these factors affecting the absorption background, it is particularly challenging to establish a standard protocol for reproducible quantitative fitting of absorption spectra based on the various SWCNT dispersions. Recently, Flavel et al. introduced the exciton–phonon sidebands to individualize the overlapped spectra by utilizing the correlations between the E_{11} and E_{22} and the exciton–phonon sidebands.⁵⁶⁷

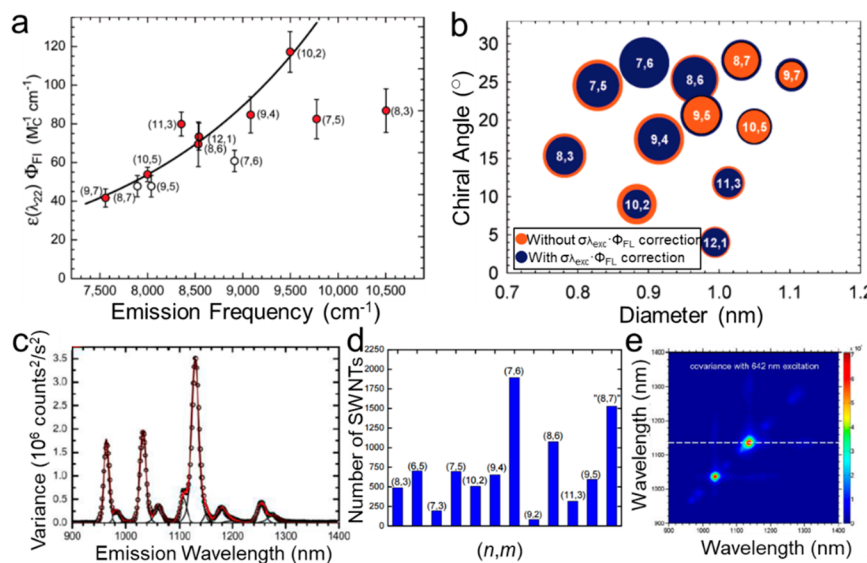


Figure 73. (a) Relation between PL action cross-section and emission frequency (ν). (b) Relative (n,m) -resolved PL distributions. Reproduced from ref 574. Copyright 2007 American Chemical Society. (c–e) Variance spectroscopy of HiPco SWCNTs excited at 660 nm (c), corresponding deduced SWCNT number abundance (d), and covariance matrix (e). Reproduced from ref 575. Copyright 2015 American Chemical Society.

This work offers the possibility of utilizing different backgrounds at different experimental conditions.

Photoluminescence. The PL spectroscopy, as well as the two-dimensional PL contour maps, readily provide an essential tool for determining the relative abundance of (n,m) for s-SWCNT.^{503,571,572} m-SWCNTs do not fluoresce. Moreover, it requires structure-dependent factors that relate the PL intensities to actual concentration to quantitatively reveal the chiral purity.

PL intensity, determined by both excitation and emission, is proportional to the species concentration, absorption cross-section at the excitation wavelength ($\sigma_{\lambda,\text{exc}}$), and corresponding PL quantum yield (Φ_{FL}).⁵⁷³ Therefore, the PL action cross-section can be termed as $\sigma_{\lambda,\text{exc}}\Phi_{\text{FL}}$. In earlier PL analysis of SWCNT samples, it was generally assumed that the PL action cross-section is independent of (n,m) .⁴⁸ Weisman et al. first reported the experimental measurement of absolute PL action cross-section of 12 s-SWCNTs by using single-nanotube NIR microscopy.⁵⁷⁴ They found that the PL action cross-section ($\sigma_{\lambda,\text{exc}}\Phi_{\text{FL}}$) generally increased with band gap (Figure 73a). Applying the empirical $\sigma_{\lambda,\text{exc}}\Phi_{\text{FL}}$ factor correction shows a tendency to decrease the measured relative abundances of SWCNTs with smaller diameters. It can be also found that after correction the abundance of the near-armchair chiralities is even higher (Figure 73b), which agrees with the results reported by Jorio and other groups.^{572,573} A new PL-based variance spectroscopy was developed by Weisman et al. to provide accurate quantitative results on the (n,m) distribution of unsorted SWCNTs and on the extraction of the spectra of single chirality from a mixture of (n,m) species.⁵⁷⁵ This approach was demonstrated by using PL spectra of unsorted SWCNT suspensions to deduce (n,m) abundances and emission efficiencies (Figure 73c,d). Moreover, correlations of intensity variations at different wavelengths is sensitive to the nanotube aggregation in suspensions (Figure 73e).

The sensitivity of PL is higher than Raman or absorption for detection, identification, and quantification of SWCNTs in trace amounts. Compared to absorption methods, essentially no PL background is needed to model and subtract. Another advantage is that there is less congestion in the PL spectrum than in absorption given that the emission peaks from (n,m) species near excitation resonance are enhanced. Therefore, the combination of PL with absorption was also employed to improve the accuracy in determining the semiconducting (n,m) abundance in an unknown sample.⁵⁷⁶ The (n,m) species was identified by PL first, and then the absorption spectrum was fitted based on the assignment results of PL. The PL also avoids the excitation problems of Raman spectroscopy since Raman requires expensive tunable or multiwavelength lasers but PL only needs tunable excitation from a lamp with a monochromator. However, the PL quantum yield depends on the tube length and environment, such as bundling effects, pH, and impurities.^{364,577,578} Therefore, it is still elaborate and difficult to make quantitative assessment of the (n,m) distribution based on PL.

Raman. The method to quantify the (n,m) population of ensemble samples through Raman is by calculating the integrated RBM intensities of each resonant (n,m) SWCNTs.^{61,579–582} However, the resonant Raman intensity depends not only on the Raman cross-section and the number of the specific (n,m) SWCNTs^{496,583,584} but also on other unknown intensity-sensitive factors, such as polarized direction,

bundling effects, and external environment,⁴⁹⁶ causing more difficulty in determining the (n,m) abundance.

4.2.2. Quantification of On-Substrate Individual SWCNTs. Different from ensemble samples, quantifying (n,m) abundance of individual SWCNT samples on substrates is mainly based on statistically counting the tube number of each (n,m) species by using Raman,^{15,18,145,221,245,485} polarization-based optical absorption,²¹² and ED.^{75,173} Raman spectral mapping is a generally used tool but is currently hindered by the requirement of tunable excitation lasers. Li et al. developed the methodology for quantifying specific chirality of SWCNTs grown with Co₇W₆ catalysts on substrate.^{15,485} They collected 1863 RBM data sets under six laser excitations with micro-Raman. An averaged tube density of 6.7 tubes/ μm^2 is calculated from 7 samples based on SEM and AFM images. It is apparent that only one RBM peak will appear even when multiple (12,6) tubes are present within the laser spot. Considering the factor that the six lasers used cover ~85% of all SWCNT chiralities,⁵⁸¹ the calibrated content of (12,6) can be estimated from the eq 4:

$$x_{(12,6)} = \frac{N_{(12,6)}\bar{n}x_{(12,6)}}{N_{(12,6)}\bar{n}x_{(12,6)} + N_{\text{others}}/0.85} \quad (4)$$

where $x_{(12,6)}$ is the calibrated content of (12,6) in the sample, $N_{(12,6)}$ is the total times that RBM for (12,6) is observed, N_{others} is the total times that RBM for all other chiralities is observed, and \bar{n} is the average number of SWCNTs under the laser spot. The calibrated content of (12,6) is 93.0% using $\bar{n} = 6.7$, in good accordance with abundance of 92.5% obtained from the UV-vis–NIR spectra and 94.9% obtained from combination of AFM and Raman measurements.¹⁵ This methodology is also used to determine the abundance of (14,4) SWCNTs.³⁹

The aforementioned polarization-based homodyne optical absorption could be an effective tool for quantifying (n,m) SWCNT arrays on substrates,⁵³¹ which avoids the “selective excitation” problem of Raman. Liu et al. measured the chirality of over 400 individual SWCNTs grown in the same conditions, which includes 240 s-SWCNTs and 162 m-SWCNTs.²¹² Therefore, the (n,m) distribution of hundreds of SWCNTs on substrates can be accurately determined. He et al. analyzed a total number of 57 individual SWCNTs grown from MgO/Co catalyst by using ED, showing that ~53% (30 out of 57) are (6,5) species.⁷⁵ In 2013, The US National Institute of Standards and Technology (NIST) released the world’s first reference material of dispersed SWCNTs known as RM8281. RM8281 has been successfully applied to develop a universal protocol to determine the purity of bulk samples. Jiang et al. adopted HRTEM/ED to statistically acquire the (n,m) distribution of the RM8281 sample, in good agreement with the results from UV-vis–NIR absorption.⁵⁷⁰

4.2.3. Limitations of Present Quantitative Methods. Let us summarize the limitations that hamper the abundance analysis of (n,m) species of SWCNTs. First of all, individually isolated or dispersed SWCNTs are needed for accurate and reliable quantification on different species of chirality. So the preparation of ideal samples is still a great challenge for the present analytical techniques.

In solution-based techniques, including absorption and PL, the dispersion of SWCNTs is always a crucial procedure. It is necessary but always difficult to reach full dispersion of all samples in solution, keeping each nanotube individually dispersed. Besides the issue of dispersion, some of the main limitations for the absorption methods are as follows: (i)

Absorption is limited by the low spectral resolution and poor differentiation between some (n,m) SWCNTs with similar E_{ii} values. (ii) Accurate and reasonable background subtraction and peak fitting of absorption spectra are still technically challenging. (iii) No calibration rule is available to correlate the peak intensity of a given (n,m) species to its abundance because the peak intensity is affected by many factors such as the tube environment.

PL can only be used for s-SWCNTs. Compared to absorption, PL intensity is more sensitive to the environment. Factors such as pH value are also responsible for changes in the PL spectra. Another technical limitation of PL is that the most commonly used InGaAs detector equipped for a PL spectrometer has a long-wavelength limit of ~ 1700 nm, only satisfactory for s-SWCNTs with $d_t < 1.3$ nm ($E_{11} > 0.73$ eV). The emission of larger diameter s-SWCNTs ($d_t > 1.3$ nm, $E_{11} < 0.73$ eV) is undetectable. This limitation can be largely overcome by using a longer-wavelength detector such as a HgCdTe detector,⁵²⁶ but the signals need to be further calibrated. With these limitations, it is impossible to get an accurate abundance of different SWCNT chiralities by PL.

The polarized absorption and Rayleigh scattering techniques are applicable to on-substrate SWCNTs, but very clean substrates are required within the laser spot. The SWCNTs should be well-aligned and long enough (normally > 5 μm), and the tube density should be suitable (normally < 0.2 tube $\cdot \mu\text{m}^{-1}$) to ensure the detection of individual tubes.

Raman spectroscopy suits all kinds of SWCNTs though it suffers from the limitation of resonance windows, which can be overcome largely by using tunable lasers or multiple wavelength lasers.

ED normally is applied for suspended SWCNTs. Unfortunately, SWCNTs with very small chiral angle normally cannot grow long. Therefore, information on such tubes might be lost due to the difficulties to grow or place them across a gap for ED detection. In order to obtain quantitative information of each sample, many spectra or patterns need to be acquired.

4.2.4. Combination of Multiple Techniques. The combination of different techniques can help to overcome the limitations of each technique. The most frequently used strategy is using microscopy (for tube visualization) and spectroscopy (to determine chiral index) together. Kappes et al. developed an approach to combine and compare the PL (spectroscopic) and AFM (topographical) information for the same individual nanotubes on a substrate.⁵⁸⁵ The structure of luminescent s-SWCNTs was probed by PL spectroscopy and the diameter and length as well as spatial position of deposited SWCNTs were accurately determined by high-resolution AFM imaging (Figure 74a–c). This approach can be employed to determine the (n,m) abundance by probing the individual nanotubes one by one. Similarly, Weisman et al. developed a combined method to measure the fraction of s-SWCNTs. The density of the on-substrate tube can be compared in images from NIR PL (to obtain s-SWCNTs) and AFM (to obtain all tubes) to calculate the semiconducting fraction.⁵⁸⁶ It has been applied to nanotubes synthesized by 6 different groups and shown to be a very reliable method. However, environmental factors such as substrate can strongly quench PL signals, which leads to insufficient estimation of the abundance of some (n,m) species.

For chirality-specific SWCNT samples on substrates, Li et al. used Raman (to detect specific (n,m) species) instead of PL to work together with AFM (to detect all tubes) in quantifying the chiral purity of SWCNTs (Figure 74c,d).¹⁵ They dispersed the

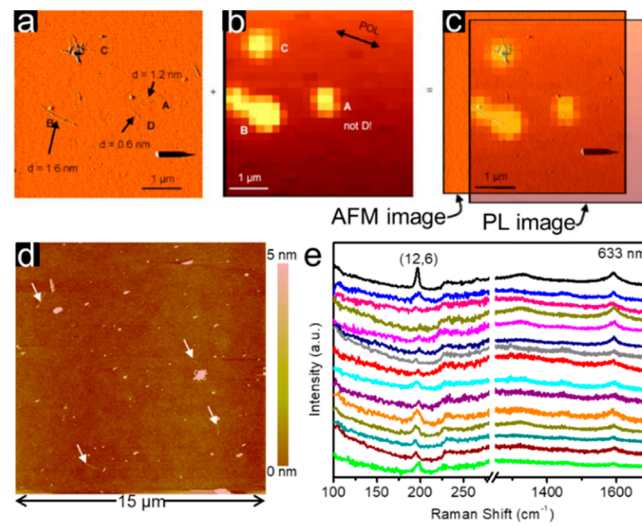


Figure 74. (a–c) AFM image (a), near-IR PL image (b), and overlay of the AFM and PL images (c). Reproduced with permission from ref 585. Copyright 2007 Wiley. (d, e) AFM image (d) and Raman spectra (e) of individual nanotubes from the (12,6) SWCNT dispersion. Reproduced with permission from ref 15. Copyright 2014 Nature Publishing Group.

SWCNTs into aqueous solution. Then the SWCNT dispersion was dropped onto a substrate, and the fraction of (12,6) SWCNTs was obtained from the ratio of (12,6) tube density (counting from Raman mapping) to total tube density (counting from AFM imaging).¹⁵ This combined method also works well for other chirality-specific samples grown on a substrate.⁵⁸⁹ The visualization of individual SWCNTs under an optical microscope makes the investigation of SWCNTs easier, which accelerates the quantitative characterization of each individual SWCNT with spectroscopy.^{539,587}

Another attempt was used to analyze the (n,m) abundance by combining absorption and PL spectroscopies.^{49,588} With better resolved peak positions of s-SWCNTs identified in PL, the absorption spectrum was fitted to reveal even the small shoulder peaks. Thus more reliable determination of the (n,m) distributions of s-SWCNTs was achieved.

5. CONCLUDING REMARKS AND PERSPECTIVES

5.1. Summary of the Present Research

Many efforts have been devoted to the controlled preparation of SWCNTs toward single-chirality. The growth of (6,5)/(7,5)-enriched SWCNTs on CoMo catalysts in 2003⁴⁸ is the prologue of chirality selective growth of SWCNTs. Since then, researchers have intensively studied the growth mechanism, the effects of catalysts, and growth conditions. Based on all these experimental and theoretical understandings, Li et al. developed a strategy of using catalysts with defined structure and unique atomic arrangements to achieve direct synthesis of SWCNTs with specific (n,m) under proper kinetic growth conditions in 2014.¹⁵ Right now, the highest chiral purity ever reported is 97% for (14,4) tubes using Co_7W_6 catalyst.⁵⁹ It is important to design catalysts with stable and unique structures that match the desired (n,m) SWCNTs and simultaneously optimize a carbon feeding condition to match the growth of this (n,m) SWCNT.⁶⁴

In parallel to efforts in controlled growth, intensive studies have been performed to develop a range of effective purification methods to achieve SWCNT separation with reasonable purity and yield. Among the techniques developed, DGU, GC, and

ATP extraction have shown to be very effective in obtaining chirality-pure SWCNTs dispersed in aqueous solution. To date, there have been 40 kinds of enriched or high-purity (n,m) species and their enantiomers obtained by different separation methods.

The characterization of SWCNTs, including optical, non-optical, and combined methods, has been developed along with the controlled preparation and sorting. At the level of ensemble nanotubes, spectroscopic methods such as Raman, absorption, and PL, are widely used to assign and quantify the concentration abundance of (n,m). At the level of individual nanotubes, counting-based methods through Raman, polarized optical absorption, Rayleigh scattering, and ED, as well as their combinations with imaging techniques including AFM and SEM, are used to quantify the number abundance of (n,m) statistically.

5.2. Remaining Challenges

Despite the achievements, many challenges remain. Here we point out some key challenges and offer our perspectives on these issues.

5.2.1. Growth Mechanism of Chirality-Controlled

SWCNTs. The mechanisms of the chirality-controlled growth of SWCNTs are still under debate. The diversity of catalysts and CVD parameters brings about great complication of the process. In recent years, direct *in situ* atomic-scale observation of SWCNT growth was achieved with the help of aberration-corrected ETEM, which however is still far from the realistic CVD systems. The gas pressure in the TEM chamber is very low (up to hundred pascals) and only a very small fraction of gases are heated and decomposed near the micrometer-scaled heating region of the ETEM chip. On the other hand, e-beam irradiation, which was found to influence (accelerate or retard) the dynamics of catalyst and nanotube growth, is often ignored. The experimental knowledge on the role of carbon atoms in or on the catalyst body or surface is still limited due to the difficulty in imaging light elements by TEM. A large amount of TEM observations are needed to reach a general statistically meaningful conclusion.

Other physical and chemical processes such as electron or charge transfer between tube and catalyst have also been proposed to explain the growth mechanism. Simulations by Chen et al. showed that catalyst structure strongly correlates with nanotube of certain chirality through charge transfer.⁵⁸⁹ *In situ* X-ray related spectroscopies such as XPS and XAFS are effective to probe the chemical characteristics of catalysts including valence state and chemical interaction during the nanotube growth. However, catalysts are inhomogeneous with different size, morphology, structure, and activities; only a small fraction of catalysts are active for growing SWCNTs. The signals from X-ray spectroscopy are averaged and are not specific for active catalysts. ETEM combined with EELS might be suitable to do this. Another challenge for *in situ* X-ray techniques is the limited resolution of time scale.

Currently, most of the *in situ* studies are mainly focused on the catalyst, but real-time tracking of the growth kinetics of SWCNTs are rarely reported. There is still no reliable way to directly track the decomposition of carbon precursor or determine the carbon feeding rate, which is crucial for optimizing the kinetic growth conditions. Linking the properties (composition, structure, etc.) of the catalysts to the growth rates of SWCNTs of various chiralities will be very important to guide the kinetic-controlled growth.

Atomistic theoretical simulation has predicted and demonstrated the growth process of SWCNTs to a certain degree but there is a need to simplify the model and process. Slight changes in setting parameters for the model will greatly influence the simulated results. Mechanisms of thermodynamics or kinetics derived chirality selectivity are still unclear. A more accurate simulation method is needed to give a clear picture of SWCNT growth.

5.2.2. Scalable Growth of Ultrapure Single-Chirality

SWCNTs and Their Quantification. The large-scale growth of chirality-specific SWCNTs with ultrahigh purity is not yet realized. The growth efficiency and chirality selectivity should be further improved. The wafer-scale growth of horizontally aligned s-SWCNT arrays with specific chirality is highly required for nanoelectronics applications. To reach this target, catalyst design and growth modulation are two indispensable factors: the selection of catalysts with desired composition and structure, the preparation of uniform catalysts with defined structure and even dispersion of catalysts on wafer-scale substrate, and the optimization of growth condition to ensure the catalyst activity and selectivity.

Though currently we have some characterization techniques to access the abundance of chiral species, there is a real necessity for developing other techniques that are reliable, accurate, and fast with nanometer-scaled spatial resolution, particularly for wafer-scale samples. In addition, quantification of single-chirality SWCNTs with ultrahigh purity is still a great challenge.

5.2.3. Low-Cost Sorting of Single-Chirality SWCNTs for

Large Scale Production. The main challenges for the application of solution-derived SWCNTs with specific (n,m) are how to improve the sorting efficiency and obtain chemically clean SWCNTs. Currently, concentrations of purified SWCNT dispersions ($\mu\text{g}\cdot\text{mL}^{-1}$) are still far below that required by practical applications. Techniques such as recycled separation and removal of dispersive agents of SWCNTs need to be explored. Strong sonication is essentially used to prepare solutions of individually dispersed SWCNTs, but it introduces defects on the tube wall and shortens the nanotube length down to $<1\ \mu\text{m}$, thus becoming unfavorable for developing high-performance electronics. Recent development in superacid-assisted dispersion of full-length SWCNTs³²¹ is encouraging and may provide a way to avoid the sonication process.

5.3. Future Outlook

Making chirality-pure SWCNTs via either CVD synthesis or solution-based separation has intrinsic scientific value. It represents advances in the precise synthesis of nanomaterials with atomic-scaled control. SWCNT-based applications, for example, electronics, have undoubtedly experienced dramatic advances in recent years. More exciting applications of chirality-pure SWCNTs have also been developed continuously, such as quantum information processing^{590,591} and biosensing and imaging.⁵⁹² There is no doubt in our mind that more unforeseeable applications will emerge if we can make steady improvement. It can be greatly promoted by the reliable and scalable production of single-chirality SWCNTs. To really achieve such a goal, more efforts should be devoted to full understanding of the chirality-controlled growth mechanism, improving the chiral purity, lowering the cost, scaling up the preparation, and developing reliable characterization techniques.

AUTHOR INFORMATION**Corresponding Authors**

Ming Zheng — Materials Science and Engineering Division, National Institute of Standards and Technology, Gaithersburg, Maryland 20899, United States;  orcid.org/0000-0002-8058-1348; Email: ming.zheng@nist.gov

Yan Li — Beijing National Laboratory for Molecular Science, Key Laboratory for the Physics and Chemistry of Nanodevices, College of Chemistry and Molecular Engineering, Peking University, Beijing 100871, China;  orcid.org/0000-0002-3828-8340; Email: yanli@pku.edu.cn

Authors

Feng Yang — Beijing National Laboratory for Molecular Science, Key Laboratory for the Physics and Chemistry of Nanodevices, College of Chemistry and Molecular Engineering, Peking University, Beijing 100871, China;  orcid.org/0000-0002-3637-814X

Meng Wang — Beijing National Laboratory for Molecular Science, Key Laboratory for the Physics and Chemistry of Nanodevices, College of Chemistry and Molecular Engineering, Peking University, Beijing 100871, China

Daqi Zhang — Beijing National Laboratory for Molecular Science, Key Laboratory for the Physics and Chemistry of Nanodevices, College of Chemistry and Molecular Engineering, Peking University, Beijing 100871, China

Juan Yang — Beijing National Laboratory for Molecular Science, Key Laboratory for the Physics and Chemistry of Nanodevices, College of Chemistry and Molecular Engineering, Peking University, Beijing 100871, China;  orcid.org/0000-0001-5502-9351

Complete contact information is available at:
<https://pubs.acs.org/10.1021/acs.chemrev.9b00835>

Notes

The authors declare no competing financial interest.

Biographies

Feng Yang received his Ph.D. degree in chemistry under Prof. Yan Li at Peking University in 2017. He subsequently held the National Postdoctoral Program for Innovative Talents fellowship and worked as a postdoctoral fellow in Prof. Yan Li's group until October 2019. Then he joined the faculty of Southern University of Science and Technology as an Assistant Professor. His interests mainly include the chirality controlled growth of SWCNTs, intermetallic catalysts, and ETEM and XAFS study on catalysts and growth mechanism of nanomaterials.

Meng Wang is a sixth-year Ph.D. candidate under Prof. Yan Li at college of chemistry of Peking University. He is working on solution processing of SWCNTs.

Daqi Zhang received his Ph.D. degree of chemistry under Prof. Yan Li at Peking University in 2017. He works on the spectroscopic characterization of SWCNTs.

Juan Yang received her Ph.D. degree from Texas A&M University in 2006. After that, she undertook postdoctoral research at Texas A&M University from 2006 to 2007 and at Pacific Northwest National Laboratory from 2007 to 2008. She joined Peking University in 2009 and became an associate professor in 2010. Her research focuses on the spectroscopic characterization of carbon-based nanomaterials and nanostructures.

Ming Zheng received B.S. and M.S. degrees in electronics from Peking University, a M.S. degree in physics from University of Utah, and a Ph.D. degree in chemistry from Princeton University in 1995. He was an American Cancer Society Postdoctoral Fellow at the US National Institutes of Health from 1996 to 2000. From 2000 to 2009, he was a principal investigator at DuPont Central Research and Development. In 2009, Ming Zheng joined the US NIST, where he is now a staff scientist. His current research focuses on carbon nanotubes and their hybrids with DNA for nanotube sorting and biosensing applications.

Yan Li received her Ph.D. from Peking University in 1993. She joined the faculty of Peking University in 1995 and was promoted to Full Professor in 2002. She was appointed a Chang Jiang Professor by the Chinese Ministry of Education in 2013. She has been appointed a distinguished visiting professor in School of Engineering, The University of Tokyo, from 2016 to 2019. She serves as associate editor and on advisory and editorial boards for several ACS and RSC journals. She is a Fellow of the Royal Society of Chemistry. Her research focuses on functional nanomaterials and nanostructures, especially carbon nanomaterials.

ACKNOWLEDGMENTS

We thank Dr. Renu Sharma from NIST for the valuable comments on the manuscript. The authors acknowledge financial support from National Natural Science Foundation of China (NSFC) under Project 21631002, Ministry of Science and Technology of China (2016YFA0201904), Shenzhen Basic Research Project (JCYJ20170817113121505), and NSFC U1632119. F.Y. acknowledges the National Postdoctoral Program for Innovative Talents (BX201700015), China Postdoctoral Science Foundation (2018M640017), and BMS Junior Fellow of Beijing National Laboratory for Molecular Science (2019BMS10012).

REFERENCES

- (1) Iijima, S. Helical Microtubules of Graphitic Carbon. *Nature* **1991**, *354*, 56–58.
- (2) Iijima, S.; Ichihashi, T. Single-Shell Carbon Nanotubes of 1-nm Diameter. *Nature* **1993**, *363*, 603–605.
- (3) De Volder, M. F.; Tawfick, S. H.; Baughman, R. H.; Hart, A. J. Carbon Nanotubes: Present and Future Commercial Applications. *Science* **2013**, *339*, 535–539.
- (4) Hong, G. S.; Diao, S. O.; Antaris, A. L.; Dai, H. J. Carbon Nanomaterials for Biological Imaging and Nanomedicinal Therapy. *Chem. Rev.* **2015**, *115*, 10816–10906.
- (5) Yu, L.; Shearer, C.; Shapter, J. Recent Development of Carbon Nanotube Transparent Conductive Films. *Chem. Rev.* **2016**, *116*, 13413–13453.
- (6) He, X.; Htoon, H.; Doorn, S. K.; Pernice, W. H. P.; Pyatkov, F.; Krupke, R.; Jeantet, A.; Chassagneux, Y.; Voisin, C. Carbon Nanotubes as Emerging Quantum-Light Sources. *Nat. Mater.* **2018**, *17*, 663–670.
- (7) Zhang, R.; Zhang, Y.; Wei, F. Horizontally Aligned Carbon Nanotube Arrays: Growth Mechanism, Controlled Synthesis, Characterization, Properties and Applications. *Chem. Soc. Rev.* **2017**, *46*, 3661–3715.
- (8) Jeon, I.; Matsuo, Y.; Maruyama, S. Single-Walled Carbon Nanotubes in Solar Cells. *Top. Curr. Chem.* **2018**, *376*, 4.
- (9) Franklin, A. D. Nanomaterials in Transistors: From High-Performance to Thin-Film Applications. *Science* **2015**, *349*, aab2750.
- (10) Rao, R.; Pint, C. L.; Islam, A. E.; Weatherup, R. S.; Hofmann, S.; Meshot, E. R.; Wu, F.; Zhou, C.; Dee, N.; Amama, P. B.; et al. Carbon Nanotubes and Related Nanomaterials: Critical Advances and Challenges for Synthesis toward Mainstream Commercial Applications. *ACS Nano* **2018**, *12*, 11756–11784.

- (11) Tu, X.; Manohar, S.; Jagota, A.; Zheng, M. DNA Sequence Motifs for Structure-Specific Recognition and Separation of Carbon Nanotubes. *Nature* **2009**, *460*, 250–253.
- (12) Liu, H.; Nishide, D.; Tanaka, T.; Kataura, H. Large-Scale Single-Chirality Separation of Single-Wall Carbon Nanotubes by Simple Gel Chromatography. *Nat. Commun.* **2011**, *2*, 309.
- (13) Liu, J.; Wang, C.; Tu, X.; Liu, B.; Chen, L.; Zheng, M.; Zhou, C. Chirality-Controlled Synthesis of Single-Wall Carbon Nanotubes Using Vapour-Phase Epitaxy. *Nat. Commun.* **2012**, *3*, 1199.
- (14) Arnold, M. S.; Green, A. A.; Hulvat, J. F.; Stupp, S. I.; Hersam, M. C. Sorting Carbon Nanotubes by Electronic Structure Using Density Differentiation. *Nat. Nanotechnol.* **2006**, *1*, 60–65.
- (15) Yang, F.; Wang, X.; Zhang, D.; Yang, J.; Luo, D.; Xu, Z.; Wei, J.; Wang, J.-Q.; Xu, Z.; Peng, F.; et al. Chirality-Specific Growth of Single-Walled Carbon Nanotubes on Solid Alloy Catalysts. *Nature* **2014**, *510*, 522–524.
- (16) Sanchez-Valencia, J. R.; Dienel, T.; Groning, O.; Shorubalko, I.; Mueller, A.; Jansen, M.; Amsharov, K.; Ruffieux, P.; Fasel, R. Controlled synthesis of single-chirality carbon nanotubes. *Nature* **2014**, *512*, 61–64.
- (17) Zhu, Z.; Wei, N.; Xie, H.; Zhang, R.; Bai, Y.; Wang, Q.; Zhang, C.; Wang, S.; Peng, L.; Dai, L.; et al. Acoustic-Assisted Assembly of an Individual Monochromatic Ultralong Carbon Nanotube for High on-Current Transistors. *Sci. Adv.* **2016**, *2*, e1601572.
- (18) Zhang, S.; Kang, L.; Wang, X.; Tong, L.; Yang, L.; Wang, Z.; Qi, K.; Deng, S.; Li, Q.; Bai, X.; et al. Arrays of Horizontal Carbon Nanotubes of Controlled Chirality Grown Using Designed Catalysts. *Nature* **2017**, *543*, 234–238.
- (19) Saito, R.; Dresselhaus, G.; Dresselhaus, M. S. *Physical Properties of Carbon Nanotubes*; Imperial College Press: London, UK, 1998.
- (20) Dresselhaus, M. S.; Dresselhaus, G.; Saito, R.; Jorio, A. Raman Spectroscopy of Carbon Nanotubes. *Phys. Rep.* **2005**, *409*, 47–99.
- (21) Kim, S. H.; Haines, C. S.; Li, N.; Kim, K. J.; Mun, T. J.; Choi, C.; Di, J. T.; Oh, Y. J.; Oviedo, J. P.; Bykova, J.; et al. Harvesting Electrical Energy from Carbon Nanotube Yarn Twist. *Science* **2017**, *357*, 773–778.
- (22) Wei, B. Q.; Vajtai, R.; Ajayan, P. M. Reliability and Current Carrying Capacity of Carbon Nanotubes. *Appl. Phys. Lett.* **2001**, *79*, 1172–1174.
- (23) Dai, L. M.; Chang, D. W.; Baek, J. B.; Lu, W. Carbon Nanomaterials for Advanced Energy Conversion and Storage. *Small* **2012**, *8*, 1130–1166.
- (24) Ni, J. F.; Li, Y. Carbon Nanomaterials in Different Dimensions for Electrochemical Energy Storage. *Adv. Energy. Mater.* **2016**, *6*, 1600278.
- (25) Peng, B.; Locascio, M.; Zapol, P.; Li, S.; Mielke, S. L.; Schatz, G. C.; Espinosa, H. D. Measurements of Near-ultimate Strength for Multiwalled Carbon Nanotubes and Irradiation-Induced Crosslinking Improvements. *Nat. Nanotechnol.* **2008**, *3*, 626–631.
- (26) Behabtu, N.; Young, C. C.; Tsentalovich, D. E.; Kleinerman, O.; Wang, X.; Ma, A. W. K.; Bengio, E. A.; ter Waarbeek, R. F.; de Jong, J. J.; Hoogerwerf, R. E.; et al. Strong, Light, Multifunctional Fibers of Carbon Nanotubes with Ultrahigh Conductivity. *Science* **2013**, *339*, 182–186.
- (27) Bai, Y. X.; Zhang, R. F.; Ye, X.; Zhu, Z. X.; Xie, H. H.; Shen, B. Y.; Cai, D. L.; Liu, B. F.; Zhang, C. X.; Jia, Z.; et al. Carbon Nanotube Bundles with Tensile Strength over 80 GPa. *Nat. Nanotechnol.* **2018**, *13*, 589–595.
- (28) Tunuguntla, R. H.; Henley, R. Y.; Yao, Y. C.; Pham, T. A.; Wanunu, M.; Noy, A. Enhanced Water Permeability and Tunable Ion Selectivity in Subnanometer Carbon Nanotube Porins. *Science* **2017**, *357*, 792–796.
- (29) Peng, L.-M.; Zhang, Z.; Qiu, C. Carbon Nanotube Digital Electronics. *Nat. Electron.* **2019**, *2*, 499–505.
- (30) Avouris, P.; Chen, Z.; Perebeinos, V. Carbon-Based Electronics. *Nat. Nanotechnol.* **2007**, *2*, 605–615.
- (31) Shulaker, M. M.; Hills, G.; Patil, N.; Wei, H.; Chen, H.; Wong, H.-S. P.; Mitra, S. Carbon Nanotube Computer. *Nature* **2013**, *501*, 526–530.
- (32) Cao, Q.; Han, S.-j.; Tersoff, J.; Franklin, A. D.; Zhu, Y.; Zhang, Z.; Tulevski, G.; Tang, J.; Haensch, W. End-bonded Contacts for Carbon Nanotube Transistors with Low, Size-Independent Resistance. *Science* **2015**, *350*, 68–72.
- (33) Brady, G. J.; Way, A. J.; Safron, N. S.; Evensen, H. T.; Gopalan, P.; Arnold, M. S. Quasi-Ballistic Carbon Nanotube Array Transistors with Current Density Exceeding Si and GaAs. *Sci. Adv.* **2016**, *2*, e1601240.
- (34) Qiu, C.; Zhang, Z.; Xiao, M.; Yang, Y.; Zhong, D.; Peng, L.-M. Scaling Carbon Nanotube Complementary Transistors to 5-nm Gate Lengths. *Science* **2017**, *355*, 271–276.
- (35) Cao, Q.; Tersoff, J.; Farmer, D.; Zhu, Y.; Han, S.-j. Carbon Nanotube Transistors Scaled to a 40-nanometer Footprint. *Science* **2017**, *356*, 1369–1372.
- (36) Shulaker, M. M.; Hills, G.; Park, R. S.; Howe, R. T.; Saraswat, K.; Wong, H. P.; Mitra, S. Three-Dimensional Integration of Nanotechnologies for Computing and Data Storage on a Single Chip. *Nature* **2017**, *547*, 74–78.
- (37) Tans, S. J.; Verschueren, A. R. M.; Dekker, C. Room-Temperature Transistor based on a Single Carbon Nanotube. *Nature* **1998**, *393*, 49–52.
- (38) Jensen, K.; Weldon, J.; Garcia, H.; Zettl, A. Nanotube Radio. *Nano Lett.* **2007**, *7*, 3508–3511.
- (39) Hills, G.; Lau, C.; Wright, A.; Fuller, S.; Bishop, M. D.; Srimani, T.; Kanhaiya, P.; Ho, R.; Amer, A.; Stein, Y.; et al. Modern Microprocessor Built from Complementary Carbon Nanotube Transistors. *Nature* **2019**, *572*, 595–602.
- (40) Wu, Z. C.; Chen, Z. H.; Du, X.; Logan, J. M.; Sippel, J.; Nikolou, M.; Kamaras, K.; Reynolds, J. R.; Tanner, D. B.; Hebard, A. F.; et al. Transparent, Conductive Carbon Nanotube Films. *Science* **2004**, *305*, 1273–1276.
- (41) Kaskela, A.; Nasibulin, A. G.; Timmermans, M. Y.; Aitchison, B.; Papadimitratos, A.; Tian, Y.; Zhu, Z.; Jiang, H.; Brown, D. P.; Zakhidov, A.; et al. Aerosol-Synthesized SWCNT Networks with Tunable Conductivity and Transparency by a Dry Transfer Technique. *Nano Lett.* **2010**, *10*, 4349–4355.
- (42) Hecht, D. S.; Heintz, A. M.; Lee, R.; Hu, L. B.; Moore, B.; Cucksey, C.; Risser, S. High Conductivity Transparent Carbon Nanotube Films Deposited from Superacid. *Nanotechnology* **2011**, *22*, No. 075201.
- (43) Jiang, S.; Hou, P. X.; Chen, M. L.; Wang, B. W.; Sun, D. M.; Tang, D. M.; Jin, Q.; Guo, Q. X.; Zhang, D. D.; Du, J. H.; et al. Ultrahigh-Performance Transparent Conductive Films of Carbon-Welded Isolated Single-Wall Carbon Nanotubes. *Sci. Adv.* **2018**, *4*, eaap9264.
- (44) Si, J.; Zhong, D.; Xu, H.; Xiao, M.; Yu, C.; Zhang, Z.; Peng, L. M. Scalable Preparation of High-Density Semiconducting Carbon Nanotube Arrays for High-Performance Field-Effect Transistors. *ACS Nano* **2018**, *12*, 627–634.
- (45) Diao, S.; Hong, G. S.; Robinson, J. T.; Jiao, L. Y.; Antaris, A. L.; Wu, J. Z.; Choi, C. L.; Dai, H. J. Chirality Enriched (12,1) and (11,3) Single-Walled Carbon Nanotubes for Biological Imaging. *J. Am. Chem. Soc.* **2012**, *134*, 16971–16974.
- (46) Jain, R. M.; Howden, R.; Tvrdy, K.; Shimizu, S.; Hilmer, A. J.; McNicholas, T. P.; Gleason, K. K.; Strano, M. S. Polymer-Free Near-Infrared Photovoltaics with Single Chirality (6,5) Semiconducting Carbon Nanotube Active Layers. *Adv. Mater.* **2012**, *24*, 4436–4439.
- (47) Pfohl, M.; Glaser, K.; Graf, A.; Mertens, A.; Tune, D. D.; Puercckhauer, T.; Alam, A.; Wei, L.; Chen, Y.; Zaumseil, J.; et al. Probing the Diameter Limit of Single Walled Carbon Nanotubes in SWCNT: Fullerene Solar Cells. *Adv. Energy. Mater.* **2016**, *6*, 1600890.
- (48) Bachilo, S. M.; Balzano, L.; Herrera, J. E.; Pompeo, F.; Resasco, D. E.; Weisman, R. B. Narrow (*n,m*)-Distribution of Single-Walled Carbon Nanotubes Grown Using A Solid Supported Catalyst. *J. Am. Chem. Soc.* **2003**, *125*, 11186–11187.
- (49) Lolli, G.; Zhang, L.; Balzano, L.; Sakulchaicharoen, N.; Tan, Y.; Resasco, D. E. Tailoring (*n,m*) Structure of Single-Walled Carbon Nanotubes by Modifying Reaction Conditions and the Nature of the Support of CoMo Catalysts. *J. Phys. Chem. B* **2006**, *110*, 2108–2115.
- (50) Li, X.; Tu, X.; Zaric, S.; Welsher, K.; Seo, W. S.; Zhao, W.; Dai, H. Selective Synthesis Combined with Chemical Separation of Single-

- Walled Carbon Nanotubes for Chirality Selection. *J. Am. Chem. Soc.* **2007**, *129*, 15770–15771.
- (51) Chiang, W. H.; Sankaran, R. M. Linking Catalyst Composition to Chirality Distributions of as-Grown Single-Walled Carbon Nanotubes by Tuning Ni_xFe_{1-x} Nanoparticles. *Nat. Mater.* **2009**, *8*, 882–886.
- (52) He, M.; Chernov, A. I.; Fedotov, P. V.; Obraztsova, E. D.; Sainio, J.; Rikkinen, E.; Jiang, H.; Zhu, Z.; Tian, Y.; Kauppinen, E. I.; et al. Predominant (6,5) Single-Walled Carbon Nanotube Growth on a Copper-Promoted Iron Catalyst. *J. Am. Chem. Soc.* **2010**, *132*, 13994–13996.
- (53) Wang, H.; Wang, B.; Quek, X. Y.; Wei, L.; Zhao, J.; Li, L. J.; Chan-Park, M. B.; Yang, Y.; Chen, Y. Selective Synthesis of (9, 8) Single Walled Carbon Nanotubes on Cobalt Incorporated TUD-1 Catalysts. *J. Am. Chem. Soc.* **2010**, *132*, 16747–16749.
- (54) Liu, B.; Ren, W.; Li, S.; Liu, C.; Cheng, H.-M. High Temperature Selective Growth of Single-Walled Carbon Nanotubes with a Narrow Chirality Distribution from a CoPt Bimetallic Catalyst. *Chem. Commun.* **2012**, *48*, 2409–2411.
- (55) Wang, H.; Yuan, Y.; Wei, L.; Goh, K.; Yu, D. S.; Chen, Y. Catalysts for Chirality Selective Synthesis of Single-Walled Carbon Nanotubes. *Carbon* **2015**, *81*, 1–19.
- (56) Li, M.; Liu, X.; Zhao, X.; Yang, F.; Wang, X.; Li, Y. Metallic Catalysts for Structure-Controlled Growth of Single-Walled Carbon Nanotubes. *Top. Curr. Chem.* **2017**, *375*, 29.
- (57) Liu, B.; Wu, F.; Gui, H.; Zheng, M.; Zhou, C. Chirality-Controlled Synthesis and Applications of Single-Wall Carbon Nanotubes. *ACS Nano* **2017**, *11*, 31–53.
- (58) Wang, X.; He, M.; Ding, F. Chirality-Controlled Synthesis of Single-Walled Carbon Nanotubes—From Mechanistic Studies toward Experimental Realization. *Mater. Today* **2018**, *21*, 845–860.
- (59) Yang, F.; Wang, X.; Si, J.; Zhao, X.; Qi, K.; Jin, C.; Zhang, Z.; Li, M.; Zhang, D.; Yang, J.; et al. Water-Assisted Preparation of High-Purity Semiconducting (14,4) Carbon Nanotubes. *ACS Nano* **2017**, *11*, 186–193.
- (60) Nish, A.; Hwang, J.-Y.; Doig, J.; Nicholas, R. J. Highly Selective Dispersion of Single Walled Carbon Nanotubes Using Aromatic Polymers. *Nat. Nanotechnol.* **2007**, *2*, 640–646.
- (61) Krupke, R.; Hennrich, F.; Lohneysen, H. v.; Kappes, M. M. Separation of Metallic from Semiconducting Single-Walled Carbon Nanotubes. *Science* **2003**, *301*, 344–347.
- (62) Zheng, M.; Jagota, A.; Semke, E. D.; Diner, B. A.; McLean, R. S.; Lustig, S. R.; Richardson, R. E.; Tassi, N. G. DNA-Assisted Dispersion and Separation of Carbon Nanotubes. *Nat. Mater.* **2003**, *2*, 338–342.
- (63) Fagan, J. A.; Khripin, C. Y.; Silvera Batista, C. A.; Simpson, J. R.; Hároz, E. H.; Hight Walker, A. R.; Zheng, M. Isolation of Specific Small-Diameter Single-Wall Carbon Nanotube Species via Aqueous Two-Phase Extraction. *Adv. Mater.* **2014**, *26*, 2800–2804.
- (64) Yang, F.; Wang, X.; Li, M.; Liu, X.; Zhao, X.; Zhang, D.; Zhang, Y.; Yang, J.; Li, Y. Templated Synthesis of Single-Walled Carbon Nanotubes with Specific Structure. *Acc. Chem. Res.* **2016**, *49*, 606–615.
- (65) Takagi, D.; Homma, Y.; Hibino, H.; Suzuki, S.; Kobayashi, Y. Single-Walled Carbon Nanotube Growth from Highly Activated Metal Nanoparticles. *Nano Lett.* **2006**, *6*, 2642–2645.
- (66) Yuan, D.; Ding, L.; Chu, H.; Feng, Y.; McNicholas, T. P.; Liu, J. Horizontally Aligned Single-Walled Carbon Nanotube on Quartz from a Large Variety of Metal Catalysts. *Nano Lett.* **2008**, *8*, 2576–2579.
- (67) Peng, F.; Liu, Y.; Cui, R. L.; Gao, D. L.; Yang, F.; Li, Y. Direct Growth of Single-Walled Carbon Nanotubes on Substrates. *Chin. Sci. Bull.* **2012**, *57*, 225–233.
- (68) Li, Y.; Cui, R.; Ding, L.; Liu, Y.; Zhou, W.; Zhang, Y.; Jin, Z.; Peng, F.; Liu, J. How Catalysts Affect the Growth of Single-Walled Carbon Nanotubes on Substrates. *Adv. Mater.* **2010**, *22*, 1508–1515.
- (69) Liu, B.; Tang, D. M.; Sun, C.; Liu, C.; Ren, W.; Li, F.; Yu, W. J.; Yin, L. C.; Zhang, L.; Jiang, C.; et al. Importance of Oxygen in the Metal-Free Catalytic Growth of Single-Walled Carbon Nanotubes from SiO_x by a Vapor-Solid-Solid Mechanism. *J. Am. Chem. Soc.* **2011**, *133*, 197–199.
- (70) Harutyunyan, A. R.; Tokune, T.; Mora, E. Liquid as a Required Catalyst Phase for Carbon Single-Walled Nanotube Growth. *Appl. Phys. Lett.* **2005**, *87*, No. 051919.
- (71) Rao, R.; Eyink, K. G.; Maruyama, B. Single-Walled Carbon Nanotube Growth from Liquid Gallium and Indium. *Carbon* **2010**, *48*, 3971–3973.
- (72) Jourdain, V.; Bichara, C. Current Understanding of the Growth of Carbon Nanotubes in Catalytic Chemical Vapour Deposition. *Carbon* **2013**, *58*, 2–39.
- (73) Helveg, S.; Lopez-Cartes, C.; Sehested, J.; Hansen, P. L.; Clausen, B. S.; Rostrup-Nielsen, J. R.; Abild-Pedersen, F.; Norskov, J. K. Atomic-Scale Imaging of Carbon Nanofibre Growth. *Nature* **2004**, *427*, 426–429.
- (74) Hofmann, S.; Sharma, R.; Ducati, C.; Du, G.; Mattevi, C.; Cepek, C.; Cantoro, M.; Pisana, S.; Parvez, A.; Cervantes-Sodi, F.; et al. In Situ Observations of Catalyst Dynamics during Surface-Bound Carbon Nanotube Nucleation. *Nano Lett.* **2007**, *7*, 602–608.
- (75) He, M.; Jiang, H.; Liu, B.; Fedotov, P. V.; Chernov, A. I.; Obraztsova, E. D.; Cavalca, F.; Wagner, J. B.; Hansen, T. W.; Anoshkin, I. V.; et al. Chiral-Selective Growth of Single-Walled Carbon Nanotubes on Lattice-Mismatched Epitaxial Cobalt Nanoparticles. *Sci. Rep.* **2013**, *3*, 1460.
- (76) Pierce, N.; Chen, G.; P. Rajukumar, L.; Chou, N. H.; Koh, A. L.; Sinclair, R.; Maruyama, S.; Terrones, M.; Harutyunyan, A. R. Intrinsic Chirality Origination in Carbon Nanotubes. *ACS Nano* **2017**, *11*, 9941–9949.
- (77) Hofmann, S.; Blume, R.; Wirth, C. T.; Cantoro, M.; Sharma, R.; Ducati, C.; Hävecker, M.; Zafeiratos, S.; Schnoerch, P.; Oestreich, A.; et al. State of Transition Metal Catalysts during Carbon Nanotube Growth. *J. Phys. Chem. C* **2009**, *113*, 1648–1656.
- (78) Raty, J.-Y.; Gygi, F.; Galli, G. Growth of Carbon Nanotubes on Metal Nanoparticles: A Microscopic Mechanism from Ab Initio Molecular Dynamics Simulations. *Phys. Rev. Lett.* **2005**, *95*, No. 096103.
- (79) Kong, J.; Cassell, A. M.; Dai, H. J. Chemical Vapor Deposition of Methane for Single-Walled Carbon Nanotubes. *Chem. Phys. Lett.* **1998**, *292*, 567–574.
- (80) Li, Y. M.; Kim, W.; Zhang, Y. G.; Rolandi, M.; Wang, D. W.; Dai, H. J. Growth of Single-Walled Carbon Nanotubes from Discrete Catalytic Nanoparticles of Various Sizes. *J. Phys. Chem. B* **2001**, *105*, 11424–11431.
- (81) Zheng, L. X.; O’Connell, M. J.; Doorn, S. K.; Liao, X. Z.; Zhao, Y. H.; Akhadv, E. A.; Hoffbauer, M. A.; Roop, B. J.; Jia, Q. X.; Dye, R. C.; et al. Ultralong Single-Wall Carbon Nanotubes. *Nat. Mater.* **2004**, *3*, 673–676.
- (82) Fiawoo, M. F.; Bonnot, A. M.; Amara, H.; Bichara, C.; Thibault-Pénisson, J.; Loiseau, A. Evidence of Correlation Between Catalyst Particles and the Single-Wall Carbon Nanotube Diameter: A First Step towards Chirality Control. *Phys. Rev. Lett.* **2012**, *108*, 195503.
- (83) Shibuta, Y.; Maruyama, S. Molecular Dynamics Simulation of Formation Process of Single-Walled Carbon Nanotubes by CCVD Method. *Chem. Phys. Lett.* **2003**, *382*, 381–386.
- (84) Ding, F.; Bolton, K.; Rosen, A. Nucleation Growth of Single-Walled Carbon Nanotubes: A Molecular Dynamics Study. *J. Phys. Chem. B* **2004**, *108*, 17369–17377.
- (85) Yuan, Q.; Xu, Z.; Yakobson, B.; Ding, F. Efficient Defect Healing in Catalytic Carbon Nanotube Growth. *Phys. Rev. Lett.* **2012**, *108*, 245505.
- (86) Neyts, E. C.; Ostrikov, K.; Han, Z. J.; Kumar, S.; van Duin, A. C. T.; Bogaerts, A. Defect Healing and Enhanced Nucleation of Carbon Nanotubes by Low-Energy Ion Bombardment. *Phys. Rev. Lett.* **2013**, *110*, No. 065501.
- (87) Xu, Z.; Qiu, L.; Ding, F. The Kinetics of Chirality Assignment in Catalytic Single-Walled Carbon Nanotube Growth and the Routes Towards Selective Growth. *Chem. Sci.* **2018**, *9*, 3056–3061.
- (88) Neyts, E. C.; van Duin, A. C. T.; Bogaerts, A. Changing Chirality during Single-Walled Carbon Nanotube Growth: A Reactive Molecular Dynamics/Monte Carlo Study. *J. Am. Chem. Soc.* **2011**, *133*, 17225–17231.

- (89) Kim, J.; Page, A. J.; Irle, S.; Morokuma, K. Dynamics of Local Chirality during SWCNT Growth: Armchair versus Zigzag Nanotubes. *J. Am. Chem. Soc.* **2012**, *134*, 9311–9319.
- (90) Li, H.-B.; Page, A. J.; Irle, S.; Morokuma, K. Single-walled Carbon Nanotube Growth from Chiral Carbon Nanorings: Prediction of Chirality and Diameter Influence on Growth Rates. *J. Am. Chem. Soc.* **2012**, *134*, 15887–15896.
- (91) Diarra, M.; Zappelli, A.; Amara, H.; Ducastelle, F.; Bichara, C. Importance of Carbon Solubility and Wetting Properties of Nickel Nanoparticles for Single Wall Nanotube Growth. *Phys. Rev. Lett.* **2012**, *109*, 185501.
- (92) Aguiar-Hualde, J.-M.; Magnin, Y.; Amara, H.; Bichara, C. Probing the Role of Carbon Solubility in Transition Metal Catalyzing Single-Walled Carbon Nanotubes Growth. *Carbon* **2017**, *120*, 226–232.
- (93) Diarra, M.; Amara, H.; Ducastelle, F.; Bichara, C. Carbon Solubility in Nickel Nanoparticles: A Grand Canonical Monte Carlo Study. *Phys. Status Solidi B* **2012**, *249*, 2629–2634.
- (94) Ding, F.; Rosén, A.; Bolton, K. The Role of the Catalytic Particle Temperature Gradient for SWNT Growth from Small Particles. *Chem. Phys. Lett.* **2004**, *393*, 309–313.
- (95) Ding, F.; Bolton, K. The Importance of Supersaturated Carbon Concentration and its Distribution in Catalytic Particles for Single-Walled Carbon Nanotube Nucleation. *Nanotechnology* **2006**, *17*, 543–548.
- (96) Ding, F.; Larsson, P.; Larsson, J. A.; Ahuja, R.; Duan, H.; Rosen, A.; Bolton, K. The Importance of Strong Carbon-Metal Adhesion for Catalytic Nucleation of Single-Walled Carbon Nanotubes. *Nano Lett.* **2008**, *8*, 463–468.
- (97) He, M.; Magnin, Y.; Jiang, H.; Amara, H.; Kauppinen, E.; Loiseau, A.; Bichara, C. Growth Modes and Chiral Selectivity of Single-Walled Carbon Nanotubes. *Nanoscale* **2018**, *10*, 6744–6750.
- (98) Amara, H.; Bichara, C. Modeling the Growth of Single-Wall Carbon Nanotubes. *Top. Curr. Chem.* **2017**, *375*, 55.
- (99) Kumakura, M.; Kozawa, A.; Saida, T.; Naritsuka, S.; Maruyama, T. Spectroscopic Study of X-ray Absorption Near-Edge Structure of Chemical States of Pt Catalyst during Growth of Single-Walled Carbon Nanotubes. *J. Cryst. Growth* **2017**, *468*, 155–158.
- (100) Yang, F.; Zhao, H.; Wang, X.; Liu, X.; Liu, Q.; Liu, X.; Jin, C.; Wang, R.; Li, Y. Atomic Scale Stability of Tungsten-Cobalt Intermetallic Nanocrystals in Reactive Environment at High Temperature. *J. Am. Chem. Soc.* **2019**, *141*, 5871–5879.
- (101) Gili, A.; Schlicker, L.; Bekheet, M. F.; Görke, O.; Kober, D.; Simon, U.; Littlewood, P.; Schomäcker, R.; Doran, A.; Gaissmaier, D.; et al. Revealing the Mechanism of Multiwalled Carbon Nanotube Growth on Supported Nickel Nanoparticles by In Situ Synchrotron X-ray Diffraction, Density Functional Theory, and Molecular Dynamics Simulations. *ACS Catal.* **2019**, *9*, 6999–7011.
- (102) Yoshida, H.; Takeda, S.; Uchiyama, T.; Kohno, H.; Homma, Y. Atomic-Scale in-situ Observation of Carbon Nanotube Growth from Solid State Iron Carbide Nanoparticles. *Nano Lett.* **2008**, *8*, 2082–2086.
- (103) Picher, M.; Lin, P. A.; Gomez-Ballesteros, J. L.; Balbuena, P. B.; Sharma, R. Nucleation of Graphene and Its Conversion to Single-Walled Carbon Nanotubes. *Nano Lett.* **2014**, *14*, 6104–6108.
- (104) Rao, R.; Sharma, R.; Abild-Pedersen, F.; Nørskov, J. K.; Harutyunyan, A. R. Insights into Carbon Nanotube Nucleation: Cap Formation Governed by Catalyst Interfacial Step Flow. *Sci. Rep.* **2015**, *4*, 6510.
- (105) Santos, E. J. G.; Nørskov, J. K.; Harutyunyan, A. R.; Abild-Pedersen, F. Toward Controlled Growth of Helicity-Specific Carbon Nanotubes. *J. Phys. Chem. Lett.* **2015**, *6*, 2232–2237.
- (106) Rodríguez-Manzo, J. A.; Terrones, M.; Terrones, H.; Kroto, H. W.; Sun, L.; Banhart, F. In Situ Nucleation of Carbon Nanotubes by the Injection of Carbon Atoms into Metal Particles. *Nat. Nanotechnol.* **2007**, *2*, 307–311.
- (107) Tang, D.-M.; Liu, C.; Yu, W.-J.; Zhang, L.-L.; Hou, P.-X.; Li, J.-C.; Li, F.; Bando, Y.; Golberg, D.; Cheng, H.-M. Structural Changes in Iron Oxide and Gold Catalysts during Nucleation of Carbon Nanotubes Studied by In Situ Transmission Electron Microscopy. *ACS Nano* **2014**, *8*, 292–301.
- (108) Zhang, L.; Hou, P.-X.; Li, S.; Shi, C.; Cong, H.-T.; Liu, C.; Cheng, H.-M. In Situ TEM Observations on the Sulfur-Assisted Catalytic Growth of Single-Wall Carbon Nanotubes. *J. Phys. Chem. Lett.* **2014**, *5*, 1427–1432.
- (109) Cao, K.; Chamberlain, T. W.; Biskupek, J.; Zoberbier, T.; Kaiser, U.; Khlobystov, A. N. Direct Correlation of Carbon Nanotube Nucleation and Growth with the Atomic Structure of Re Nanocatalysts Stimulated and Imaged by the Electron Beam. *Nano Lett.* **2018**, *18*, 6334–6339.
- (110) Lin, P. A.; Gomez-Ballesteros, J. L.; Burgos, J. C.; Balbuena, P. B.; Natarajan, B.; Sharma, R. Direct Evidence of Atomic-Scale Structural Fluctuations in Catalyst Nanoparticles. *J. Catal.* **2017**, *349*, 149–155.
- (111) Zhu, H.; Suenaga, K.; Hashimoto, A.; Urata, K.; Hata, K.; Iijima, S. Atomic-Resolution Imaging of the Nucleation Points of Single-Walled Carbon Nanotubes. *Small* **2005**, *1*, 1180–1183.
- (112) Pohl, D.; Schäffel, F.; Rümmeli, M. H.; Mohn, E.; Täschner, C.; Schultz, L.; Kisielowski, C.; Rellinghaus, B. Understanding the Metal-Carbon Interface in FePt Catalyzed Carbon Nanotubes. *Phys. Rev. Lett.* **2011**, *107*, 185501.
- (113) Sharma, R.; Moore, E.; Rez, P.; Treacy, M. M. Site-Specific Fabrication of Fe Particles for Carbon Nanotube Growth. *Nano Lett.* **2009**, *9*, 689–694.
- (114) Gomez-Ballesteros, J. L.; Burgos, J. C.; Lin, P. A.; Sharma, R.; Balbuena, P. B. Nanocatalyst Shape and Composition during Nucleation of Single-Walled Carbon Nanotubes. *RSC Adv.* **2015**, *5*, 106377–106386.
- (115) Kohigashi, Y.; Yoshida, H.; Homma, Y.; Takeda, S. Structurally Inhomogeneous Nanoparticulate Catalysts in Cobalt-Catalyzed Carbon Nanotube Growth. *Appl. Phys. Lett.* **2014**, *105*, No. 073108.
- (116) Magnin, Y.; Zappelli, A.; Amara, H.; Ducastelle, F.; Bichara, C. Size Dependent Phase Diagrams of Nickel-Carbon Nanoparticles. *Phys. Rev. Lett.* **2015**, *115*, 205502.
- (117) Wirth, C. T.; Bayer, B. C.; Gamalski, A. D.; Esconjauregui, S.; Weatherup, R. S.; Ducati, C.; Baehtz, C.; Robertson, J.; Hofmann, S. The Phase of Iron Catalyst Nanoparticles during Carbon Nanotube Growth. *Chem. Mater.* **2012**, *24*, 4633–4640.
- (118) Wu, J.; Helveg, S.; Ullmann, S.; Peng, Z.; Bell, A. T. Growth of Encapsulating Carbon on Supported Pt Nanoparticles Studied by In Situ TEM. *J. Catal.* **2016**, *338*, 295–304.
- (119) Zhang, L.; He, M.; Hansen, T.; Kling, J.; Jiang, H.; Kauppinen, E. I.; Loiseau, A.; Wagner, J. B. Growth Termination and Multiple Nucleation of Single-Wall Carbon Nanotubes Evidenced by In Situ Transmission Electron Microscopy. *ACS Nano* **2017**, *11*, 4483–4493.
- (120) Mazzucco, S.; Wang, Y.; Tanase, M.; Picher, M.; Li, K.; Wu, Z.; Irle, S.; Sharma, R. Direct Evidence of Active and Inactive Phases of Fe Catalyst Nanoparticles for Carbon Nanotube Formation. *J. Catal.* **2014**, *319*, 54–60.
- (121) He, M.; Jin, H.; Zhang, L.; Jiang, H.; Yang, T.; Cui, H.; Fossard, F.; Wagner, J. B.; Karppinen, M.; Kauppinen, E. I.; Loiseau, A. Environmental Transmission Electron Microscopy Investigations of Pt- Fe_2O_3 Nanoparticles for Nucleating Carbon Nanotubes. *Carbon* **2016**, *110*, 243–248.
- (122) He, M.; Amara, H.; Jiang, H.; Hassinen, J.; Bichara, C.; Ras, R. H.; Lehtonen, J.; Kauppinen, E.; Loiseau, A. Key Roles of Carbon Solubility in Single-Walled Carbon Nanotube Nucleation and Growth. *Nanoscale* **2015**, *7*, 20284–20289.
- (123) Rao, R.; Liptak, D.; Cherukuri, T.; Yakobson, B. I.; Maruyama, B. In Situ Evidence for Chirality-Dependent Growth Rates of Individual Carbon Nanotubes. *Nat. Mater.* **2012**, *11*, 213–216.
- (124) Bedewy, M.; Viswanath, B.; Meshot, E. R.; Zakharov, D. N.; Stach, E. A.; Hart, A. J. Measurement of the Dewetting, Nucleation, and Deactivation Kinetics of Carbon Nanotube Population Growth by Environmental Transmission Electron Microscopy. *Chem. Mater.* **2016**, *28*, 3804–3813.

- (125) Hamilton, G. L.; Kang, E. J.; Mba, M.; Toste, F. D. A Powerful Chiral Counterion Strategy for Asymmetric Transition Metal Catalysis. *Science* **2007**, *317*, 496–499.
- (126) Reich, S.; Li, L.; Robertson, J. Control the Chirality of Carbon Nanotubes by Epitaxial Growth. *Chem. Phys. Lett.* **2006**, *421*, 469–472.
- (127) Reich, S.; Li, L.; Robertson, J. Epitaxial Growth of Carbon Caps on Ni for Chiral Selectivity. *Phys. Status Solidi B* **2006**, *243*, 3494–3499.
- (128) Gómez-Gualdrón, D. A.; Zhao, J.; Balbuena, P. B. Nanocatalyst Structure as a Template to Define Chirality of Nascent Single-Walled Carbon Nanotubes. *J. Chem. Phys.* **2011**, *134*, No. 014705.
- (129) Dutta, D.; Chiang, W.-H.; Sankaran, R. M.; Bhethanabotla, V. R. Epitaxial Nucleation Model for Chiral-Selective Growth of Single-Walled Carbon Nanotubes on Bimetallic Catalyst Surfaces. *Carbon* **2012**, *50*, 3766–3773.
- (130) Zhu, H.; Suenaga, K.; Wei, J.; Wang, K.; Wu, D. A Strategy to Control the Chirality of Single-Walled Carbon Nanotubes. *J. Cryst. Growth* **2008**, *310*, 5473–5476.
- (131) Page, A. J.; Ohta, Y.; Irle, S.; Morokuma, K. Mechanisms of Single-Walled Carbon Nanotube Nucleation, Growth, and Healing Determined Using QM-MD Methods. *Acc. Chem. Res.* **2010**, *43*, 1375–1385.
- (132) Page, A. J.; Yamane, H.; Ohta, Y.; Irle, S.; Morokuma, K. QM/MD Simulation of SWNT Nucleation on Transition-Metal Carbide Nanoparticles. *J. Am. Chem. Soc.* **2010**, *132*, 15699–15707.
- (133) Reich, S.; Li, L.; Robertson, J. Structure and Formation Energy of Carbon Nanotube Caps. *Phys. Rev. B: Condens. Matter Mater. Phys.* **2005**, *72*, 165423.
- (134) Ohta, Y.; Okamoto, Y.; Page, A. J.; Irle, S.; Morokuma, K. Quantum Chemical Molecular Dynamics Simulation of Single-Walled Carbon Nanotube Cap Nucleation on an Iron Particle. *ACS Nano* **2009**, *3*, 3413–3420.
- (135) Artyukhov, V. I.; Penev, E. S.; Yakobson, B. I. Why Nanotubes Grow Chiral. *Nat. Commun.* **2014**, *5*, 4892.
- (136) Yuan, Q.; Ding, F. How a Zigzag Carbon Nanotube Grows. *Angew. Chem., Int. Ed.* **2015**, *54*, 5924–5928.
- (137) Luo, M.; Penev, E. S.; Harutyunyan, A. R.; Yakobson, B. I. Effect of Cap–Catalyst Structural Correlation on the Nucleation of Carbon Nanotubes. *J. Phys. Chem. C* **2017**, *121*, 18789–18794.
- (138) Ding, F.; Harutyunyan, A. R.; Yakobson, B. I. Dislocation Theory of Chirality-Controlled Nanotube Growth. *Proc. Natl. Acad. Sci. U. S. A.* **2009**, *106*, 2506–2509.
- (139) Wang, Q.; Ng, M. F.; Yang, S. W.; Yang, Y.; Chen, Y. The Mechanism of Single-Walled Carbon Nanotube Growth and Chirality Selection Induced by Carbon Atom and Dimer Addition. *ACS Nano* **2010**, *4*, 939–946.
- (140) Liu, B.; Liu, J.; Tu, X.; Zhang, J.; Zheng, M.; Zhou, C. Chirality-Dependent Vapor-Phase Epitaxial Growth and Termination of Single-Wall Carbon Nanotubes. *Nano Lett.* **2013**, *13*, 4416–4421.
- (141) Kharlamova, M. V.; Kramberger, C.; Saito, T.; Sato, Y.; Suenaga, K.; Pichler, T.; Shiozawa, H. Chirality-Dependent Growth of Single-Wall Carbon Nanotubes as Revealed inside Nano-Test Tubes. *Nanoscale* **2017**, *9*, 7998–8006.
- (142) Hedman, D.; Reza Barzegar, H.; Rosén, A.; Wågberg, T.; Andreas Larsson, J. On the Stability and Abundance of Single Walled Carbon Nanotubes. *Sci. Rep.* **2015**, *5*, 16850.
- (143) Magnin, Y.; Amara, H.; Ducastelle, F.; Loiseau, A.; Bichara, C. Entropy-Driven Stability of Chiral Single-Walled Carbon Nanotubes. *Science* **2018**, *362*, 212–215.
- (144) Wang, X.; Ding, F. How a Solid Catalyst Determines the Chirality of the Single-Wall Carbon Nanotube Grown on It. *J. Phys. Chem. Lett.* **2019**, *10*, 735–741.
- (145) Yang, F.; Wang, X.; Zhang, D.; Qi, K.; Yang, J.; Xu, Z.; Li, M.; Zhao, X.; Bai, X.; Li, Y. Growing Zigzag (16,0) Carbon Nanotubes with Structure-Defined Catalysts. *J. Am. Chem. Soc.* **2015**, *137*, 8688–8691.
- (146) Yao, Y.; Li, Q.; Zhang, J.; Liu, R.; Jiao, L.; Zhu, Y. T.; Liu, Z. Temperature-Mediated Growth of Single-Walled Carbon-Nanotube Intramolecular Junctions. *Nat. Mater.* **2007**, *6*, 283.
- (147) Lu, C.; Liu, J. Controlling the Diameter of Carbon Nanotubes in Chemical Vapor Deposition Method by Carbon Feeding. *J. Phys. Chem. B* **2006**, *110*, 20254–20257.
- (148) Picher, M.; Anglaret, E.; Arenal, R.; Jourdain, V. Processes Controlling the Diameter Distribution of Single-Walled Carbon Nanotubes during Catalytic Chemical Vapor Deposition. *ACS Nano* **2011**, *5*, 2118–2125.
- (149) Li, Y.; Liu, J.; Wang, Y.; Wang, Z. L. Preparation of Monodispersed Fe-Mo Nanoparticles as the Catalyst for CVD Synthesis of Carbon Nanotubes. *Chem. Mater.* **2001**, *13*, 1008–1014.
- (150) Cheung, C. L.; Kurtz, A.; Park, H.; Lieber, C. M. Diameter-Controlled Synthesis of Carbon Nanotubes. *J. Phys. Chem. B* **2002**, *106*, 2429–2433.
- (151) An, L.; Owens, J. M.; McNeil, L. E.; Liu, J. Synthesis of Nearly Uniform Single-Walled Carbon Nanotubes Using Identical Metal-Containing Molecular Nanoclusters as Catalysts. *J. Am. Chem. Soc.* **2002**, *124*, 13688–13689.
- (152) Ago, H.; Ayagaki, T.; Ogawa, Y.; Tsuji, M. Ultrahigh-Vacuum-Assisted Control of Metal Nanoparticles for Horizontally Aligned Single-Walled Carbon Nanotubes with Extraordinary Uniform Diameters. *J. Phys. Chem. C* **2011**, *115*, 13247–13253.
- (153) Li, P.; Zhang, X.; Liu, J. Aligned Single-Walled Carbon Nanotube Arrays from Rhodium Catalysts with Unexpected Diameter Uniformity Independent of the Catalyst Size and Growth Temperature. *Chem. Mater.* **2016**, *28*, 870–875.
- (154) Choi, H. C.; Kim, W.; Wang, D.; Dai, H. Delivery of Catalytic Metal Species onto Surfaces with Dendrimer Carriers for the Synthesis of Carbon Nanotubes with Narrow Diameter Distribution. *J. Phys. Chem. B* **2002**, *106*, 12361–12365.
- (155) Lu, J.; Yi, S. S.; Kopley, T.; Qian, C.; Liu, J.; Gulari, E. Fabrication of Ordered Catalytically Active Nanoparticles Derived from Block Copolymer Micelle Templates for Controllable Synthesis of Single-Walled Carbon Nanotubes. *J. Phys. Chem. B* **2006**, *110*, 6655–6660.
- (156) Muller, A.; Das, S. K.; Kogerler, P.; Bogge, H.; Schmidtmann, M.; Trautwein, A. X.; Schunemann, V.; Krickemeyer, E.; Preetz, W. A New Type of Supramolecular Compound: Molybdenum-oxide-based Composites Consisting of Magnetic Nanocapsules with Encapsulated Keggin-Ion Electron Reservoirs Cross-Linked to a Two-Dimensional Network. *Angew. Chem.* **2000**, *112*, 3555–3559.
- (157) Chen, G.; Seki, Y.; Kimura, H.; Sakurai, S.; Yumura, M.; Hata, K.; Futaba, D. N. Diameter Control of Single-Walled Carbon Nanotube Forests from 1.3–3.0 nm by Arc Plasma Deposition. *Sci. Rep.* **2015**, *4*, 3804.
- (158) Jeong, G. H.; Yamazaki, A.; Suzuki, S.; Yoshimura, H.; Kobayashi, Y.; Homma, Y. Cobalt-Filled Apoferritin for Suspended Single-Walled Carbon Nanotube Growth with Narrow Diameter Distribution. *J. Am. Chem. Soc.* **2005**, *127*, 8238–8239.
- (159) Takagi, D.; Yamazaki, A.; Otsuka, Y.; Yoshimura, H.; Kobayashi, Y.; Homma, Y. Gold-Filled Apo-Ferritin for Investigation of Single-Walled Carbon Nanotube Growth on Substrate. *Chem. Phys. Lett.* **2007**, *445*, 213–216.
- (160) Zhang, Y.; Li, Y.; Kim, W.; Wang, D.; Dai, H. Imaging as-Grown Single-Walled Carbon Nanotubes Originated from Isolated Catalytic Nanoparticles. *Appl. Phys. A: Mater. Sci. Process.* **2002**, *74*, 325–328.
- (161) Fu, Q.; Huang, S.; Liu, J. Chemical Vapor Depositions of Single-Walled Carbon Nanotubes Catalyzed by Uniform Fe_2O_3 Nanoclusters Synthesized Using Diblock Copolymer Micelles. *J. Phys. Chem. B* **2004**, *108*, 6124–6129.
- (162) Putaj, P.; Lefebvre, F. Polyoxometalates Containing Late Transition and Noble Metal Atoms. *Coord. Chem. Rev.* **2011**, *255*, 1642–1685.
- (163) Peng, F.; Luo, D.; Sun, H.; Wang, J.; Yang, F.; Li, R.; Yang, J.; Li, Y. Diameter-Controlled Growth of Aligned Single-Walled Carbon Nanotubes on Quartz Using Molecular Nanoclusters as Catalyst Precursors. *Chin. Sci. Bull.* **2013**, *58*, 433–439.
- (164) Goss, K.; Kamra, A.; Spudat, C.; Meyer, C.; Kögerler, P.; Schneider, C. M. CVD Growth of Carbon Nanotubes Using Molecular Nanoclusters as Catalyst. *Phys. Status Solidi B* **2009**, *246*, 2494–2497.

- (165) Anderson, R. E.; Colorado, R., Jr.; Crouse, C.; Ogrin, D.; Maruyama, B.; Pender, M. J.; Edwards, C. L.; Whitsitt, E.; Moore, V. C.; Koveal, D.; et al. A Study of the Formation, Purification and Application as a SWNT Growth Catalyst of the Nanocluster $[H_xPMo_{12}O_{40}CH_4Mo_{72}Fe_{30}(O_2CMe)_{15}O_{254}(H_2O)_{98}]$. *Dalton Trans.* **2006**, 3097–3107.
- (166) Li, J.; Ke, C.-T.; Liu, K.; Li, P.; Liang, S.; Finkelstein, G.; Wang, F.; Liu, J. Importance of Diameter Control on Selective Synthesis of Semiconducting Single-Walled Carbon Nanotubes. *ACS Nano* **2014**, 8, 8564–8572.
- (167) Zhang, S.; Tong, L.; Hu, Y.; Kang, L.; Zhang, J. Diameter-specific Growth of Semiconducting SWNTs Arrays Using Uniform Mo₂C Solid Catalyst. *J. Am. Chem. Soc.* **2015**, 137, 8904–8907.
- (168) Chen, J.; Xu, X.; Zhang, L.; Huang, S. Controlling the Diameter of Single-Walled Carbon Nanotubes by Improving the Dispersion of the Uniform Catalyst Nanoparticles on Substrate. *Nano-Micro Lett.* **2015**, 7, 353–359.
- (169) Bouanis, F. Z.; Cojocaru, C. S.; Huc, V.; Norman, E.; Chaigneau, M.; Maurice, J. L.; Mallah, T.; Pribat, D. Direct Synthesis and Integration of Individual, Diameter-Controlled Single-Walled Nanotubes (SWNTs). *Chem. Mater.* **2014**, 26, 5074–5082.
- (170) Yamada, T.; Namai, T.; Hata, K.; Futaba, D. N.; Mizuno, K.; Fan, J.; Yudasaka, M.; Yumura, M.; Iijima, S. Size-Selective Growth of Double-Walled Carbon Nanotube Forests from Engineered Iron Catalysts. *Nat. Nanotechnol.* **2006**, 1, 131–136.
- (171) Barzegar, H. R.; Nitze, F.; Sharifi, T.; Ramstedt, M.; Tai, C. W.; Malolepszy, A.; Stobinski, L.; Wågberg, T. Simple Dip-Coating Process for the Synthesis of Small Diameter Single-Walled Carbon Nanotubes—Effect of Catalyst Composition and Catalyst Particle Size on Chirality and Diameter. *J. Phys. Chem. C* **2012**, 116, 12232–12239.
- (172) Javey, A.; Dai, H. J. Regular Arrays of 2 nm Metal Nanoparticles for Deterministic Synthesis of Nanomaterials. *J. Am. Chem. Soc.* **2005**, 127, 11942–11943.
- (173) Zhang, F.; Hou, P.-X.; Liu, C.; Wang, B.-W.; Jiang, H.; Chen, M.-L.; Sun, D.-M.; Li, J.-C.; Cong, H.-T.; Kauppinen, E. I.; et al. Growth of Semiconducting Single-Wall Carbon Nanotubes with A Narrow Band-Gap Distribution. *Nat. Commun.* **2016**, 7, 11160.
- (174) Hu, Y.; Kang, L.; Zhao, Q.; Zhong, H.; Zhang, S.; Yang, L.; Wang, Z.; Lin, J.; Li, Q.; Zhang, Z.; et al. Growth of High-Density Horizontally Aligned SWNT Arrays Using Trojan Catalysts. *Nat. Commun.* **2015**, 6, 6099.
- (175) Li, M.; Yang, F.; Ding, L.; Liu, X.; Zhang, Z.; Zhang, D.; Zhao, X.; Yang, J.; Li, Y. Diameter-Specific Growth of Single-Walled Carbon Nanotubes Using Tungsten Supported Nickel Catalysts. *Carbon* **2017**, 118, 485–492.
- (176) Baliyan, A.; Nakajima, Y.; Fukuda, T.; Uchida, T.; Hanajiri, T.; Maekawa, T. Synthesis of an Ultra Dense Forest of Vertically Aligned Triple-Walled Carbon Nanotubes of Uniform Diameter and Length Using Hollow Catalytic Nanoparticles. *J. Am. Chem. Soc.* **2014**, 136, 1047–1053.
- (177) Ciuparu, D.; Chen, Y.; Lim, S.; Haller, G. L.; Pfefferle, L. Uniform-Diameter Single-Walled Carbon Nanotubes Catalytically Grown in Cobalt-Incorporated MCM-41. *J. Phys. Chem. B* **2004**, 108, 503–507.
- (178) Chen, Y.; Ciuparu, D.; Lim, S.; Yang, Y.; Haller, G. L.; Pfefferle, L. Synthesis of Uniform Diameter Single Wall Carbon Nanotubes in Co-MCM-41: Effects of CO Pressure and Reaction Time. *J. Catal.* **2004**, 226, 351–362.
- (179) Chen, Y.; Ciuparu, D.; Lim, S.; Yang, Y.; Haller, G. L.; Pfefferle, L. Synthesis of Uniform Diameter Single-Wall Carbon Nanotubes in Co-MCM-41: Effects of the Catalyst Prereduction and Nanotube Growth Temperatures. *J. Catal.* **2004**, 225, 453–465.
- (180) Loebick, C. Z.; Derrouiche, S.; Marinkovic, N.; Wang, C.; Hennrich, F.; Kappes, M. M.; Haller, G. L.; Pfefferle, L. D. Effect of Manganese Addition to the Co-MCM-41 Catalyst in the Selective Synthesis of Single Wall Carbon Nanotubes. *J. Phys. Chem. C* **2009**, 113, 21611–21620.
- (181) Zoican Loebick, C.; Derrouiche, S.; Fang, F.; Li, N.; Haller, G. L.; Pfefferle, L. D. Effect of Chromium Addition to the Co-MCM-41 Catalyst in the Synthesis of Single Wall Carbon Nanotubes. *Appl. Catal., A* **2009**, 368, 40–49.
- (182) Lee, S.; Zoican Loebick, C.; Pfefferle, L. D.; Haller, G. L. High-Temperature Stability of Cobalt Grafted on Low-Loading Incorporated Mo-MCM-41 Catalyst for Synthesis of Single-Walled Carbon Nanotubes. *J. Phys. Chem. C* **2011**, 115, 1014–1024.
- (183) Lim, S.; Ciuparu, D.; Pak, C.; Dobek, F.; Chen, Y.; Harding, D.; Pfefferle, L. D.; Haller, G. L. Synthesis and Characterization of Highly Ordered Co-MCM-41 for Production of Aligned Single Walled Carbon Nanotubes (SWNT). *J. Phys. Chem. B* **2003**, 107, 11048–11056.
- (184) Hou, B.; Wu, C.; Inoue, T.; Chiashi, S.; Xiang, R.; Maruyama, S. Extended Alcohol Catalytic Chemical Vapor Deposition for Efficient Growth of Single-Walled Carbon Nanotubes Thinner than (6,5). *Carbon* **2017**, 119, S02–S10.
- (185) He, M.; Liu, B.; Chernov, A. I.; Obraztsova, E. D.; Kauppi, I.; Jiang, H.; Anoshkin, I.; Cavalca, F.; Hansen, T. W.; Wagner, J. B.; et al. Growth Mechanism of Single-Walled Carbon Nanotubes on Iron–Copper Catalyst and Chirality Studies by Electron Diffraction. *Chem. Mater.* **2012**, 24, 1796–1801.
- (186) Cui, K.; Kumamoto, A.; Xiang, R.; An, H.; Wang, B.; Inoue, T.; Chiashi, S.; Ikuhara, Y.; Maruyama, S. Synthesis of Subnanometer-Diameter Vertically Aligned Single-Walled Carbon Nanotubes with Copper-Anchored Cobalt Catalysts. *Nanoscale* **2016**, 8, 1608–1617.
- (187) Wang, B.; Yang, Y.; Li, L.-J.; Chen, Y. Effect of Different Catalyst Supports on the (n,m) Selective Growth of Single-Walled Carbon Nanotube from Co–Mo Catalyst. *J. Mater. Sci.* **2009**, 44, 3285–3295.
- (188) Xiang, R.; Maruyama, S. Revisiting Behaviour of Monometallic Catalysts in Chemical Vapour Deposition Synthesis of Single-Walled Carbon Nanotubes. *R. Soc. Open Sci.* **2018**, 5, 180345.
- (189) He, M.; Magnin, Y.; Amara, H.; Jiang, H.; Cui, H.; Fossard, F.; Castan, A.; Kauppinen, E.; Loiseau, A.; Bichara, C. Linking Growth Mode to Lengths of Single-Walled Carbon Nanotubes. *Carbon* **2017**, 113, 231–236.
- (190) Yamada, K.; Kato, H.; Homma, Y. Narrow Diameter Distribution of Horizontally Aligned Single-Walled Carbon Nanotubes Grown Using Size-Controlled Gold Nanoparticles. *Jpn. J. Appl. Phys.* **2013**, 52, No. 035105.
- (191) Nasibulin, A. G.; Pikhitsa, P. V.; Jiang, H.; Kauppinen, E. I. Correlation Between Catalyst Particle and Single-Walled Carbon Nanotube Diameters. *Carbon* **2005**, 43, 2251–2257.
- (192) Diaz, M. C.; Jiang, H.; Kauppinen, E. I.; Sharma, R.; Balbuena, P. B. Can Single-Walled Carbon Nanotube Diameter Be Defined by Catalyst Particle Diameter? *J. Phys. Chem. C* **2019**, 123, 30305–30317.
- (193) Homma, Y. Gold Nanoparticles as the Catalyst of Single-Walled Carbon Nanotube Synthesis. *Catalysts* **2014**, 4, 38–48.
- (194) Zhou, W.; Zhan, S.; Ding, L.; Liu, J. General Rules for Selective Growth of Enriched Semiconducting Single Walled Carbon Nanotubes with Water Vapor as *in-situ* Etchant. *J. Am. Chem. Soc.* **2012**, 134, 14019–14026.
- (195) Ding, L.; Tselev, A.; Wang, J.; Yuan, D.; Chu, H.; McNicholas, T. P.; Li, Y.; Liu, J. Selective Growth of Well-Aligned Semiconducting Single-Walled Carbon Nanotubes. *Nano Lett.* **2009**, 9, 800–805.
- (196) Ibrahim, I.; Kalbacova, J.; Engemaier, V.; Pang, J.; Rodriguez, R. D.; Grimm, D.; Gemming, T.; Zahn, D. R. T.; Schmidt, O. G.; Eckert, J.; et al. Confirming the Dual Role of Etchants during the Enrichment of Semiconducting Single Wall Carbon Nanotubes by Chemical Vapor Deposition. *Chem. Mater.* **2015**, 27, 5964–5973.
- (197) Che, Y.; Wang, C.; Liu, J.; Liu, B.; Lin, X.; Parker, J.; Beasley, C.; Wong, H. S. P.; Zhou, C. Selective Synthesis and Device Applications of Semiconducting Single-Walled Carbon Nanotubes Using Isopropanol as Feedstock. *ACS Nano* **2012**, 6, 7454–7462.
- (198) Yu, B.; Liu, C.; Hou, P.-X.; Tian, Y.; Li, S.; Liu, B.; Li, F.; Kauppinen, E. I.; Cheng, H.-M. Bulk Synthesis of Large Diameter Semiconducting Single-Walled Carbon Nanotubes by Oxygen-Assisted Floating Catalyst Chemical Vapor Deposition. *J. Am. Chem. Soc.* **2011**, 133, 5232–5235.
- (199) Qin, X.; Peng, F.; Yang, F.; He, X.; Huang, H.; Luo, D.; Yang, J.; Wang, S.; Liu, H.; Peng, L.; et al. Growth of Semiconducting Single-

- Walled Carbon Nanotubes by Using Ceria as Catalyst Supports. *Nano Lett.* **2014**, *14*, 512–517.
- (200) Tang, L.; Li, T.; Li, C.; Ling, L.; Zhang, K.; Yao, Y. CoPt/CeO₂ Catalysts for the Growth of Narrow Diameter Semiconducting Single-Walled Carbon Nanotubes. *Nanoscale* **2015**, *7*, 19699–19704.
- (201) Li, Y.; Mann, D.; Rolandi, M.; Kim, W.; Ural, A.; Hung, S.; Javey, A.; Cao, J.; Wang, D.; Yenilmez, E.; et al. Preferential Growth of Semiconducting Single-Walled Carbon Nanotubes by a Plasma Enhanced CVD Method. *Nano Lett.* **2004**, *4*, 317–321.
- (202) Hong, G.; Zhang, B.; Peng, B.; Zhang, J.; Choi, W. M.; Choi, J. Y.; Kim, J. M.; Liu, Z. Direct Growth of Semiconducting Single-Walled Carbon Nanotube Array. *J. Am. Chem. Soc.* **2009**, *131*, 14642–14643.
- (203) Li, W.-S.; Hou, P.-X.; Liu, C.; Sun, D.-M.; Yuan, J.; Zhao, S.-Y.; Yin, L.-C.; Cong, H.; Cheng, H.-M. High Quality, Highly Concentrated Semiconducting Single-Wall Carbon Nanotubes for Use in Field Effect Transistors and Biosensors. *ACS Nano* **2013**, *7*, 6831–6839.
- (204) Wang, J.; Jin, X.; Liu, Z.; Yu, G.; Ji, Q.; Wei, H.; Zhang, J.; Zhang, K.; Li, D.; Yuan, Z.; et al. Growing Highly Pure Semiconducting Carbon Nanotubes by Electrotwisting the Helicity. *Nat. Catal.* **2018**, *1*, 326–331.
- (205) Ke, J.; Xiao, J.-W.; Zhu, W.; Liu, H.; Si, R.; Zhang, Y.-W.; Yan, C.-H. Dopant-Induced Modification of Active Site Structure and Surface Bonding Mode for High-Performance Nanocatalysts: CO Oxidation on Capping-free (110)-oriented CeO₂: Ln (Ln= La–Lu) Nanowires. *J. Am. Chem. Soc.* **2013**, *135*, 15191–15200.
- (206) Kang, L.; Hu, Y.; Liu, L.; Wu, J.; Zhang, S.; Zhao, Q.; Ding, F.; Li, Q.; Zhang, J. Growth of Close Packed Semiconducting Single-walled Carbon Nanotube Arrays Using Oxygen-Deficient TiO₂ Nanoparticles as Catalysts. *Nano Lett.* **2015**, *15*, 403–409.
- (207) Kang, L.; Zhang, S.; Li, Q.; Zhang, J. Growth of Horizontal Semiconducting SWNT Arrays with Density Higher than 100 Tubes/ μm Using Ethanol/Methane CVD. *J. Am. Chem. Soc.* **2016**, *138*, 6727–6730.
- (208) Zhang, S.; Hu, Y.; Wu, J.; Liu, D.; Kang, L.; Zhao, Q.; Zhang, J. Selective Scission of C–O and C–C Bonds in Ethanol Using Bimetal Catalysts for the Preferential Growth of Semiconducting SWNTs Arrays. *J. Am. Chem. Soc.* **2015**, *137*, 1012–1015.
- (209) Sakurai, S.; Yamada, M.; Sakurai, H.; Sekiguchi, A.; Futaba, D. N.; Hata, K. A Phenomenological Model for Selective Growth of Semiconducting Single-Walled Carbon Nanotube Based on Catalyst Deactivation. *Nanoscale* **2016**, *8*, 1015–1023.
- (210) Franklin, A. D. The Road to Carbon Nanotube Transistors. *Nature* **2013**, *498*, 443–444.
- (211) Zhou, W.; Ding, L.; Yang, S.; Liu, J. Synthesis of High Density, Large-Diameter and Aligned Single-Walled Carbon Nanotubes by Multiple-Cycle Growth Methods. *ACS Nano* **2011**, *5*, 3849–3857.
- (212) Li, J.; Liu, K.; Liang, S.; Zhou, W.; Pierce, M.; Wang, F.; Peng, L.; Liu, J. Growth of High-Density Aligned and Semiconducting-Enriched Single Walled Carbon Nanotubes: Decoupling the Conflict Between Density and Selectivity. *ACS Nano* **2014**, *8*, 554–562.
- (213) Kang, L.; Hu, Y.; Zhong, H.; Si, J.; Zhang, S.; Zhao, Q.; Lin, J.; Li, Q.; Zhang, Z.; Peng, L.; et al. Large-Area Growth of Ultra-High-Density Single-Walled Carbon Nanotube Arrays on Sapphire Surface. *Nano Res.* **2015**, *8*, 3694–3703.
- (214) Xiang, R.; Einarsson, E.; Murakami, Y.; Shiomi, J.; Chiashi, S.; Tang, Z.; Maruyama, S. Diameter Modulation of Vertically Aligned Single-Walled Carbon Nanotubes. *ACS Nano* **2012**, *6*, 7472–7479.
- (215) Maruyama, S.; Kojima, R.; Miyauchi, Y.; Chiashi, S.; Kohno, M. Low-Temperature Synthesis of High-Purity Single-Walled Carbon Nanotubes from Alcohol. *Chem. Phys. Lett.* **2002**, *360*, 229–234.
- (216) Miyauchi, Y.; Chiashi, S.; Murakami, Y.; Hayashida, Y.; Maruyama, S. Fluorescence Spectroscopy of Single-Walled Carbon Nanotubes Synthesized from Alcohol. *Chem. Phys. Lett.* **2004**, *387*, 198–203.
- (217) He, M.; Fedotov, P. V.; Obraztsova, E. D.; Viitanen, V.; Sainio, J.; Jiang, H.; Kauppinen, E. I.; Niemelä, M.; Lehtonen, J. Chiral-Selective Growth of Single-Walled Carbon Nanotubes on Stainless Steel Wires. *Carbon* **2012**, *50*, 4294–4297.
- (218) He, M.; Fedotov, P. V.; Chernov, A.; Obraztsova, E. D.; Jiang, H.; Wei, N.; Cui, H.; Sainio, J.; Zhang, W.; Jin, H.; et al. Chiral-Selective Growth of Single-Walled Carbon Nanotubes on Fe-based Catalysts Using CO as Carbon Source. *Carbon* **2016**, *108*, 521–528.
- (219) He, M.; Chernov, A. I.; Obraztsova, E. D.; Jiang, H.; Kauppinen, E. I.; Lehtonen, J. Synergistic Effects in FeCu Bimetallic Catalyst for Low Temperature Growth of Single-Walled Carbon Nanotubes. *Carbon* **2013**, *52*, 590–594.
- (220) Qiu, L.; Ding, F. Contact-Induced Phase Separation of Alloy Catalyst to Promote Carbon Nanotube Growth. *Phys. Rev. Lett.* **2019**, *123*, 256101.
- (221) An, H.; Kumamoto, A.; Takezaki, H.; Ohyama, S.; Qian, Y.; Inoue, T.; Ikuhara, Y.; Chiashi, S.; Xiang, R.; Maruyama, S. Chirality Specific and Spatially Uniform Synthesis of Single-Walled Carbon Nanotubes from Sputtered Co-W Bimetallic Catalyst. *Nanoscale* **2016**, *8*, 14523–14529.
- (222) An, H.; Kumamoto, A.; Xiang, R.; Inoue, T.; Otsuka, K.; Chiashi, S.; Bichara, C.; Loiseau, A.; Li, Y.; Ikuhara, Y.; et al. Atomic-Scale Structural Identification and Evolution of Co-W-C Ternary SWCNT Catalytic Nanoparticles: High-Resolution STEM Imaging on SiO₂. *Sci. Adv.* **2019**, *5*, eaat9459.
- (223) He, M.; Chernov, A. I.; Fedotov, P. V.; Obraztsova, E. D.; Rikkinen, E.; Zhu, Z.; Sainio, J.; Jiang, H.; Nasibulin, A. G.; Kauppinen, E. I.; et al. Selective Growth of SWNTs on Partially Reduced Monometallic Cobalt Catalyst. *Chem. Commun.* **2011**, *47*, 1219–1221.
- (224) Xu, B.; Kaneko, T.; Shibuta, Y.; Kato, T. Preferential Synthesis of (6,4) Single-Walled Carbon Nanotubes by Controlling Oxidation Degree of Co Catalyst. *Sci. Rep.* **2017**, *7*, 11149.
- (225) He, M.; Wang, X.; Zhang, L.; Wu, Q.; Song, X.; Chernov, A. I.; Fedotov, P. V.; Obraztsova, E. D.; Sainio, J.; Jiang, H.; et al. Anchoring Effect of Ni²⁺ in Stabilizing Reduced Metallic Particles for Growing Single-Walled Carbon Nanotubes. *Carbon* **2018**, *128*, 249–256.
- (226) Wu, Q.; Ji, Z.; Xin, L.; Li, D.; Zhang, L.; Liu, C.; Yang, T.; Wen, Z.; Wang, H.; Xin, B.; et al. Iron Silicide-Catalyzed Growth of Single-Walled Carbon Nanotubes with a Narrow Diameter Distribution. *Carbon* **2019**, *149*, 139–143.
- (227) He, M.; Li, D.; Yang, T.; Shang, D.; Chernov, A. I.; Fedotov, P. V.; Obraztsova, E. D.; Liu, Q.; Jiang, H.; Kauppinen, E. A Robust Co_xMg_{1-x}O Catalyst for Predominantly Growing (6, 5) Single-Walled Carbon Nanotubes. *Carbon* **2019**, *153*, 389–395.
- (228) Tang, L.; Luo, Y.; Zhang, S.; Zhang, Q.; Yao, Y.; Zhang, J. Substrate-Anchored Solid Solution Catalysts for High density SWNTs Growth. *Carbon* **2018**, *126*, 313–318.
- (229) Ohashi, T.; Shima, T. Synthesis of Vertically Aligned Single-Walled Carbon Nanotubes with Metallic Chirality through Facet Control of Catalysts. *Carbon* **2015**, *87*, 453–461.
- (230) Ishigami, N.; Ago, H.; Imamoto, K.; Tsuji, M.; Iakoubovskii, K.; Minami, N. Crystal Plane dependent Growth of Aligned Single-Walled Carbon Nanotubes on Sapphire. *J. Am. Chem. Soc.* **2008**, *130*, 9918–9924.
- (231) Harutyunyan, A. R.; Chen, G.; Paronyan, T. M.; Pigos, E. M.; Kuznetsov, O. A.; Hewaparakrama, K.; Kim, S. M.; Zakharov, D.; Stach, E. A.; Sumanasekera, G. U. Preferential Growth of Single-Walled Carbon Nanotubes with Metallic Conductivity. *Science* **2009**, *326*, 116–120.
- (232) Fouquet, M.; Bayer, B. C.; Esconjauregui, S.; Thomsen, C.; Hofmann, S.; Robertson, J. Effect of Catalyst Pre-Treatment on Chirality-Selective Growth of Single-Walled Carbon Nanotubes. *J. Phys. Chem. C* **2014**, *118*, 5773–5781.
- (233) Wang, H.; Goh, K.; Xue, R.; Yu, D.; Jiang, W.; Lau, R.; Chen, Y. Sulfur Doped Co/SiO₂ Catalysts for Chirally Selective Synthesis of Single Walled Carbon Nanotubes. *Chem. Commun.* **2013**, *49*, 2031–2033.
- (234) Yuan, Y.; Karahan, H. E.; Yıldırım, C.; Wei, L.; Birer, Ö.; Zhai, S.; Lau, R.; Chen, Y. “Smart Poisoning” of Co/SiO₂ Catalysts by Sulfidation for Chirality Selective Synthesis of (9,8) Single-Walled Carbon Nanotubes. *Nanoscale* **2016**, *8*, 17705–17713.
- (235) Zhu, Z.; Jiang, H.; Susi, T.; Nasibulin, A. G.; Kauppinen, E. I. The Use of NH₃ to Promote the Production of Large-Diameter Single-

- Walled Carbon Nanotubes with a Narrow (*n,m*) Distribution. *J. Am. Chem. Soc.* **2011**, *133*, 1224–1227.
- (236) Wang, H.; Yang, L.; Sui, X.; Karahan, H. E.; Wang, X.; Chen, Y. Selective Synthesis of Single Walled Carbon Nanotubes on Metal (Iron, Nickel or Cobalt) Sulfate-based Catalysts. *Carbon* **2018**, *129*, 128–136.
- (237) Sundaram, R. M.; Koziol, K. K. K.; Windle, A. H. Continuous Direct Spinning of Fibers of Single Walled Carbon Nanotubes with Metallic Chirality. *Adv. Mater.* **2011**, *23*, 5064–5068.
- (238) Wang, H.; Wei, L.; Ren, F.; Wang, Q.; Pfefferle, L. D.; Haller, G. L.; Chen, Y. Chiral-Selective $\text{CoSO}_4/\text{SiO}_2$ Catalyst for (9,8) Single-Walled Carbon Nanotube Growth. *ACS Nano* **2013**, *7*, 614–626.
- (239) Li, J.; Otsuka, K.; Zhang, X.; Maruyama, S.; Liu, J. Selective Synthesis of Large Diameter, Highly Conductive and High Density Single-Walled Carbon Nanotubes by Thiophene-Assisted Chemical Vapor Deposition Method on Transparent Substrates. *Nanoscale* **2016**, *8*, 14156–14162.
- (240) Wang, H.; Ren, F.; Liu, C.; Si, R.; Yu, D.; Pfefferle, L. D.; Haller, G. L.; Chen, Y. $\text{CoSO}_4/\text{SiO}_2$ Catalyst for Selective Synthesis of (9,8) Single-Walled Carbon Nanotubes: Effect of catalyst calcination. *J. Catal.* **2013**, *300*, 91–101.
- (241) Maruyama, T.; Kozawa, A.; Saida, T.; Naritsuka, S.; Iijima, S. Low Temperature Growth of Single-Walled Carbon Nanotubes from Rh Catalysts. *Carbon* **2017**, *116*, 128–132.
- (242) Page, A. J.; Saha, S.; Li, H.-B.; Irle, S.; Morokuma, K. Quantum Chemical Simulation of Carbon Nanotube Nucleation on Al_2O_3 Catalysts via CH_4 Chemical Vapor Deposition. *J. Am. Chem. Soc.* **2015**, *137*, 9281–9288.
- (243) Tang, D. M.; Zhang, L. L.; Liu, C.; Yin, L. C.; Hou, P. X.; Jiang, H.; Zhu, Z.; Li, F.; Liu, B.; Kauppinen, E. I.; et al. Heteroepitaxial Growth of Single-Walled Carbon Nanotubes from Boron Nitride. *Sci. Rep.* **2012**, *2*, 971.
- (244) Takagi, D.; Kobayashi, Y.; Homma, Y. Carbon Nanotube Growth from Diamond. *J. Am. Chem. Soc.* **2009**, *131*, 6922–6923.
- (245) Zhao, X.; Yang, F.; Chen, J.; Ding, L.; Liu, X.; Yao, F.; Li, M.; Zhang, D.; Zhang, Z.; Liu, X.; et al. Selective Growth of Chirality-Enriched Carbon Semiconducting Carbon Nanotubes by Using Bimetallic Catalysts from Salt Precursors. *Nanoscale* **2018**, *10*, 6922–6927.
- (246) Dumlich, H.; Reich, S. Chirality-dependent Growth Rate of Carbon Nanotubes: A theoretical Study. *Phys. Rev. B: Condens. Matter Mater. Phys.* **2010**, *82*, No. 085421.
- (247) Zhu, Z.; Wei, N.; Cheng, W.; Shen, B.; Sun, S.; Gao, J.; Wen, Q.; Zhang, R.; Xu, J.; Wang, Y.; et al. Rate-Selected Growth of Ultrapure Semiconducting Carbon Nanotube Arrays. *Nat. Commun.* **2019**, *10*, 4467.
- (248) Zhao, Q.; Xu, Z.; Hu, Y.; Ding, F.; Zhang, J. Chemical Vapor Deposition Synthesis of Near-Zigzag Single-Walled Carbon Nanotubes with Stable Tube-Catalyst Interface. *Sci. Adv.* **2016**, *2*, e1501729.
- (249) He, M.; Jiang, H.; Kauppinen, E. I.; Lehtonen, J. Diameter and Chiral Angle Distribution Dependencies on the Carbon Precursors in Surface-Grown Single-Walled Carbon Nanotubes. *Nanoscale* **2012**, *4*, 7394–7398.
- (250) Wang, B.; Poa, C. H. P.; Wei, L.; Li, L. J.; Yang, Y.; Chen, Y. (*n,m*) Selectivity of Single-Walled Carbon Nanotubes by Different Carbon Precursors on Co-Mo Catalysts. *J. Am. Chem. Soc.* **2007**, *129*, 9014–9019.
- (251) Geohegan, D. B.; Puretzky, A. A.; Jackson, J. J.; Rouleau, C. M.; Eres, G.; More, K. L. Flux-Dependent Growth Kinetics and Diameter Selectivity in Single-Wall Carbon Nanotube Arrays. *ACS Nano* **2011**, *5*, 8311–8321.
- (252) Wang, B.; Wei, L.; Yao, L.; Li, L. J.; Yang, Y.; Chen, Y. Pressure-Induced Single-Walled Carbon Nanotube (*n,m*) Selectivity on Co-Mo Catalysts. *J. Phys. Chem. C* **2007**, *111*, 14612–14616.
- (253) Inoue, T.; Hasegawa, D.; Badar, S.; Aikawa, S.; Chiashi, S.; Maruyama, S. Effect of Gas Pressure on the Density of Horizontally Aligned Single-Walled Carbon Nanotubes Grown on Quartz Substrates. *J. Phys. Chem. C* **2013**, *117*, 11804–11810.
- (254) Ghorannevis, Z.; Kato, T.; Kaneko, T.; Hatakeyama, R. Narrow-Chirality Distributed Single-Walled Carbon Nanotube Growth from Nonmagnetic Catalyst. *J. Am. Chem. Soc.* **2010**, *132*, 9570–9572.
- (255) Kato, T.; Hatakeyama, R. Direct Growth of Short Single-Walled Carbon Nanotubes with Narrow-Chirality Distribution by Time-Programmed Plasma Chemical Vapor Deposition. *ACS Nano* **2010**, *4*, 7395–7400.
- (256) Ostrikov, K.; Mehdioui, H. Nanoscale Plasma Chemistry Enables Fast, Size-Selective Nanotube Nucleation. *J. Am. Chem. Soc.* **2012**, *134*, 4303–4312.
- (257) Nikolaev, P.; Bronikowski, M. J.; Bradley, R. K.; Rohmund, F.; Colbert, D. T.; Smith, K. A.; Smalley, R. E. Gas-Phase Catalytic Growth of Single-Walled Carbon Nanotubes from Carbon Monoxide. *Chem. Phys. Lett.* **1999**, *313*, 91–97.
- (258) Wang, Y.; Liu, Y.; Li, X.; Cao, L.; Wei, D.; Zhang, H.; Shi, D.; Yu, G.; Kajiura, H.; Li, Y. Direct Enrichment of Metallic Single-Walled Carbon Nanotubes Induced by the Different Molecular Composition of Monohydroxy Alcohol Homologues. *Small* **2007**, *3*, 1486–1490.
- (259) Gómez-Gualdrón, D. A.; Beetge, J. M.; Burgos, J. C.; Balbuena, P. B. Effects of Precursor Type on the CVD Growth of Single-Walled Carbon Nanotubes. *J. Phys. Chem. C* **2013**, *117*, 10397–10409.
- (260) Liao, Y.; Jiang, H.; Wei, N.; Laiho, P.; Zhang, Q.; Khan, S. A.; Kauppinen, E. I. Direct Synthesis of Colorful Single-Walled Carbon Nanotube Thin Films. *J. Am. Chem. Soc.* **2018**, *140*, 9797–9800.
- (261) In, J. B.; Grigoropoulos, C. P.; Chernov, A. A.; Noy, A. Hidden Role of Trace Gas Impurities in Chemical Vapor Deposition Growth of Vertically-Aligned Carbon Nanotube Arrays. *Appl. Phys. Lett.* **2011**, *98*, 153102.
- (262) Rao, R.; Pierce, N.; Liptak, D.; Hooper, D.; Sargent, G.; Semiatin, S.; Curtarolo, S.; Harutyunyan, A. R.; Maruyama, B. Revealing the Impact of Catalyst Phase Transition on Carbon Nanotube Growth by In Situ Raman Spectroscopy. *ACS Nano* **2013**, *7*, 1100–1107.
- (263) Zoican Loebick, C.; Podila, R.; Reppert, J.; Chudow, J.; Ren, F.; Haller, G. L.; Rao, A. M.; Pfefferle, L. D. Selective Synthesis of Subnanometer Diameter Semiconducting Single-Walled Carbon Nanotubes. *J. Am. Chem. Soc.* **2010**, *132*, 11125–11131.
- (264) Otsuka, K.; Yamamoto, S.; Inoue, T.; Koyano, B.; Ukai, H.; Yoshikawa, R.; Xiang, R.; Chiashi, S.; Maruyama, S. Digital Isotope Coding to Trace the Growth Process of Individual Single-Walled Carbon Nanotubes. *ACS Nano* **2018**, *12*, 3994–4001.
- (265) Xiang, R.; Hou, B.; Einarsson, E.; Zhao, P.; Harish, S.; Morimoto, K.; Miyachi, Y.; Chiashi, S.; Tang, Z.; Maruyama, S. Carbon Atoms in Ethanol Do Not Contribute Equally to Formation of Single-Walled Carbon Nanotubes. *ACS Nano* **2013**, *7*, 3095–3103.
- (266) Kang, L.; Deng, S.; Zhang, S.; Li, Q.; Zhang, J. Selective Growth of Subnanometer Diameter Single-Walled Carbon Nanotube Arrays in Hydrogen-free CVD. *J. Am. Chem. Soc.* **2016**, *138*, 12723–12726.
- (267) Zhang, S.; Wang, X.; Yao, F.; He, M.; Lin, D.; Ma, H.; Sun, Y.; Zhao, Q.; Liu, K.; Ding, F.; et al. Controllable Growth of (*n*, *n*–1) Family of Semiconducting Carbon Nanotubes. *Chem.* **2019**, *5*, 1182.
- (268) Artyukhov, V. I.; Liu, M.; Peney, E. S.; Yakobson, B. I. A Jellium Model of a Catalyst Particle in Carbon Nanotube Growth. *J. Chem. Phys.* **2017**, *146*, 244701.
- (269) Yoshikawa, R.; Hisama, K.; Ukai, H.; Takagi, Y.; Inoue, T.; Chiashi, S.; Maruyama, S. Molecular Dynamics of Chirality Definable Growth of Single-Walled Carbon Nanotubes. *ACS Nano* **2019**, *13*, 6506–6512.
- (270) Khalilov, U.; Bogaerts, A.; Neyts, E. C. Atomic Scale Simulation of Carbon Nanotube Nucleation from Hydrocarbon Precursors. *Nat. Commun.* **2015**, *6*, 10306.
- (271) Qi, H.; Yuan, D. N.; Liu, J. Two-Stage Growth of Single-Walled Carbon Nanotubes. *J. Phys. Chem. C* **2007**, *111*, 6158–6160.
- (272) Wang, Y.; Kim, M. J.; Shan, H.; Kittrell, C.; Fan, H.; Ericson, L. M.; Hwang, W.-F.; Arepalli, S.; Hauge, R. H.; Smalley, R. E. Continued Growth of Single-Walled Carbon Nanotubes. *Nano Lett.* **2005**, *5*, 997–1002.
- (273) Smalley, R. E.; Li, Y.; Moore, V. C.; Price, B. K.; Colorado, R.; Schmidt, H. K.; Hauge, R. H.; Barron, A. R.; Tour, J. M. Single Wall

- Carbon Nanotube Amplification: En Route to a Type-Specific Growth Mechanism. *J. Am. Chem. Soc.* **2006**, *128*, 15824–15829.
- (274) Ogrin, D.; Anderson, R. E.; Colorado, R., Jr.; Maruyama, B.; Pender, M. J.; Moore, V. C.; Pheasant, S. T.; McJilton, L.; Schmidt, H. K.; Hauge, R. H.; et al. Amplification of Single-Walled Carbon Nanotubes from Designed Seeds: Separation of Nucleation and Growth. *J. Phys. Chem. C* **2007**, *111*, 17804–17806.
- (275) Yao, Y.; Feng, C.; Zhang, J.; Liu, Z. “Cloning” of Single-Walled Carbon Nanotubes via Open-End Growth Mechanism. *Nano Lett.* **2009**, *9*, 1673–1677.
- (276) Yu, X.; Zhang, J.; Choi, W.; Choi, J.-Y.; Kim, J. M.; Gan, L.; Liu, Z. Cap Formation Engineering: From Opened C_{60} to Single-Walled Carbon Nanotubes. *Nano Lett.* **2010**, *10*, 3343–3349.
- (277) Liu, B.; Liu, J.; Li, H.-B.; Bhola, R.; Jackson, E. A.; Scott, L. T.; Page, A.; Irle, S.; Morokuma, K.; Zhou, C. Nearly Exclusive Growth of Small Diameter Semiconducting Single-Wall Carbon Nanotubes from Organic Chemistry Synthetic End-Cap Molecules. *Nano Lett.* **2015**, *15*, 586–595.
- (278) Ibrahim, I.; Zhang, Y.; Popov, A.; Dunsch, L.; Büchner, B.; Cuniberti, G.; Rümmeli, M. H. Growth of All-Carbon Horizontally Aligned Single-Walled Carbon Nanotubes Nucleated from Fullerene-based Structures. *Nanoscale Res. Lett.* **2013**, *8*, 265.
- (279) Rao, F.; Li, T.; Wang, Y. Growth of “All-Carbon” Single-Walled Carbon Nanotubes from Diamonds and Fullerenes. *Carbon* **2009**, *47*, 3580–3584.
- (280) Omachi, H.; Nakayama, T.; Takahashi, E.; Segawa, Y.; Itami, K. Initiation of Carbon Nanotube Growth by Well-Defined Carbon Nanorings. *Nat. Chem.* **2013**, *5*, 572–576.
- (281) Lim, H. E.; Miyata, Y.; Kitaura, R.; Nishimura, Y.; Nishimoto, Y.; Irle, S.; Warner, J. H.; Kataura, H.; Shinohara, H. Growth of Carbon Nanotubes via Twisted Graphene Nanoribbons. *Nat. Commun.* **2013**, *4*, 2548.
- (282) Lin, D.; Zhang, S.; Zheng, Z.; Hu, W.; Zhang, J. Microwave-Assisted Regeneration of Single-Walled Carbon Nanotubes from Carbon Fragments. *Small* **2018**, *14*, 1800033.
- (283) Fort, E. H.; Donovan, P. M.; Scott, L. T. Diels-Alder Reactivity of Polycyclic Aromatic Hydrocarbon Bay Regions: Implications for Metal-Free Growth of Single-Chirality Carbon Nanotubes. *J. Am. Chem. Soc.* **2009**, *131*, 16006–16007.
- (284) Hitosugi, S.; Yamasaki, T.; Isobe, H. Bottom-up Synthesis and Thread-in-Bead Structures of Finite ($n,0$)-Zigzag Single-Wall Carbon Nanotubes. *J. Am. Chem. Soc.* **2012**, *134*, 12442–12445.
- (285) Segawa, Y.; Yagi, A.; Matsui, K.; Itami, K. Design and Synthesis of Carbon Nanotube Segments. *Angew. Chem., Int. Ed.* **2016**, *55*, 5136.
- (286) Povie, G.; Segawa, Y.; Nishihara, T.; Miyauchi, Y.; Itami, K. Synthesis of a Carbon Nanobelt. *Science* **2017**, *356*, 172–175.
- (287) Wang, H.; Yamada, C.; Liu, J.; Liu, B.; Tu, X.; Zheng, M.; Zhou, C.; Homma, Y. Re-Growth of Single-Walled Carbon Nanotube by Hot-Wall and Cold-Wall Chemical Vapor Deposition. *Carbon* **2015**, *95*, 497–502.
- (288) Michel, T.; Paillet, M.; Nakabayashi, D.; Picher, M.; Jourdain, V.; Meyer, J. C.; Zahab, A. A.; Sauvajol, J. L. Indexing of Individual Single-Walled Carbon Nanotubes from Raman Spectroscopy. *Phys. Rev. B: Condens. Matter Mater. Phys.* **2009**, *80*, 245416.
- (289) Hároz, E. H.; Duque, J. G.; Barros, E. B.; Telg, H.; Simpson, J. R.; Hight Walker, A. R.; Khripin, C. Y.; Fagan, J. A.; Tu, X.; Zheng, M.; et al. Asymmetric Excitation Profiles in the Resonance Raman Response of Armchair Carbon Nanotubes. *Phys. Rev. B: Condens. Matter Mater. Phys.* **2015**, *91*, 205446.
- (290) Tu, X.; Hight Walker, A. R.; Khripin, C. Y.; Zheng, M. Evolution of DNA Sequences Toward Recognition of Metallic Armchair Carbon Nanotubes. *J. Am. Chem. Soc.* **2011**, *133*, 12998–3001.
- (291) Hároz, E. H.; Rice, W. D.; Lu, B. Y.; Ghosh, S.; Hauge, R. H.; Weisman, R. B.; Doorn, S. K.; Kono, J. Enrichment of Armchair Carbon Nanotubes via Density Gradient Ultracentrifugation: Raman Spectroscopy Evidence. *ACS Nano* **2010**, *4*, 1955–1962.
- (292) Hároz, E. H.; Duque, J. G.; Lu, B. Y.; Nikolaev, P.; Arepalli, S.; Hauge, R. H.; Doorn, S. K.; Kono, J. Unique Origin of Colors of Armchair Carbon Nanotubes. *J. Am. Chem. Soc.* **2012**, *134*, 4461–4464.
- (293) Mueller, A.; Amsharov, K. Y.; Jansen, M. Synthesis of End-Cap Precursor Molecules for (6,6) Armchair and (9,0) Zig-zag Single-Walled Carbon Nanotubes. *Tetrahedron Lett.* **2010**, *51*, 3221–3225.
- (294) Mueller, A.; Amsharov, K. Y.; Jansen, M. End-Cap Precursor Molecules for the Controlled Growth of Single-Walled Carbon Nanotubes. *Fullerenes, Nanotubes, Carbon Nanostruct.* **2012**, *20*, 401–404.
- (295) Abdurakhmanova, N.; Mueller, A.; Stepanow, S.; Rauschenbach, S.; Jansen, M.; Kern, K.; Amsharov, K. Y. Bottom up Fabrication of (9, 0) Zigzag and (6, 6) Armchair Carbon Nanotube End-Caps on the Rh(111) Surface. *Carbon* **2015**, *84*, 444–447.
- (296) Hashimoto, A.; Suenaga, K.; Gloter, A.; Urita, K.; Iijima, S. Direct Evidence for Atomic Defects in Graphene Layers. *Nature* **2004**, *430*, 870–873.
- (297) Picher, M.; Navas, H.; Arenal, R.; Quesnel, E.; Anglaret, E.; Jourdain, V. Influence of the Growth Conditions on the Defect Density of Single-walled Carbon Nanotubes. *Carbon* **2012**, *50*, 2407–2416.
- (298) Penev, E. S.; Artyukhov, V. I.; Yakobson, B. I. Extensive Energy Landscape Sampling of Nanotube End-Caps Reveals No Chiral-Angle Bias for Their Nucleation. *ACS Nano* **2014**, *8*, 1899–1906.
- (299) Hersam, M. C. Progress Towards Monodisperse Single-Walled Carbon Nanotubes. *Nat. Nanotechnol.* **2008**, *3*, 387–394.
- (300) Zheng, M. Sorting Carbon Nanotubes. *Top. Curr. Chem.* **2017**, *375*, 13.
- (301) Cui, J.; Yang, D.; Zeng, X.; Zhou, N.; Liu, H. Recent Progress on the Structure Separation of Single-Wall Carbon Nanotubes. *Nanotechnology* **2017**, *28*, 452001.
- (302) Lefebvre, J.; Ding, J.; Li, Z.; Finnie, P.; Lopinski, G.; Malenfant, P. R. L. High-Purity Semiconducting Single-Walled Carbon Nanotubes: A Key Enabling Material in Emerging Electronics. *Acc. Chem. Res.* **2017**, *50*, 2479–2486.
- (303) Lei, T.; Pochorovski, I.; Bao, Z. Separation of Semiconducting Carbon Nanotubes for Flexible and Stretchable Electronics Using Polymer Removable Method. *Acc. Chem. Res.* **2017**, *50*, 1096–1104.
- (304) Janas, D. Towards monochiral carbon nanotubes: A Review of Progress in Sorting of Single-Wall Carbon Nanotubes. *Mater. Chem. Front.* **2018**, *2*, 36–63.
- (305) Qiu, S.; Wu, K.; Gao, B.; Li, L.; Jin, H.; Li, Q. Solution-Processing of High-Purity Semiconducting Single-Walled Carbon Nanotubes for Electronics Devices. *Adv. Mater.* **2019**, *31*, 1800750.
- (306) Li, H.; Gordeev, G.; Garrity, O.; Peyyety, N. A.; Selvasundaram, P. B.; Dehm, S.; Krupke, R.; Cambre, S.; Wenseleers, W.; Reich, S.; et al. Separation of Specific Single Enantiomer Single-Wall Carbon Nanotubes in the Large Diameter Regime. *ACS Nano* **2020**, DOI: 10.1021/acsnano.9b08244.
- (307) Liu, J.; Rinzler, A. G.; Dai, H. J.; Hafner, J. H.; Bradley, R. K.; Boul, P. J.; Lu, A.; Iverson, T.; Shelimov, K.; Huffman, C. B.; et al. *Science* **1998**, *280*, 1253–1256.
- (308) Chen, J.; Hamon, M. A.; Hu, H.; Chen, Y. S.; Rao, A. M.; Eklund, P. C.; Haddon, R. C. Solution Properties of Single-Walled Carbon Nanotubes. *Science* **1998**, *282*, 95–98.
- (309) Georgakilas, V.; Kordatos, K.; Prato, M.; Guldi, D. M.; Holzinger, M.; Hirsch, A. Organic Functionalization of Carbon Nanotubes. *J. Am. Chem. Soc.* **2002**, *124*, 760–761.
- (310) Strano, M. S.; Dyke, C. A.; Usrey, M. L.; Barone, P. W.; Allen, M. J.; Shan, H.; Kittrell, C.; Hauge, R. H.; Tour, J. M.; Smalley, R. E. Electronic Structure Control of Single-Walled Carbon Nanotube Functionalization. *Science* **2003**, *301*, 1519–1522.
- (311) Strano, M. S.; Moore, V. C.; Miller, M. K.; Allen, M. J.; Haroz, E. H.; Kittrell, C.; Hauge, R. H.; Smalley, R. E. The Role of Surfactant Adsorption during Ultrasonication in the Dispersion of Single-Walled Carbon Nanotubes. *J. Nanosci. Nanotechnol.* **2003**, *3*, 81–86.
- (312) Moore, V. C.; Strano, M. S.; Haroz, E. H.; Hauge, R. H.; Smalley, R. E.; Schmidt, J.; Talmon, Y. Individually Suspended Single-Walled Carbon Nanotubes in Various Surfactants. *Nano Lett.* **2003**, *3*, 1379–1382.
- (313) Wenseleers, W.; Vlasov, I. I.; Goovaerts, E.; Obraztsova, E. D.; Lobach, A. S.; Bouwen, A. Efficient Isolation and Solubilization of

- Pristine Single-Walled Nanotubes in Bile Salt Micelles. *Adv. Funct. Mater.* **2004**, *14*, 1105–1112.
- (314) O'Connell, M. J.; Bachilo, S. M.; Huffman, C. B.; Moore, V. C.; Strano, M. S.; Haroz, E. H.; Rialon, K. L.; Boul, P. J.; Noon, W. H.; Kittrell, C.; et al. Band Gap Fluorescence from Individual Single-Walled Carbon Nanotubes. *Science* **2002**, *297*, 593–596.
- (315) Chen, R. J.; Zhang, Y. G.; Wang, D. W.; Dai, H. J. Noncovalent Sidewall Functionalization of Single-Walled Carbon Nanotubes for Protein Immobilization. *J. Am. Chem. Soc.* **2001**, *123*, 3838–3839.
- (316) Peng, X.; Komatsu, N.; Bhattacharya, S.; Shimawaki, T.; Aonuma, S.; Kimura, T.; Osuka, A. Optically Active Single-Walled Carbon Nanotubes. *Nat. Nanotechnol.* **2007**, *2*, 361–365.
- (317) Koh, B.; Kim, G.; Yoon, H. K.; Park, J. B.; Kopelman, R.; Cheng, W. Fluorophore and Dye-Assisted Dispersion of Carbon Nanotubes in Aqueous Solution. *Langmuir* **2012**, *28*, 11676–11686.
- (318) Ozawa, H.; Fujigaya, T.; Niidome, Y.; Hotta, N.; Fujiki, M.; Nakashima, N. Rational Concept to Recognize/Extract Single-Walled Carbon Nanotubes with a Specific Chirality. *J. Am. Chem. Soc.* **2011**, *133*, 2651–2657.
- (319) Yurekli, K.; Mitchell, C. A.; Krishnamoorti, R. Small-Angle Neutron Scattering from Surfactant-Assisted Aqueous Dispersions of Carbon Nanotubes. *J. Am. Chem. Soc.* **2004**, *126*, 9902–9903.
- (320) Islam, M. F.; Rojas, E.; Bergey, D. M.; Johnson, A. T.; Yodh, A. G. High Weight Fraction Surfactant Solubilization of Single-Wall Carbon Nanotubes in Water. *Nano Lett.* **2003**, *3*, 269–273.
- (321) Wang, P.; Kim, M.; Peng, Z.; Sun, C. F.; Mok, J.; Lieberman, A.; Wang, Y. Superacid-Surfactant Exchange: Enabling Nondestructive Dispersion of Full-Length Carbon Nanotubes in Water. *ACS Nano* **2017**, *11*, 9231–9238.
- (322) Hagen, A.; Hertel, T. Quantitative Analysis of Optical Spectra from Individual Single-Wall Carbon Nanotubes. *Nano Lett.* **2003**, *3*, 383–388.
- (323) Liang, L. Y.; Xie, W. Y.; Fang, S. X.; He, F.; Yin, B. H.; Tlili, C.; Wang, D. Q.; Qiu, S.; Li, Q. W. High-Efficiency Dispersion and Sorting of Single-Walled Carbon Nanotubes via Non-Covalent Interactions. *J. Mater. Chem. C* **2017**, *5*, 11339–11368.
- (324) Zheng, M.; Jagota, A.; Strano, M. S.; Santos, A. P.; Barone, P.; Chou, S. G.; Diner, B. A.; Dresselhaus, M. S.; McLean, R. S.; Onoa, G. B.; et al. Structure-Based Carbon Nanotube Sorting by Sequence-Dependent DNA Assembly. *Science* **2003**, *302*, 1545–1548.
- (325) Nakashima, N.; Okuzono, S.; Murakami, H.; Nakai, T.; Yoshikawa, K. DNA Dissolves Single-Walled Carbon Nanotubes in Water. *Chem. Lett.* **2003**, *32*, 456–457.
- (326) Kato, Y.; Inoue, A.; Niidome, Y.; Nakashima, N. Thermodynamics on Soluble Carbon Nanotubes: How Do DNA Molecules Replace Surfactants on Carbon Nanotubes? *Sci. Rep.* **2012**, *2*, 733.
- (327) Ju, S. Y.; Abanulo, D. C.; Badalucco, C. A.; Gascon, J. A.; Papadimitrakopoulos, F. Handedness Enantioselection of Carbon Nanotubes Using Helical Assemblies of Flavin Mononucleotide. *J. Am. Chem. Soc.* **2012**, *134*, 13196–13199.
- (328) Hirano, A.; Tanaka, T.; Kataura, H.; Kameda, T. Arginine Side Chains as a Dispersant for Individual Single-Wall Carbon Nanotubes. *Chem. - Eur. J.* **2014**, *20*, 4922–4930.
- (329) Grigoryan, G.; Kim, Y. H.; Acharya, R.; Axelrod, K.; Jain, R. M.; Willis, L.; Drndic, M.; Kikkawa, J. M.; DeGrado, W. F. Computational Design of Virus-Like Protein Assemblies on Carbon Nanotube Surfaces. *Science* **2011**, *332*, 1071–1076.
- (330) Dieckmann, G. R.; Dalton, A. B.; Johnson, P. A.; Razal, J.; Chen, J.; Giordano, G. M.; Munoz, E.; Musselman, I. H.; Baughman, R. H.; Draper, R. K. Controlled Assembly of Carbon Nanotubes by Designed Amphiphilic Peptide Helices. *J. Am. Chem. Soc.* **2003**, *125*, 1770–1777.
- (331) Zorbas, V.; Smith, A. L.; Xie, H.; Ortiz-Acevedo, A.; Dalton, A. B.; Dieckmann, G. R.; Draper, R. K.; Baughman, R. H.; Musselman, I. H. Importance of Aromatic Content for Peptide/Single-Walled Carbon Nanotube Interactions. *J. Am. Chem. Soc.* **2005**, *127*, 12323–12328.
- (332) Calvaresi, M.; Zerbetto, F. The Devil and Holy Water: Protein and Carbon Nanotube Hybrids. *Acc. Chem. Res.* **2013**, *46*, 2454–2463.
- (333) Nakashima, N.; Tomonari, Y.; Murakami, H. Water-Soluble Single-Walled Carbon Nanotubes via Noncovalent Sidewall-Function-
- alization with a Pyrene-Carrying Ammonium Ion. *Chem. Lett.* **2002**, *31*, 638–639.
- (334) Tomonari, Y.; Murakami, H.; Nakashima, N. Solubilization of Single-Walled Carbon Nanotubes by Using Polycyclic Aromatic Ammonium Amphiphiles in Water—Strategy for the Design of High-Performance Solubilizers. *Chem. - Eur. J.* **2006**, *12*, 4027–4034.
- (335) Tian, L. L.; Meziani, M. J.; Lu, F. S.; Kong, C. Y.; Cao, L.; Thorne, T. J.; Sun, Y. P. Graphene Oxides for Homogeneous Dispersion of Carbon Nanotubes. *ACS Appl. Mater. Interfaces* **2010**, *2*, 3217–3222.
- (336) Li, Y. L.; Yang, J.; Zhao, Q. H.; Li, Y. Dispersing Carbon-Based Nanomaterials in Aqueous Phase by Graphene Oxides. *Langmuir* **2013**, *29*, 13527–13534.
- (337) Fukushima, T.; Kosaka, A.; Ishimura, Y.; Yamamoto, T.; Takigawa, T.; Ishii, N.; Aida, T. Molecular Ordering of Organic Molten Salts Triggered by Single-Walled Carbon Nanotubes. *Science* **2003**, *300*, 2072–2074.
- (338) Furtado, C. A.; Kim, U. J.; Gutierrez, H. R.; Pan, L.; Dickey, E. C.; Eklund, P. C. Debundling and Dissolution of Single-Walled Carbon Nanotubes in Amide Solvents. *J. Am. Chem. Soc.* **2004**, *126*, 6095–6105.
- (339) Wang, J. Y.; Chu, H. B.; Li, Y. Why Single-Walled Carbon Nanotubes Can Be Dispersed in Imidazolium-Based Ionic Liquids. *ACS Nano* **2008**, *2*, 2540–2546.
- (340) Bellayer, S.; Gilman, J. W.; Eidelman, N.; Bourbigot, S.; Flambard, X.; Fox, D. M.; De Long, H. C.; Trulove, P. C. Preparation of Homogeneously Dispersed Multiwalled Carbon Nanotube/Polystyrene Nanocomposites via Melt Extrusion Using Trialkyl Imidazolium Compatibilizer. *Adv. Funct. Mater.* **2005**, *15*, 910–916.
- (341) Heller, D. A.; Mayrhofer, R. M.; Baik, S.; Grinkova, Y. V.; Usrey, M. L.; Strano, M. S. Concomitant Length and Diameter Separation of Single-Walled Carbon Nanotubes. *J. Am. Chem. Soc.* **2004**, *126*, 14567–14573.
- (342) Arnold, M. S.; Stupp, S. I.; Hersam, M. C. Enrichment of Single-Walled Carbon Nanotubes by Diameter in Density Gradients. *Nano Lett.* **2005**, *5*, 713–718.
- (343) Huang, X. Y.; McLean, R. S.; Zheng, M. High-Resolution Length Sorting and Purification of DNA-Wrapped Carbon Nanotubes by Size-Exclusion Chromatography. *Anal. Chem.* **2005**, *77*, 6225–6228.
- (344) Hennrich, F.; Krupke, R.; Arnold, K.; Stutz, J. A. R.; Lebedkin, S.; Koch, T.; Schimmel, T.; Kappes, M. M. The Mechanism of Cavitation-Induced Scission of Single-Walled Carbon Nanotubes. *J. Phys. Chem. B* **2007**, *111*, 1932–1937.
- (345) Tanaka, T.; Jin, H.; Miyata, Y.; Fujii, S.; Suga, H.; Naitoh, Y.; Minari, T.; Miyadera, T.; Tsukagoshi, K.; Kataura, H. Simple and Scalable Gel-Based Separation of Metallic and Semiconducting Carbon Nanotubes. *Nano Lett.* **2009**, *9*, 1497–1500.
- (346) Tanaka, T.; Urabe, Y.; Nishide, D.; Kataura, H. Continuous Separation of Metallic and Semiconducting Carbon Nanotubes Using Agarose Gel. *Appl. Phys. Express* **2009**, *2*, 125002.
- (347) Wang, H.; Bao, Z. Conjugated Polymer Sorting of Semiconducting Carbon Nanotubes and Their Electronic Applications. *Nano Today* **2015**, *10*, 737–758.
- (348) Khripin, C. Y.; Fagan, J. A.; Zheng, M. Spontaneous Partition of Carbon Nanotubes in Polymer-Modified Aqueous Phases. *J. Am. Chem. Soc.* **2013**, *135*, 6822–6825.
- (349) Lustig, S. R.; Jagota, A.; Khripin, C.; Zheng, M. Theory of Structure-Based Carbon Nanotube Separations by Ion-Exchange Chromatography of DNA/CNT Hybrids. *J. Phys. Chem. B* **2005**, *109*, 2559–2566.
- (350) Zheng, M.; Semke, E. D. Enrichment of Single Chirality Carbon Nanotubes. *J. Am. Chem. Soc.* **2007**, *129*, 6084–6085.
- (351) Fagan, J. A.; Zheng, M.; Rastogi, V.; Simpson, J. R.; Khripin, C. Y.; Silvera Batista, C. A.; Hight Walker, A. R. Analyzing surfactant structures on Length and Chirality Resolved (6,5) Single-Wall Carbon Nanotubes by Analytical Ultracentrifugation. *ACS Nano* **2013**, *7*, 3373–3387.
- (352) Moshammer, K.; Hennrich, F.; Kappes, M. M. Selective Suspension in Aqueous Sodium Dodecyl Sulfate According to

- Electronic Structure Type Allows Simple Separation of Metallic from Semiconducting Single-Walled Carbon Nanotubes. *Nano Res.* **2009**, *2*, 599–606.
- (353) Liu, H.; Tanaka, T.; Kataura, H. Optical Isomer Separation of Single-Chirality Carbon Nanotubes Using Gel Column Chromatography. *Nano Lett.* **2014**, *14*, 6237–6243.
- (354) Akazaki, K.; Toshimitsu, F.; Ozawa, H.; Fujigaya, T.; Nakashima, N. Recognition and One-Pot Extraction of Right- and Left-Handed Semiconducting Single-Walled Carbon Nanotube Enantiomers Using Fluorene-Binaphthol Chiral Copolymers. *J. Am. Chem. Soc.* **2012**, *134*, 12700–12707.
- (355) Kanai, Y.; Grossman, J. C. Role of Semiconducting and Metallic Tubes in P3HT/Carbon-Nanotube Photovoltaic Heterojunctions: Density Functional Theory Calculations. *Nano Lett.* **2008**, *8*, 908–912.
- (356) Wang, H.; Hsieh, B.; Jimenez-Oses, G.; Liu, P.; Tassone, C. J.; Diao, Y.; Lei, T.; Houk, K. N.; Bao, Z. Solvent Effects on Polymer Sorting of Carbon Nanotubes with Applications in Printed Electronics. *Small* **2015**, *11*, 126–133.
- (357) Lei, T.; Lai, Y.-C.; Hong, G.; Wang, H.; Hayoz, P.; Weitz, R. T.; Chen, C.; Dai, H.; Bao, Z. Diketopyrrolopyrrole (DPP)-Based Donor-Acceptor Polymers for Selective Dispersion of Large-Diameter Semiconducting Carbon Nanotubes. *Small* **2015**, *11*, 2946–2954.
- (358) Venema, L. C.; Wildoer, J. W. G.; Janssen, J. W.; Tans, S. J.; Tuinstra, H. L. J. T.; Kouwenhoven, L. P.; Dekker, C. Imaging Electron Wave Functions of Quantized Energy Levels in Carbon Nanotubes. *Science* **1999**, *283*, 52–55.
- (359) Welsher, K.; Sherlock, S. P.; Dai, H. J. Deep-Tissue Anatomical Imaging of Mice Using Carbon Nanotube Fluorophores in the Second Near-Infrared Window. *Proc. Natl. Acad. Sci. U. S. A.* **2011**, *108*, 8943–8948.
- (360) Bonard, J. M.; Stora, T.; Salvetat, J. P.; Maier, F.; Stockli, T.; Duschl, C.; Forro, L.; deHeer, W. A.; Chatelain, A. Purification and Size-Selection of Carbon Nanotubes. *Adv. Mater.* **1997**, *9*, 827–831.
- (361) Khripin, C. Y.; Tu, X.; Howarter, J.; Fagan, J.; Zheng, M. Concentration Measurement of Length-Fractionated Colloidal Single-Wall Carbon Nanotubes. *Anal. Chem.* **2012**, *84*, 8733–8739.
- (362) Chen, B. L.; Selegue, J. P. Separation and Characterization of Single-Walled and Multiwalled Carbon Nanotubes by Using Flow Field-Flow Fractionation. *Anal. Chem.* **2002**, *74*, 4774–4780.
- (363) Chun, J.; Fagan, J. A.; Hobbie, E. K.; Bauer, B. J. Size Separation of Single-Wall Carbon Nanotubes by Flow-Field Flow Fractionation. *Anal. Chem.* **2008**, *80*, 2514–2523.
- (364) Sun, X.; Zaric, S.; Daranciang, D.; Welsher, K.; Lu, Y.; Li, X.; Dai, H. Optical Properties of Ultrashort Semiconducting Single-Walled Carbon Nanotube Capsules Down to Sub-10 nm. *J. Am. Chem. Soc.* **2008**, *130*, 6551–6555.
- (365) Fagan, J. A.; Becker, M. L.; Chun, J.; Hobbie, E. K. Length Fractionation of Carbon Nanotubes Using Centrifugation. *Adv. Mater.* **2008**, *20*, 1609–1613.
- (366) Ohmori, S.; Saito, T.; Shukla, B.; Yumura, M.; Iijima, S. Fractionation of Single Wall Carbon Nanotubes by Length Using Cross Flow Filtration Method. *ACS Nano* **2010**, *4*, 3606–3610.
- (367) Khripin, C. Y.; Manohar, S.; Zheng, M.; Jagota, A. Measurement of Electrostatic Properties of DNA-Carbon Nanotube Hybrids by Capillary Electrophoresis. *J. Phys. Chem. C* **2009**, *113*, 13616–13621.
- (368) Gui, H.; Chen, H.; Khripin, C. Y.; Liu, B.; Fagan, J. A.; Zhou, C.; Zheng, M. A Facile and Low-Cost Length Sorting of Single-Wall Carbon Nanotubes by Precipitation and Applications for Thin-Film Transistors. *Nanoscale* **2016**, *8*, 3467–3473.
- (369) Khripin, C. Y.; Tu, X.; Heddleston, J. M.; Silvera-Batista, C.; Walker, A. R. H.; Fagan, J.; Zheng, M. High-Resolution Length Fractionation of Surfactant-Dispersed Carbon Nanotubes. *Anal. Chem.* **2013**, *85*, 1382–1388.
- (370) Khripin, C. Y.; Arnold-Medabalimi, N.; Zheng, M. Molecular-Crowding-Induced Clustering of DNA-Wrapped Carbon Nanotubes for Facile Length Fractionation. *ACS Nano* **2011**, *5*, 8258–8266.
- (371) Ziegler, K. J.; Schmidt, D. J.; Rauwald, U.; Shah, K. N.; Flor, E. L.; Haage, R. H.; Smalley, R. E. Length-Dependent Extraction of Single-Walled Carbon Nanotubes. *Nano Lett.* **2005**, *5*, 2355–2359.
- (372) Chattopadhyay, D.; Lastella, S.; Kim, S.; Papadimitrakopoulos, F. Length Separation of Zwitterion-Functionalized Single Wall Carbon Nanotubes by GPC. *J. Am. Chem. Soc.* **2002**, *124*, 728–729.
- (373) Kim, Y.; Lee, D.; Oh, Y.; Choi, J.; Baik, S. The Effects of Acid Treatment Methods on the Diameter Dependent Length Separation of Single Walled Carbon Nanotubes. *Synth. Met.* **2006**, *156*, 999–1003.
- (374) Wang, P.; Barnes, B.; Wu, X.; Qu, H.; Zhang, C.; Shi, Y.; Headrick, R. J.; Pasquali, M.; Wang, Y. Self-Sorting of 10-μm-Long Single-Walled Carbon Nanotubes in Aqueous Solution. *Adv. Mater.* **2019**, *31*, 1901641.
- (375) Strano, M. S.; Zheng, M.; Jagota, A.; Onoa, G. B.; Heller, D. A.; Barone, P. W.; Usrey, M. L. Understanding the Nature of the DNA-Assisted Separation of Single-Walled Carbon Nanotubes Using Fluorescence and Raman Spectroscopy. *Nano Lett.* **2004**, *4*, 543–550.
- (376) Cambre, S.; Wenseleers, W. Separation and Diameter-Sorting of Empty (End-Capped) and Water-Filled (Open) Carbon Nanotubes by Density Gradient Ultracentrifugation. *Angew. Chem., Int. Ed.* **2011**, *50*, 2764–2768.
- (377) Liu, H.; Feng, Y.; Tanaka, T.; Urabe, Y.; Kataura, H. Diameter-Selective Metal/Semiconductor Separation of Single-Wall Carbon Nanotubes by Agarose Gel. *J. Phys. Chem. C* **2010**, *114*, 9270–9276.
- (378) Chen, F.; Wang, B.; Chen, Y.; Li, L.-J. Toward the extraction of Single Species of Single-Walled Carbon Nanotubes Using Fluorene-Based Polymers. *Nano Lett.* **2007**, *7*, 3013–3017.
- (379) Gomulya, W.; Diaz Costanzo, G.; Figueiredo de Carvalho, E. J.; Bisri, S. Z.; Derenskyi, V.; Fritsch, M.; Froehlich, N.; Allard, S.; Gordiichuk, P.; Herrmann, A.; et al. Semiconducting Single-Walled Carbon Nanotubes on Demand by Polymer Wrapping. *Adv. Mater.* **2013**, *25*, 2948–2956.
- (380) Yanagi, K.; Itsuka, T.; Fujii, S.; Kataura, H. Separations of Metallic and Semiconducting Carbon Nanotubes by Using Sucrose as a Gradient Medium. *J. Phys. Chem. C* **2008**, *112*, 18889–18894.
- (381) Silvera-Batista, C. A.; Scott, D. C.; McLeod, S. M.; Ziegler, K. J. A Mechanistic Study of the Selective Retention of SDS-Suspended Single-Wall Carbon Nanotubes on Agarose Gels. *J. Phys. Chem. C* **2011**, *115*, 9361–9369.
- (382) Li, H. B.; Jin, H. H.; Zhang, J.; Wen, X. N.; Song, Q. J.; Li, Q. W. Understanding the Electrophoretic Separation of Single-Walled Carbon Nanotubes Assisted by Thionine as a Probe. *J. Phys. Chem. C* **2010**, *114*, 19234–19238.
- (383) Gui, H.; Li, H.; Tan, F.; Jin, H.; Zhang, J.; Li, Q. Binary Gradient Elution of Semiconducting Single-Walled Carbon Nanotubes by Gel Chromatography for Their Separation according to Chirality. *Carbon* **2012**, *50*, 332–335.
- (384) Liu, H.; Tanaka, T.; Urabe, Y.; Kataura, H. High-Efficiency Single-Chirality Separation of Carbon Nanotubes Using Temperature-Controlled Gel Chromatography. *Nano Lett.* **2013**, *13*, 1996–2003.
- (385) Tulevski, G. S.; Franklin, A. D.; Afzali, A. High Purity Isolation and Quantification of Semiconducting Carbon Nanotubes via Column Chromatography. *ACS Nano* **2013**, *7*, 2971–2976.
- (386) Streit, J. K.; Lam, S.; Piao, Y.; Hight Walker, A. R.; Fagan, J. A.; Zheng, M. Separation of Double-Wall Carbon Nanotubes by Electronic Type and Diameter. *Nanoscale* **2017**, *9*, 2531–2540.
- (387) Wei, L.; Flavel, B. S.; Krupke, R.; Chen, Y.; Li, W. Exploring the Upper Limit of Single-Walled Carbon Nanotube Purity by Multiple-Cycle Aqueous Two-Phase Separation. *Nanoscale* **2017**, *9*, 11640–11646.
- (388) Subbaiyan, N. K.; Parra-Vasquez, A. N. G.; Cambre, S.; Cordoba, M. A. S.; Yalcin, S. E.; Hamilton, C. E.; Mack, N. H.; Blackburn, J. L.; Doorn, S. K.; Duque, J. G. Bench-Top Aqueous Two-Phase Extraction of Isolated Individual Single-Walled Carbon Nanotubes. *Nano Res.* **2015**, *8*, 1755–1769.
- (389) Gui, H.; Streit, J. K.; Fagan, J. A.; Hight Walker, A. R.; Zhou, C.; Zheng, M. Redox Sorting of Carbon Nanotubes. *Nano Lett.* **2015**, *15*, 1642–1646.
- (390) Wang, J.; Nguyen, T. D.; Cao, Q.; Wang, Y.; Tan, M. Y.; Chan-Park, M. B. Selective Surface Charge Sign Reversal on Metallic Carbon Nanotubes for Facile Ultrahigh Purity Nanotube Sorting. *ACS Nano* **2016**, *10*, 3222–3232.

- (391) Jagota, A.; Diner, B. A.; Bouss, S.; Zheng, M. Carbon Nanotube–Biomolecule Interactions: Applications in Carbon Nanotube Separation and Biosensing. *Applied Physics of Carbon Nanotubes: Fundamentals of Theory, Optics and Transport Devices*; Springer: Berlin, 2005; pp 285–261.
- (392) Fong, D.; Adronov, A. Recent Developments in the Selective Dispersion of Single-Walled Carbon Nanotubes Using Conjugated Polymers. *Chem. Sci.* **2017**, *8*, 7292–7305.
- (393) Hwang, J.-Y.; Nish, A.; Doig, J.; Douven, S.; Chen, C.-W.; Chen, L.-C.; Nicholas, R. J. Polymer Structure and Solvent Effects on the Selective Dispersion of Single-Walled Carbon Nanotubes. *J. Am. Chem. Soc.* **2008**, *130*, 3543–3553.
- (394) Stuerzl, N.; Hennrich, F.; Lebedkin, S.; Kappes, M. M. Near Monochiral Single-Walled Carbon Nanotube Dispersions in Organic Solvents. *J. Phys. Chem. C* **2009**, *113*, 14628–14632.
- (395) Gerstel, P.; Klumpp, S.; Hennrich, F.; Altintas, O.; Eaton, T. R.; Mayor, M.; Barner-Kowollik, C.; Kappes, M. M. Selective Dispersion of Single-Walled Carbon Nanotubes via Easily Accessible Conjugated Click Polymers. *Polym. Chem.* **2012**, *3*, 1966–1970.
- (396) Lemasson, F.; Berton, N.; Tittmann, J.; Hennrich, F.; Kappes, M. M.; Mayor, M. Polymer Library Comprising Fluorene and Carbazole Homo- and Copolymers for Selective Single-Walled Carbon Nanotubes Extraction. *Macromolecules* **2012**, *45*, 713–722.
- (397) Mistry, K. S.; Larsen, B. A.; Blackburn, J. L. High-Yield Dispersions of Large-Diameter Semiconducting Single-Walled Carbon Nanotubes with Tunable Narrow Chirality Distributions. *ACS Nano* **2013**, *7*, 2231–2239.
- (398) Brady, G. J.; Joo, Y.; Wu, M.-Y.; Shea, M. J.; Gopalan, P.; Arnold, M. S. Polyfluorene-Sorted, Carbon Nanotube Array Field-Effect Transistors with Increased Current Density and High On/Off Ratio. *ACS Nano* **2014**, *8*, 11614–11621.
- (399) Li, H.; Gordeev, G.; Wasserroth, S.; Chakravadhanula, V. S. K.; Neelakandhan, S. K. C.; Hennrich, F.; Jorio, A.; Reich, S.; Krupke, R.; Flavel, B. S. Inner- and Outer-Wall Sorting of Double-Walled Carbon Nanotubes. *Nat. Nanotechnol.* **2017**, *12*, 1176–1182.
- (400) Wang, H.; Koleilat, G. I.; Liu, P.; Jimenez-Oses, G.; Lai, Y. C.; Vosgueritchian, M.; Fang, Y.; Park, S.; Houk, K. N.; Bao, Z. High-Yield Sorting of Small-Diameter Carbon Nanotubes for Solar Cells and Transistors. *ACS Nano* **2014**, *8*, 2609–2617.
- (401) Li, H.; Zhang, F.; Qiu, S.; Lv, N.; Zhao, Z.; Li, Q.; Cui, Z. Designing Large-Plane Conjugated Copolymers for the High-Yield Sorting of Semiconducting Single-Walled Carbon Nanotubes. *Chem. Commun.* **2013**, *49*, 10492–10494.
- (402) Zhang, X.; Zhao, J.; Tange, M.; Xu, W.; Xu, W.; Zhang, K.; Guo, W.; Okazaki, T.; Cui, Z. Sorting Semiconducting Single Walled Carbon Nanotubes by Poly(9,9-Dioctylfluorene) Derivatives and Application for Ammonia Gas Sensing. *Carbon* **2015**, *94*, 903–910.
- (403) Liang, S.; Subrahmanyam, A. V.; Khadem, M.; Zhao, Y. M.; Adronov, A. Selective Dispersion of Single-Walled Carbon Nanotubes with Electron-Rich Fluorene-Based Copolymers. *RSC Adv.* **2016**, *6*, 25733–25740.
- (404) Gao, W.; Xu, W.; Ye, J.; Liu, T.; Wang, J.; Tan, H.; Lin, Y.; Tange, M.; Sun, D.; Wu, L.; et al. Selective Dispersion of Large-Diameter Semiconducting Carbon Nanotubes by Functionalized Conjugated Dendritic Oligothiophenes for Use in Printed Thin Film Transistors. *Adv. Funct. Mater.* **2017**, *27*, 1703938.
- (405) Jakubka, F.; Schiessl, S. P.; Martin, S.; Englert, J. M.; Hauke, F.; Hirsch, A.; Zaumseil, J. Effect of Polymer Molecular Weight and Solution Parameters on Selective Dispersion of Single-Walled Carbon Nanotubes. *ACS Macro Lett.* **2012**, *1*, 815–819.
- (406) Qian, L.; Xu, W.; Fan, X.; Wang, C.; Zhang, J.; Zhao, J.; Cui, Z. Electrical and Photoresponse Properties of Printed Thin-Film Transistors Based on Poly(9,9-dioctylfluorene-co-bithiophene) Sorted Large-Diameter Semiconducting Carbon Nanotubes. *J. Phys. Chem. C* **2013**, *117*, 18243–18250.
- (407) Xu, W.; Zhao, J.; Qian, L.; Han, X.; Wu, L.; Wu, W.; Song, M.; Zhou, L.; Su, W.; Wang, C.; et al. Sorting of Large-Diameter Semiconducting Carbon Nanotube and Printed Flexible Driving Circuit for Organic Light Emitting Diode (OLED). *Nanoscale* **2014**, *6*, 1589–1595.
- (408) Toshimitsu, F.; Nakashima, N. Semiconducting Single-Walled Carbon Nanotubes Sorting with a Removable Solubilizer Based on Dynamic Supramolecular Coordination Chemistry. *Nat. Commun.* **2014**, *5*, 5041.
- (409) Rice, N. A.; Subrahmanyam, A. V.; Laengert, S. E.; Adronov, A. The Effect of Molecular Weight on the Separation of Semiconducting Single-Walled Carbon Nanotubes Using Poly(2,7-carbazole)s. *J. Polym. Sci., Part A: Polym. Chem.* **2015**, *53*, 2510–2516.
- (410) Toshimitsu, F.; Nakashima, N. Facile Isolation of Adsorbent-Free Long and Highly-Pure Chirality-Selected Semiconducting Single-Walled Carbon Nanotubes Using a Hydrogen-bonding Supramolecular Polymer. *Sci. Rep.* **2015**, *5*, 18066.
- (411) Fong, D.; Bodnaryk, W. J.; Rice, N. A.; Saem, S.; Moran-Mirabal, J. M.; Adronov, A. Influence of Polymer Electronics on Selective Dispersion of Single-Walled Carbon Nanotubes. *Chem. - Eur. J.* **2016**, *22*, 14560–14566.
- (412) Ouyang, J.; Ding, J.; Lefebvre, J.; Li, Z.; Guo, C.; Kell, A. J.; Malenfant, P. R. L. Sorting of Semiconducting Single-Walled Carbon Nanotubes in Polar Solvents with an Amphiphilic Conjugated Polymer Provides General Guidelines for Enrichment. *ACS Nano* **2018**, *12*, 1910–1919.
- (413) Lei, T.; Chen, X.; Pitner, G.; Wong, H.-S. P.; Bao, Z. Removable and Recyclable Conjugated Polymers for Highly Selective and High-Yield Dispersion and Release of Low-Cost Carbon Nanotubes. *J. Am. Chem. Soc.* **2016**, *138*, 802–805.
- (414) Pochorovski, I.; Wang, H.; Feldblyum, J. I.; Zhang, X.; Antaris, A. L.; Bao, Z. H-Bonded Supramolecular Polymer for the Selective Dispersion and Subsequent Release of Large-Diameter Semiconducting Single-Walled Carbon Nanotubes. *J. Am. Chem. Soc.* **2015**, *137*, 4328–4331.
- (415) Ghosh, S.; Bachilo, S. M.; Weisman, R. B. Advanced Sorting of Single-Walled Carbon Nanotubes by Nonlinear Density-Gradient Ultracentrifugation. *Nat. Nanotechnol.* **2010**, *5*, 443–450.
- (416) Green, A. A.; Hersam, M. C. Nearly Single-Chirality Single-Walled Carbon Nanotubes Produced via Orthogonal Iterative Density Gradient Ultracentrifugation. *Adv. Mater.* **2011**, *23*, 2185–2190.
- (417) Zhao, P.; Einarsson, E.; Xiang, R.; Murakami, Y.; Maruyama, S. Controllable Expansion of Single-Walled Carbon Nanotube Dispersions Using Density Gradient Ultracentrifugation. *J. Phys. Chem. C* **2010**, *114*, 4831–4834.
- (418) Kawai, M.; Kyakuno, H.; Suzuki, T.; Igarashi, T.; Suzuki, H.; Okazaki, T.; Kataura, H.; Maniwa, Y.; Yanagi, K. Single Chirality Extraction of Single-Wall Carbon Nanotubes for the Encapsulation of Organic Molecules. *J. Am. Chem. Soc.* **2012**, *134*, 9545–9548.
- (419) Yomogida, Y.; Tanaka, T.; Zhang, M.; Yudasaka, M.; Wei, X.; Kataura, H. Industrial-Scale Separation of High-Purity Single-Chirality Single-Wall Carbon Nanotubes for Biological Imaging. *Nat. Commun.* **2016**, *7*, 12056.
- (420) Zeng, X.; Hu, J.; Zhang, X.; Zhou, N.; Zhou, W.; Liu, H.; Xie, S. Ethanol-Assisted Gel Chromatography for Single-Chirality Separation of Carbon Nanotubes. *Nanoscale* **2015**, *7*, 16273–16281.
- (421) Ichinose, Y.; Eda, J.; Yomogida, Y.; Liu, Z.; Yanagi, K. Extraction of High-Purity Single-Chirality Single-Walled Carbon Nanotubes through Precise pH Control Using Carbon Dioxide Bubbling. *J. Phys. Chem. C* **2017**, *121*, 13391–13395.
- (422) Flavel, B. S.; Kappes, M. M.; Krupke, R.; Hennrich, F. Separation of Single-Walled Carbon Nanotubes by 1-Dodecanol-Mediated Size-Exclusion Chromatography. *ACS Nano* **2013**, *7*, 3557–3564.
- (423) Flavel, B. S.; Moore, K. E.; Pfohl, M.; Kappes, M. M.; Hennrich, F. Separation of Single-Walled Carbon Nanotubes with a Gel Permeation Chromatography System. *ACS Nano* **2014**, *8*, 1817–1826.
- (424) Hirano, A.; Tanaka, T.; Urabe, Y.; Kataura, H. pH- and Solute-Dependent Adsorption of Single-Wall Carbon Nanotubes onto Hydrogels: Mechanistic Insights into the Metal/Semiconductor Separation. *ACS Nano* **2013**, *7*, 10285–10295.

- (425) Tanaka, T.; Urabe, Y.; Hirakawa, T.; Kataura, H. Simultaneous Chirality and Enantiomer Separation of Metallic Single-Wall Carbon Nanotubes by Gel Column Chromatography. *Anal. Chem.* **2015**, *87*, 9467–9472.
- (426) Fagan, J. A.; Haroz, E. H.; Ihly, R.; Gui, H.; Blackburn, J. L.; Simpson, J. R.; Lam, S.; Walker, A. R. H.; Doorn, S. K.; Zheng, M. Isolation of > 1 nm Diameter Single-Wall Carbon Nanotube Species Using Aqueous Two-Phase Extraction. *ACS Nano* **2015**, *9*, 5377–5390.
- (427) Subbaiyan, N. K.; Cambre, S.; Parra-Vasquez, A. N. G.; Haroz, E. H.; Doorn, S. K.; Duque, J. G. Role of Surfactants and Salt in Aqueous Two-Phase Separation of Carbon Nanotubes toward Simple Chirality Isolation. *ACS Nano* **2014**, *8*, 1619–1628.
- (428) Li, H.; Gordeev, G.; Garrity, O.; Reich, S.; Flavel, B. S. Separation of Small-Diameter Single-Walled Carbon Nanotubes in One to Three Steps with Aqueous Two-Phase Extraction. *ACS Nano* **2019**, *13*, 2567–2578.
- (429) Ao, G.; Khrapin, C. Y.; Zheng, M. DNA-Controlled Partition of Carbon Nanotubes in Polymer Aqueous Two-Phase Systems. *J. Am. Chem. Soc.* **2014**, *136*, 10383–10392.
- (430) Zheng, M.; Diner, B. A. Solution Redox Chemistry of Carbon Nanotubes. *J. Am. Chem. Soc.* **2004**, *126*, 15490–15494.
- (431) Kim, S. N.; Kuang, Z.; Grote, J. G.; Farmer, B. L.; Naik, R. R. Enrichment of (6,5) Single Wall Carbon Nanotubes Using Genomic DNA. *Nano Lett.* **2008**, *8*, 4415–4420.
- (432) Ao, G.; Streit, J. K.; Fagan, J. A.; Zheng, M. Differentiating Left- and Right-handed Carbon Nanotubes by DNA. *J. Am. Chem. Soc.* **2016**, *138*, 16677–16688.
- (433) Lyu, M.; Meany, B.; Yang, J.; Li, Y.; Zheng, M. Towards Complete Resolution of DNA/Carbon Nanotube Hybrids by Aqueous Two-phase Systems. *J. Am. Chem. Soc.* **2019**, *141*, 20177–20186.
- (434) Tange, M.; Okazaki, T.; Iijima, S. Selective Extraction of Large-Diameter Single-Wall Carbon Nanotubes with Specific Chiral Indices by Poly(9,9-diptylfluorene-alt-benzothiadiazole). *J. Am. Chem. Soc.* **2011**, *133*, 11908–11911.
- (435) Gerstel, P.; Klumpp, S.; Hennrich, F.; Poschlade, A.; Meded, V.; Blasco, E.; Wenzel, W.; Kappes, M. M.; Barner-Kowollik, C. Highly Selective Dispersion of Single-Walled Carbon Nanotubes via Polymer Wrapping: a Combinatorial Study via Modular Conjugation. *ACS Macro Lett.* **2014**, *3*, 10–15.
- (436) Ozawa, H.; Ide, N.; Fujigaya, T.; Niidome, Y.; Nakashima, N. One-Pot Separation of Highly Enriched (6,5)-Single-walled Carbon Nanotubes Using a Fluorene-based Copolymer. *Chem. Lett.* **2011**, *40*, 239–241.
- (437) Peng, X. B.; Komatsu, N.; Kimura, T.; Osuka, A. Improved Optical Enrichment of SWNTs through Extraction with Chiral Nanotweezers of 2,6-Pyridylene-Bridged Diporphyrins. *J. Am. Chem. Soc.* **2007**, *129*, 15947–15953.
- (438) Peng, X.; Komatsu, N.; Kimura, T.; Osuka, A. Simultaneous Enrichments of Optical Purity and (n,m) Abundance of SWNTs through Extraction with 3,6-Carbazolylene-Bridged Chiral Diporphyrin Nanotweezers. *ACS Nano* **2008**, *2*, 2045–2050.
- (439) Green, A. A.; Duch, M. C.; Hersam, M. C. Isolation of Single-Walled Carbon Nanotube Enantiomers by Density Differentiation. *Nano Res.* **2009**, *2*, 69–77.
- (440) Wang, F.; Matsuda, K.; Rahman, A. F. M. M.; Peng, X.; Kimura, T.; Komatsu, N. Simultaneous Discrimination of Handedness and Diameter of Single-Walled Carbon Nanotubes (SWNTs) with Chiral Diporphyrin Nanotweezers Leading to Enrichment of a Single Enantiomer of (6,5)-SWNTs. *J. Am. Chem. Soc.* **2010**, *132*, 10876–10881.
- (441) Wang, F.; Matsuda, K.; Rahman, A. F. M. M.; Kimura, T.; Komatsu, N. Improved Selectivity in Discriminating Handedness and Diameter of Single-Walled Carbon Nanotubes with N-Substituted 3,6-Carbazolylene-Bridged Chiral Diporphyrin Nanotweezers. *Nanoscale* **2011**, *3*, 4117–4124.
- (442) Marquis, R.; Kulikiewicz, K.; Lebedkin, S.; Kappes, M. M.; Mioskowski, C.; Meunier, S.; Wagner, A. Axially Chiral Facial Amphiphiles with a Dihydronaphthopentaphene Structure as Molecular Tweezers for SWNTs. *Chem. - Eur. J.* **2009**, *15*, 11187–11196.
- (443) Peng, X. B.; Wang, F.; Bauri, A. K.; Rahman, A. F. M. M.; Komatsu, N. Optical Resolution of Single-Walled Carbon Nanotubes through Molecular Recognition with Chiral Diporphyrin Nanotweezers. *Chem. Lett.* **2010**, *39*, 1022–1027.
- (444) Liu, G.; Wang, F.; Chauchaiyakul, S.; Saito, Y.; Bauri, A. K.; Kimura, T.; Kuwahara, Y.; Komatsu, N. Simultaneous Discrimination of Diameter, Handedness, and Metallicity of Single-Walled Carbon Nanotubes with Chiral Diporphyrin Nanocalipers. *J. Am. Chem. Soc.* **2013**, *135*, 4805–4814.
- (445) Ghosh, S.; Bachilo, S. M.; Weisman, R. B. Structure-dependent Optical Activity of Single-walled Carbon Nanotube Enantiomers. *Fullerenes, Nanotubes, Carbon Nanostruct.* **2014**, *22*, 269–279.
- (446) Wei, X. J.; Tanaka, T.; Yomogida, Y.; Sato, N.; Saito, R.; Kataura, H. Experimental Determination of Excitonic Band Structures of Single-Walled Carbon Nanotubes Using Circular Dichroism Spectra. *Nat. Commun.* **2016**, *7*, 12899.
- (447) Dukovic, G.; Balaz, M.; Doak, P.; Berova, N. D.; Zheng, M.; McLean, R. S.; Brus, L. E. Racemic Single-Walled Carbon Nanotubes Exhibit Circular Dichroism When Wrapped with DNA. *J. Am. Chem. Soc.* **2006**, *128*, 9004–9005.
- (448) Streit, J. K.; Fagan, J. A.; Zheng, M. A Low Energy Route to DNA-Wrapped Carbon Nanotubes via Replacement of Bile Salt Surfactants. *Anal. Chem.* **2017**, *89*, 10496–10503.
- (449) Yudasaka, M.; Zhang, M.; Iijima, S. Diameter-Selective Removal of Single-Wall Carbon Nanotubes through Light-Assisted Oxidation. *Chem. Phys. Lett.* **2003**, *374*, 132–136.
- (450) Huang, H.; Maruyama, R.; Noda, K.; Kajiwara, H.; Kadono, K. Preferential Destruction of Metallic Single-Walled Carbon Nanotubes by Laser Irradiation. *J. Phys. Chem. B* **2006**, *110*, 7316–7320.
- (451) Collins, P. C.; Arnold, M. S.; Avouris, P. Engineering Carbon Nanotubes and Nanotube Circuits Using Electrical Breakdown. *Science* **2001**, *292*, 706–709.
- (452) Otsuka, K.; Inoue, T.; Chiashi, S.; Maruyama, S. Selective Removal of Metallic Single-Walled Carbon Nanotubes in Full Length by Organic Film-Assisted Electrical Breakdown. *Nanoscale* **2014**, *6*, 8831–8835.
- (453) Li, J.; Franklin, A. D.; Liu, J. Gate-Free Electrical Breakdown of Metallic Pathways in Single-Walled Carbon Nanotube Crossbar Networks. *Nano Lett.* **2015**, *15*, 6058.
- (454) Zhang, G.; Qi, P.; Wang, X.; Lu, Y.; Li, X.; Tu, R.; Bangsaruntip, S.; Mann, D.; Zhang, L.; Dai, H. Selective Etching of Metallic Carbon Nanotubes by Gas-Phase Reaction. *Science* **2006**, *314*, 974–977.
- (455) Xie, X.; Jin, S. H.; Wahab, M. A.; Islam, A. E.; Zhang, C.; Du, F.; Seabron, E.; Lu, T.; Dunham, S. N.; Cheong, H. I.; et al. A Microwave Purification of Large-Area Horizontally Aligned Arrays of Single-Walled Carbon Nanotubes. *Nat. Commun.* **2014**, *5*, 5332.
- (456) Li, P.; Zhang, J. Sorting out Semiconducting Single-Walled Carbon Nanotube Arrays by Preferential Destruction of Metallic Tubes Using Water. *J. Mater. Chem.* **2011**, *21*, 11815–11821.
- (457) Li-Pook-Than, A.; Lefebvre, J.; Finnie, P. Type-and Species-Selective Air Etching of Single-Walled Carbon Nanotubes Tracked with In Situ Raman Spectroscopy. *ACS Nano* **2013**, *7*, 6507–6521.
- (458) Liu, B.; Jiang, H.; Krasheninnikov, A. V.; Nasibulin, A. G.; Ren, W.; Liu, C.; Kauppinen, E. I.; Cheng, H.-M. Chirality-Dependent Reactivity of Individual Single-Walled Carbon Nanotubes. *Small* **2013**, *9*, 1379–1386.
- (459) Maeda, Y.; Higo, J.; Amagai, Y.; Matsui, J.; Ohkubo, K.; Yoshigoe, Y.; Hashimoto, M.; Eguchi, K.; Yamada, M.; Hasegawa, T.; et al. Helicity Selective Photoreaction of Single-walled Carbon Nanotubes with Organosulfur Compounds in the Presence of Oxygen. *J. Am. Chem. Soc.* **2013**, *135*, 6356–6362.
- (460) Yu, Q.; Wu, C.; Guan, L. Direct Enrichment of Metallic Single-Walled Carbon Nanotubes by Using NO₂ as Oxidant to Selectively Etch Semiconducting Counterparts. *J. Phys. Chem. Lett.* **2016**, *7*, 4470–4474.
- (461) Yu, F.; Zhou, H.; Yang, H.; Chen, M.; Wang, G.; Sun, L. Preferential Elimination of Thin Single-Walled Carbon Nanotubes by Iron Etching. *Chem. Commun.* **2012**, *48*, 1042–1044.

- (462) Banerjee, S.; Wong, S. S. Demonstration of Diameter-Selective Reactivity in the Sidewall Ozonation of SWNTs by Resonance Raman Spectroscopy. *Nano Lett.* **2004**, *4*, 1445–1450.
- (463) Li, S. S.; Liu, C.; Hou, P. X.; Sun, D. M.; Cheng, H. M. Enrichment of Semiconducting Single-Walled Carbon Nanotubes by Carbothermic Reaction for Use in All-Nanotube Field Effect Transistors. *ACS Nano* **2012**, *6*, 9657–9661.
- (464) Pop, E. The Role of Electrical and Thermal Contact Resistance for Joule Breakdown of Single-Wall Carbon Nanotubes. *Nanotechnology* **2008**, *19*, 295202.
- (465) Liao, A.; Alizadeh, R.; Ong, Z.-Y.; Dutta, S.; Xiong, F.; Hsia, K. J.; Pop, E. Thermal Dissipation and Variability in Electrical Breakdown of Carbon Nanotube Devices. *Phys. Rev. B: Condens. Matter Mater. Phys.* **2010**, *82*, 205406.
- (466) Jin, S. H.; Dunham, S. N.; Song, J.; Xie, X.; Kim, J.-h.; Lu, C.; Islam, A.; Du, F.; Kim, J.; Felts, J.; et al. Using Nanoscale Thermocapillary Flows to Create Arrays of Purely Semiconducting Single-Walled Carbon Nanotubes. *Nat. Nanotechnol.* **2013**, *8*, 347–355.
- (467) Li-Pook-Than, A.; Finnie, P. Observation of the Metallic-Type Selective Etching of Single Walled Carbon Nanotubes by Real-Time In Situ Two-Laser Raman Spectroscopy. *Carbon* **2015**, *89*, 232–241.
- (468) Zhang, H.; Liu, Y.; Cao, L.; Wei, D.; Wang, Y.; Kajiwara, H.; Li, Y.; Noda, K.; Luo, G.; Wang, L.; et al. A Facile, Low-Cost, and Scalable Method of Selective Etching of Semiconducting Single-Walled Carbon Nanotubes by a Gas Reaction. *Adv. Mater.* **2009**, *21*, 813–816.
- (469) Hassanien, A.; Tokumoto, M.; Umek, P.; Vrbanić, D.; Mozetič, M.; Mihailović, D.; Venturini, P. Selective Etching of Metallic Single-Wall Carbon Nanotubes with Hydrogen Plasma. *Nanotechnology* **2005**, *16*, 278–281.
- (470) Yang, C.-M.; An, K. H.; Park, J. S.; Park, K. A.; Lim, S. C.; Cho, S.-H.; Lee, Y. S.; Park, W.; Park, C. Y.; Lee, Y. H. Preferential Etching of Metallic Single-Walled Carbon Nanotubes with Small Diameter by Fluorine Gas. *Phys. Rev. B: Condens. Matter Mater. Phys.* **2006**, *73*, No. 075419.
- (471) Chattopadhyay, D.; Galeska, L.; Papadimitrakopoulos, F. A. A Route for Bulk Separation of Semiconducting from Metallic Single-Wall Carbon Nanotubes. *J. Am. Chem. Soc.* **2003**, *125*, 3370–3375.
- (472) LeMieux, M. C.; Roberts, M.; Barman, S.; Jin, Y. W.; Kim, J. M.; Bao, Z. N. Self-Sorted, Aligned Nanotube Networks for Thin-Film Transistors. *Science* **2008**, *321*, 101–104.
- (473) Hong, G.; Zhou, M.; Zhang, R. O. X.; Hou, S. M.; Choi, W.; Woo, Y. S.; Choi, J. Y.; Liu, Z. F.; Zhang, J. Separation of Metallic and Semiconducting Single-Walled Carbon Nanotube Arrays by “Scotch Tape”. *Angew. Chem., Int. Ed.* **2011**, *50*, 6819–6823.
- (474) Zhang, D.; Yang, J.; Li, Y. Spectroscopic Characterization of the Chiral Structure of Individual Single-Walled Carbon Nanotubes and the Edge Structure of Isolated Graphene Nanoribbons. *Small* **2013**, *9*, 1284–1304.
- (475) Odom, T. W.; Huang, J.-L.; Kim, P.; Lieber, C. M. Atomic Structure and Electronic Properties of Single-Walled Carbon Nanotubes. *Nature* **1998**, *391*, 62–64.
- (476) Wilder, J. W. G.; Venema, L. C.; Rinzler, A. G.; Smalley, R. E.; Dekker, C. Electronic Structure of Atomically Resolved Carbon Nanotubes. *Nature* **1998**, *391*, 59–62.
- (477) Qin, L. C. Electron-Diffraction from Cylindrical Nanotubes. *J. Mater. Res.* **1994**, *9*, 2450–2456.
- (478) Qin, L.-C. Electron Diffraction from Carbon Nanotubes. *Rep. Prog. Phys.* **2006**, *69*, 2761–2821.
- (479) Kataura, H.; Kumazawa, Y.; Maniwa, Y.; Umezawa, I.; Suzuki, S.; Ohtsuka, Y.; Achiba, Y. Optical Properties of Single-Wall Carbon Nanotubes. *Synth. Met.* **1999**, *103*, 2555–2558.
- (480) Wei, X.; Tanaka, T.; Yomogida, Y.; Sato, N.; Saito, R.; Kataura, H. Experimental Determination of Excitonic Band Structures of Single-Walled Carbon Nanotubes Using Circular Dichroism Spectra. *Nat. Commun.* **2016**, *7*, 12899.
- (481) Fantini, C.; Jorio, A.; Souza, M.; Strano, M.; Dresselhaus, M.; Pimenta, M. Optical Transition Energies for Carbon Nanotubes from Resonant Raman Spectroscopy: Environment and Temperature Effects. *Phys. Rev. Lett.* **2004**, *93*, 147406.
- (482) Araujo, P.; Jorio, A. The Role of Environmental Effects on the Optical Transition Energies and Radial Breathing Mode Frequency of Single Wall Carbon Nanotubes. *Phys. Status Solidi B* **2008**, *245*, 2201–2204.
- (483) Maultzsch, J.; Telg, H.; Reich, S.; Thomsen, C. Radial Breathing Mode of Single-Walled Carbon Nanotubes: Optical Transition Energies and Chiral-Index Assignment. *Phys. Rev. B: Condens. Matter Mater. Phys.* **2005**, *72*, 205438.
- (484) Soares, J. S.; Cançado, L. G.; Barros, E. B.; Jorio, A. The Kataura Plot for Single Wall Carbon Nanotubes on Top of Crystalline Quartz. *Phys. Status Solidi B* **2010**, *247*, 2835–2837.
- (485) Zhang, D.; Yang, J.; Yang, F.; Li, R.; Li, M.; Ji, D.; Li, Y. (*n,m*) Assignments and Quantification for Single-Walled Carbon Nanotubes on SiO₂/Si Substrates by Resonant Raman Spectroscopy. *Nanoscale* **2015**, *7*, 10719–10727.
- (486) Araujo, P.; Maciel, I.; Pesce, P.; Pimenta, M.; Doorn, S.; Qian, H.; Hartschuh, A.; Steiner, M.; Grigorian, L.; Hata, K.; et al. Nature of the Constant Factor in the Relation Between Radial Breathing Mode Frequency and Tube Diameter for Single-Wall Carbon Nanotubes. *Phys. Rev. B: Condens. Matter Mater. Phys.* **2008**, *77*, 241403.
- (487) Yang, J.; Zhang, D.; Hu, Y.; Xia, C.; Sun, S.; Li, Y. Bilayer Plots for Accurately Determining the Chirality of Single-Walled Carbon Nanotubes under Complex Environments. *ACS Nano* **2017**, *11*, 10509–10518.
- (488) www.chem.pku.edu.cn/cnt_assign.
- (489) Farhat, H.; Berciaud, S.; Kalbac, M.; Saito, R.; Heinz, T.; Dresselhaus, M.; Kong, J. Observation of Electronic Raman Scattering in Metallic Carbon Nanotubes. *Phys. Rev. Lett.* **2011**, *107*, 157401.
- (490) Zhang, D.; Yang, J.; Hasdeo, E. H.; Liu, C.; Liu, K.; Saito, R.; Li, Y. Multiple Electronic Raman Scatterings in a Single Metallic Carbon Nanotube. *Phys. Rev. B: Condens. Matter Mater. Phys.* **2016**, *93*, 245428.
- (491) Zhang, D.; Yang, J.; Li, M.; Li, Y. (*n,m*) Assignments of Metallic Single-Walled Carbon Nanotubes by Raman Spectroscopy: The Importance of Electronic Raman Scattering. *ACS Nano* **2016**, *10*, 10789–10797.
- (492) Jorio, A.; Saito, R.; Hafner, J.; Lieber, C.; Hunter, M.; McClure, T.; Dresselhaus, G.; Dresselhaus, M. Structural (*n,m*) Determination of Isolated Single-Wall Carbon Nanotubes by Resonant Raman Scattering. *Phys. Rev. Lett.* **2001**, *86*, 1118–1121.
- (493) O’Connell, M. J.; Sivaram, S.; Doorn, S. K. Near-Infrared Resonance Raman Excitation Profile Studies of Single-Walled Carbon Nanotube Intertube Interactions: A Direct Comparison of Bundled and Individually Dispersed HiPco Nanotubes. *Phys. Rev. B: Condens. Matter Mater. Phys.* **2004**, *69*, 235415.
- (494) Meyer, J.; Paillet, M.; Michel, T.; Moréac, A.; Neumann, A.; Duesberg, G.; Roth, S.; Sauvajol, J.-L. Raman Modes of Index-Identified Freestanding Single-Walled Carbon Nanotubes. *Phys. Rev. Lett.* **2005**, *95*, No. 217401.
- (495) Chiashi, S.; Kono, K.; Matsumoto, D.; Shitaba, J.; Homma, N.; Beniya, A.; Yamamoto, T.; Homma, Y. Adsorption Effects on Radial Breathing Mode of Single-Walled Carbon Nanotubes. *Phys. Rev. B: Condens. Matter Mater. Phys.* **2015**, *91*, 155415.
- (496) Fantini, C.; Jorio, A.; Santos, A. P.; Peressinotto, V. S. T.; Pimenta, M. A. Characterization of DNA-Wrapped Carbon Nanotubes by Resonance Raman and Optical Absorption Spectroscopies. *Chem. Phys. Lett.* **2007**, *439*, 138–142.
- (497) Lebedkin, S.; Arnold, K.; Kiowski, O.; Hennrich, F.; Kappes, M. M. Raman Study of Individually Dispersed Single-Walled Carbon Nanotubes under Pressure. *Phys. Rev. B: Condens. Matter Mater. Phys.* **2006**, *73*, No. 094109.
- (498) Liu, K.; Wang, W.; Wu, M.; Xiao, F.; Hong, X.; Aloni, S.; Bai, X.; Wang, E.; Wang, F. Intrinsic Radial Breathing Oscillation in Suspended Single-Walled Carbon Nanotubes. *Phys. Rev. B: Condens. Matter Mater. Phys.* **2011**, *83*, 113404.
- (499) Jungen, A.; Popov, V. N.; Stampfer, C.; Durrer, L.; Stoll, S.; Hierold, C. Raman Intensity Mapping of Single-Walled Carbon

- Nanotubes. *Phys. Rev. B: Condens. Matter Mater. Phys.* **2007**, *75*, No. 041405.
- (500) Wang, J.; Yang, J.; Zhang, D.; Li, Y. Structure Dependence of the Intermediate-Frequency Raman Modes in Isolated Single-Walled Carbon Nanotubes. *J. Phys. Chem. C* **2012**, *116*, 23826–23832.
- (501) Araujo, P. T.; Doorn, S. K.; Kilina, S.; Tretiak, S.; Einarsson, E.; Maruyama, S.; Chacham, H.; Pimenta, M. A.; Jorio, A. Third and Fourth Optical Transitions in Semiconducting Carbon Nanotubes. *Phys. Rev. Lett.* **2007**, *98*, No. 067401.
- (502) Jorio, A.; Fantini, C.; Pimenta, M.; Capaz, R.; Samsonidze, G.; Dresselhaus, G.; Dresselhaus, M.; Jiang, J.; Kobayashi, N.; Grüneis, A.; et al. Resonance Raman Spectroscopy (n,m)-Dependent Effects in Small-Diameter Single-Wall Carbon Nanotubes. *Phys. Rev. B: Condens. Matter Mater. Phys.* **2005**, *71*, No. 075401.
- (503) Bachilo, S. M.; Strano, M. S.; Kittrell, C.; Hauge, R. H.; Smalley, R. E.; Weisman, R. B. Structure-Assigned Optical Spectra of Single-Walled Carbon Nanotubes. *Science* **2002**, *298*, 2361–2366.
- (504) Telg, H.; Maultzsch, J.; Reich, S.; Hennrich, F.; Thomsen, C. Chirality Distribution and Transition Energies of Carbon Nanotubes. *Phys. Rev. Lett.* **2004**, *93*, 177401.
- (505) Chu, H.; Wang, J.; Ding, L.; Yuan, D.; Zhang, Y.; Liu, J.; Li, Y. Decoration of Gold Nanoparticles on Surface-Grown Single-Walled Carbon Nanotubes for Detection of Every Nanotube by Surface-Enhanced Raman Spectroscopy. *J. Am. Chem. Soc.* **2009**, *131*, 14310–14316.
- (506) Kumar, R.; Zhou, H.; Cronin, S. B. Surface-Enhanced Raman Spectroscopy and Correlated Scanning Electron Microscopy of Individual Carbon Nanotubes. *Appl. Phys. Lett.* **2007**, *91*, 223105.
- (507) Kneipp, K.; Kneipp, H.; Corio, P.; Brown, S. D.; Shafer, K.; Motz, J.; Perelman, L. T.; Hanlon, E. B.; Marucci, A.; Dresselhaus, G.; et al. Surface-Enhanced and Normal Stokes and Anti-Stokes Raman Spectroscopy of Single-Walled Carbon Nanotubes. *Phys. Rev. Lett.* **2000**, *84*, 3470–3473.
- (508) Brown, S.; Jorio, A.; Corio, P.; Dresselhaus, M.; Dresselhaus, G.; Saito, R.; Kneipp, K. Origin of the Breit-Wigner-Fano Lineshape of the Tangential G-Band Feature of Metallic Carbon Nanotubes. *Phys. Rev. B: Condens. Matter Mater. Phys.* **2001**, *63*, 155414.
- (509) Michel, T.; Paillet, M.; Zahab, A.; Nakabayashi, D.; Jourdain, V.; Parret, R.; Sauvajol, J. L. About the Indexing of the Structure of Single-Walled Carbon Nanotubes from Resonant Raman Scattering. *Adv. Nat. Sci.: Nanosci. Nanotechnol.* **2010**, *1*, No. 045007.
- (510) Házor, E. H.; Duque, J. G.; Rice, W. D.; Densmore, C. G.; Kono, J.; Doorn, S. K. Resonant Raman Spectroscopy of Armchair Carbon Nanotubes: Absence of broad G⁺ feature. *Phys. Rev. B: Condens. Matter Mater. Phys.* **2011**, *84*, 121403.
- (511) Zhang, Y.; Son, H.; Zhang, J.; Dresselhaus, M. S.; Kong, J.; Liu, Z. Raman Spectra Variation of Partially Suspended Individual Single-Walled Carbon Nanotubes. *J. Phys. Chem. C* **2007**, *111*, 1983–1987.
- (512) Souza, M.; Jorio, A.; Fantini, C.; Neves, B. R. A.; Pimenta, M. A.; Saito, R.; Ismach, A.; Joselevich, E.; Brar, V. W.; Samsonidze, G. G.; et al. Single- and Double-Resonance Raman G-Band Processes in Carbon Nanotubes. *Phys. Rev. B: Condens. Matter Mater. Phys.* **2004**, *69*, 241403.
- (513) Wang, B.; Gupta, A. K.; Huang, J.; Vedala, H.; Hao, Q.; Crespi, V. H.; Choi, W.; Eklund, P. C. Effect of Bending on Single-Walled Carbon Nanotubes: A Raman Scattering Study. *Phys. Rev. B: Condens. Matter Mater. Phys.* **2010**, *81*, 115422.
- (514) Jorio, A.; Souza Filho, A.; Dresselhaus, G.; Dresselhaus, M.; Swan, A.; Ünlü, M.; Goldberg, B.; Pimenta, M.; Hafner, J.; Lieber, C.; et al. G-Band Resonant Raman Study of 62 Isolated Single-Wall Carbon Nanotubes. *Phys. Rev. B: Condens. Matter Mater. Phys.* **2002**, *65*, 155412.
- (515) Telg, H.; Duque, J. G.; Staiger, M.; Tu, X.; Hennrich, F.; Kappes, M. M.; Zheng, M.; Maultzsch, J.; Thomsen, C.; Doorn, S. K. Chiral Index Dependence of the G⁺ and G⁻ Raman Modes in Semiconducting Carbon Nanotubes. *ACS Nano* **2012**, *6*, 904–911.
- (516) Levshov, D. I.; Tran, H. N.; Paillet, M.; Arenal, R.; Than, X. T.; Zahab, A. A.; Yuzyuk, Y. I.; Sauvajol, J. L.; Michel, T. Accurate Determination of the Chiral Indices of Individual Carbon Nanotubes by Combining Electron Diffraction and Resonant Raman Spectroscopy. *Carbon* **2017**, *114*, 141–159.
- (517) Jorio, A.; Pimenta, M. A.; Souza Filho, A. G.; Samsonidze, G. G.; Swan, A. K.; Ünlü, M. S.; Goldberg, B. B.; Saito, R.; Dresselhaus, G.; Dresselhaus, M. S. Resonance Raman Spectra of Carbon Nanotubes by Cross-Polarized Light. *Phys. Rev. Lett.* **2003**, *90*, 107403.
- (518) Popov, V. N.; Lambin, P. Radius and Chirality Dependence of the Radial Breathing Mode and the G-Band Phonon Modes of Single-Walled Carbon Nanotubes. *Phys. Rev. B: Condens. Matter Mater. Phys.* **2006**, *73*, No. 085407.
- (519) Kalbac, M.; Kavan, L.; Zukalová, M.; Dunsch, L. The Intermediate Frequency Modes of Single- and Double-Walled Carbon Nanotubes: A Raman Spectroscopic and In Situ Raman Spectroelectrochemical Study. *Chem. - Eur. J.* **2006**, *12*, 4451–4457.
- (520) Souza Filho, A. G.; Jorio, A.; Swan, A. K.; Ünlü, M. S.; Goldberg, B. B.; Saito, R.; Hafner, J. H.; Lieber, C. M.; Pimenta, M. A.; Dresselhaus, G.; et al. Anomalous Two-Peak G-Band Raman Effect in One Isolated Single-Wall Carbon Nanotube. *Phys. Rev. B: Condens. Matter Mater. Phys.* **2002**, *65*, No. 085417.
- (521) Souza Filho, A. G.; Jorio, A.; Samsonidze, G. G.; Dresselhaus, G.; Dresselhaus, M. S.; Swan, A. K.; Ünlü, M. S.; Goldberg, B. B.; Saito, R.; Hafner, J. H.; et al. Probing the Electronic Trigonal Warping Effect in Individual Single-Wall Carbon Nanotubes Using Phonon Spectra. *Chem. Phys. Lett.* **2002**, *354*, 62–68.
- (522) Hartschuh, A.; Pedrosa, H. N.; Novotny, L.; Krauss, T. D. Simultaneous Fluorescence and Raman Scattering from Single Carbon Nanotubes. *Science* **2003**, *301*, 1354–1356.
- (523) Lefebvre, J.; Fraser, J.; Finnie, P.; Homma, Y. Photoluminescence from an Individual Single-Walled Carbon Nanotube. *Phys. Rev. B: Condens. Matter Mater. Phys.* **2004**, *69*, No. 075403.
- (524) Sturzl, N.; Lebedkin, S.; Peng, F.; Li, Y.; Hennrich, F.; Kappes, M. M. Simultaneous Detection of Raman Scattering and Near-Infrared Photoluminescence in One Imaging Microscope. *Rev. Sci. Instrum.* **2012**, *83*, No. 063709.
- (525) Kono, K.; Matsumoto, D.; Chiashi, S.; Homma, Y. Simultaneous Measurement of Photoluminescence and Raman Scattering Spectra from suspended Single-Walled Carbon Nanotubes. *Surf. Interface Anal.* **2012**, *44*, 686–689.
- (526) Steiner, M.; Freitag, M.; Tsang, J. C.; Perebeinos, V.; Bol, A. A.; Failla, A. V.; Avouris, P. How Does the Substrate Affect the Raman and Excited State Spectra of a Carbon Nanotube? *Appl. Phys. A: Mater. Sci. Process.* **2009**, *96*, 271–282.
- (527) Kiowski, O.; Lebedkin, S.; Kappes, M. M. Photoluminescence Microscopy of As-Grown Individual Single-Walled Carbon Nanotubes on Si/SiO₂ Substrates. *Phys. Status Solidi B* **2006**, *243*, 3122–3125.
- (528) Schweiger, M.; Zakharko, Y.; Gannott, F.; Grimm, S. B.; Zaumseil, J. Photoluminescence Enhancement of Aligned Arrays of Single-Walled Carbon Nanotubes by Polymer Transfer. *Nanoscale* **2015**, *7*, 16715–16720.
- (529) Weisman, R. B.; Bachilo, S. M. Dependence of Optical Transition Energies on Structure for Single-Walled Carbon Nanotubes in Aqueous Suspension: an Empirical Kataura Plot. *Nano Lett.* **2003**, *3*, 1235–1238.
- (530) Blancon, J.-C.; Paillet, M.; Tran, H. N.; Than, X. T.; Guebrou, S. A.; Ayari, A.; Miguel, A. S.; Phan, N.-M.; Zahab, A.-A.; Sauvajol, J.-L.; et al. Direct Measurement of the Absolute Absorption Spectrum of Individual Semiconducting Single-Wall Carbon Nanotubes. *Nat. Commun.* **2013**, *4*, 2542.
- (531) Liu, K.; Hong, X.; Zhou, Q.; Jin, C.; Li, J.; Zhou, W.; Liu, J.; Wang, E.; Zettl, A.; Wang, F. High-Throughput Optical Imaging and Spectroscopy of Individual Carbon Nanotubes in Devices. *Nat. Nanotechnol.* **2013**, *8*, 917–922.
- (532) Yao, F.; Liu, C.; Chen, C.; Zhang, S.; Zhao, Q.; Xiao, F.; Wu, M.; Li, J.; Gao, P.; Zhao, J.; et al. Measurement of Complex Optical Susceptibility for Individual Carbon Nanotubes by Elliptically Polarized Light Excitation. *Nat. Commun.* **2018**, *9*, 3387.
- (533) Sfeir, M. Y.; Wang, F.; Huang, L. M.; Chuang, C. C.; Hone, J.; O'Brien, S. P.; Heinz, T. F.; Brus, L. E. Probing electronic transitions in

- Individual Carbon Nanotubes by Rayleigh Scattering. *Science* **2004**, *306*, 1540–1543.
- (534) Sfeir, M. Y.; Beetz, T.; Wang, F.; Huang, L.; Huang, X. M.; Huang, M.; Hone, J.; O'Brien, S.; Misewich, J. A.; Heinz, T. F.; et al. Optical Spectroscopy of Individual Single-Walled Carbon Nanotubes of Defined Chiral Structure. *Science* **2006**, *312*, 554–556.
- (535) Wang, F.; Sfeir, M. Y.; Huang, L. M.; Huang, X. M. H.; Wu, Y.; Kim, J. H.; Hone, J.; O'Brien, S.; Brus, L. E.; Heinz, T. F. Interactions Between Individual Carbon Nanotubes Studied by Rayleigh Scattering Spectroscopy. *Phys. Rev. Lett.* **2006**, *96*, 167401.
- (536) Berciaud, S.; Deshpande, V. V.; Caldwell, R.; Miyauchi, Y.; Voisin, C.; Kim, P.; Hone, J.; Heinz, T. F. All-Optical Structure Assignment of Individual Single-Walled Carbon Nanotubes from Rayleigh and Raman Scattering Measurements. *Phys. Status Solidi B* **2012**, *249*, 2436–2441.
- (537) Liu, K.; Deslippe, J.; Xiao, F.; Capaz, R. B.; Hong, X.; Aloni, S.; Zettl, A.; Wang, W.; Bai, X.; Louie, S. G.; et al. An Atlas of Carbon Nanotube Optical Transitions. *Nat. Nanotechnol.* **2012**, *7*, 325–329.
- (538) Joh, D. Y.; Herman, L. H.; Ju, S. Y.; Kinder, J.; Segal, M. A.; Johnson, J. N.; Chan, G. K. L.; Park, J. On-Chip Rayleigh Imaging and Spectroscopy of Carbon Nanotubes. *Nano Lett.* **2011**, *11*, 1–7.
- (539) Wu, W.; Yue, J.; Lin, X.; Li, D.; Zhu, F.; Yin, X.; Zhu, J.; Wang, J.; Zhang, J.; Chen, Y.; et al. True-Color Real-Time Imaging and Spectroscopy of Carbon Nanotubes on Substrates by Enhanced Rayleigh Scattering. *Nano Res.* **2015**, *8*, 2721–2732.
- (540) Sánchez-Castillo, A.; Román-Velázquez, C.; Noguera, C. Optical Circular Dichroism of Single-Wall Carbon Nanotubes. *Phys. Rev. B: Condens. Matter Mater. Phys.* **2006**, *73*, No. 045401.
- (541) Chen, Y.; Shen, Z.; Xu, Z.; Hu, Y.; Xu, H.; Wang, S.; Guo, X.; Zhang, Y.; Peng, L.; Ding, F.; et al. Helicity-Dependent Single-Walled Carbon Nanotube Alignment on Graphite for Helical Angle and Handedness Recognition. *Nat. Commun.* **2013**, *4*, 2205.
- (542) Chen, Y.; Hu, Y.; Liu, M.; Xu, W.; Zhang, Y.; Xie, L.; Zhang, J. Chiral Structure Determination of Aligned Single-Walled Carbon Nanotubes on Graphite Surface. *Nano Lett.* **2013**, *13*, 5666–5671.
- (543) Qin, L.-C. Determination of the Chiral Indices (*n,m*) of Carbon Nanotubes by Electron Diffraction. *Phys. Chem. Chem. Phys.* **2007**, *9*, 31–48.
- (544) Jiang, H.; Nasibulin, A. G.; Brown, D. P.; Kauppinen, E. I. Unambiguous Atomic Structural Determination of Single-Walled Carbon Nanotubes by Electron Diffraction. *Carbon* **2007**, *45*, 662–667.
- (545) <https://research.physics.unc.edu/lcqin/www/nds/hdsh/hdsh.html>.
- (546) Liu, Z. J.; Qin, L. C. A Direct Method to Determine the Chiral Indices of Carbon Nanotubes. *Chem. Phys. Lett.* **2005**, *408*, 75–79.
- (547) Jiang, H.; Brown, D.; Nasibulin, A.; Kauppinen, E. Robust Bessel-Function-Based Method for Determination of the (*n,m*) Indices of Single-Walled Carbon Nanotubes by Electron Diffraction. *Phys. Rev. B: Condens. Matter Mater. Phys.* **2006**, *74*, No. 035427.
- (548) Gao, M.; Zuo, J.; Tweten, R.; Petrov, I.; Nagahara, L.; Zhang, R. Structure Determination of Individual Single-Wall Carbon Nanotubes by Nanoarea Electron Diffraction. *Appl. Phys. Lett.* **2003**, *82*, 2703–2705.
- (549) He, M.; Dong, J.; Zhang, K.; Ding, F.; Jiang, H.; Loiseau, A.; Lehtonen, J.; Kauppinen, E. I. Precise Determination of the Threshold Diameter for a Single-Walled Carbon Nanotube to Collapse. *ACS Nano* **2014**, *8*, 9657–9663.
- (550) Barkelid, M.; Steele, G. A.; Zwiller, V. Probing Optical Transitions in Individual Carbon Nanotubes Using Polarized Photocurrent Spectroscopy. *Nano Lett.* **2012**, *12*, 5649–5653.
- (551) Vijayaraghavan, A.; Blatt, S.; Marquardt, C.; Dehm, S.; Wah, R.; Hennrich, F.; Krupke, R. Imaging Electronic Structure of Carbon Nanotubes by Voltage-Contrast Scanning Electron Microscopy. *Nano Res.* **2008**, *1*, 321–332.
- (552) Li, J.; He, Y.; Han, Y.; Liu, K.; Wang, J.; Li, Q.; Fan, S.; Jiang, K. Direct Identification of Metallic and Semiconducting Single-Walled Carbon Nanotubes in Scanning Electron Microscopy. *Nano Lett.* **2012**, *12*, 4095–4101.
- (553) Lu, W.; Xiong, Y.; Hassanien, A.; Zhao, W.; Zheng, M.; Chen, L. W. A Scanning Probe Microscopy Based Assay for Single-Walled Carbon Nanotube Metallicity. *Nano Lett.* **2009**, *9*, 1668–1672.
- (554) Shi, Z.; Hong, X.; Bechtel, H. A.; Zeng, B.; Martin, M. C.; Watanabe, K.; Taniguchi, T.; Shen, Y.-R.; Wang, F. Observation of a Luttinger-Liquid Plasmon in Metallic Single-Walled Carbon Nanotubes. *Nat. Photonics* **2015**, *9*, 515–519.
- (555) Torrents, O. N.; Milkie, D. E.; Zheng, M.; Kikkawa, J. M. Photoluminescence from Intertube Carrier Migration in Single-Walled Carbon Nanotube Bundles. *Nano Lett.* **2006**, *6*, 2864–2867.
- (556) Tan, P. H.; Rozhin, A. G.; Hasan, T.; Hu, P.; Scardaci, V.; Milne, W. I.; Ferrari, A. C. Photoluminescence Spectroscopy of Carbon Nanotube Bundles: Evidence for Exciton Energy Transfer. *Phys. Rev. Lett.* **2007**, *99*, 137402.
- (557) Lefebvre, J.; Finnie, P. Photoluminescence and Forster Resonance Energy Transfer in Elemental Bundles of Single-Walled Carbon Nanotubes. *J. Phys. Chem. C* **2009**, *113*, 7536–7540.
- (558) Kiowski, O.; Jester, S.-S.; Lebedkin, S.; Jin, Z.; Li, Y.; Kappes, M. Photoluminescence Spectral Imaging of Ultralong Single-Walled Carbon Nanotubes: Micromanipulation-Induced Strain, Rupture, and Determination of Handedness. *Phys. Rev. B: Condens. Matter Mater. Phys.* **2009**, *80*, No. 075426.
- (559) Liu, K.; Hong, X.; Choi, S.; Jin, C.; Capaz, R. B.; Kim, J.; Wang, W.; Bai, X.; Louie, S. G.; Wang, E.; et al. Systematic Determination of Absolute Absorption Cross-Section of Individual Carbon Nanotubes. *Proc. Natl. Acad. Sci. U. S. A.* **2014**, *111*, 7564–7569.
- (560) Liu, K.; Jin, C.; Hong, X.; Kim, J.; Zettl, A.; Wang, E.; Wang, F. Van Der Waals-Coupled Electronic States in Incommensurate Double-Walled Carbon Nanotubes. *Nat. Phys.* **2014**, *10*, 737–742.
- (561) Carlson, L. J.; Maccagnano, S. E.; Zheng, M.; Silcox, J.; Krauss, T. D. Fluorescence Efficiency of Individual Carbon Nanotubes. *Nano Lett.* **2007**, *7*, 3698–3703.
- (562) Schöppeler, F.; Mann, C.; Hain, T. C.; Neubauer, F. M.; Privitera, G.; Bonaccorso, F.; Chu, D.; Ferrari, A. C.; Hertel, T. Molar Extinction Coefficient of Single-Wall Carbon Nanotubes. *J. Phys. Chem. C* **2011**, *115*, 14682–14686.
- (563) Berciaud, S.; Cognet, L.; Lounis, B. Luminescence Decay and the Absorption Cross Section of Individual Single-Walled Carbon Nanotubes. *Phys. Rev. Lett.* **2008**, *101*, No. 077402.
- (564) Oudjedi, L.; Parra-Vasquez, A. N.; Godin, A. G.; Cognet, L.; Lounis, B. Metrological Investigation of the (6,5) Carbon Nanotube Absorption Cross Section. *J. Phys. Chem. Lett.* **2013**, *4*, 1460–1464.
- (565) Streit, J. K.; Bachilo, S. M.; Ghosh, S.; Lin, C. W.; Weisman, R. B. Directly Measured Optical Absorption Cross Sections for Structure-Selected Single-Walled Carbon Nanotubes. *Nano Lett.* **2014**, *14*, 1530–1536.
- (566) Vialla, F.; Roquelet, C.; Langlois, B.; Delport, G.; Santos, S. M.; Deleporte, E.; Roussignol, P.; Delalande, C.; Voisin, C.; Lauret, J. S. Chirality Dependence of the Absorption Cross Section of Carbon Nanotubes. *Phys. Rev. Lett.* **2013**, *111*, 137402.
- (567) Pfohl, M.; Tune, D. D.; Graf, A.; Zaumseil, J.; Krupke, R.; Flavel, B. S. Fitting Single-Walled Carbon Nanotube Optical Spectra. *ACS omega* **2017**, *2*, 1163–1171.
- (568) Nair, N.; Usrey, M. L.; Kim, W.-J.; Braatz, R. D.; Strano, M. S. Estimation of the (*n,m*) Concentration Distribution of Single-Walled Carbon Nanotubes from Photoabsorption Spectra. *Anal. Chem.* **2006**, *78*, 7689–7696.
- (569) Naumov, A. V.; Ghosh, S.; Tsyboulski, D. A.; Bachilo, S. M.; Weisman, R. B. Analyzing Absorption Backgrounds in Single-Walled Carbon Nanotube Spectra. *ACS Nano* **2011**, *5*, 1639–1648.
- (570) Tian, Y.; Jiang, H.; Anoshkin, I. V.; Kauppinen, L. J. I.; Mustonen, K.; Nasibulin, A. G.; Kauppinen, E. I. A Reference Material of Single-Walled Carbon Nanotubes: Quantitative Chirality Assessment using Optical Absorption Spectroscopy. *RSC Adv.* **2015**, *5*, 102974–102980.
- (571) Rocha, J. D. R.; Bachilo, S. M.; Ghosh, S.; Arepalli, S.; Weisman, R. B. Efficient Spectrofluorimetric Analysis of Single-Walled Carbon Nanotube Samples. *Anal. Chem.* **2011**, *83*, 7431–7437.

- (572) Jorio, A.; Fantini, C.; Pimenta, M. A.; Heller, D. A.; Strano, M. S.; Dresselhaus, M. S.; Oyama, Y.; Jiang, J.; Saito, R. Carbon Nanotube Population Analysis from Raman and Photoluminescence Intensities. *Appl. Phys. Lett.* **2006**, *88*, No. 023109.
- (573) Oyama, Y.; Saito, R.; Sato, K.; Jiang, J.; Samsonidze, G. G.; Grüneis, A.; Miyachi, Y.; Maruyama, S.; Jorio, A.; Dresselhaus, G.; et al. Photoluminescence Intensity of Single-Wall Carbon Nanotubes. *Carbon* **2006**, *44*, 873–879.
- (574) Tsybouski, D. A.; Rocha, J. D. R.; Bachilo, S. M.; Cognet, L.; Weisman, R. B. Structure-Dependent Fluorescence Efficiencies of Individual Single-Walled Carbon Nanotubes. *Nano Lett.* **2007**, *7*, 3080–3085.
- (575) Streit, J. K.; Bachilo, S. M.; Sanchez, S. R.; Lin, C. W.; Weisman, R. B. Variance Spectroscopy. *J. Phys. Chem. Lett.* **2015**, *6*, 3976–3981.
- (576) Luo, Z.; Pfefferle, L. D.; Haller, G. L.; Papadimitrakopoulos, F. (*n,m*) Abundance Evaluation of Single-Walled Carbon Nanotubes by Fluorescence and Absorption Spectroscopy. *J. Am. Chem. Soc.* **2006**, *128*, 15511–15516.
- (577) Piao, Y.; Meany, B.; Powell, L. R.; Valley, N.; Kwon, H.; Schatz, G. C.; Wang, Y. Brightening of Carbon Nanotube Photoluminescence through the Incorporation of sp^3 Defects. *Nat. Chem.* **2013**, *5*, 840–845.
- (578) Ju, S. Y.; Kopcha, W. P.; Papadimitrakopoulos, F. Brightly Fluorescent Single-Walled Carbon Nanotubes via an Oxygen-Excluding Surfactant Organization. *Science* **2009**, *323*, 1319–1323.
- (579) Qu, L.; Du, F.; Dai, L. Preferential Syntheses of Semiconducting Vertically Aligned Single-Walled Carbon Nanotubes for Direct Use in Fets. *Nano Lett.* **2008**, *8*, 2682–2687.
- (580) Ohashi, T.; Iwama, H.; Shima, T. Growth of Vertically Aligned Single-Walled Carbon Nanotubes with Metallic Chirality through Faceted Fept-Au Catalysts. *J. Appl. Phys.* **2016**, *119*, No. 084303.
- (581) Fouquet, M.; Bayer, B.; Esconjauregui, S.; Blume, R.; Warner, J.; Hofmann, S.; Schlägl, R.; Thomsen, C.; Robertson, J. Highly Chiral-Selective Growth of Single-Walled Carbon Nanotubes with a Simple Monometallic Co Catalyst. *Phys. Rev. B: Condens. Matter Mater. Phys.* **2012**, *85*, 235411.
- (582) Tian, Y.; Jiang, H.; Laiho, P.; Kauppinen, E. I. On the Validity of Measuring Metallic and Semiconducting SWCNT Fractions by Quantitative Raman Spectroscopy. *Anal. Chem.* **2018**, *90*, 2517–2525.
- (583) Popov, V.; Henrard, L.; Lambin, P. Electron-Phonon and Electron-Photon Interactions and Resonant Raman Scattering from the Radial-Breathing Mode of Single-Walled Carbon Nanotubes. *Phys. Rev. B: Condens. Matter Mater. Phys.* **2005**, *72*, No. 035436.
- (584) Jorio, A.; Santos, A. P.; Ribeiro, H. B.; Fantini, C.; Souza, M.; Vieira, J. P. M.; Furtado, C. A.; Jiang, J.; Saito, R.; Balzano, L.; et al. Quantifying Carbon-Nanotube Species with Resonance Raman Scattering. *Phys. Rev. B: Condens. Matter Mater. Phys.* **2005**, *72*, No. 075207.
- (585) Jester, S.-S.; Kiowski, O.; Lebedkin, S.; Hennrich, F.; Fischer, R.; Stürzl, N.; Hawecker, J.; Kappes, M. M. Combination of Atomic Force Microscopy and Photoluminescence Microscopy for the Investigation of Individual Carbon Nanotubes on Sapphire Surfaces. *Phys. Status Solidi B* **2007**, *244*, 3973–3977.
- (586) Naumov, A. V.; Kuznetsov, O. A.; Harutyunyan, A. R.; Green, A. A.; Hersam, M. C.; Resasco, D. E.; Nikolaev, P. N.; Weisman, R. B. Quantifying the Semiconducting Fraction in Single-Walled Carbon Nanotube Samples through Comparative Atomic Force and Photoluminescence Microscopies. *Nano Lett.* **2009**, *9*, 3203–3208.
- (587) Chu, H.; Cui, R.; Wang, J.; Yang, J.; Li, Y. Visualization of Individual Single-Walled Carbon Nanotubes Under an Optical Microscope as a Result of Decoration with Gold Nanoparticles. *Carbon* **2011**, *49*, 1182–1188.
- (588) Yuan, Y.; Wei, L.; Jiang, W.; Goh, K.; Jiang, R.; Lau, R.; Chen, Y. Sulfur-Induced Chirality Changes in Single-Walled Carbon Nanotube Synthesis by Ethanol Chemical Vapor Deposition on a Co/SiO₂ Catalyst. *J. Mater. Chem. A* **2015**, *3*, 3310–3319.
- (589) Wang, Q.; Yang, S.-W.; Yang, Y.; Chan-Park, M. B.; Chen, Y. Charge Transfer Between Metal Clusters and Growing Carbon Structures in Chirality-Controlled Single-Walled Carbon Nanotube Growth. *J. Phys. Chem. Lett.* **2011**, *2*, 1009–1014.
- (590) Srinivasan, K.; Zheng, M. Nanotube Chemistry Tunes Light. *Nat. Photonics* **2017**, *11*, 535–537.
- (591) Saha, A.; Gifford, B. J.; He, X. W.; Ao, G. Y.; Zheng, M.; Kataura, H.; Htoon, H.; Kilina, S.; Tretiak, S.; Doorn, S. K. Narrow-Band Single-Photon Emission through Selective Aryl Functionalization of Zigzag Carbon Nanotubes. *Nat. Chem.* **2018**, *10*, 1089–1095.
- (592) Galassi, T. V.; Jena, P. V.; Shah, J.; Ao, G.; Molitor, E.; Bram, Y.; Frankel, A.; Park, J.; Jessurun, J.; Ory, D. S.; et al. An Optical Nanoreporter of Endolysosomal Lipid Accumulation Reveals Enduring Effects of Diet on Hepatic Macrophages in Vivo. *Sci. Transl. Med.* **2018**, *10*, eaar2680.